Flushing Ballast Tanks

A thesis submitted to Department of Mechanical Engineering,
University College London
for the degree of Doctor of Philosophy

Zhixin Qi
April 2015

Declaration

I, Zhixin Qi, confirm that the work presented in this thesis is my own. Where information has been derived from other sources, I confirm that this has been indicated in the thesis.

Abstract

The non-indigenous species (NIS) transported by ships' ballast water lead to destructive failure of the main ecologies giving rise to economic implications of many countries dependent on aquatic organisms. The International Maritime Organisation currently requires that ballast tanks are flushed three times with far ocean water. New protocols for cleaning technologies are still in discussion internationally. Current lacking is the science to understand how ballast tanks geometry and ballast water composition affect the NIS removal rate. This thesis describes a major contribution to this effort and identifies key engineering principles that should be taken into account to improve flushing efficiency.

A combined experimental and theoretical study of flushing from ballast tanks is described. A hierarchy of laboratory scale models are designed, built and tested to understand the effect of geometry and stratification, with complexity increasing from 1×7, 2×2, 3×3 to 5×4 configurations. The experimental study is based on an optical method of interrogating the fraction of each compartment and whole tank that is cleaned.

By drawing on modelling approaches applied in related areas, notably building engineering, a number of new mathematical models are developed that have no free variables (when resistance of pathways is the same) or require the use of closures for pressure drop coefficients. For homogeneous flow where stratification is negligible, the agreement between predictions and experiments is within 1.2%. Likewise, when resistances are different, the model is accurate, except when the inhomogeneity is significant. Three models are developed to include the influence of stratification. For miscible fluids, the stratified mixing model is accurate within 5% at Richardson

number between 30 and 1000.

We apply the validated models to examine how to change practical ballast tanks and how cleaning efficiency affects the total NIS removal. To enhance flushing, a single outlet should be placed far from the inlet.

Acknowledgement

I would like to express my first and sincere gratitude to my principal supervisor, Prof Ian Eames, whose insightful suggestions and continuous encouragement helped me during the period of my PhD research. Ian is undoubtedly a talented scientist in fluid mechanics. I am often enlightened by his creative ideas and greatly touched by his devotion to academia. Thanks to his trust and support, I had opportunities to gain teaching and tutoring experience, and attend international conferences. Besides, he found funding for my existence after my scholarship ended, without which I would have been in financial trouble. My appreciation to his generous help is beyond my words. I hope my work to scientific research could repay him to some extent. Also, I would like to acknowledge my second supervisor, Dr Alistair Greig, who gave me advice on my paper writing and experimental equipment design. Both of my supervisors sent me literatures which they found useful to my research in the first time.

My second appreciation goes to my funding body, the European Commission, who offered me the Erasmus Mundus scholarship for 34 months to study at University College London for my PhD degree. This overseas experience is definitely an invaluable wealth to my whole life. Mr Marco Federighi, Mrs Elisabeth Axell, and other coordinators of this program, have always done their best to render whatever service they could and I am grateful to them for their endeavour. Also, I acknowledge the Graduate School and Prof Nicos Ladommatos, the previous Head of Department of Mechanical Engineering, who financially funded my travel to the United States for the 66th APS DFD Meeting.

I thank Mr Peter Kelley, the superintendent of the departmental workshop, Mr Richard Winn and Mr Barry Carter, two hard-working technicians in the workshop.

They made every effort to maintain the operation of the lab facilities. I thank Mr Philip Jeavons for building my experimental equipment.

My colleague, Amir Samsudin, is a kind ophthalmologist working in the same lab with me. Chatting with him was always a good relaxation when I felt tired. Another two colleagues, Hendrik Ülpre and Christian Klettner, helped me with the coding of computational fluid dynamics and proofread of thesis, respectively.

Especially, I would like to thank my father and grandmother, who are full of solicitude towards me all the time from my home country. I am willing to try my best to reward them in the future. Also, I want to express my love to my mother in the heaven. I wish everything goes well with her in her world. Finally, I thank all of my other relatives and friends.

Contents

List of Figures

List of Tables

Nomenclature

Latin Letters

$\bar{C}$	Average flushed fraction
$\boldsymbol{u}$	Velocity field
$\boldsymbol{v}$	Eigenvector of matrix
$\hat{\boldsymbol{n}}$	Unit normal vector
$\hat{\boldsymbol{z}}$	Unit upwards vector
$\hat{h}$	Normalised height
A	Area
b	Plume radius
C	Concentration/Flushed fraction
C_d	Discharge coefficient
C_I	Depth integrated flushed fraction
D	Diameter
F	Mass flux
f	Internal flow rate
g	Gravitational acceleration, 9.8 m/s^2
H	Height
h	Height
H_I	Interface height
I	Light intensity
I_t	Turbulence intensity
k	Fraction of length

L	Length
l	Distance
M	Momentum
p	Pressure
Q	Flow rate
r	Rank
Re	Reynolds number
Ri	Richardson number
Sa	Salinity
T	Dimensionless time, Qt/V
t	Real time
$T_{\frac{1}{2}}$	Half flushed time
Te	Temperature
U	Velocity
u	Horizontal velocity
V	Volume
v	Vertical velocity
v_T	Terminal fall velocity
W	Width
w	Width
z	Vertical distance
$\mathcal{H}$	Heaviside function
D	Total derivative
R	NIS removal rate

Greek Letters

$\alpha_{\frac{1}{2}}$	Flushing rate at half time
$\boldsymbol{\tau}$	Tensor
Δ	Difference
δ	Difference

η	Treatment efficiency
κ	Entrainment coefficient
λ	Eigenvalue of matrix
μ	Dynamic viscosity
ν	Kinematic viscosity
ϕ	Flow allocation ratio
ρ	Density
ρ_0	Water density at 1 atm
Σ	Sum
τ	Dimensionless time, $Qt/V_{[i][j]}$
ζ	Pressure loss coefficient

Superscripts

t	Time

Subscripts

0	Initial value
$[i][j]$	Compartment notation
h	Horizontal
i	Compartment notation
j	Layer notation
l	Lower
m	Middle
n	Nozzle
p	Plume
RMS	Root mean square
t	Tank
u	Upper
v	Vertical

Chapter 1

Introduction

1.1 Research background and objective

Flow-through dilution of ballast water is a currently recommended and widely employed offshore method for controlling the introduction of NIS (non-indigenous species) by ships (Murphy et al., 2004). The IMO (International Maritime Organization, 2004) introduces specific legislation to reduce the potential for NIS being transported globally by ballast tanks. For ships employing the pumping-through method, Regulation D-1 of the 2004 Ballast Water Management (BWM) Convention requires that pumping open-ocean water into a full ballast tank should achieve a volumetric flushing efficiency ($\bar{C}$, defined as the fraction of the incoming water volume over the total water volume) of 95% and be carried out at least 200 nautical miles away from the mainland. The IMO requirements have put forward many technical challenges to ship design (Chen et al., 2013).

How to effectively improve ballast water flushing efficiency has become a meaningful scientific question. This study will approach this problem from the viewpoint of fluid mechanics by providing general principles to estimate, analyse and possibly improve the NIS removal in ballast tank water for current/future management systems. The purpose of this study is to

1. understand the compartmental and global flow features in a ballast tank, and analyse the fundamentals of fluids spreading in and transporting around it;

2. analyse the factors that influence ballast tank flushing efficiency, and investigate the effect of tank geometry, outlet setting, inflow rate and density contrast;

3. analyse the flushing from practical ballast tanks on satisfying the IMO standards, and provide management strategy of ballast water systems, involving structure optimization, and pumping rate control and valve setting.

1.2 Thesis structure

This research thesis has the following structure: Chapter 2 explores the literature on typical ballast tank structure, current ballast water treatment technology and exchange. To quantify how the flushing efficiency depends on ballast tank geometry, outlet arrangements and exchange volumes, multizone models of fluid flows and mass transfer are developed in multiply-connected chambers under unstratified conditions, and applied to a 2×2 tank in Chapter 3. The models are validated against a laboratory experimental study. In Chapter 4, the experimental methodology is described, including the experimental design considerations, experimental apparatus, image processing principle, analytical and diagnostic tools. In Chapter 5, the unstratified flushing from three homogeneous networks (2×2, 3×3 and 5×4 tanks) is analysed by comparing experimental measurements with model predictions, and the model is applied to identical configurations. In Chapter 6, the unstratified flushing is analysed by testing the hole resistance and compartment capacitance in a 2×2 tank, and then the model is applied to more complex inhomogeneous configurations. In Chapter 7, the model is extended to analyse the flushing when density effects exist in a linear network. The theoretical predictions are compared with the experimental measurements in a 1×7 linear tank. In Chapter 8, the stratified flushing is further analysed in 2×2 and 5×4 tanks. In Chapter 9, the mathematical models are applied to typical practical ballast tanks to analyse the influence of tank geometry on the flushing. In Chapter 10, the influencing factors of ballast tank flushing are summarised, the implications for ship design and operation of ballast water management system within IMO protocols are provided and possible research topics for the future

are indicated.

Chapter 2

Literature Review

2.1 Introduction

Shipping is the dominant mode of the world's trade transport with an estimated fraction of 90% by volume and 60% by value (UNEP, ITC and ICTSD, 2012). For the safe operation of ships, ballast is needed to ensure stability, trim, bridge visibility and structural integrity by maintaining shear stresses and bending moments within acceptable limits. The ballast on most ships is usually achieved using water, which is taken on board a ship in specially designed tanks located along the length of ships. Shipping transfers approximately 3 to 5 billion tonnes of ballast water globally every year, and a similar volume may also be transferred domestically within countries and regions annually (Partnerships, 2012). Ballast water capacity varies as a function of cargo carrying capacity and vessel type. Ships usually discharge ballast water in ports while loading and take up ballast water in destination ports while unloading, where water is shallow and rich in aquatic organisms, shown in Figure 2.1. Typically, ballast is taken up from submergent ports but discharged over board. In some cases, but in much smaller amounts they take ballast aboard to adjust trim and draft during journey to suit prevailing sea conditions.

Ballast water enables the transportation of harmful aquatic organisms through out the whole world in much greater rate than any other physical process. For instance, out of the 65 non-indigenous species (NIS) discovered in the Great Lakes basin that

Figure 2.1: Photograph of ballast water discharge from a ship.

are new arrivals to the inland waters of North America, ballast water release introduced 43 species (Rothlisberger and Lodge, 2013). Most marine species carried in ballast water cannot survive the journey, as the ballasting and deballasting cycle and the environment inside ballast tanks can be quite hostile to organism survival. Even for those that do survive a voyage and are discharged, their survival opportunities in the new environmental conditions are further reduced. However, under favourable conditions, a newly introduced species which survives to establish a reproductive population in the new environment may become invasive, out-competing native species and multiplying into pest proportions (Partnerships, 2012), if there are not natural predators to control its population. It is estimated that at least 7000 marine species are transported daily around the world either attached to the hull or entrained within the ballast tanks, comprising anything small enough to pass through the intakes and pumps (Endresen et al., 2004; MacPhee, 2006). There are numerous examples of

serious aquatic bio-invasions around the world and the International Maritime Organization (IMO) has published a list with the 'ten most unwanted' organisms. These species could be bacteria, microbes, as well as small invertebrates, eggs, cysts and larvae. The fact that virtually all marine species have life cycles that include planktonic stages complicates the problem (Partnerships, 2012).

The introduction of non-indigenous species (NIS) into new marine areas, whether through ships' ballast water, attached to ships' hulls or via other means, has been identified as one of the four main threats to the world's oceans, which can damage the biodiversity, cause extremely severe ecological disturbance and economic loss, and threaten public health. Ballast water possesses substances capable of inducing genotoxic effects on plant and animal life (Olorunfemi et al., 2012), and contains bacteria that is a potential risk to human health (Altug et al., 2012). Some invasive unicellular algae can cause harmful algal blooms and produce toxins that build up in food chains. The impacts of NIS are different from other forms of marine pollution, because most are irreversible (Partnerships, 2012).

It has only been in the last two decades (since 1988) that the international community has recognised the causes of NIS. Since then there has been a great deal of effort on the legislative side and on practical methods for managing contaminated ballast water. The International Maritime Organization (IMO) adopted the 'International Convention for the Control and Management of Ships' Ballast Water and Sediments' (BWM Convention) in February 2004 in London. The Convention will be applied 12 months after not less than 30 countries representing 35% of world merchant shipping tonnage ratify it. The aim of the Convention is to prevent, minimise and ultimately eliminate the transfer of the harmful aquatic organisms through the control and management of ship ballast water. Up to 30 September 2014 there were 41 contracting states that contributed 30.25% of the world tonnage (Partnerships, 2012). Countries such as Canada, Brazil, Japan, Australia, New Zealand and USA have adopted their own regulations for the ships entering their waters, including mandatory requirements for ballast water exchange.

Ballast water discharge is a great international environmental challenge. To prevent the transfer of NIS through ballast water, besides disemploying ballast tanks

from ships, there are two approaches to deal with the contaminated ballast water: (1) to perform ballast water exchange with mid ocean water; (2) to treat the ballast water itself. The first is still the most effective practical method and is based on the fact that deep mid ocean water contains few organisms and those taken from the coastal or fresh water environment will not survive. The related BWM regulation B-4 Ballast Water Exchange mandates all ships whenever possible to conduct ballast water exchange at least 200 nautical miles from the nearest land and in water at least 200 meters deep. Under circumstances where this is not possible the ballast water exchange should take place as far from the nearest land as possible and in all cases at least 50 nautical miles from the nearest land and in water at least 200 metres in depth.

Technologies and methods have been tested for many years. Most of them have the basis in well known municipal and industrial water and wastewater applications but major barriers still exist in scaling them up to deal effectively with the huge quantities of ballast water carried by large ships (e.g. about 60,000 tonnes of ballast water on a 200,000 tonnes DWT (Dead-Weight-Tonnage) bulk carrier). The main treatment options are (a) mechanical, such as filtration and separation, (b) physical, such as ultra-violet (UV) light, sterilisation by ozone, electric currents and heat treatment and (c) chemical treatment such as adding biocides to ballast water to kill organisms.

The original intention of the Ballast Water Convention was that the water exchange technique would be a short term solution and be replaced by water treatment. When the Convention was written no ballast water treatment plants were in production. Their development has been slower than expected due to various reasons including an underestimation of the technical challenges, insufficient resources and market economics (see King et al., 2012). The magnitude of the logistical effort required for effective enforcement and regulation of various aspects of the Convention have also been identified as potential barriers to implementation (see Wright, 2012). These are some of the reasons why the Convention is still not ratified even though some of its initial deadlines for implementation have already passed. The situation is complex but the outcome is that ballast water exchange is still in widespread use and will continue to be so for quite some time. Moreover some authorities are now insisting

on a combination of ballast water exchange and treatment. It is also becoming clear that a much more detailed understanding of the flow behaviour within ballast tanks is required for compliance assessment and enforcement once ballast water treatment is introduced.

The efficiency of current and future technologies for cleaning ballast water depends partly or wholly on the transport and mixing that occurs within a ballast tank. Previous reviews have mainly focused on legislation/compliance (Gollasch et al., 2007) or treatment technologies (Goncalves and Gagnon, 2012; Tsolaki and Diamadopoulos, 2010). Gollasch et al. (2007) reviewed the IMO international convention and guidelines on ballast water management from perspectives of biological, shipping and regulatory concerns. Drillet et al. (2013) reviewed some of the effects of temperature on plankton organisms as well as on the efficacy of chemical treatment of ballast water. Heyer et al. (2013) reviewed structural properties of ship ballast tanks, including predominant environmental conditions. In this chapter, a state of the art review on ballast tank system and studies on ballast water exchange is conducted, which not only reviews research in the whole ballast system, but also extracts information from the viewpoint of fluid mechanics. It includes an overview of necessity of ballast water management, ballast tank structure, ballast water and NIS, IMO regulations, ballast water exchange and modelling approaches, which provides a comprehensive understanding of the characteristics of ballast water exchange system, as well as guidance on the research methodologies.

2.2 Ballast tank system

2.2.1 Structure of ballast tanks

Ballast water is carried in purpose built tanks whose location and size depend on vessel type and shipbuilder. Dry bulk carriers, tankers and liquefied natural gas (LNG) carriers require large amount of ballast water, primarily for journeys when the ship is unloaded. Bulk carriers and tankers account for 39% and 37% of the global ballast water transported annually. Container ships, ferries, general cargo ships, passenger

ships, roll-on roll-off (Ro-Ro) ferries, fishing ships and military ships require much smaller amounts of ballast water (the remaining 24% of global transport) in almost all loading conditions to control stability, trim and heel.

The ship ballast water system is mainly comprised of ballast water pump, ballast water pipe and ballast tank. Located between the outer and inner hulls, one ballast tank at the centre or several tanks on either side can be provided in a ship's lowermost region and below the machinery room to hold ballast water. Ballast tank designs are currently driven entirely by structural considerations of the vessel, customised for maximum cargo capacity and practicality of human access and construction. The number of ballast tanks depends on the ship's size, design, and requirement, the size depends on ship's type, function and tonnage, and the volume should normally be 30-50% of the total cargo hold volume in a ship. For instance, when the cargo hold is 15,000 m^3, the typical volume of the ballast tank is around 5,000 m^3. Ballast capacities range from single cubic meters for sailing boats up to 200,000 m^3 for large cargo carriers, and inner surface areas are classically in the range of 1.57 million m^2 (Heyer et al., 2013).

Ballast tanks are structurally complex and composed of interconnected bays, longitudinal and transverse stringers/stiffeners to improve the strength of the vessel. To reduce weight these tanks have lightening holes cut into them. The usual layout of ballast tanks on a bulk carrier consists of the tanks located at the fore peak, aft peak, upper/topside wing, lower/hopper wing and bottom. The double bottom tank and hopper tank are unified and in some cases are connected with the upper wing/topside tanks by a trunk that allows the ballast water to flow between them. The dimension of a typical double bottom and hopper ballast tank in a bulk carrier is shown in Figure 2.2(a), and the structure of a typical double hull ballast tank of a cargo vessel is shown in Figure 2.2(b).

Figure 2.2(c) is a physical representation of a hopper side and upper wing ballast tank from a typical 35,000 dwt handy-size bulk carrier, including a total of three rows by ten columns of double bottom tanks, hopper side tanks, and topside tank bays. Inside the tank, individual compartments are generated by crossing longitudinal and transverse stiffeners and frames with lightening holes. The neighbouring

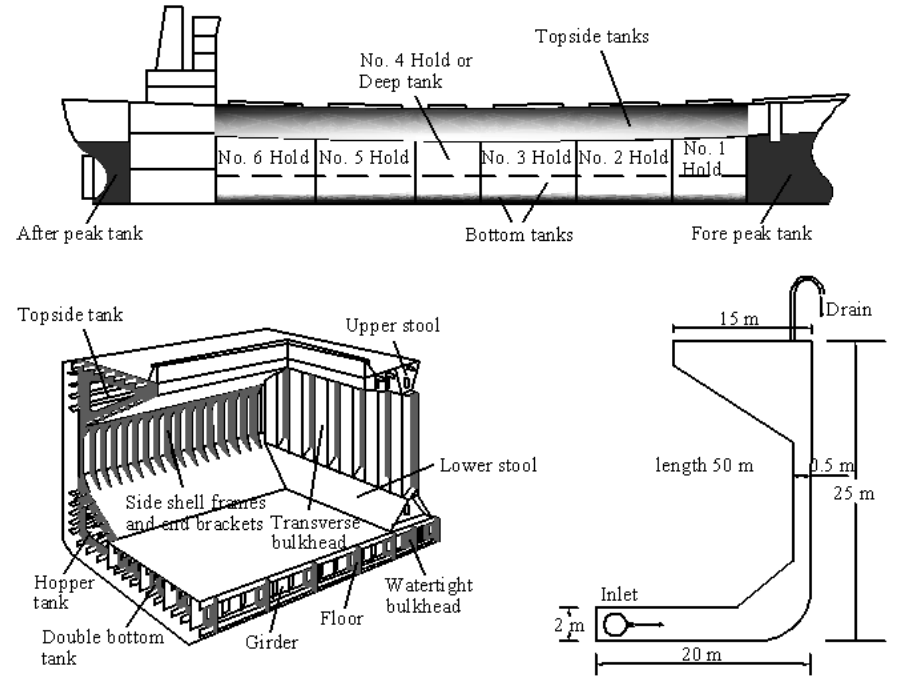
Topside tanks
No. 4 Hold or
Deep tank
No. 6 Hold
No. 5 Hold
No. 3 Hold
No. 2 Hold
No. 1
Hold
After peak tank
Bottom tanks
Fore peak tank
Topside tank
Upper stool
Lower stool
Side shell frames
and end brackets
Transverse
bulkhead
Hopper
tank
Double bottom
tank
Girder
Floor
Watertight
bulkhead
15 m
Drain
length 50 m
0.5 m
25 m
Inlet
2 m
20 m

(a)

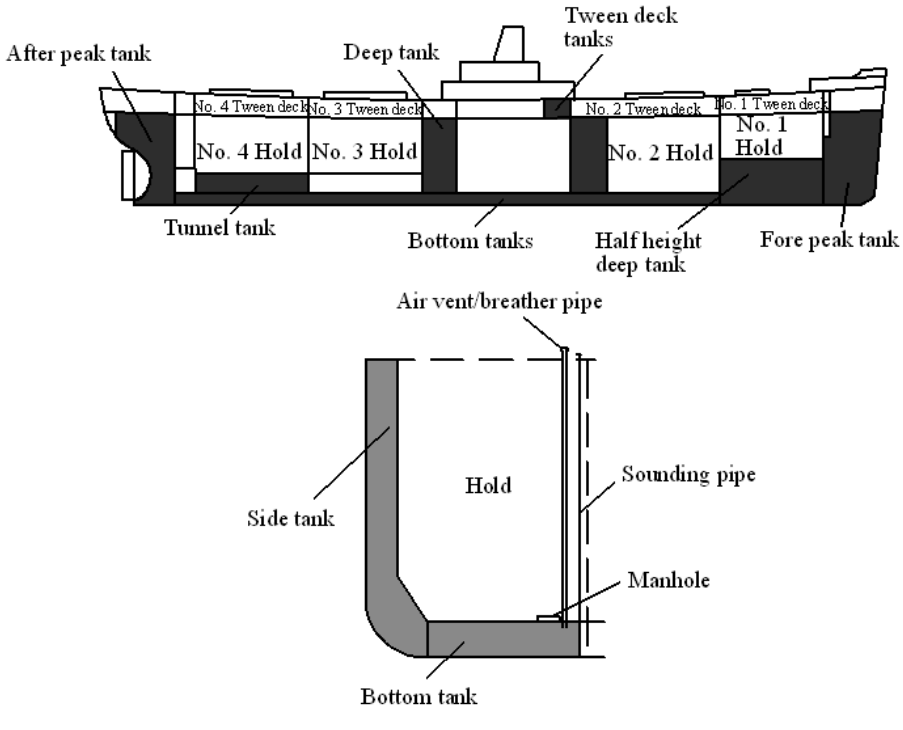
After peak tank
Deep tank
Tween deck
tanks
No. 4 Tween deck
No. 3 Tween deck
No. 2 Tween deck
No. 1 Tween deck
No. 4 Hold
No. 3 Hold
No. 2 Hold
No. 1
Hold
Tunnel tank
Bottom tanks
Half height
deep tank
Fore peak tank
Air vent/breather pipe
Hold
Sounding pipe
Side tank
Manhole
Bottom tank

(b)

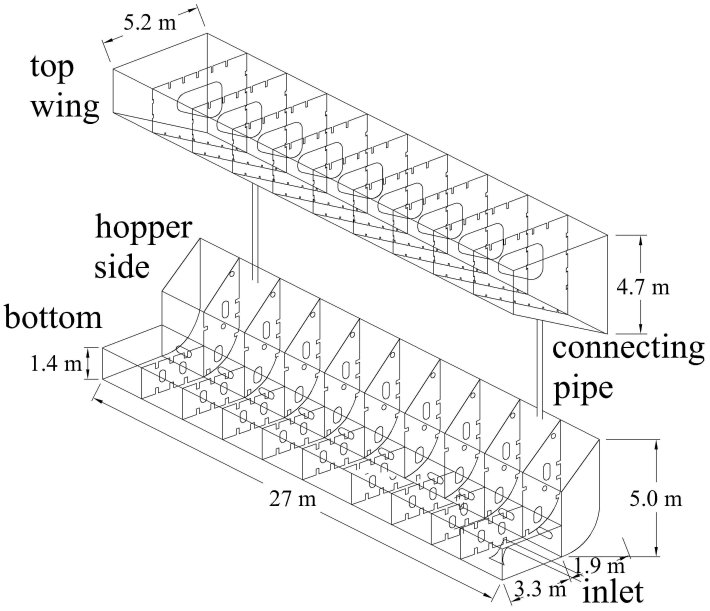
5.2 m
top
wing
hopper
side
bottom
1.4 m
4.7 m
connecting
pipe
27 m
5.0 m
1.9 m
3.3 m
inlet

(c)

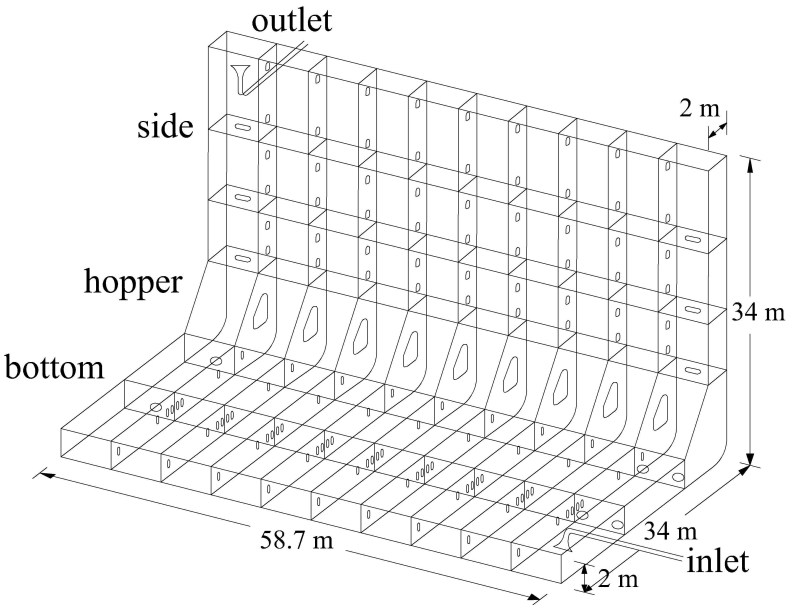
outlet
side
2 m
hopper
34 m
bottom
58.7 m
34 m
inlet
2 m

(d)

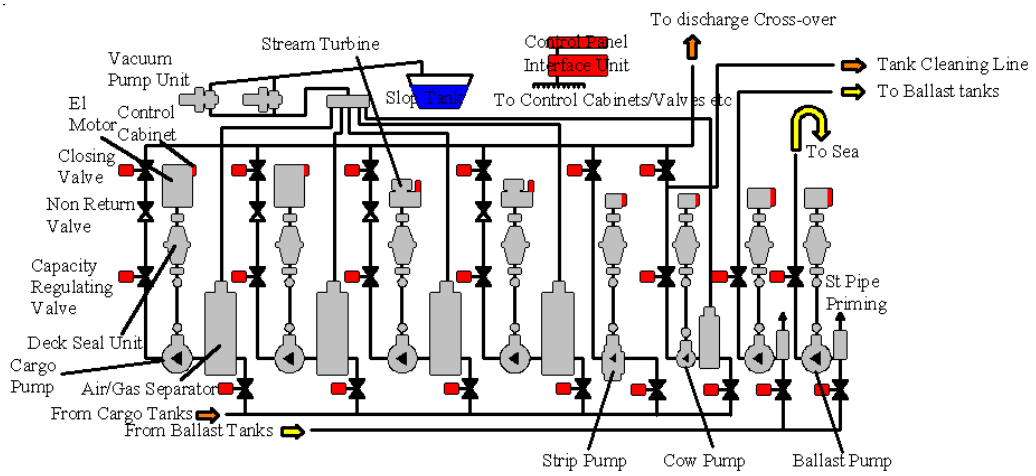

(e)

Figure 2.2: Schematics of ballast tank structure showing (a) a ballast tank typical of a bulk carrier (redrawn from Eames et al. (2008); Sutton et al. (1998); Wilson et al. (2006)), (b) a ballast tank typical of a cargo vessel (redrawn from Sutton et al. (1998)), (c) a double bottom and hopper ballast tank with internal structure (redrawn from Chang III et al. (2009)), (d) a double hull tank with internal structure (redrawn from American Bureau of Shipping (2004)) and (e) a typical cargo/ballast pumping system (redrawn from Hamworthy (2012)).

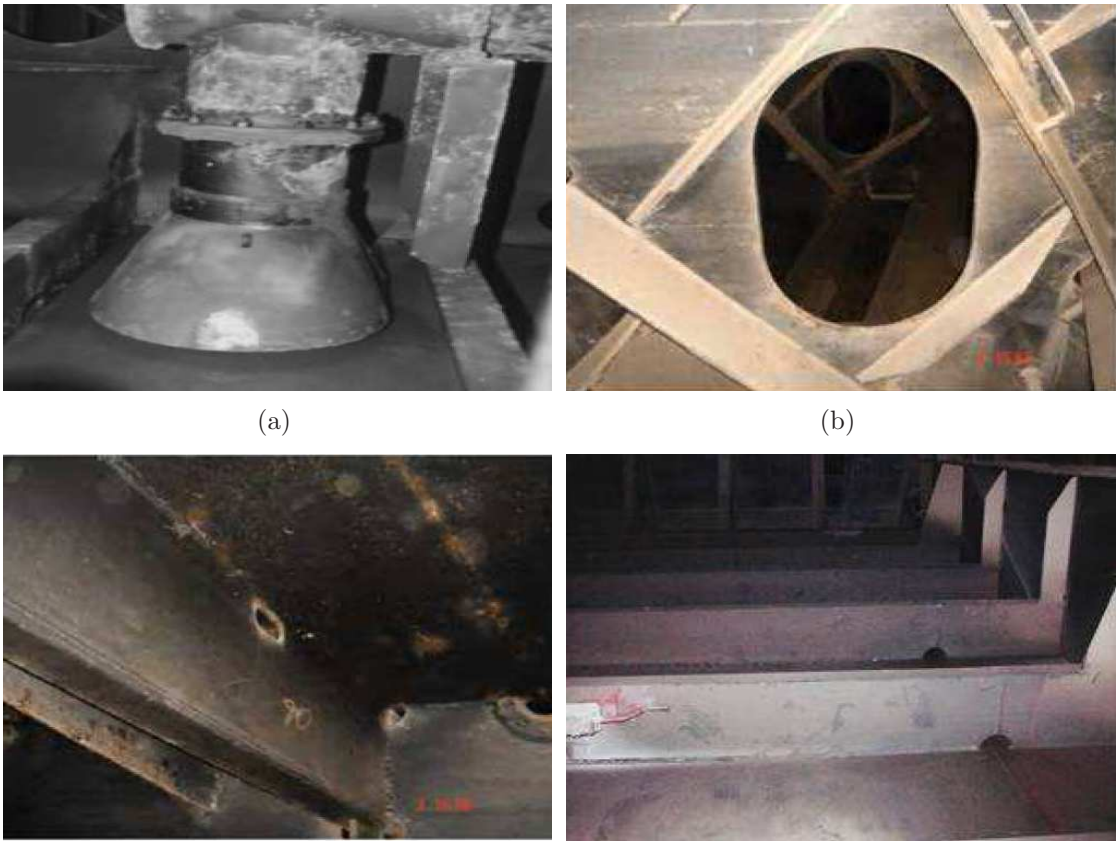

(a) (b)

(c) (d)

Figure 2.3: Photographs of the interior geometry of a ballast tank showing (a) an inlet nozzle, (b) a lightening hole, (c) top limber holes, and (d) stringers with lower limber holes (taken from Steinhauer (2007)).

compartments are associated with lightening holes, stringers and limber holes, shown in Figure 2.3. The hopper tank bays are connected to the topside tank bays via two connection pipes of typically 0.15-0.2 m in diameter. The ballast tank flushing is achieved either from the inlet by the sequential (empty/refill) method or through overflow arrangements by the flushing-through method. For the flushing-through method, the incoming fluid is pumped into the tank via a single inlet bell-mouth, and exits to the deck or side under an overflow condition from the top of the two compartments directly above the two connection pipes.

Figure 2.2(d) shows the geometry of a 'J'-type bottom and side ballast tank with a volume of 14,267 m^3, which is 58.7 m long, 34 m wide and 34 m high. There are 9 transverse frames with 5.87 m spacing between the transverse bulkheads, and 14 ballast vent holes of 0.8 m by 0.6 m on each frame. The polygon manhole adjacent to the turn of the bilge has an area of 7.52 m^2. Three stringers are located at 9.6 m, 16.6 m and 24.6 m above the base line, respectively. On each stringer, there are 2 access holes of 0.75 m by 1.8 m, one located at the aft end and the other at the forward end. Between transverse frames on each stringer, there are 4 drain holes of 0.12 m by 0.24 m with 1.468 m of spacing at the sides of the longitudinal inner skin bulkhead and side shell plating. There is a side girder located 13 m off the centreline, and another side girder under the longitudinal bulkhead located 25.35 m off the centreline. On each side girder, there is an access manhole of 1.2 m by 0.8 m at the aft end and two of 1 m by 0.8 m at the forward end.

The ship's ballast pumping system is located at the lowermost region of the machinery room and below the seawater line to supply necessary suction head for the ballast pumps. Ballast water can be alternately pumped into or out of ballast tanks through openings, which are connected to a ballast system through the pump and piping system. Dedicated high capacity ballast pumps are provided for the ballasting process to pump seawater in vertical or horizontal orientations, and non-return valves are set in the pipelines near the openings for safety. A pipe running under the bench connect the forward and aft tanks and a complicated system of valves controls at each pump (Hamworthy, 2012) (see Figure 2.2(e)).

To put the work into context, two components need to be appreciated in ballast

tanks. The first is the composition of the water, and the second is the material in the water, which can include non-indigenous species (NIS), biological matter and sediment.

2.2.2 Characteristics of ballast water

Ballast tanks are charged near or in seaports, so the constituent properties of the ballast water, such as density depends on seawater density distribution. The distributions of worldwide sea surface salinity and temperature are shown in Figures 2.4(a,b), and the relationship between water density and salinity as well as temperature is shown in Figure 2.4(c) (Millero and Poissont, 1981). The density of sea surface water depends on its salinity and temperature, through the relationship $\partial\rho/\partial Sa < 0$ and $\partial\rho/\partial Te > 0$, where ρ is the density, Sa is the salinity, and Te is the temperature.

Temperature in the sea surface layers depends on sun radiation, absorption, evaporation, rainfall and heat exchange with the atmosphere, varying in the range from 2 to 28℃; seawater contains NaCl, with a salinity ranging between 3.3% and 3.8%, and a neutral pH between 7.5 and 8.3 (Heyer et al., 2013).

2.2.3 Characteristics of NIS

Ballast water will contain anything that is small enough to pass through ships' ballast water intake ports and pumps. The NIS that can be drawn into a ballast tank range from bacteria (Burkholder et al., 2007; Rivera et al., 2012) and other microbes (Ruiz et al., 2000), the adult and larval stages of the many marine and coastal plants and animals (Baek et al., 2012; DiBacco et al., 2012; Mills et al., 1993), such as algae (Flöder and Kilroy, 2009; Hallegraeff and Bolch, 1992), mussels (Orlova et al., 2005; Therriault et al., 2005), clams (de Oliveira et al., 2006), fish eggs, crabs (Dittel and Epifanio, 2009; Rudnick et al., 2003; See and Feist, 2009; Yamada and Kosro, 2009) and fish (see Wonham et al., 2005).

The most infamous example is the zebra mussel (*Dreissena polymorpha*), native to the Black sea and the Caspian Sea region of Asia but introduced via ballast water to eastern half of North America, especially the Great Lakes. It fouls all available

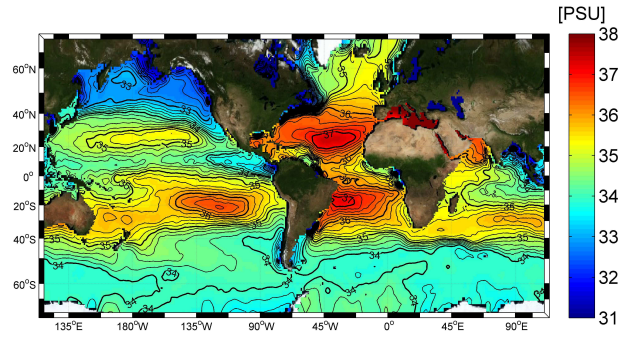

(a)

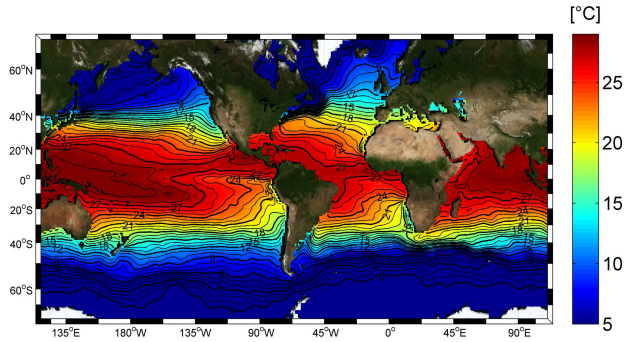

(b)

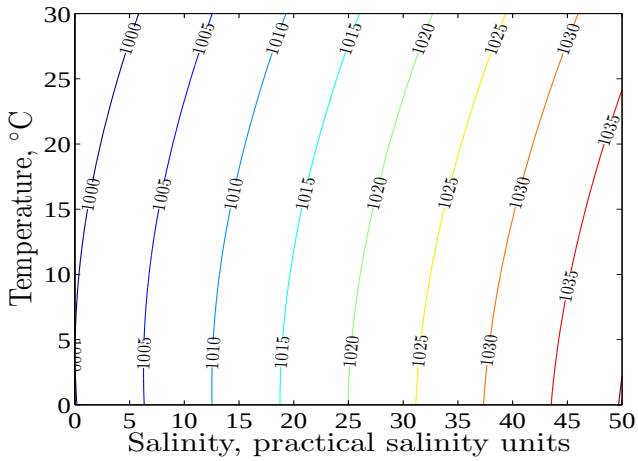

(c)

Figure 2.4: Schematics of sea surface salinity, temperature and density. (a) shows worldwide sea surface salinity (CATDS Ocean Salinity Expert Center, 2013), practical salinity units, (b) shows worldwide sea surface temperature (CATDS Ocean Salinity Expert Center, 2013), ℃ and (c) shows relationship between density and the above two factors, kg/m^3.

hard surfaces causing severe problems on infrastructure and vessels by blocking water intake pipes, sluices and irrigation ditches. It displaces native aquatic species altering the ecosystems of the Great Lakes by reducing phytoplankton, the foundation of the local food chain. Approximately $ 1 billion has been spent in the USA between 1989 and 2000 to remediate the damages (Endresen et al., 2004; Pimentel et al., 2000). The Chinese mitten crab (*Eriocheir sinensis*), native to northern Asia and introduced to Western Europe, Baltic Sea and the west coast of North America is also a classic example of invasive species. It experiences mass migrations for reproductive purposes and competition with native fishes and invertebrate species has led to the local extinction of some species. Additionally the mitten crab burrows into riverbanks and dykes causing erosion and siltation, and damages the fishing communities directly by destroying their nets and catches. Some cholera epidemics appear to be associated with ballast water as well. In 1991, a cholera epidemic started simultaneously in three separate ports in Peru, swept across South America affecting more than a million people and killed more than ten thousand by 1994. Consumption of contaminated shellfish from non-indigenous toxic algae, by humans has also been associated with severe illness and deaths. The European green crab, native of freshwater and estuarine habitats along the east coast of Asia, has a life cycle of around one year, including egg, larvae and adult stages. It is typically 30-100 mm in width, and its typical population density is about 5 individuals per square meter. Dinoflagellates, typical microscopic algae, are widely dispersed all over the world, and their concentrations can become quite high when they bloom. They are often no larger than 2 mm in diameter, and have a life span from a few days to several weeks. Mussels (for instance, zebra mussel and quagga mussel), have a life span of up to 5 years, which includes egg, juvenile and adult stages. Their sizes are from microscopic to about 50 mm long, and their population density may reach thousands of individuals per square meter. Zebra mussels at the pre-juvenile stage may attach to the ship's hull and then increase their removal difficulty. Burkholder et al. (2007) sampled from 9 ports on the west coast and 4 ports on the east coast of USA, and observed that the bio-loading is extremely variable, for instance, phytoplankton concentration had a mean of 3.2×10^4 viable cells/m^3; median, 7.9×10^3 cells/m^3. The loading was dominated by chain-forming

diatoms and dinoflagellates, and viable organisms comprised about half of the total cells.

The settling or swimming velocity of NIS, ranges from 0.1 to 150 mm/s (see Magill et al., 2006; Wong and Piedrahita, 2000). Many NIS has a small body size and a density comparable to water (e.g. bacteria, plankton, fish eggs). Large species, such as macro-algae, can survive and be transported in microscopic forms (Flagella et al., 2007). Some NIS can rise and sink in the water by changing their body density and this makes them hard to be separated from water by gravitational methods. In all, many NIS moves with water inside ballast tanks and can be considered dynamically passive.

2.2.4 Sampling and analysis of ballast water

Ballast water sampling is very important for assessing the risk of biological invasions. Basurko and Mesbahi (2011) proposed that 16% of a ship's ballast water must be sampled to be representative of the whole ballast water discharged. Due to the various dimensions and behaviours of species distributed in the large volume of ballast water, and the differences in ship construction, it is very difficult to provide samples which are representative of the whole discharge of ballast water (Carney et al., 2013). Thus, there is no uniform ballast water sampling methodology currently established worldwide. There are two main sampling types: one was through ballast water sounding pipes with specially designed equipment (in-tank sampling), and the other was at the fire-fighting system (at-discharge sampling) (David and Perkovic, 2004).

Various chemical and biological methods have been applied to analyse ballast water, including Organic matter fluorescence (Murphy et al., 2013), PCR (polymerase chain reaction) (Deagle et al., 2003; Harvey et al., 2009; Patil et al., 2005), NASBA (nucleic acid sequence based amplification) (Fykse et al., 2012), flight mass spectrometry (Emami et al., 2012) and micro-fluid differential resistive pulse sensor (Song et al., 2012). To estimate whether a vessel may discharge ballast water and the quantity of ballast water to be discharged, David et al. (2012) developed a generic assessment model based on the vessel cargo operation and vessel dimensions.

2.3 IMO regulations on ballast water management

Table 2.1: Ballast Water Treatment Performance Standard

Organism category	Regulation of discharge ballast water
Plankton, >50 μm in minimum dimension	<10 cells/m^3
Plankton, 10-50 μm	<10 cells/ml
Toxicogenic *Vibrio cholera* (O1 and O139)	<1 cfu[a]/100 ml
Escherichia coli	<250 cfu[a]/100 ml
Intestinal Enterococci	<100 cfu[a]/100 ml

[a] cfu = colony forming unit.

According to the Ballast Water Exchange Standard, Regulation D-1 of the 2004 Ballast Water Management (BWM) Convention, ships making use of exchange method need to exchange ballast water at least 95% by volume; for ships exchanging ballast water by the pumping-through method, pumping through three times the volume of each ballast tank shall be considered to meet the standard. Pumping through less than three times the volume may be acceptable if the ship can demonstrate that it can remove at least 95% original ballast water by volume. The 95% flushing efficiency requirement should be achieved by the whole ballast tank rather than each single compartment.

Regulation D-2 of the BWM Convention - Ballast Water Treatment Performance Standard requires that the discharged ballast water contain less than 10 viable ≥ 50 μm organisms per m^3 and less than 10 viable 10-50 μm organisms per ml; and discharge of the indicator microbes shall not exceed the specified concentrations, see Table 2.1. Based on Regulation B-3 of the Convention, which is Ballast Water Management for Ships, ships need to satisfy either Regulation D-1 or D-2, depending on both their ballast water capability and their construction year. However, due to technical problems in counting rare organisms and difficulties in assessing smaller non-motile organisms, comprehensive testing for full D-2 compliance will be a complex, time-consuming operation (Wright, 2012). The Marine Environment Protection

Committee adopted the 'Guidelines for ballast water exchange design and construction standards' in 2006, calling for special consideration on the feasibility of combining ballast exchange methods with treatment technologies to meet the standards of Regulation D-2. According to the success criteria for shipboard testing - 2.2.2.5 of IMO Guidelines for approval of ballast water management systems (G8), the viable organism concentration of the ballast water to be treated should exceed 10 times the maximum permitted values in Regulation D-2.1. This indicates an equivalent NIS removal rate of at least 90% for shipboard testing (International Maritime Organization, 2008). The NIS removal rate (R) is defined as $R = (C_0 - C(t))/C_0 \times 100\%$, where C_0 is the original NIS average concentration of the ballast system and $C(t)$ is the NIS average concentration of the system varying with time. R measures the total removal of NIS from the whole system.

2.4 Ballast water exchange

Ballast water exchange is the method of transferring the water from a ship's ballast system to the environment, with a simultaneous or subsequent uptake of water to refill the ballast to reduce the concentration of coastal organisms, which is usually conducted in distant seas, as the mid-oceanic species which will be taken into ballast tanks are considered unlikely to survive in nearshore waters. Ballast water exchange is the prevailing procedures for the time being, although it has drawbacks as follows: (1) sediments and residual water cannot be fully removed from the bottom of ballast tanks; (2) organisms attaching to the sides of ballast tanks or supporting structures in them cannot be easily removed, and residual organisms may be discharged with ballast water into seaports, so the actual risk by the discharge of ballast water in ports remains high (Simard et al., 2011); and (3) it is dangerous to exchange ballast water when it is stormy at sea. There are two reasons to consider the ballast water exchange from viewpoint of fluid mechanics. First, this is the recommended and most widely applied method in ballast water treatment at the moment. It is based on the principle that far from the coast and in deep waters, few types of species will exist. Therefore, ballast water exchange may replace coastal water with open-ocean water

during a sea voyage and reduces the density of potentially invasive coastal organisms and replace them with oceanic organisms with a lower probability of survival in nearshore waters (Tsolaki and Diamadopoulos, 2010). In spite of a large number of ballast water management techniques in development, ballast water exchange in open oceans, as the recommended treatment option, is the only widely used management technique at present (McCluskey et al., 2005). Multiattribute decision analysis of questionnaires for ballast water management measures in the US Great Lakes shows that ballast water exchange proved to be more favoured than filtration/UV and heat (Yang, 2004). Capital and operational costs for ballast water exchange are low because no additional material or operator training is needed. The second reason to consider fluid mechanics is that any continuous treatment process, based on recycling of ballast water through the tank, requires knowledge of the fluid flows.

2.4.1 Ballast water exchange types

There are two approaches of ballast water exchange: sequential exchange (also known as the empty/fill method) and continuous exchange (also known as the flushing-through method and dilution method).

Sequential exchange is a process by which a ballast tank intended for the carriage of ballast water is first emptied and then refilled with replacement ballast water. This method is recognised as being very effective for removing NIS but it is less favoured because it imposes significant loads on the ship's structure due to the mismatch of weight and buoyancy forces along the ship's length. It can also lead to a loss of stability. It is thought that this was the cause of the near capsize of the 55,000 tonne car transporter Cougar Ace off Aleutian Islands in July 2006 (Krüger and Kluwe, 2010).

For continuous exchange, the ballast tank remains full and replacement water is continuously pumped into the tank allowing water to exit through overflow or other arrangements. Figure 2.5(a) shows a schematic of the current open-loop ballast flushing system, where seawater is continuously pumped in to the ballast tank and flush the ballast water out. The fluid mechanics of flushing depends on the tank

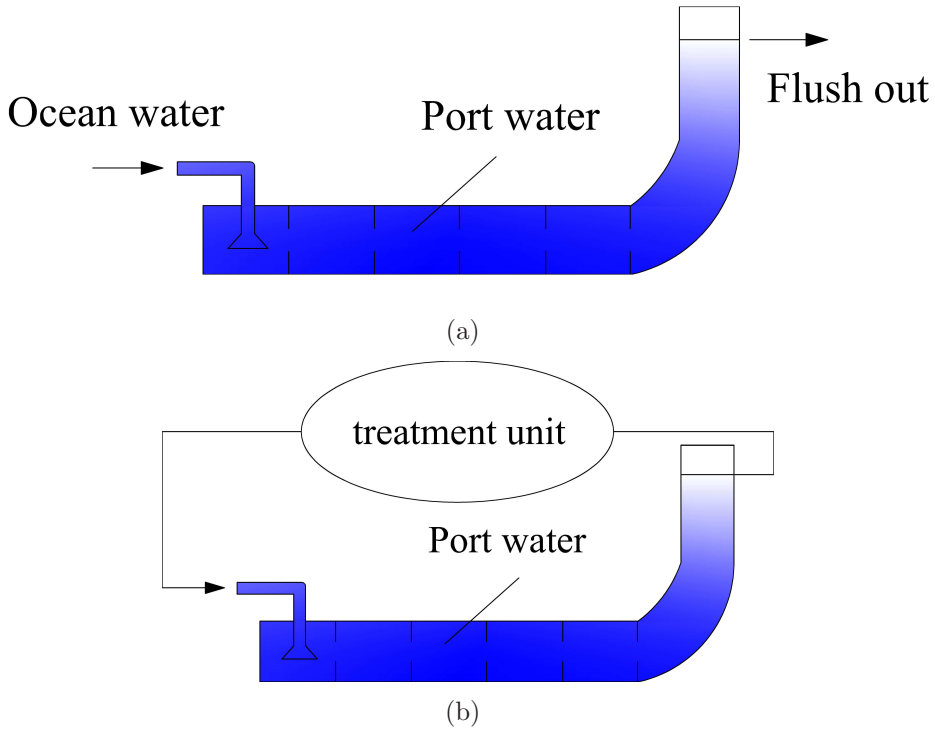

Figure 2.5: Schematics of ballast water management systems. (a) shows the open-loop flushing-through system, while (b) shows the closed-loop system where the outflow is treated and re-injected (Brodie et al., 2003).

geometry and the property of the water injected into the tank as well as the water initially present, largely expressed by the bulk density of the water. This flushing-through method would keep ships safe by making sure that tanks contain water at all times. With the exception of some newly built ships, the world fleet of ships were not designed to accommodate any form of ballast water treatment or flushing. The existing pipework has to be used, through which water has to be pumped into the base of the tanks and allowed to escape from the vent holes and/or access hatches at their top. There are some risks associated with this procedure as the ships were never designed with this process in mind. The procedure is particularly hazardous in winter when ice formation might occur. Pumping through three times the volume of each ballast tank is considered to meet the IMO standard. If perfect mixing takes place a three tank volume exchange will result in 95% of the original fluid being removed. It is recommended by the American Bureau of Shipping (2010) that the inlet and outlet piping connections be located as remotely from each other as practicable; aft and fore peak tanks are required to be provided with additional pipework to improve mixing; the total cross sectional area of the ballast water discharge pipes on the upper deck is not to be less than twice that of the filling/suction pipe; the discharge pipe located closer to the filling/suction pipe is to have a smaller diameter than the other discharge pipe located further away from the filling/suction pipe.

In the future, ships need to employ mechanical, physical, or chemical technologies to treat NIS. Most treatment systems will be a combination of two or more methods essentially to improve the NIS treatment efficiency. The mechanical mechanisms, such as filtration (Parsons, 2003; Parsons and Harkins, 2002; Tang et al., 2006, 2009) and hydrocyclone (Badran and Abu-Khader, 2004; Martínez et al., 2007; Wang and Wang, 2009), can be used as pretreatment to remove NIS from ballast water, the removal rate of which depends on the size or density of the NIS. These techniques also remove debris that is suspended in the water. The physical and chemical methods, including ultraviolet (UV) radiation (Hess-Erga et al., 2008; Mamlook et al., 2007; Wang et al., 2013; Werschkun et al., 2012), ultrasound (Holm et al., 2008), cavitation (Helu, 2005), plasma (Sun et al., 2011), deoxygenation (de Lafontaine and Despatie, 2014; de Lafontaine et al., 2013; Hua and Hwang, 2012; McCollin et al., 2007), electrolysis (Bai

et al., 2007), electrodialysis (Kim and Jang, 2009), electrochlorination (Añasco et al., 2008), ozonation (Juretić et al., 2011), chlorine dioxide (Maranda et al., 2013) and peracetic acid (Alekseev et al., 2010), are aimed at deactivating and terminating any NIS. Numerous research attempts on various ballast water treatment methods result in the conclusion that there is still no scientific opinion on the final choice of methods for wide application on board (Kurtela and Komadina, 2010). No treatment option, however, can totally solve the NIS problem (Perakis and Yang, 2003), because none has been shown to be 100% biologically effective, environmental friendly, economic, safe and practical at the same time (Goncalves and Gagnon, 2012). For ships utilising a physical method, such as UV, ultrasound, cavitation, plasma and electrolysis, a closed-loop system has been suggested by Brodie et al. (2003) to further enhance the ballast water treatment, shown in Figure 2.5(b). This circulating system consists of a treatment unit and a flushing unit, where ballast water is continuously treated and flushed back to the tank. The advantage of this system include accommodating low water qualities, saving power and allowing long treatment time in transit. The NIS removal depends upon both the process of treatment and that of flushing.

2.4.2 Theoretical studies on ballast water exchange

There are comparatively few theoretical studies of the flow within multi-compartment tanks. Computational fluid dynamics (CFD) modelling is useful to understand ballast tank flow and predict the flushing efficiency, but appropriate resolution of tank structure and cell grid densities of CFD have to be allowed for maximum benefit (Chang III et al., 2009). Kent and Parsons (2004) used CFD software (FLUENT) to evaluate the flow-through ballast exchange method for a rectangular double bottom tank, a 'J'-type bottom and side tank, as well as a hopper side and upper wing tank. They found that the performance of the flushing exceeded the performance of the prefect mixing mode for the double bottom tank; the single trunk, single-port design gave the best flushing performance for the hopper side/upper wing tank; only the dual-trunk, single-port design exceeded the perfect mixing assumption for the hopper side/upper wing tank. The most extensive study to-date of flow within ballast tanks

was imitated by Wilson et al. (2006) and Chang III et al. (2009), who developed a computational model to investigate the impact of ballast tank structure by comparing the case of a tank with and without stringers. The former case which is the more complex case and also more realistic was shown by CFD modelling to produce more effective mixing. When density contrast between the incoming seawater and the original freshwater was relatively large, the predicted flushing efficiency did not meet the required 95% replacement after three tank volumes exchange for the simulated tank geometry, due to trappage in the tank tops. The CFD model for a 1/3-scale double bottom tank and a full-scale ballast tank from a typical bulk carrier predicted the experimental saltwater effluent volume fraction and mixedness data within the tank. The significant finding in this study was that the perfect mixing assumption for the whole tank was challenged for the real ship tank geometry and that redesign for ballast tanks and pumping systems would advance the effectiveness of ballast water exchange. The introduction of stringers encouraged plug flow where it might be expected that a more complex internal geometry would enhance mixing. Also, they inferred that the addition of vent holes in the tank tops would allow for some movement of the trapped fluid. The main difficulty is to find appropriate resolution of tank structure and CFD cell grid densities.

Armstrong (1997) considered the effect of improving the flow within ballast tanks by modifying internal distribution pipework. If pumps are installed above the bottom of ballast tanks, residual water and sediments may be got rid of, and thus the risk of introduction of NIS will be reduced. The bottom of ballast tanks could also be redesigned to be sloping to drain residual water and sediments into a pump. For sequential exchange, Chen et al. (2010a) used a non-dominated sorting genetic algorithm to optimise the ship's subdivision arrangement. To design an optimal integral sequential plan that requires the minimum of a ship's structural strength and keeps the ship at an optimum gesture at sea, Chen et al. (2010b) combined a mathematical model of symmetrical multi-tank strategy with a specially designed multi-objective genetic algorithm (MOGA); Chen et al. (2010c) combined a mathematical model of diagonal one-tank strategy with a specially designed MOGA; Chen et al. (2013) proposed a heuristic exchanging strategy for ships with very small design margins.

2.4.3 Experimental studies on ballast water exchange

Meanwhile, there are few experimental studies of the flow and flushing in ballast tanks, most researchers have concentrated on conducted macro-scale trials using dyes, salinity, and sampling of the marine life at points within a real ballast tank. The original work was conducted for the Australian Department of Agriculture, Fisheries and Forestry in 1993. Their results indicated that the problem was more complex than assuming a simple homogeneous mixing, the proportion of the surviving NIS did not match the proportion of original water remaining, and that the removal rate of NIS was not consistent across the range of species measured, suggesting that size and hence mixing regime are also important. Drake et al. (2002) sampled the microbial community in exchanged and unexchanged ballast-water holds onboard a commercial bulk carrier during a transoceanic voyage, and results indicated that all microbial metrics tested had decreased 1.6% to 34% from initial values five days following the exchange process. Due to the highly variable virus abundance in ballast tanks, the water exchange needs consideration of the dynamics of specific viruses in future studies (Leichsenring and Lawrence, 2011). Reported experimental studies on ballast water exchange are shown in Figure 2.6 according to the typical Re and Ri in the tested tank. For field measurement, at three volumes flushing, the ballast water exchange efficiency is 99% for commercial oil tankers (Ruiz et al., 2005), 95% for bulk carrier (Rigby and Hallegraeff, 1994) and 87% for container ships (Ruiz and Reid, 2007). Kamada et al. (2004) used a 2D 1 m square tank model and measured the dilution rate of the inside fluid with an optical method, analysed the motion of inside fluid of tank by a numerical calculation method, compared with the experiment results, and confirmed that the flushing-through method can dilute about 95% when volume of three times the capacity of the model tank has entered a single compartment tank and overflowed. Wilson et al. (2006) tested a 1/3-scale double bottom tank, and the flushing efficiency at once volume exchange agreed with the numerical calculation result. When density contrast was large and inflow rate was low, there was still mostly unmixed original fluid trapped between the stringers near the tank tops after three volume exchanges. They found that decreasing the density contrast and increasing the inflow rate may improve mixing within the tank. Eames et al. (2008) looked at the

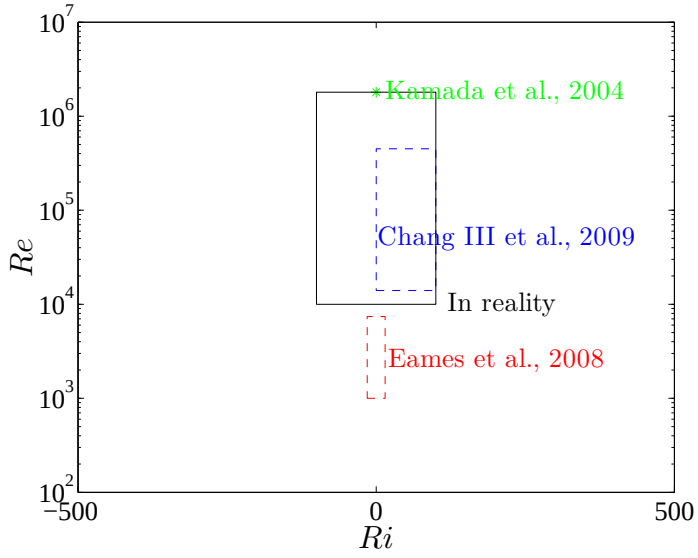

Figure 2.6: Reported experimental studies on ballast water exchange according to the typical Re and Ri in the tested tank (Chang III et al., 2009; Eames et al., 2008; Kamada et al., 2004).

density effect with moderate Re, limited parameter region and identical geometry by studying the flushing of a 'J'-type ballast tank using simplified mixing models, which in some sense gave a general insight into the dominant physical processes from planar tanks. In the absence of density contrast between the ballast water and that used to flush the tank, the high aspect ratio of tank geometry (along the base and the vertical sections), meant that a bulk Péclet number (based on a turbulent diffusivity) was high (>100) so that the transport out of the tank was largely through displacement.

2.5 Studies on the multizone flow models

Multizone flow models, also know as flow network models, are an alternative to CFD models for investigating heat and pollutant transport in multi-room structure, for the computing cost of the multizone models is much lower than CFD as it takes only a few minutes to conduct an hour-by-hour dynamic simulation of a whole building (Wang and Chen, 2007a,b). These models simplify the behaviour of spatially distributed

physical systems into a topological network where nodes represent rooms/spaces and the connectors represent pathways. The system enables the average flow and mass transfer rate between different rooms based on the mass conservation and energy balance equations to approximate how materials or energies are transmitted among the compartments of the multibody fluid delivery system by assuming each room homogeneous (see Chang et al., 2003). The multizone models are powerful to predict air exchange rate and ventilation efficiency in an entire building (Chen, 2009; Chen et al., 2010d).

2.5.1 Studies on the fluid flow and pressure loss

Many studies have focussed on the fluid flow between rooms or boxes (Engdahl, 1999; Hirano et al., 2006; Montazeri et al., 2010). Within each room, the fluid flow is conserved, i.e. the amount of the flow that enters a room is equivalent to that leaves the room (Haghighat, 1989). In the context of the ventilation literature, researchers dealt with an algebraic set of equations detailing the flux between rooms/windows with empirical closures for the pressure drop coefficients characterising the flow between spaces (Cao et al., 2011). At the steady state, the relationship between the flow rate through a hole and the pressure difference between neighbouring rooms can be obtained from the Bernoulli equation. The pressure loss through a hole is resulted from the friction caused by the hole edge that also changes the area of flow. Most studies of the multi-zone models used the following equation to relate the pressure difference to the flow rate (Linden, 1999)

$$\Delta p = \frac{1}{2}\zeta \rho u^2, \tag{2.1}$$

where Δp is the pressure difference between neighbouring rooms, ζ is the pressure loss coefficient, ρ is the fluid density and u is the average velocity. Chu et al. (2009) tested a wind tunnel, and found that the discharge coefficient is a function of Reynolds number and airflow direction, but independent of external turbulence intensity and wall porosity. Chu et al. (2010) investigated wind-driven cross ventilation in partitioned buildings by wind tunnel experiments, and found that the pressure loss coefficient

is dependent on the porosity, but independent of the configuration and location of the holes. Yang et al. (2005) and Chu and Wang (2009) used an empirical closure to estimate the pressure coefficient by the ratio of area of the hole to the area of the wall. Ye et al. (2009) related the pressure coefficient to the ratio of diameter of the hole to the diameter of the pipe.

2.5.2 Studies on the mass transfer

The multizone models are based on the assumption that the whole space can be considered as a set of well-mixed regions or zones of homogeneous composition (Sandberg, 1984). This assumption can be acceptable when the openings between regions or zones are relatively small, as compared to the size of the regions or zones (Mora et al., 2003). Eames et al. (2009) examined the transient concentration of a continuous source of passive dye that was injected into an acrylic model, and validated the perfect mixing assumption in a single room.

The equation describing the mass transfer in a multizone region was first proposed by Sinden (1978) to calculate the time evolution of the spread of the tracer gas concentration from known flow rates. Initially a known concentration of tracer gas uniformly exists in each zone, and no tracer gas is generated in the system after time zero. The incoming air is assumed to be instantaneously and uniformly diffused to a zone. The time evolution of the concentration of the tracer gas in zone i is based on the mass conservation as

$$V_i \frac{\mathrm{d}C_i}{\mathrm{d}t} = \sum Q_{i,\mathrm{in}} C_{i,\mathrm{in}} - \sum Q_{i,\mathrm{out}} C_i, \tag{2.2}$$

where V_i is volume of zone i, t is time, C_i is the concentration of the tracer gas in zone i, $C_{i,\mathrm{in}}$ is the concentration in the zone(s) which flows into zone i, $Q_{i,\mathrm{in}}$ and $Q_{i,\mathrm{out}}$ are the inflow rate and outflow rate of zone i, respectively. Waters and Simons (1987) examined the solutions to the equation array for the distribution of tracer gas in each zone in the matrix form.

The multizone models are widely applied to building ventilation (Chu et al., 2009; Zhao et al., 2003) and cardiovascular system (Violon, 2012). When the internal airflow

is studied, the building is commonly represented as a number of interconnected perfect mixing rooms. Sandberg (1984) added a time-dependent source term to the mass transfer equation to represent the release of a contaminant. The assumptions of the model include

1. the contaminants are dynamically passive, i.e. they follow the air movements in the room;

2. the contaminants are conserved, i.e. the amount of the contaminants that enter the system is equivalent to that leave the system;

3. the physical quantities of each room such as flow velocity, pressure and concentration are mean values.

2.5.3 Studies on the stratified flow

There are a few studies on the stratified flow in in-line space. Gladstone et al. (1998) combined the displacement ventilation with the hydraulic air exchange through a hole into another room, and developed a model to show how the interface varies as a function of time. Lin and Linden (2002) extended a single-room displacement ventilation model based on plume theory to a space consisting of two equal-height chambers connected by a top hole and a bottom hole on the vertical dividing wall. The flow between the two chambers were driven by a single source of buoyancy in one of the chambers. They tested the variation of interface height and density with time and the vertical distribution of density. Further experimental tests have been done on similar configurations, e.g. two chambers connected by a top hole and a middle hole (Tovar et al., 2009), or two rooms with a buoyancy source located in the ceiling of the first room and an unforced vent opened in the ceiling of the other room (Tovar et al., 2007).

2.6 Summary

This chapter has given an overview of the characteristics of ballast tank, ballast water and the NIS, the exchange technology and the feasible and potential treatment technologies in mitigating the NIS. The current legislation deals with the number of exchange volumes that are required to achieve a level of flushing. Although continuous flushing mode may be disbanded in the future, for all but the largest ships, some of the new treatment technologies which will be employed will use circulated flushing to treat ballast water while the ship is in transit.

It is necessary to examine the influencing factors on ballast water flushing. There requires a general insight into the types of flows generated and the efficiency of ballast water flushing, which is affected by fluid conditions. This indicates the importance of ballast tank geometry, flow rate and density contrast between fluids. Eames et al. (2008) pointed out the necessity of new research to build design principles for ballast water tanks (and their associated pumping and pipe systems), and protocols for flushing out NIS. It is important to clarify the site location of inlet and outlet of ballast tank, and to employ a good flushing strategy for ballast water. The review of the ballast tank geometry specifically highlights the complex internal form of the ballast tanks, especially for large tankers, which tend to have multi-compartmental regions. Current approach is to use simple bulk diagnostics (such as the average concentration in the tank) or point measurements of dye concentration. The major problem here is the lack of a methodology for understanding inertial flows in complex interconnected spaces. In order to have an impact on the internal design of ballast tanks to improve the flushing technology, it is necessary to understand how the NIS concentration in each compartment varies with time. For the future closed-loop strategy, knowledge of the distribution of treated ballast water will be useful.

Currently, there is a significant gap in understanding how water that is initially in ballast tanks is exchanged by flushing. First, there is currently no method to describe the flow through multiple regions which are geometrically complex. The available CFD studies are restricted to particular geometries, and are poorly resolved. Secondly, there is currently a lack of diagnostic tools to analyse how NIS spread through these

Table 2.2: Summarisation of methodologies for analysing ballast tank flushing.

Methodologies	Advantages	Disadvantages
Field measurements	Valid	Expensive; Time consuming; Difficult to interpret
CFD	Detailed analysis; Whole field datasets	Difficult to validate; Unclear physical model
Multizone network model	Time saving; Easy to extend	Restricted to simple flows; Restricted validity
Small scale experiments	Inexpensive; Easy to operate	Restricted validity

compartments. Thirdly, there are few experimental studies that involve investigating movement within sufficiently geometrically complex geometries that have a direct bearing on the practical problem. Therefore, available techniques and new tools are needed for analysing the flow, the concentration field and the effects of fluid density contrast on them; moreover, it is necessary to explore how these above subjects are affected by ballast tank geometry.

A number of methodologies can be applied to study the movement of NIS in a ballast tank, including field measurements, CFD (computational fluid dynamics), reduced models and laboratory scale experiments, summarised in Table 2.2. Although field measurements are the most convincing, they tend to be expensive to undertake and restricted to specific types, and therefore cannot provide general guidelines for all kinds of ships. Due to limitations on tank access and sampling equipment, on-board experiments generally rely on measurements taken at the overflow outlet of the tank which do not necessarily represent the volume mixture that remains in the ballast tank (Wilson et al., 2006). CFD can provide detailed results, but the major challenge is grid generation for such complex geometry and grid resolution. There is limited understanding of the vortex shedding flow due to the sharp edge of the lightening holes

between compartments. The flow network model is restricted to simple flows, but time saving and easy to extend. The dimensionless groups characterising laboratory scale tests may not match those of field problems, which may restrict their applicability, but they tend to be easier to operate. In next chapter, a multizone model will be derived to enable the flow through a ballast tank to be understood in terms of average flushing efficiency. The predictive framework is analysed in greater detail against laboratory scale experiments in later chapters.

Chapter 3

Multizone Flow Modelling

3.1 Introduction

From the literature review in Chapter 2, it can be seen that there is a need to quantify the fluid exchange in ballast tanks. Currently, the property of the flow inside ballast tanks is not fully understood. To provide a means of predicting how the ballast water is flushed out of each compartment of a ballast tank, the modelling needs to have a predictive capability that can be used for complex geometries. CFD needs a deep insight into fluid mechanics and is complex and time-consuming due to the grid construction and the solution convergence in most cases (Chang et al., 2003; Hanby et al., 2006). It is difficult to test parameters, as even a small change of structure requires a large amount of effort in rerunning the simulation. In contrast, a multizone network model does not need meshing so that it can be set up more quickly and will run faster with fewer parameters. The model has more flexibility in testing the various geometrical influencing factors existing in complex ballast tanks. Therefore, multizone network models are more suitable than CFD to analyse the fluid exchange in a ballast tank.

This chapter aims to develop a multizone flow model to describe the movement of fluid in a ballast tank, on scenarios where flushing occurs in waters with similar density of the port water so that buoyancy has a dynamically negligible effect. The modelling technique draws on the research into the spread of contaminants in buildings (Zhao

et al., 1998). In this chapter, the property of the fluid flow in a typical ballast tank is analysed at first, and then the multizone model is derived in general and further illustrated in a simple 2× 2 tank at the end.

3.2 Characteristics of the fluid flow in a ballast tank

The characteristics of the fluid flow in a typical ballast tank are going to be discussed, as the removal of NIS in ballast water depends on tank geometry and the fluid nature (Eames et al., 2008). The flow in a ballast tank is characterised by two dimensionless variables: Richardson number (Ri) and Reynolds number (Re),

$$Ri = \frac{\Delta\rho g L}{\rho U^2}, \qquad Re = \frac{UL}{\nu}, \tag{3.1}$$

where $\Delta\rho$ is the density difference between the incoming water and the existing water, ρ the denser fluid, g the gravitational acceleration, 9.8 m/s^2, U the characteristic velocity, L the characteristic length, and ν the kinematic viscosity. Now the fluid flow in a real ship's ballast tank shown in Figure 3.1 is considered. This tank is large with a simple box design, and has a capacity of 81383.3 m^3 of water serviced by pumps with a flow rate of 2,500 m^3/h (or ≈ 0.7 m^3/s). It is characterised by a typical length $L = 50$ m, width $W_h = 20$ m of the base and $W_v = 0.5$ m of the vertical region, height $H_h = 2$ m of the horizontal region and $H_v = 25$ m of the vertical region, and the nominal diameter of the inlet nozzle $D = 0.5$ m. Further away from the inlet nozzle, the mean flow decays quite quickly. It is important to estimate typical values as these variables determine the type of modelling approach and the validity of the experimental analogue. The mean flow velocity through the nozzle is $U_n = 4Q/\pi D^2 \sim 3.6$ m/s. The inlet nozzle Reynolds number $Re_n = U_n D/\nu \sim 1.8 \times 10^6$. Based on the horizontal section, $U_h \geq Q/0.5\pi W_h H_h \sim 10^{-2}$ m/s, $Re_h = U_h H_h/\nu \sim 10^4$. Up the riser section, $U_v = Q/LW_v \sim 10^{-2}$ m/s, so $Re_v = U_v W_v/\nu \sim 10^4$. Thus the flow in a ballast tank is inertially dominant so that Re is high and the flow is turbulent. The density difference between ballast water and external fluid is $\Delta\rho/\rho \sim -0.035 \rightarrow 0.035$,

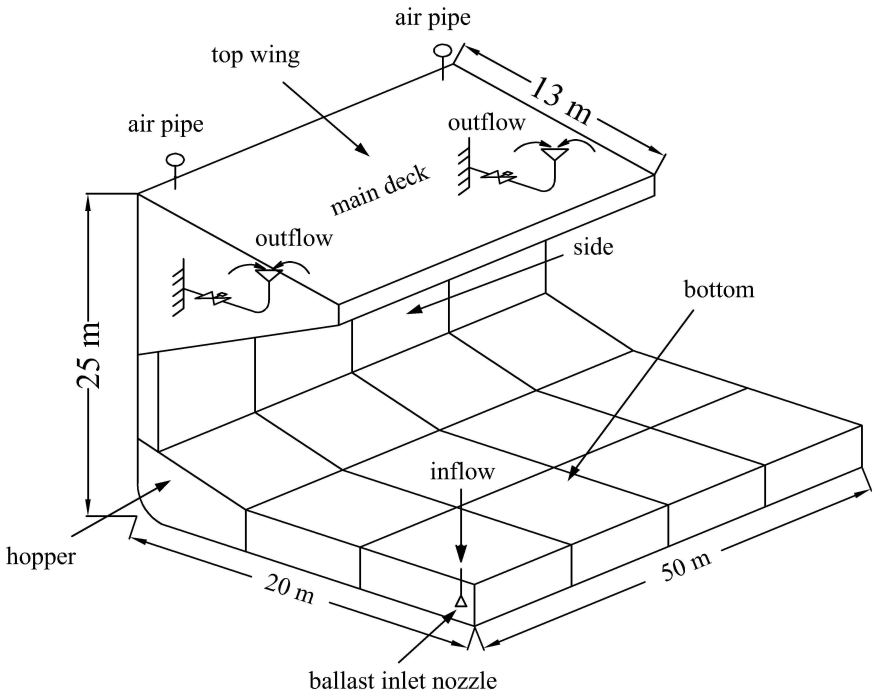

(a)

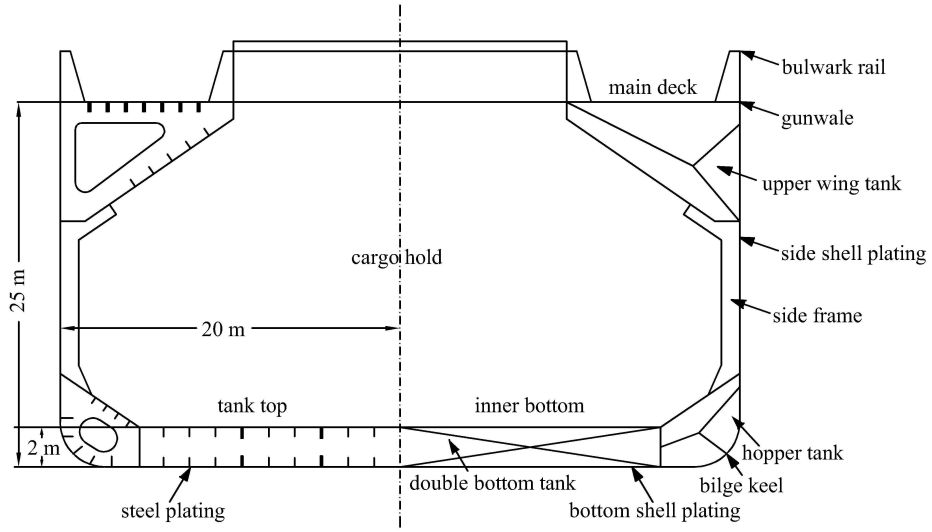

(b)

Figure 3.1: Schematic drawings showing (a) oblique and (b) cross-section view of a typical ballast tank. The tank is separated into port and starboard chambers (redrawn from Armstrong (1997)).

so that the Richardson number is about $-10^2 \rightarrow 10^2$ inside the tank.

The movement of fluid within a ballast tank is influenced by Ri. When $Ri \rightarrow +\infty$, that is when denser fluid is injected slowly into the tank, a stable interface forms between the injected and initial fluid (see Figure 3.2(a, b)). The lighter water in the ballast tank is vertically displaced when it is flushed by the injected denser water from below. If the NIS is assumed to have the same density with the original ballast water and suspend in it, the concentration of NIS in ballast water of a single compartment ballast tank, C, decreases linearly with time as $C/C_0 = 1 - T$, where C_0 is the original NIS concentration, and $T = Qt/V$ (Q is the flow rate, t the flushing time and V the ballast tank volume), until the NIS is completely removed. When $Ri \rightarrow 0$, that is when the density contrast is very small or the flow velocity is very high, perfect mixing occurs. In the absence of density effect, decrease of NIS in a single compartment ballast tank follows the perfect mixing rule, $C/C_0 = \exp(-T)$ (Parsons, 1998). That is, NIS concentration decreases exponentially with time, shown in Figure 3.2(c, d). The flushing-through method was confirmed to achieve an efficiency of 95% at three volumes flushing in a square tank (Kamada et al., 2004). When $Ri \rightarrow -\infty$, that is when lighter fluid is slowly injected, the fluid bypasses much of the tank and a portion of the initial NIS remains after three tank volumes flushing (see Figure 3.2(e, f)). The NIS cannot be effectively removed in this case so this practice should be avoided. If the flushing direction is reversed, the bypassing is then transformed to displacement.

The assumption of uniform density (i.e. $Ri = 0$) is appropriate especially when ballast water is taken in a seawater port such as Singapore and the water used to flush through the ballast tank is taken from deep ocean. For those ports near estuaries (e.g. Shanghai, New York, Hamburg, etc.), the change in density may be significant, this assumption is clearly not appropriate.

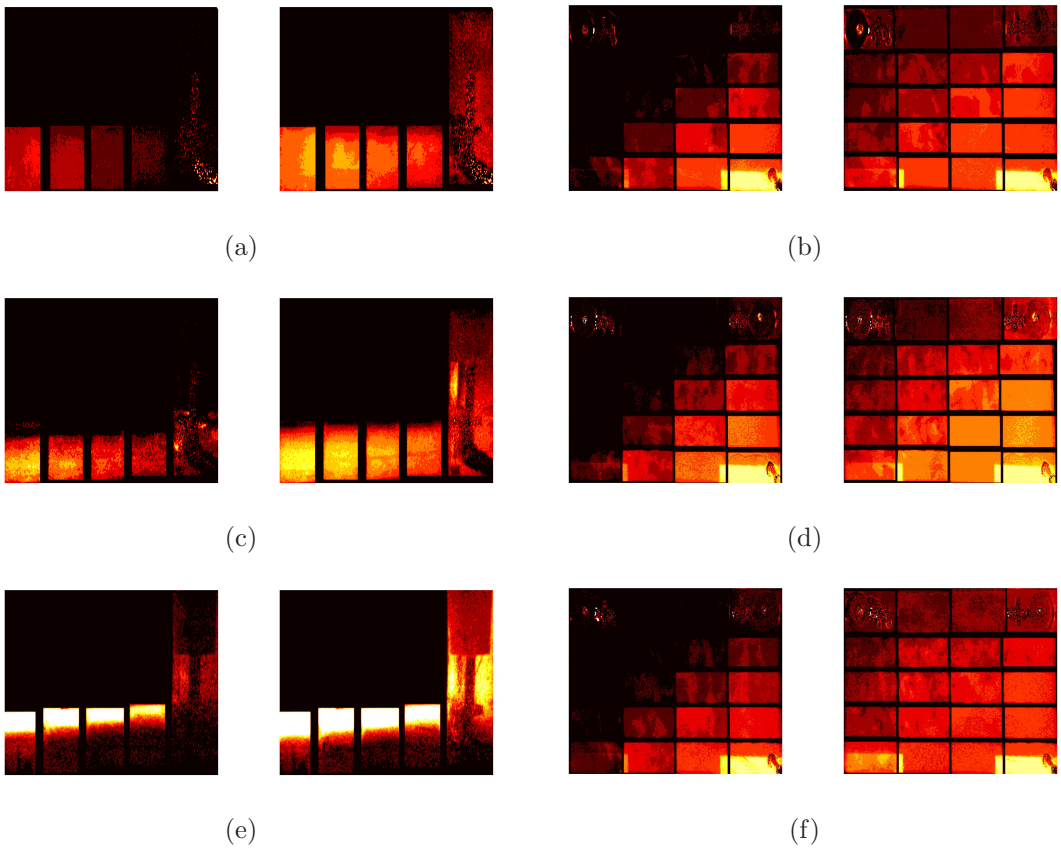

Figure 3.2: Integrated concentration field of water exchange by the flushing-through method in a multi-compartment tank (Dunsby, 2009). The figures correspond to the case of (a) injecting salt water into fresh water, (c) injecting fresh water into salt water and (e) injecting fresh water into salt water from the side view; (b), (d) and (f) are the corresponding plan view of (a), (c) and (e), respectively.

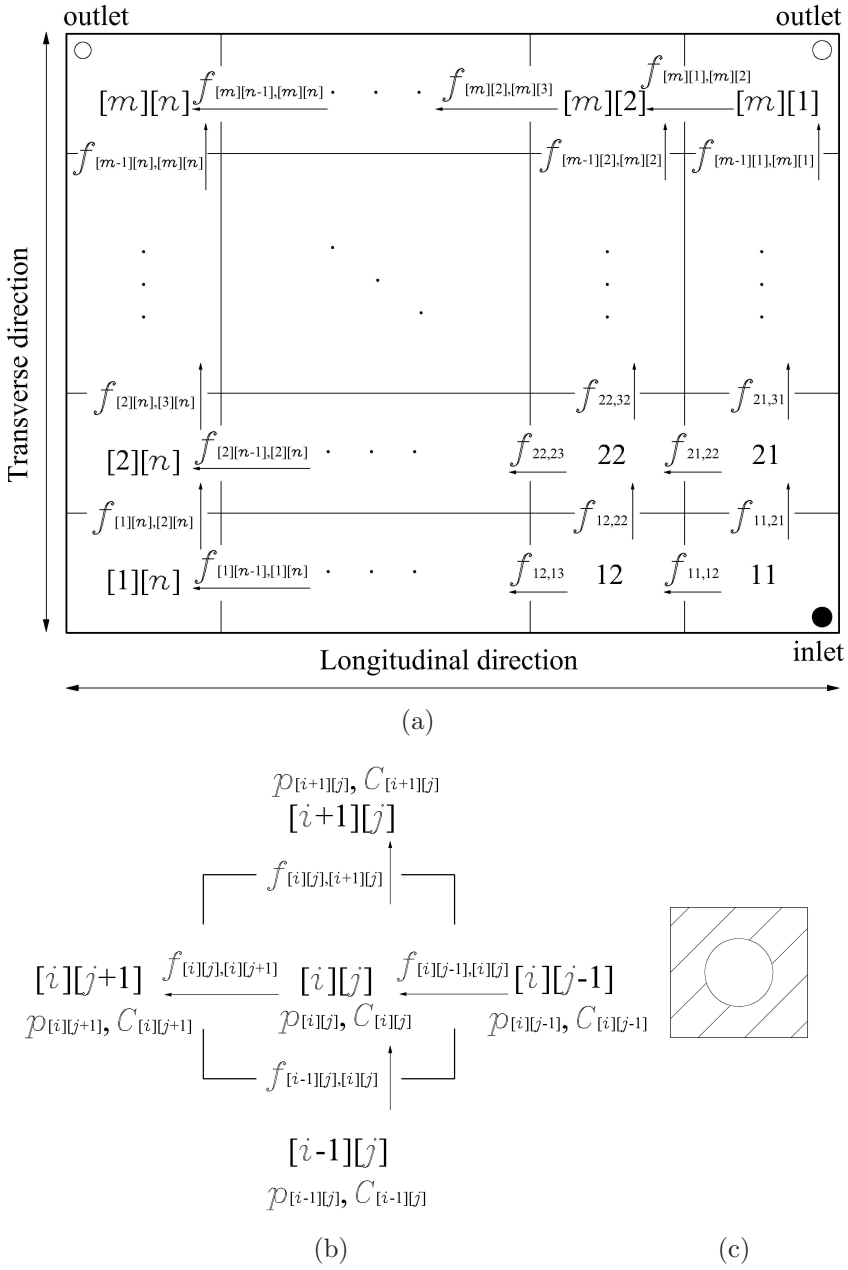

Figure 3.3: Schematics of the configuration of an $m \times n$ tank with one inlet and two outlets. (a) shows the plan view of the tank; (b) shows its generic compartment $[i][j]$ with notations of pressure, flushed fraction as well as flow rate; (c) shows a baffle with a hole between two neighbouring compartments. Inlet is taken to be located in compartment 11 and two outlets are in compartments $[m][1]$ and $[m][n]$, respectively.

3.3 Mathematical modelling

3.3.1 Notations and definitions

A flow network model typically represents rooms, compartments or subdivisions as nodes to the network (Joekar-Niasar et al., 2010; Weinläder et al., 2012; Wu et al., 2012). A node is characterised by capacitance, and the connection between the nodes represents the flow pathways and is characterised by resistance. In the context of ballast tanks, capacitance and resistance correspond to volume of compartments/rooms and size/shape of connecting passages. Figure 3.3(a) shows a schematic plan view of a general tank configuration consisting of m rows by n columns interconnected rectangular compartments and the notation used in the mathematical model. The box structure of most ballast tanks means that this topological network is appropriate. This type of analysis is easily extendable to other topological networks. A compartment at the i-th row and the j-th column of the tank is referenced as $[i][j]$. The bottom right-hand corner compartment is the pipe entrance to the ballast tank, while the top left-hand and right-hand corner compartments are two outlets. The tank is not constrained to the horizontal plane and may 'fold' as it progresses from the double bottom of a ship up its sides. Water with the same density as the water in the tank is injected through the inlet. Figure 3.3(b) shows a schematic of a generic compartment within the ballast tank. $p_{[i][j]}$ is the pressure of the centre of compartment $[i][j]$. The volumetric flux from compartment $[i_1][j_1]$ to its neighbouring compartment $[i_2][j_2]$ (here $i_1 = i_2$, $|j_1 - j_2| = 1$ or $j_1 = j_2$, $|i_1 - i_2| = 1$) through a hole (shown in Figure 3.3(c)) with cross sectional area $A_{[i_1][j_1],[i_2][j_2]}$ is defined as

$$f_{[i_1][j_1],[i_2][j_2]} = \int_{A_{[i_1][j_1],[i_2][j_2]}} \boldsymbol{u} \cdot \hat{\boldsymbol{n}} \mathrm{d}A, \tag{3.2}$$

where $\boldsymbol{u}$ is velocity, $\hat{\boldsymbol{n}}$ is a unit normal vector directed from compartment $[i_1][j_1]$ to compartment $[i_2][j_2]$. The fraction of water in compartment $[i][j]$ (of volume $V_{[i][j]}$) that has been flushed out is denoted as $C_{[i][j]}$. The flushed fraction is calculated as a

function of dimensionless time T, based on flushing the total tank volume (V), i.e.

$$T = \frac{Qt}{V}, \tag{3.3}$$

where $T = 0$ corresponds to the tank starting to be flushed. If all the compartments of the tank are identical, τ is defined as

$$\tau = \frac{Qt}{V_{[i][j]}}. \tag{3.4}$$

The fraction of fluid in the whole tank that has been flushed out, $\bar{C}$, is defined as

$$\bar{C}(T) = \frac{\sum_i \sum_j C_{[i][j]} V_{[i][j]}}{\sum_i \sum_j V_{[i][j]}}. \tag{3.5}$$

3.3.2 Governing equations

A system of ordinary differential equations is developed by integrating over individual compartments. The inertial force of the fluid is sufficiently large when compared to the buoyancy force that the latter can be ignored. The assumptions of the model are that (a) the incoming matter is well mixed, (b) the NIS are dynamically passive so that the removal of the NIS can be represented by the water exchange in the tank, and (c) the pressure (p) is the same within each compartment, but the gradients of p and C between compartments are important. Focusing on the generality of the formulation, the flow through the network is driven by volumetric sources at inlet nodes and pressure at outlet nodes. The network is characterised by a high level of turbulence at the nodes due to the sharp edges in the lightening frames in ballast tanks. As such, fluid is assumed to mix perfectly at each node and stratification effects tend to be weak. Small species in ballast water are essentially advected with the flow and can be regarded as passive during flushing. Since the species are dynamically passive, the fraction of the original water that is flushed out of the ballast tank can be used as a proxy for estimating the removal of NIS from the tanks.

The mass conservation is described by the continuity equation

$$\boldsymbol{\nabla} \cdot \boldsymbol{u} = 0, \tag{3.6}$$

where $\boldsymbol{u}$ is the fluid velocity vector; satisfies the Boussinesq equation

$$\rho \frac{\mathrm{D}\boldsymbol{u}}{\mathrm{D}t} = -\boldsymbol{\nabla} p + \mu \nabla^2 \boldsymbol{u} + \Delta\rho g \hat{\boldsymbol{z}}, \tag{3.7}$$

where ρ is the density of the fluid originally in the tank, $\Delta\rho$ the density contrast between the incoming fluid and the original fluid, t time, p pressure, μ the dynamic viscosity, g=9.81 m/s^2 the gravity acceleration, and $\hat{\boldsymbol{z}}$ the unit upwards vector. The transport of the fluid is described by an advection equation

$$\frac{\mathrm{D}C}{\mathrm{D}t} = 0. \tag{3.8}$$

The boundary conditions for solving these equations are

1. on all the walls, $\boldsymbol{u} \cdot \hat{\boldsymbol{n}} = 0$ (kinematic boundary condition) and $(\boldsymbol{u} \times \hat{\boldsymbol{n}}) \times \hat{\boldsymbol{n}} = \boldsymbol{0}$ (no-slip condition). The flux of C, $\boldsymbol{u}C \cdot \hat{\boldsymbol{n}} = 0$, therefore, $\boldsymbol{\nabla} C \cdot \hat{\boldsymbol{n}} = 0$;

2. on the inlet, $\boldsymbol{u} \cdot \hat{\boldsymbol{n}} = Q/(\pi R^2)$ and $C = 1$.

Now the limits of $Ri \to 0$ are examined in an $m \times n$ tank. From the governing equations, lumped models are developed by integrating over individual compartments. Integrating (3.6) over compartment $[i][j]$ gives

$$0 = \int_{V_{[i][j]}} \boldsymbol{\nabla} \cdot \boldsymbol{u} \mathrm{d}V = \int_{S_{[i][j]}} \boldsymbol{u} \cdot \hat{\boldsymbol{n}} \mathrm{d}S, \tag{3.9}$$

where $S_{[i][j]}$ is the surface of compartment $[i][j]$. Substituting (3.2) into (3.9) gives

$$\sum f_{[i][j],\mathrm{in}} - \sum f_{[i][j],\mathrm{out}} = 0, \tag{3.10}$$

where $f_{[i][j],\mathrm{in}}$ and $f_{[i][j],\mathrm{out}}$ are the volumetric inflow rate and volumetric outflow rate of compartment $[i][j]$, respectively.

For steady flows, the multizone model of flow between compartments employs a semi-empirical closure model to relate the pressure drop with the average velocity through the holes. Integrating the steady momentum equation over compartment $[i][j]$ gives

$$\rho \int_{S_{[i][j]}} (\boldsymbol{u} \cdot \hat{\boldsymbol{n}}) \boldsymbol{u} \mathrm{d}S = - \int_{S_{[i][j]}} p \hat{\boldsymbol{n}} \mathrm{d}S + \int_{S_{[i][j]}} \boldsymbol{\tau} \cdot \hat{\boldsymbol{n}} \mathrm{d}S. \tag{3.11}$$

The approach adopted here is consistent with that of other studies (Chu et al., 2009; Mora et al., 2003; Tan and Glicksman, 2005). The pressure difference between two neighbouring compartments $[i_1][j_1]$ and $[i_2][j_2]$ is

$$p_{[i_1][j_1]} - p_{[i_2][j_2]} = \zeta_{[i_1][j_1],[i_2][j_2]} \rho \frac{|f_{[i_1][j_1],[i_2][j_2]}| f_{[i_1][j_1],[i_2][j_2]}}{A_{[i_1][j_1],[i_2][j_2]}{}^2}, \tag{3.12}$$

where $\zeta_{[i_1][j_1],[i_2][j_2]}$ is the local pressure loss coefficient between compartments $[i_1][j_1]$ and $[i_2][j_2]$. The pressure loss coefficient ζ is usually determined empirically. Different forms of the closure have been developed to account for windows, doors and sharp openings in a circular pipe. At high Reynolds numbers, Heiselberg et al. (2001) and Chu et al. (2010) found that ζ depends primarily on the ratio (β) of the hole area to the partition wall area. For square holes between rooms, Chu and Wang (2010) found that ζ increases rapidly with β when $0 \leq \beta \leq 5\%$. Meizig and Schmidt (1965) found that ζ increases approximately linearly with $\sqrt{\beta}$ for $5\% \leq \beta \leq 50\%$. Typically, $\beta \leq 20\%$ for ballast tanks. To estimate the pressure drop coefficient of a hole between two neighbouring compartments in this study ($3.27\% \leq \beta \leq 39.6\%$), a square root fit is used based on the wind tunnel testing results of Meizig and Schmidt (1965),

$$\zeta = 4.24 \sqrt{\beta}, \tag{3.13}$$

for $0 \leq \beta \leq 50\%$.

The fluid is transported by the mean flow and mixed by turbulent dispersion (Eames et al., 2008). The mean flow is largest in the passage between compartments and is smallest within compartments. The sharp edge of the lightening hole means that vortex shedding occurs and in this class of flows, the level of turbulence is

comparable to the mean flow, i.e. $I_t = u_{RMS}/|\boldsymbol{u}| \sim 1$ within compartments. In the hole between compartments, a straining flow leads to a suppressing of the turbulence (Tao and Thiagarajan, 2003) and I_t is reduced. Consequently the fluid tends to be rapidly mixed by turbulent dispersion within a compartment so that $C \simeq C_{[i][j]}$. For compartment $[i][j]$, an approximate model is used to describe the variation of the flushed fraction with time, i.e.

$$V_{[i][j]}\frac{\mathrm{d}C_{[i][j]}}{\mathrm{d}t} = \sum f_{[i][j],\mathrm{in}} C_{[i][j],\mathrm{in}} - \sum f_{[i][j],\mathrm{out}} C_{[i][j]}, \tag{3.14}$$

where $C_{[i][j],\mathrm{in}}$ is the flushed fraction in the compartment(s) flowing into compartment $[i][j]$. The matrix form of equation array (3.14) is shown in Appendix A.

3.3.3 General form

The ballast tank from the plan view, as shown in Figure 3.3(a), is composed of m rows by n columns compartments. It has one inlet node (source) - compartment 11 and two outlets (sink nodes) - compartments $[m][1]$ and $[m][n]$. The external fluid is injected with a steady flow rate Q into compartment 11 (source node). The original fluid exits from compartment $[m][1]$ and compartment $[m][n]$ at outflow rate $Q_{[m][1],\mathrm{out}}$ and $Q_{[m][n],\mathrm{out}}$, respectively. Inside the tank, there is a constant flow from one compartment to another. Based on the conservation of the flow (see equation (3.10)), the sum of the flow into compartment $[i][j]$ is equal to that out of compartment $[i][j]$. Therefore, the flow rates for all compartments in the tank have the following relationships:

$$\begin{aligned}
&Q = f_{11,12} + f_{11,21},\\
&f_{[1][n-1],[1][n]} = f_{[1][n],[2][n]},\\
&f_{[m-1][1],[m][1]} = f_{[m][1],[m][2]} + Q_{[m][1],\mathrm{out}},\\
&f_{[m-1][n],[m][n]} + f_{[m][n-1],[m][n]} = Q_{[m][n],\mathrm{out}},\\
&f_{[1][j-1],[1][j]} = f_{[1][j],[1][j+1]} + f_{[1][j],[2][j]}, \quad j = 2, 3, \cdots, n-1,\\
&f_{[m][j-1],[m][j]} + f_{[m-1][j],[m][j]} = f_{[m][j],[m][j+1]}, \quad j = 2, 3, \cdots, n-1,\\
&f_{[i-1][1],[i][1]} = f_{[i][1],[i][2]} + f_{[i][1],[i+1][1]}, \quad i = 2, 3, \cdots, m-1,
\end{aligned}$$

$$f_{[i-1][n],[i][n]} + f_{[i][n-1],[i][n]} = f_{[i][n],[i+1][n]}, \quad i = 2, 3, \cdots, m-1,$$
$$f_{[i-1][j],[1][j]} + f_{[i][j-1],[i][j]} = f_{[i][j],[i][j+1]} + f_{[i][j],[i+1][j]}, \quad i = 2, 3, \cdots, m-1 \quad \text{and}$$
$$j = 2, 3, \cdots, n-1. \tag{3.15}$$

For different outlet arrangements, the boundary conditions are different. When only the far outlet (compartment $[m][n]$) is open, $Q_{[m][1],\text{out}} = 0$, $p_{[m][n]} = 0$; when only the near outlet (compartment $[m][1]$) is open, $Q_{[m][n],\text{out}} = 0$, $p_{[m][1]} = 0$; when both outlets are open, $p_{[m][1]} = p_{[m][n]} = 0$.

Each compartment is assumed to be characterised by a volume, a pressure and a flushed fraction. Based on equation 3.12, the pressure difference between neighbouring compartments depends on the drop coefficient and the flow rate, which can be expressed as below:

$$p_{[i][j]} - p_{[i][j+1]} = \zeta_{[i][j],[i][j+1]} \rho \frac{|f_{[i][j],[i][j+1]}| f_{[i][j],[i][j+1]}}{A_{[i][j],[i][j+1]}^2}, \quad i = 1, 2, \cdots, m \quad \text{and}$$
$$j = 1, 2, \cdots, n-1;$$
$$p_{[i][j]} - p_{[i+1][j]} = \zeta_{[i][j],[i+1][j]} \rho \frac{|f_{[i][j],[i+1][j]}| f_{[i][j],[i+1][j]}}{A_{[i][j],[i+1][j]}^2}, \quad i = 1, 2, \cdots, m-1 \quad \text{and}$$
$$j = 1, 2, \cdots, n. \tag{3.16}$$

The drop coefficient ζ is estimated by equation (3.13). Given the inflow rate Q and the pressure drop coefficient (ζ), all the flow rates can be calculated. According to equation (3.14), the variation of the flushed fraction in a compartment depends on the compartment volume and the difference of the mass variation (fC), which varies in time as

$$\frac{\mathrm{d}C_{11}}{\mathrm{d}T} = \frac{V}{V_{11}}(1 - C_{11}),$$
$$\frac{\mathrm{d}C_{[1][n]}}{\mathrm{d}T} = \frac{V}{V_{[1][n]}} \left(\frac{f_{[1][n-1],[1][n]}}{Q} C_{[1][n-1]} - \frac{f_{[1][n],[2][n]}}{Q} C_{[1][n]} \right),$$

$$
\begin{aligned}
\frac{\mathrm{d}C_{[m][1]}}{\mathrm{d}T} =& \frac{V}{V_{[m][1]}}\left(\frac{f_{[m-1][1],[m][1]}}{Q}C_{[m-1][1]} - \frac{f_{[m][1],[m][2]}}{Q}(\mathcal{H}(f_{[m][1],[m][2]})C_{[m][1]}\right.\\
&\left.+\mathcal{H}(-f_{[m][1],[m][2]})C_{[m][2]}) - \frac{Q_{[m][1],\mathrm{out}}}{Q}C_{[m][1]}\right),\\
\frac{\mathrm{d}C_{[m][n]}}{\mathrm{d}T} =& \frac{V}{V_{[m][n]}}\left(\frac{f_{[m-1][n],[m][n]}}{Q}C_{[m-1][n]} + \frac{f_{[m][n-1],[m][n]}}{Q}(\mathcal{H}(f_{[m][n-1],[m][n]})C_{[m][n-1]}\right.\\
&\left.+\mathcal{H}(-f_{[m][n-1],[m][n]})C_{[m][n]}) - \frac{Q_{[m][n],\mathrm{out}}}{Q}C_{[m][n]}\right),\\
\frac{\mathrm{d}C_{[1][j]}}{\mathrm{d}T} =& \frac{V}{V_{[1][j]}}\left(\frac{f_{[1][j-1],[1][j]}}{Q}C_{[1][j-1]} - \frac{f_{[1][j],[2][j]}}{Q}C_{[1][j]} - \frac{f_{[1][j],[1][j+1]}}{Q}C_{[1][j]}\right),\\
& j = 2,3,\cdots,n-1,\\
\frac{\mathrm{d}C_{[m][j]}}{\mathrm{d}T} =& \frac{V}{V_{[m][j]}}\left(\frac{f_{[m][j-1],[m][j]}}{Q}(\mathcal{H}(f_{[m][j-1],[m][j]})C_{[m][j-1]} + \mathcal{H}(-f_{[m][j-1],[m][j]})C_{[m][j]})\right.\\
&+ \frac{f_{[m-1][j],[m][j]}}{Q}C_{[m-1][j]} - \frac{f_{[m][j],[m][j+1]}}{Q}(\mathcal{H}(f_{[m][j],[m][j+1]})C_{[m][j]}\\
&\left.+\mathcal{H}(-f_{[m][j],[m][j+1]})C_{[m][j+1]})\right), \qquad j = 2,3,\cdots,n-1,\\
\frac{\mathrm{d}C_{[i][1]}}{\mathrm{d}T} =& \frac{V}{V_{[i][1]}}\left(\frac{f_{[i-1][1],[i][1]}}{Q}C_{[i-1][1]} - \frac{f_{[i][1],[i][2]}}{Q}(\mathcal{H}(f_{[i][1],[i][2]})C_{[i][1]}\right.\\
&\left.+\mathcal{H}(-f_{[i][1],[i][2]})C_{[i][2]}) - \frac{f_{[i][1],[i+1][1]}}{Q}C_{[i][1]}\right), \qquad i = 2,3,\cdots,m-1,\\
\frac{\mathrm{d}C_{[i][n]}}{\mathrm{d}T} =& \frac{V}{V_{[i][n]}}\left(\frac{f_{[i-1][n],[i][n]}}{Q}C_{[i-1][n]} + \frac{f_{[i][n-1],[i][n]}}{Q}(\mathcal{H}(f_{[i][n-1],[i][n]})C_{[i][n-1]}\right.\\
&\left.+\mathcal{H}(-f_{[i][n-1],[i][n]})C_{[i][n]}) - \frac{f_{[i][n],[i+1][n]}}{Q}C_{[i][n]}\right), \qquad i = 2,3,\cdots,m-1,\\
\frac{\mathrm{d}C_{[i][j]}}{\mathrm{d}T} =& \frac{V}{V_{[i][j]}}\left(\frac{f_{[i][j-1],[i][j]}}{Q}(\mathcal{H}(f_{[i][j-1],[i][j]})C_{[i][j-1]} + \mathcal{H}(-f_{[i][j-1],[i][j]})C_{[i][j]})\right.\\
&+ \frac{f_{[i-1][j],[i][j]}}{Q}C_{[i-1][j]} - \frac{f_{[i][j],[i][j+1]}}{Q}(\mathcal{H}(f_{[i][j],[i][j+1]})C_{[i][j]}\\
&\left.+\mathcal{H}(-f_{[i][j],[i][j+1]})C_{[i][j+1]}) - \frac{f_{[i][j],[i+1][j]}}{Q}C_{[i][j]}\right),\\
& i = 2,3,\cdots,m-1 \quad \text{and} \quad j = 2,3,\cdots,n-1
\end{aligned}
\tag{3.17}
$$

along with

$$C_{[i][j]}|_{T=0} = 0.$$

Here $\mathcal{H}(X)$ is the Heaviside step function with the property $\mathcal{H}(X) = 1$ for $X \geq 0$ and $\mathcal{H}(X) = 0$ for $X < 0$, which is needed to make sure that the expression for the mass variation is correct. For instance, when the flow is from compartment $[m][1]$ to $[m][2]$, i.e. $f_{[m][1],[m][2]} > 0$, $\mathcal{H}(f_{[m][1],[m][2]}) = 1$ and $\mathcal{H}(-f_{[m][1],[m][2]}) = 0$, the expression for the mass variation in compartment $[m][1]$ should be

$$\frac{\mathrm{d}C_{[m][1]}}{\mathrm{d}T} = \frac{V}{V_{[m][1]}} \left(\frac{f_{[m-1][1],[m][1]}}{Q} C_{[m-1][1]} - \frac{f_{[m][1],[m][2]}}{Q} C_{[m][1]} - \frac{Q_{[m][1],\mathrm{out}}}{Q} C_{[m][1]} \right);$$

when the flow is from compartment $[m][2]$ to $[m][1]$, i.e. $f_{[m][1],[m][2]} < 0$, $\mathcal{H}(f_{[m][1],[m][2]}) = 0$ and $\mathcal{H}(-f_{[m][1],[m][2]}) = 1$, the expression becomes

$$\frac{\mathrm{d}C_{[m][1]}}{\mathrm{d}T} = \frac{V}{V_{[m][1]}} \left(\frac{f_{[m-1][1],[m][1]}}{Q} C_{[m-1][1]} - \frac{f_{[m][1],[m][2]}}{Q} C_{[m][2]} - \frac{Q_{[m][1],\mathrm{out}}}{Q} C_{[m][1]} \right).$$

3.3.4 Diagnostic tools

The mathematical model generates a time series for the flushed fraction of water in each compartment. A set of diagnostic tools are required to quantify the timescale when each compartment is flushed and the rate at which they are flushed by the incoming water. The dimensionless characteristic time $T_{\frac{1}{2},[i][j]}$ for flushing is identified when compartment $[i][j]$ is flushed to half of its maximum, interpreted as 'half flushed time'

$$T_{\frac{1}{2},[i][j]} = T \Big|_{C_{[i][j]}=\frac{1}{2}}, \tag{3.18}$$

and $\alpha_{\frac{1}{2},[i][j]}$ represents the characteristic flushing rate, at which compartment $[i][j]$ is being flushed when half of its contents have been flushed (that is, when $T = T_{\frac{1}{2},[i][j]}$),

$$\alpha_{\frac{1}{2},[i][j]} = \frac{V_{[i][j]}}{V} \frac{\mathrm{d}C_{[i][j]}}{\mathrm{d}T} \Big|_{T=T_{\frac{1}{2},[i][j]}}. \tag{3.19}$$

The diagnostics are applied to analyse the results from the multizone model and the experimental results.

3.4 Model calculation

Matlab software is employed to calculate the mathematical equation arrays and plot the outputs.

3.4.1 Calculation of the flow rate

A main script M-file and a function script M-file are used to calculate the flow rates between neighbouring compartments within a ballast tank. All these flow rates are defined as global variables in both files. In the main file, the system function 'fsolve' in Matlab is employed, which solves systems of non-linear algebraic equations of several variables using a quasi-Newton method. This function has a format of 'X = fsolve(FUN, X0)', which starts at the vector X0 (initial values of flow rates and pressures for iteration, set as 0) and tries to solve the equations in the function file 'FUN'. 'FUN' accepts input 'X' and returns a vector of equation values 'F' evaluated at 'X'. The iterations end when $\Sigma(F(X_i) - F(X_{i+1}))^2 < 10^{-3}$. In the function file, the pressure drop coefficients are estimated by using equation (3.13), the sectional areas of the holes between neighbouring compartments are given, and all the mass conservations equations (3.10) and pressure drop equations (3.12) are listed in vector 'F'. The calculation times depend on the number of the compartments, varying from a few hundred to over 1,000 for the tested tanks.

3.4.2 Calculation of the flushed fraction

A main script M-file and a function script M-file are used to calculate the flushed fractions within each compartment of the ballast tank. In the main file, the flushed fractions are calculated by Matlab function 'ode45', which is based on an explicit Runge-Kutta 4th and 5th order algorithm. The function has a format of '[TOUT,YOUT] = ode45(ODEFUN, [T0 T1 ... TFINAL]', Y0)', which numerically integrates the system of differential equations (3.14) saved in the function file 'ODEFUN' with initial conditions 'Y0'. The column vector '[T0 T1 ... TFINAL]" is the time series from 'T0' to 'TFINAL'. Since three volumes exchange is looked at, the time series is set

from 0 to 3 with an interval of $\Delta T = 0.1$. 'Y0' is a zero vector, corresponding to the initial values of the flushed fractions in each compartment for iteration. The function 'ODEFUN' returns the solution array 'YOUT' and the corresponding series of time 'T' is returned as the column vector 'TOUT'. Each column in 'YOUT' corresponds to a time series of flushed fractions in a compartment, '$C_{[i][j]}$'. The default relative error tolerance is 10^{-3} and the default absolute tolerance is 10^{-6} for each compartment. The loop times vary from about a hundred to about 2,000 for the tested tanks.

3.4.3 Calculation of the half flushed time and the characteristic flushing rate

From Section 3.4.2, a time series of the flushed fractions has been calculated for each compartment. The time points and the flushed fractions are saved in the time vector 'T' and the flushed fraction vector 'C', respectively. $T_{\frac{1}{2}}$ ('Thalf') is estimated by using function 'interp1' in Matlab. The function 'Thalf = interp1(C, T, 0.5)' linearly interpolates to find 'Thalf', the corresponding value in 'T' at the query point '0.5' in 'C'. $\alpha_{\frac{1}{2}}$ ('Alphahalf') is estimated by using $(C(i+1)-C(i))/(T(i+1)-T(i))$, where $C(i) < 0.5 < C(i+1)$.

3.5 Model application to a 2×2 tank

In this section, the effect of outlet arrangement on flushing is illustrated in a simple tank configuration. To maintain a high degree of complexity but reduce the number of variables, the model is applied to a 2×2 network shown in Figure 3.4(a), for it is analytically tractable. The network physically corresponds to a tank with four interconnected compartments, denoted as 11, 12, 21 and 22. The inlet to the network is node 11, while two outlets are nodes 21 and 22. $k_1 L$ and $k_2 W$ are used to represent the length and width of compartment 11, where the tank has length L and width W, and thus $L_2 = (1-k_1)L$, $W_2 = (1-k_2)W$. The internal flow rates are determined

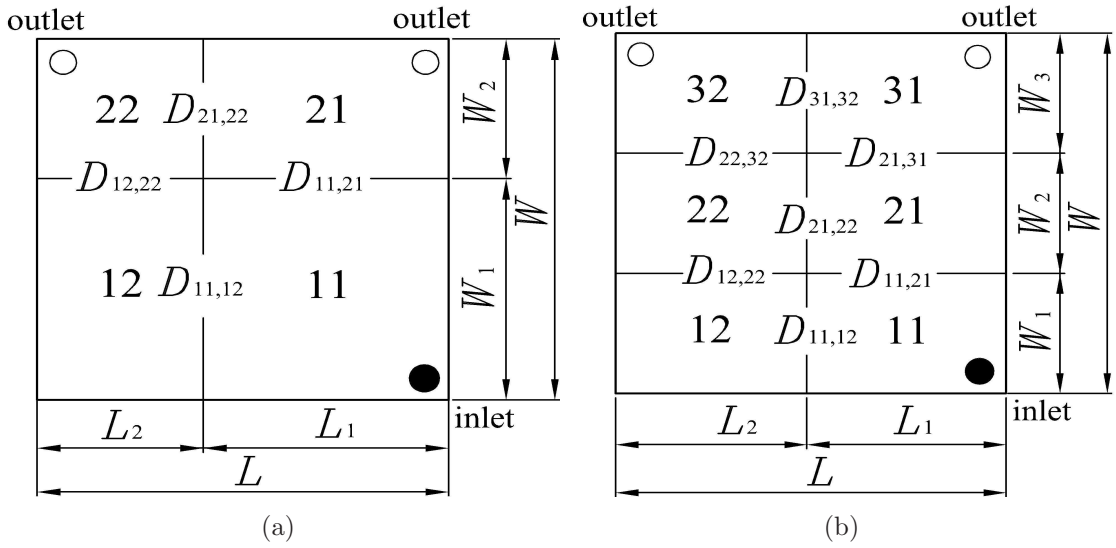

Figure 3.4: Schematic of a (a) 2×2 and (b) 3×2 inhomogeneous tank with one inlet and two outlets. $D_{[i_1][j_1],[i_2][j_2]}$ is the diameter of the hole between compartment $[i_1][j_1]$ and $[i_2][j_2]$; L, L_1 and L_2 are the length of the tank, compartment 11 and compartment 12, respectively; W, W_1, W_2 and W_3 are the width of the tank, compartment 11, compartment 21 and compartment 31, respectively. For the 2×2 tank, $L_1 = k_1 L$ and $W_1 = k_2 W$.

Table 3.1: Solution to the flow rates in the 2×2 tank.

	ϕ	$f_{11,12}$	$f_{12,22}$	$f_{11,21}$	$f_{21,22}$	$Q_{21,\text{out}}$	$Q_{22,\text{out}}$
Far open ($p_{22}=0$)	$\frac{1}{1+\left(\frac{\psi_{11,12}+\psi_{12,22}}{\psi_{11,21}+\psi_{21,22}}\right)^{\frac{1}{2}}}$	ϕQ	ϕQ	$(1-\phi)Q$	$(1-\phi)Q$	0	Q
Near open ($p_{21}=0$)	$\frac{1}{1+\left(\frac{\psi_{11,12}+\psi_{12,22}+\psi_{21,22}}{\psi_{11,21}}\right)^{\frac{1}{2}}}$	ϕQ	ϕQ	$(1-\phi)Q$	$-\phi Q$	Q	0
Both open ($p_{21}=p_{22}=0$)	$\frac{1}{1+\left(\frac{\psi_{11,12}+\psi_{12,22}}{\psi_{11,21}}\right)^{\frac{1}{2}}}$	ϕQ	ϕQ	$(1-\phi)Q$	0	$(1-\phi)Q$	ϕQ

by four flow equations as well as four pressure loss equations as below:

$$f_{11,12} + f_{11,21} = Q, \quad f_{11,12} = f_{12,22}, \quad f_{11,21} = f_{21,22} + Q_{21,\text{out}}, \quad f_{12,22} + f_{21,22} = Q_{22,\text{out}}; \tag{3.20}$$

$$\begin{aligned} p_{11} - p_{12} &= \psi_{11,12}\rho|f_{11,12}|f_{11,12}, \qquad & p_{21} - p_{22} &= \psi_{21,22}\rho|f_{21,22}|f_{21,22}, \\ p_{11} - p_{21} &= \psi_{11,21}\rho|f_{11,21}|f_{11,21}, \qquad & p_{12} - p_{22} &= \psi_{12,22}\rho|f_{12,22}|f_{12,22}, \end{aligned} \tag{3.21}$$

where $\psi = \zeta A^{-2}$. The solution to the flow rates is listed in Table 3.1. To simplify the notation, ϕ is defined as $f_{11,12}/Q$, thus $f_{11,21}/Q = 1 - \phi$.

The flushed fraction in each compartment evolves according to

$$\begin{aligned} \frac{\mathrm{d}C_{11}}{\mathrm{d}T} =& \frac{1}{k_1 k_2}\left(1 - C_{11}\right), \\ \frac{\mathrm{d}C_{12}}{\mathrm{d}T} =& \frac{1}{(1-k_1)k_2}\left(\phi C_{11} - \phi C_{12}\right), \\ \frac{\mathrm{d}C_{21}}{\mathrm{d}T} =& \frac{1}{k_1(1-k_2)}\left((1-\phi)C_{11} - \frac{f_{21,22}}{Q}(\mathcal{H}(f_{21,22})C_{21} + \mathcal{H}(-f_{21,22})C_{22}) - \frac{Q_{21,\text{out}}}{Q}C_{21}\right), \\ \frac{\mathrm{d}C_{22}}{\mathrm{d}T} =& \frac{1}{(1-k_1)(1-k_2)}\left(\phi C_{12} + \frac{f_{21,22}}{Q}(\mathcal{H}(f_{21,22})C_{21} + \mathcal{H}(-f_{21,22})C_{22}) - \frac{Q_{22,\text{out}}}{Q}C_{22}\right), \end{aligned} \tag{3.22}$$

and satisfies the initial condition,

$$C_{[i][j]}|_{T=0} = 0.$$

The system of the coupled linear differential equations can be solved analytically. The matrix expression for the flushed fraction in each compartment and the detailed analytical solutions in the case of $k_1 = k_2 = 1/2$ (That is, the four compartments of the tank have the same volume.) are given in Appendix B.

Now the case when the geometry of the lightening holes is the same ($\psi_{11,12} = \psi_{21,22} = \psi_{11,21} = \psi_{12,22}$) is considered. When only the far outlet is open ($Q_{21,\text{out}} = 0$,

$p_{22} = 0$), the solution to equation array (3.23) is

$$f_{11,12} = f_{11,21} = f_{12,22} = f_{21,22} = \frac{Q}{2}, \quad Q_{22,\text{out}} = Q; \tag{3.23}$$

$$\begin{aligned} C_{11} &= 1 - \exp(-4T), \\ C_{12} &= 1 - 2\exp(-2T) + \exp(-4T), \\ C_{21} &= 1 - 2\exp(-2T) + \exp(-4T), \\ C_{22} &= 1 - 4\exp(-2T) + (4T + 3)\exp(-4T); \end{aligned} \tag{3.24}$$

when only the near outlet is open ($Q_{22,\text{out}} = 0$, $p_{21} = 0$), after manipulation, the solution is

$$f_{11,12} = f_{12,22} = \frac{(\sqrt{3} - 1)Q}{2}, \quad f_{21,22} = \frac{(1 - \sqrt{3})Q}{2}, \quad f_{11,21} = \frac{(3 - \sqrt{3})Q}{2}, \quad Q_{21,\text{out}} = Q; \tag{3.25}$$

$$\begin{aligned} C_{11} &= 1 - \exp(-4T), \\ C_{12} &= 1 - \frac{\sqrt{3} + 3}{3}\exp((2 - 2\sqrt{3})T) + \frac{\sqrt{3}}{3}\exp(-4T), \\ C_{21} &= 1 - \frac{12T + \sqrt{3} - 3}{9}\exp((2 - 2\sqrt{3})T) + \frac{(12\sqrt{3} - 48)T + \sqrt{3} - 12}{9}\exp(-4T), \\ C_{22} &= 1 - \frac{4\sqrt{3}T + 2}{3}\exp((2 - 2\sqrt{3})T) - \frac{1}{3}\exp(-4T); \end{aligned} \tag{3.26}$$

when both outlets are open ($p_{21} = p_{22} = 0$), the fluxes between the compartments are

$$f_{11,12} = f_{12,22} = Q_{22,\text{out}} = (\sqrt{2} - 1)Q, \quad f_{21,22} = 0, \quad f_{11,21} = Q_{21,\text{out}} = (2 - \sqrt{2})Q; \tag{3.27}$$

$$
\begin{aligned}
C_{11} &= 1 - \exp(-4T), \\
C_{12} &= 1 - \frac{\sqrt{2}+2}{2}\exp((4-4\sqrt{2})T) + \frac{\sqrt{2}}{2}\exp(-4T), \\
C_{21} &= 1 - (\sqrt{2}+1)\exp((4\sqrt{2}-8)T) + \sqrt{2}\exp(-4T), \\
C_{22} &= 1 - \frac{4\sqrt{2}T+1}{2}\exp((4-4\sqrt{2})T) - \frac{1}{2}\exp(-4T).
\end{aligned} \tag{3.28}
$$

Validating the mathematical model is crucial to have some faith in the fidelity of the predictions. The gold standard is to validate against experimental results, over a variety of parameters. This model will be tested in 2×2 and 3×3 and 5×4 networks. For the 2×2 homogeneous network and 3×3 network, there is no difference of resistance between compartments so that there is no need to employ the closure model for the pressure loss coefficient; for the 5×4 network and 2×2 inhomogeneous network, the estimation of the flow resistance (3.13) is needed. The model will be first validated by testing a 2×2 square tank, a 3×3 square tank and a 5×4 'J'-type tank with different outlet arrangements in Chapter 5, and the influence of the structural inhomogeneity on the flushing from a 2×2 tank capable of varying hole resistance and compartment capacitance will be further studied in Chapter 6. The following 4 tests will be considered:

(1) examining the temporal/spatial variation of the passive matter through the system with steady release of flow to a node;

(2) examining the influence of flux constrained outlets versus pressure controlled outflow;

(3) examining the influence of resistance by varying the size of the interconnecting holes, for fixed capacitance;

(4) examining the influence of capacitance by varying the size of the compartments, for fixed resistance.

Chapter 4

Experimental Design and Methodology

4.1 Introduction

The purpose of the experimental study is to provide a means of testing the model predictions and developing a general understanding of the physics. A series of experiments were undertaken to test quantitatively the capability of the flushing model to capture the exchange processes in multi-compartment tanks. As discussed in Chapter 3, the key influencing factors of ballast tank flushing can be represented by the dynamical variables (Re and Ri) and geometrical features, including tank configuration, outlet arrangement, hole size, resistance and compartment capacity. As defined by equation (3.1), Re reflects the ratio of inertial force to viscous force, depending on flow rate, hole size and resistance. Ri reflects the ratio of buoyancy to inertial force, depending on the density contrast, inflow rate, hole size and resistance. The experimental study includes four parts:

1. The tank configuration is homogeneous (Here 'homogeneous' means that compartments of the tank have the same size in the horizontal and vertical section, respectively, and that the holes between compartments are the same across the longitudinal direction and along the transverse direction, respectively.) and no

density contrast exists between the incoming flushing water and the original tank water;

2. The tank configuration is inhomogeneous (Here 'inhomogeneous' means that compartments of the tank have different sizes, and/or that the holes between compartments are not the same.) and no density contrast exists between the incoming flushing water and the original ballast water;

3. The tank configuration is in-line (Here 'in-line' means that compartments of the tank are connected in line and thus each compartment has only one inlet and only one outlet) and homogeneous, and density contrast exists between the incoming flushing water and the original tank water;

4. The tank configuration is rectangular and density contrast exists.

To test the predictions, a number of new experimental facilities need to be designed and built. The design elements mainly consist of a system for measuring the temporal/spatial variation of dye concentration in model ballast tanks. A geometrically complex tank is needed to analyse the entire system; a geometrically simple but capable of varying resistance/capacitance is needed to look at the characteristic in each compartment; and a geometrically very simple tank (with compartments connected in line) capable of studying the fluid interface is needed to test the stratification model.

4.2 Design of experimental apparatus considerations

To quantify the flushing efficiency of multi-compartment tanks, this laboratory scale experiment is to use an optical method to test the variation of the mean dye concentration within each compartment of the transparent models. A model tank should be placed inside a holding tank with light sources and can be flushed through with water. During the flushing, the front and plan view of the tank need to be continuously recorded. The variation of the mean dye concentration needs to be quantitatively

measured by an image processing software. The geometry of the tank, the pumping speed and the water density (salinity) can be changed.

1. Design of a square tank. This tank is used to test how the fluid exchange depends on geometry, so it needs to be closed during flushing and easily decomposed for changing internal structure. The tank requires a base with a draining slot and a cover with pipes as potential inlets and outlets. Clamps and sealing trips are needed to give a water tight seal to the tank. Acrylic was selected as the material of the tank for its strength and transparency. This tank needs to be divided to different compartment configurations (2×2 and 3×3), so different plates with different holes need to be built to segment the tank.

2. Design of a 'J'-type tank. This acrylic tank simulates the typical geometry of a ballast tank, composed of an enclosed horizontal section and an open vertical section. It is sealed by silicone sealant and has a fixed structure. A pipe is needed to be inserted to a corner compartment as an inlet, and two funnels are needed in two vertical compartments as exits.

3. Design of an in-line tank. This tank is used to vertically visualise the fluid exchange and analyse the mass transfer in the stratified case. It is supposed to be composed of a line of connected compartments. A pipe is needed to be inserted to the first compartment as the inlet, and a rectangular hole is needed to be dug on the topside of the last compartment for the water to spill out of the tank.

4. Design of the holding tank. A large open transparent tank is needed to hold the model tank in the lab. This holding tank requires a slot on the bottom that is connected to a large drainage hole in the lab. Water drained into this hole can be pumped out of the lab. Light sources should be placed below and beside the holding tank and diffused by large plates. For camera to capture the plan view and the front view of the tank at the same time, a mirror is needed to set inclined above the tank to provide the plan view.

Table 4.1: The range of Re and Ri in each of the model tanks used in the experiment.

Item	Re	Ri
Real tank	$10^4 \rightarrow 10^6$	$-10^2 \rightarrow 10^2$
Square tank	$\sim 10^4$	$-10^2 \rightarrow 10^2$
'J'-type tank	$\sim 10^4$	$-10^2 \rightarrow 10^2$
In-line tank	$10^3 \rightarrow 10^4$	$-10^3 \rightarrow 10^3$

5. Pumping and piping. A submersible centrifugal pump (maximum flow rate: 4.7×10^{-3} m^3/s; maximum head: 7.5 m) is used to provide momentum for the external water to flush the internal water through a model tank. A control valve is used to adjust the flow rate and a flow meter is set on the pipe to read the flow rate. To fill the tank with clear water, the tank inlet is connected to the water tap with a pipe. A three-way pipe is used to combine the tank inlet to both the pump and the water tap. For the square tank, the two outlets are connected to the draining hole with two long soft pipes. The water flushed out of the 'J'-type tank drains by gravity through the hole of the holding tank.

6. Scaling. According to the size of the laboratory, the geometrical scale of the model tanks to a real ballast tank is about 1/100. The dynamical property of the flow inside a ballast tank can be represented by Ri and Re. As discussed in Section 3.2, the typical Ri and Re are about $-10^2 \rightarrow 10^2$ and $\sim 10^4$ inside the tank, respectively. The experimental Ri and Re need to match the practical values in a real ballast tank as close as possible by changing the inflow rate and the salinity of the flushing water. In the unstratified tests, the inflow rate is set as 2.5×10^{-3} m^3/s, and the diameter of the inlet pipe is 0.02 m so that the local Re near the nozzle and the model tank is about $10^3 \rightarrow 10^4$. To test the density effect in the in-line tank, the density contrast between the tank water and the water used to flush the tank ($\Delta\rho/\rho$) varies from -0.04 to 0.04, and the inflow rate varies from 2.5×10^{-4} to 2.5×10^{-3} m^3/s, so that the Ri varies from -10^3 to 10^3 inside the tank, which covers the range of real Ri. The range of Re and

Ri inside each of the model tanks are listed in Table 4.1.

7. Data recording. The variation of dye concentration during flushing is measured by analysing the change of light intensity in the tank. Thus there needs a camera to record images continuously from different views of the tank. The camera on a tripod should stand at a fixed position in front of the tank, with a distance that can make it capture the whole view of the tank. The images taken by the camera need to be saved in a computer and analysed by Matlab Image Processing Toolbox.

4.3 Experimental apparatus

Three acrylic model tanks were employed in the experimental study. The first one was a closed square tank of width 0.61 m and height 0.2 m, shown in Figure 4.1(a,b,c), which was designed based on the geometry of a double bottom tank. Three PVC pipes with valves were inserted through the cover into the tank as potential inlets, and on the other side of the cover, another three PVC pipes were inserted into the tank as potential outlets. To generate the 2×2 and 3×3 internal configurations, six plates in total were employed, each of which was 0.61 m long, 0.2 m high and 0.01 m thick. There was a 0.1 m long and 0.01 m thick gap in the middle of each plate, so that the two plates, shown in Figure 4.2(a,b), could be crossed with each other and inserted into the tank to generate the 2×2 internal configuration (see Figure 4.1(b,c)). The four plates each of which had three circular holes could be crossed with each other to generate the 3×3 internal configuration (see Figure 4.1(d)). All of these circular holes had an diameter of 0.1 m and located in the middle height between two neighbouring compartments. The tank volume is 0.075 m^3.

The second one was a 'J'-type tank consisting of 5×4 compartments with one inlet and two outlets (see Figure 4.1(d)), which was designed based on the geometry of a double hull tank. The holes between compartments in the longitudinal and transverse directions were different. This tank was charactered by a closed horizontal section (bottom and hopper tank), open turning section (side tank), internal geometry with

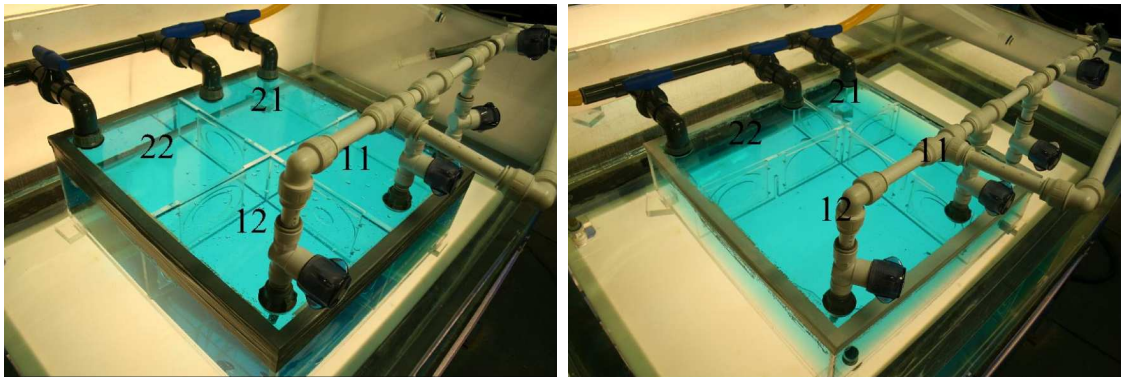

(a)

(b)

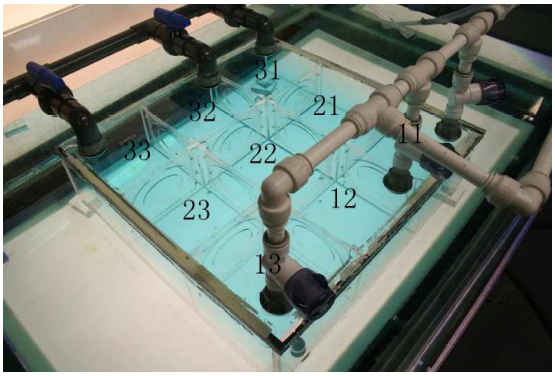

(c)

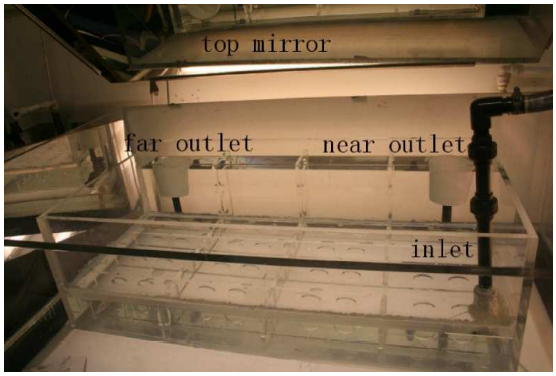

(d)

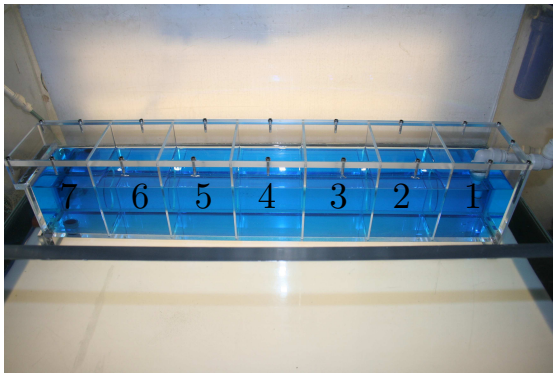

(e)

Figure 4.1: Photographs of (a) the 2×2 square tank with interconnecting holes of different sizes, (b) the 2×2 square tank with compartments of different sizes, (c) the 3×3 square tank, (d) the 5×4 'J'-type tank, and (e) the 1×7 tank used in the experimental study.

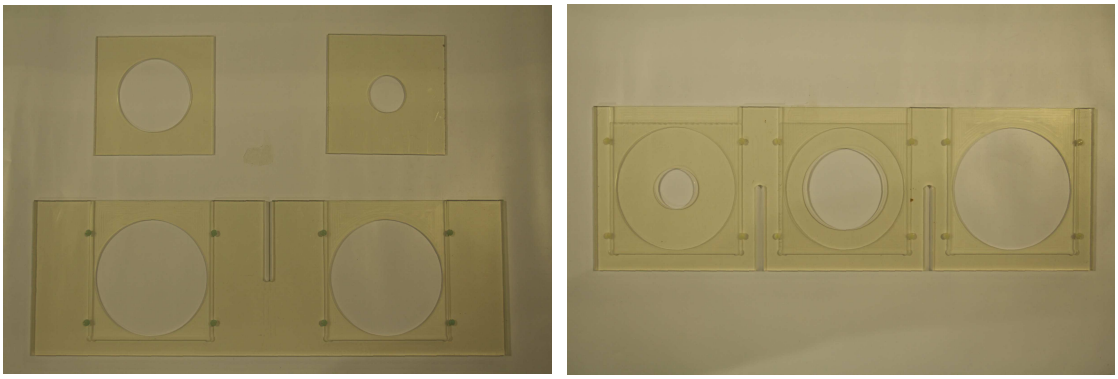

(a) (b)

Figure 4.2: Photographs of (a) a rectangular plate with two holes and two square plates with different sizes of holes, and (b) a rectangular plate with three holes used in the experimental study.

Table 4.2: The structure and dimensions of the 5×4 model tank used in the experiment.

Item	Horizontal section	Vertical section
Row number	4	1
Column number	4	4
Compartment length (m)	0.25	0.25
Compartment width (m)	0.1	0.13
Compartment height (m)	0.1	0.3
Number of lightening holes between two compartments	Longitudinal 1 Transverse 2	3
Diameter of lightening holes (m)	0.005	0.008

longitudinal and transverse frames, the filling pipes and two overflow arrangements with fixed height. Semicircular limber holes with radius 0.005 m were added at the top and bottom of each interconnecting wall, which helped to flush air out of the tank. The model tank was designed to be geometrically complex, the detailed structure and dimension of which are listed in Table 4.2. Water was pumped in through a 0.02 m diameter hole at the ceiling of the horizontal section, and exited from funnels fixed at height 0.28 m of the tank. The total volume of the tank is 0.075 m^3: each of the 16 horizontal compartments has a volume of 0.0025 m^3, and the volume of compartments 51, 52, 53 and 54 is 0.008 m^3, 0.0095 m^3, 0.0095 m^3 and 0.008 m^3, respectively.

The third tank was composed of seven compartments connected in line, which was 1.13 m long, 0.18 m wide and 0.26 m high inside, shown in Figure 4.1(e). Each compartment had an internal square base (0.15 m $\times$ 0.15 m) and height 0.2 m. Between neighbouring compartments, a rectangular plate (0.205 m high $\times$ 0.16 m wide $\times$ 0.0005 m thick) with a circular hole (diameter 0.0075 m) was inserted to the groove of the tank. A rectangular opening with a sloped weir underneath was adopted as the outlet on the left side of the tank. The opening on the top of the side wall was 0.15 m wide and 0.05 m high. The tank could hold water at a height of 0.15 m inside. A cover was screwed onto the tank. An inlet PVC pipe with a valve was inserted to the first side compartment through the right side of the tank, and a 90 degree elbow pipe was connected to guide the incoming fluid downward. There was a draining pipe hole on the base of the outlet compartment on the left side, and another 90 degree elbow pipe was used to guide the flow out of the tank. A rubber cork was used to block the hole during the flushing experiment. Sealing strips were pasted underneath the edge of the tank to prevent discharged fluid flowing back to the bottom of the tank to influence image processing.

The acrylic model tank was placed in a holding tank with length 1.5 m, width 1 m and height 0.5 m. The holding tank had a hole of diameter 0.02 m, which was used to drain the fluid pumped out of the model tank. The holding tank was illuminated by uniform diffuse light sources placed beneath and behind; an inclined mirror was placed above it to obtain the plan view (see Figure 4.1(e)). A submersible pump was employed to supply inflow with a pipe via a flow meter, from a large water bucket of

volume 0.6 m^3.

4.4 Experimental procedure

At the start of each experiment, the model tank was filled with clear water, and then a dilute methylene blue dye solution (concentration 0.1 mg/l) was pumped into the model tank via the inlet. In the unstratified experiments, the inflow rate was fixed at 2.5×10^{-4} m^3/s (according to test (1) described at the end of Section 3.5). For each tank configuration, the Reynolds number at the nozzle exit was $Re_n \sim 8000$; in the stratified experiments, the inflow rate varied from 2.5×10^{-5} to 2.5×10^{-4} m^3/s. During the flushing, a black and white C-Mount camera with a Megapixel progressive 2/3 CCD was set at a fixed position in front of the model tank, which was able to capture the front view of the model tank directly as well as the plan view from the top mirror. Images of size 1280 pixel $\times$ 960 pixel were taken at a rate of 7.5 frames per second by the camera and saved as a BMP file every 100 frames in a desktop computer.

To test the influence of boundary conditions (test (2) described at the end of Section 3.5), for each tank configuration in the unstratified experiments, three outlet arrangements were considered: only the far outlet was open ('far open' case), only the near outlet was open ('near open' case), and both outlets were open ('both open' case); for the stratified case, only the far outlet was kept open for the square/rectangular tanks.

4.5 Experimental principle

The experiments involved measuring the fraction of initial water in each compartment that is flushed out when water is injected into the tank. With the help of the inclined mirror, the camera captured a plan view of the tank. Dye water was injected into the tank (Kamada et al., 2004). An optical method was used to assess the mass of dye within each compartment based on classical absorption theory of Lambert-Beer (Rahim et al., 2010; Suhling et al., 2001; Zeng et al., 2010). The image processing was

based on the principle that the depth integrated dye concentration at a point in water can be related to the intensity of light passing through the dye water and the distance travelled by the light in the water, shown in Figure 4.3. The dye concentration at point (x, y) can then be related to the change in light intensity through

$$C_I(x,y) = \int_0^l C(x,y,z)\mathrm{d}z = f\left(\log\frac{I_0(x,y)}{I(x,y)}\right), \tag{4.1}$$

where l is the distance in the z-direction that the light travels in the water, I_0 is the light intensity after the light travels through clear water, and I is the light intensity after the light travels through dye water. The function $f(x)$ is determined by a series of calibration tests for fixed l. The volume averaged flushed fraction in compartment $[i][j]$ is

$$C_{[i][j]}(T) = \frac{\int_{A_{[i][j]}} C_I(x,y)\mathrm{d}x\mathrm{d}y}{\int_{A_{[i][j]}} C_{I_0}(x,y)\mathrm{d}x\mathrm{d}y}, \tag{4.2}$$

where $C_{I_0}(x,y)$ is the depth integrated dye concentration at point (x,y) when compartment $[i][j]$ is completely filled with dye water.

4.5.1 Calibration

A calibration test was undertaken by studying the fractional attenuation of light intensity as a function of the dye concentration in the water, so as to determine the dye dosage of the flushing water. Several dyestuffs including methylene blue (Kamada et al., 2004), Rhodamine-6G dye (Wilson et al., 2006) and food colouring dye (Kim et al., 2009) were used to make colourful water in previous studies. In this study, methylene blue hydrate puriss was selected, which was mixed with water in the large holding bucket. A rectangular tank of length 0.296 m, width 0.194 m and height 0.2 m was used for calibration. Methylene blue was mixed with water to make the condensate dye solution at a concentration of 0.4 g/l, and then the condensate dye solution was added to the tank which had contained 10 litres clear water. The volume of the condensate dye solution added to the tank was from 0 to 5 ml with a step of 0.5 ml, so the corresponding dye concentration in the tank was from 0 to 0.2 mg/l

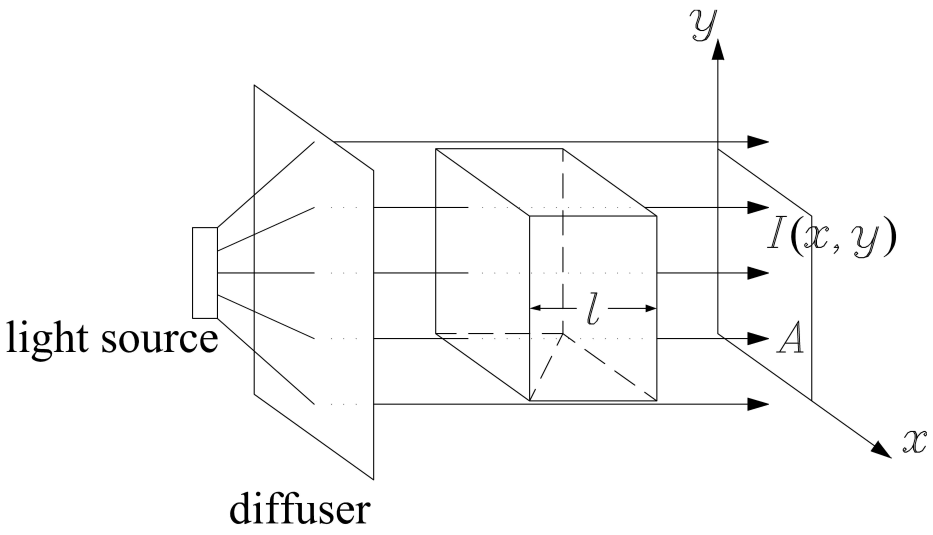

Figure 4.3: Schematic of the image processing principle. The light source is diffused by a white plate, then travelled through a rectangular compartment with dye concentration C. The projection plane is assumed to locate behind the compartment forward the light travel direction, with area A.

with a step of 0.02 mg/l. For each dye concentration, an image was taken by the camera at a fixed position in front of the tank, saved as a BMP file.

To work out the attenuation of the light intensity through the tank against different dye concentrations, Matlab Image Processing Toolbox (Curran and Davies, 2004; Santosh et al., 2007; Shrestha et al., 2008) was employed. There were 11 images taken for dye concentration from 0 to 0.2 mg/l. When a BMP image file was loaded in Matlab, it was represented as a 960×1280 matrix of unsigned 8-bit integers, the value range of which was between 0 and 255. The value of a point in the matrix represented the light intensity of its corresponding point in the image. The value of a black point was 0, while that of a white point was 255. That is, the darker a point was, the smaller its value was; and the lighter the larger. The image taken from the tank with clear water (without methylene blue) was the base image, represented as the base matrix; and the images taken with methylene blue were named as concentration images, represented by concentration matrices. Two steps were needed to obtain $\log(I_0/I)/l$ versus dye concentrations:

1. The front view of the tank was masked off from the base image, and saved as a 960×1280 logical matrix, the size of which was the same as that of the base image and the values in which were either 0 or 1. The value of a point inside the mask region was 1, while that outside the mask region was 0. For each concentration, the front view of the tank was represented as a 960×1280 matrix, each number in which was the product of the corresponding number in the image matrix and that in the mask matrix.

2. The light attenuations were worked out for different concentrations. The ratio of the light intensity of each point in the base matrix to that in each concentration matrix was taken logarithm individually, and then divided by the width of the tank. The obtained values of all the points in the front view matrix for each concentration were averaged.

$\log(I_0/I)/l$ versus dye concentration in the tank is plotted in Figure 4.4. Below 0.2 mg/l, the relationship between the light attenuation and the methylene blue concentration is close to be linear. The concentration range from 0 to 0.2 mg/l can be used for the flushing experiments. The methylene blue concentration in the flushing water was determined as 0.1 mg/l.

4.5.2 Analytical tools

For the flushing experiments, Matlab Image Processing Toolbox was used to determine the fraction of initial fluid in each compartment that was removed, as a function of time.

1. Each compartment of the tank was masked off. An image of the tank with clear water was taken as the base image. Each compartment of the tank was individually masked off from the base image as a mask file. The light intensity of a compartment was represented as a 960×1280 matrix, each number in which was the product of the corresponding number in the image matrix and the corresponding value in the corresponding mask matrix.

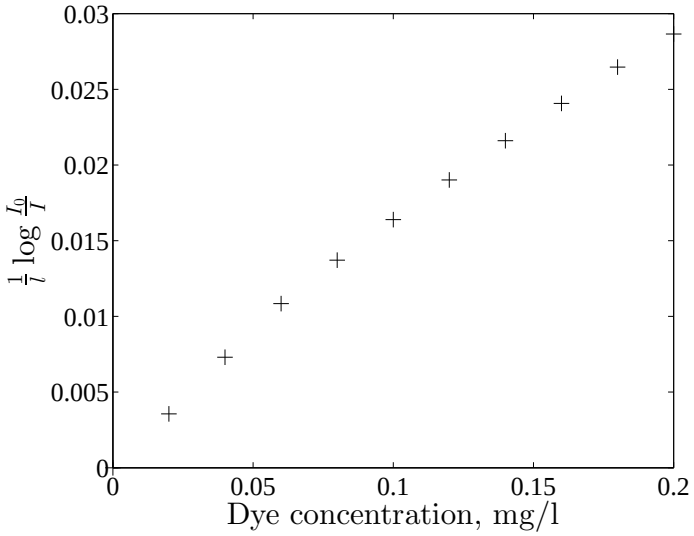

Figure 4.4: Calibration of $\log(I_0/I)/l$ against dye concentration.

2. Time series of $C_{[i][j]}$ was plotted. The relative dye concentration in each compartment varying over time could be figured out by analysing its plan view in the images. When dye water was pumped to mix with clear water in the tank, the light intensity of the mixed region became darker. Thus, the ratio of the original light intensity (the number in the base image matrix) of a point in a compartment, to the light intensity of the same point in other images was able to be calculated. As light intensity attenuation is proportional to the exponential of dye concentration and the distance it travels through the light absorbent, the logarithm of the above ratio was divided by the corresponding distance it travelled through the compartment. For each image, this quotient was proportional to the dye concentration in the point at the time that the image corresponded to. Since the inflow rate, the effective tank volume and the time interval between two neighbouring images were known, the dimensionless time that each image represented could be worked out. The final image was taken when the tank was completely filled with dye water, so the concentration of each intermediate image could be normalised by being divided by the quotient calculated from the base image and the final image. The relative concentration of each

compartment was the average value of the relative concentrations of all selected points in this compartment. Thus, times series of $C_{[i][j]}$ was worked out.

3. Time series of $\bar{C}$ was plotted. The normalised dye concentration of the whole tank $\bar{C}$ against time was worked out, which was the average value of the mean relative concentration of each compartment against time. Then the normalized mean concentration curve of the whole tank over time was plotted.

4. $\alpha_{\frac{1}{2},[i][j]}$ versus $T_{\frac{1}{2},[i][j]}$ was plotted. $T_{\frac{1}{2},[i][j]}$, the time when the relative mean concentration of compartment $[i][j]$ reached 0.5, and $\alpha_{\frac{1}{2},[i][j]}$, the corresponding gradient of the normalized mean concentration curve of compartment $[i][j]$ from the plan view when $T_{\frac{1}{2},[i][j]} = 0.5$ were figured out. $T_{\frac{1}{2},[i][j]}$ was estimated by interpolating $C_{[i][j]}$ to determine when $C_{[i][j]} = 0.5$. There were two vectors, one representing the relative concentration, and the other representing the corresponding time. By interpolation and difference quotient, the corresponding time when the concentration was equal to 0.5 would be worked out. $\alpha_{\frac{1}{2},[i][j]}$ was estimated by linearly regressing $C_{[i][j]}$ with T over the interval $|C_{[i][j]} - 0.5| \leq 0.1$ and identified $\alpha_{\frac{1}{2},[i][j]}$ proportional to the slope of the curve. $\alpha_{\frac{1}{2},[i][j]}$ versus $T_{\frac{1}{2},[i][j]}$ was plotted.

5. The plan view and the front view of the tank against T were contour plotted respectively. For an image, the plan and front view of each compartment were individually masked off and then integrated, respectively. Different values in the image matrix were represented with different colour intensities. Values varying from 0 to 1 were plotted from black, red, yellow to white. The time series of the integrated concentration field showed the variation of the visual information of the fluid flow within each compartment of the tank.

4.6 Diagnostic tools

The diagnostic tools defined in §3.3.4 to analyse the model predictions were applied to analyse the experimental data. For images captured from the experiments, each

compartment from the plan view was individually masked so that its time series (4.2) could be evaluated.

4.7 Experimental errors

The major errors of the experimental measurement were caused by masking and calibration. From a series of calibration tests, a standard error of 1.75% was observed in relating dye concentration to light intensity. On the top and bottom of the tank, lack of transparency in some points may decrease the measured dye concentration by about 0.5%. The compartments of the tank are individually assessed by masking part of the total image. The compartments had dimensions of around 100×100 pixels; masking is accurate to within 5 pixels and thus gives an error of 0.25% in the masked area. During the pumping and flushing, small bubbles attached to the wall that form due to temperature change inside the tank may lead to a maximum error of 0.5%. The total experimental measurements have an error less than 3%. More systematic errors occur for the multiple outlets ('both open') configuration because of the difficulty of setting the pressure on the two outlets to be equal.

4.8 Summary

Experimental methodology and diagnostic tools were built up. Three clear model tanks were constructed to test the fluid exchange when dye water was pumped in. An optical method was used to analyse the variation of dye concentration in each compartment of the tank. Calibration results show that the logarithm of light intensity attenuation increases linearly with the methylene blue concentration at the range of 0-0.2 mg/l. Matlab Image Processing Toolbox was used either to determine the fraction of exchanged fluid in each compartment, or to visualise the fluid exchange in it. The experimental measurements had an error less than 3%. The diagnostic tools adopted for the model predictions are applied for analysing the experimental data.

Chapter 5

Flushing Homogeneous Tanks

5.1 Introduction

A series of experiments were undertaken to provide a means of testing quantitatively the capability of the multizone model to capture the exchange processes in multi-compartment tanks. The effect of geometry on flushing is illustrated by examining a series of tanks with increasing geometrical complexity from a 2×2, 3×3 to 5×4 tank. It will be seen how the theoretical predictions and experimental measurements match each other. The validation of the model provides implications on the effect of subdividing an identical ballast tank for different outlet arrangements. To reduce the number of variables, the flow rate was fixed to examine different outlet arrangements for each tank. As described at the end of Section 3.5, this study will examine (1) the fluid exchange by steadily releasing flow to a node and (2) the influence of flux constrained outlets versus pressure controlled outflow. These two test cases are analysed using the following constraints to the model:

(1) flushed fraction $C = 1$ at inlet and $C = 0$ at $T = 0$ in the tank, for fixed flux rate Q. Experimentally, $C = 1$ corresponds to the fully dyed water that is used to flush the tank; $C = 0$ corresponds to the clear water that is originally inside the tank. The exchange volume T varies from 0 to 3, as the IMO regulation focuses on three exchange volumes.

(2) the outlet arrangements are set as flux constrained ($Q_{22,\text{out}} = Q$ corresponding to 'far open' or $Q_{21,\text{out}} = Q$ corresponding to 'near open') or pressure controlled ($p_{21} = p_{22} = 0$ corresponding to 'both open').

5.2 Comparison between theoretical and experimental results

To build up a physical picture of the dynamics, the simplest configuration - a four connected compartment arrangement with one inlet and two outlets is first analysed, shown in Figure 5.1(a). In order to simplify the analysis, the four compartments are assumed to have the same shape and dimensions, and all the four holes between neighbouring compartments are assumed to be the same thin-wall circular holes in size, height and resistance. Similarly for the 3×3 case (see Figure 5.1(b)), all the circular holes between neighbouring compartments are geometrically congruent and same in height.

5.2.1 Flushing the 2×2 square tank

Figure 5.2 shows the vertically integrated flushed fraction field from the plan view of the 2×2 tank at T =0.5, 1.0, 2.0, and 3.0 for the 'far open', 'near open' and 'both open' cases in the experiment. For all cases, compartment 11 was well mixed, due to the severe turbulence near the inlet. For the 'far open' case shown in Figure 5.2(a), the flushed fraction of compartment 12 and that of compartment 21 are roughly symmetrical according to the diagonal line at all times; for 'near open' shown in Figure 5.2(b), the flushed fraction of compartment 21 seemed to be averagely higher than that of compartment 12 at $T = 0.5$ and $T = 1.0$, but averagely lower at $T = 2.0$ and $T = 3.0$, because compartment 12 was flushed by compartment 22, and compartment 22 was flushed very slowly so that a large amount of initial water remained in it; for 'both open' shown in Figure 5.2(c), $C_{21} > C_{12}$ because $f_{11,21} > f_{11,12}$. The flushed fraction for 'both open' seemed lower than that for 'far open', but higher than that for 'near open', which agreed with the model prediction.

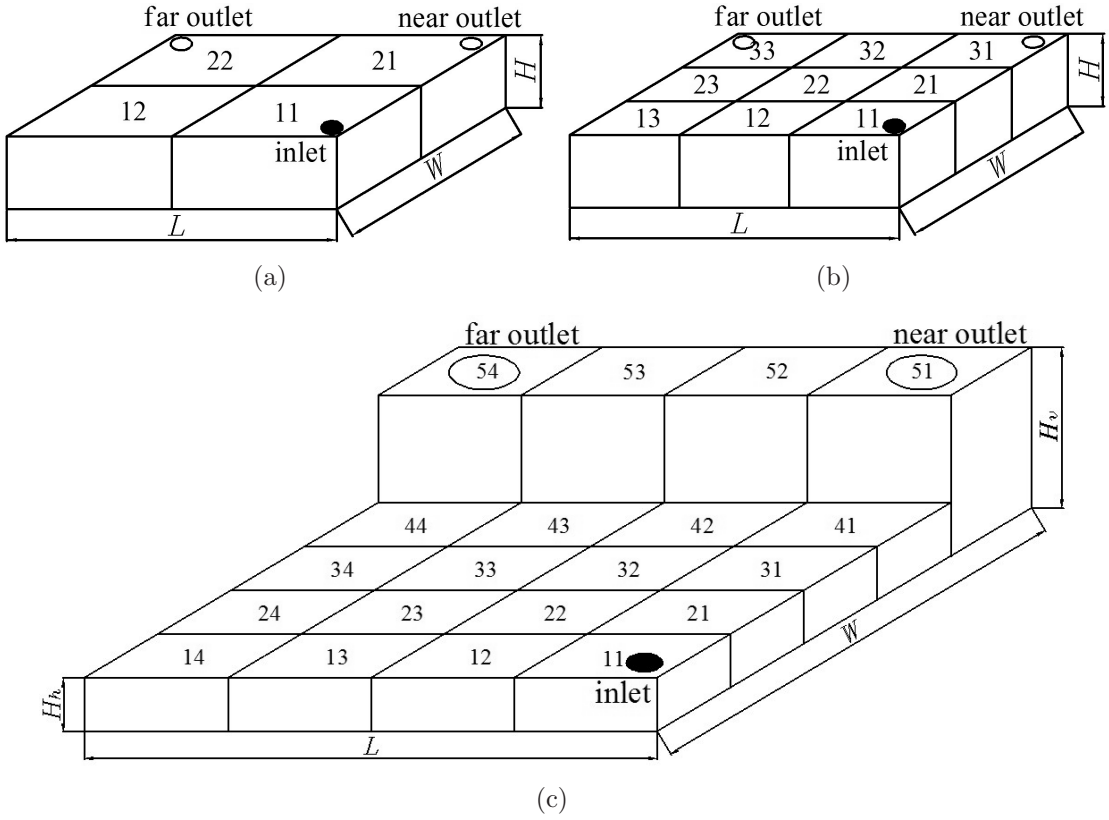

Figure 5.1: Elevated schematics of a (a) 2×2 square tank, (b) 3×3 square tank, and (c) 5×4 'J'-type tank with one inlet and two outlets. The inlet and outlets on the top of the tanks are indicated.

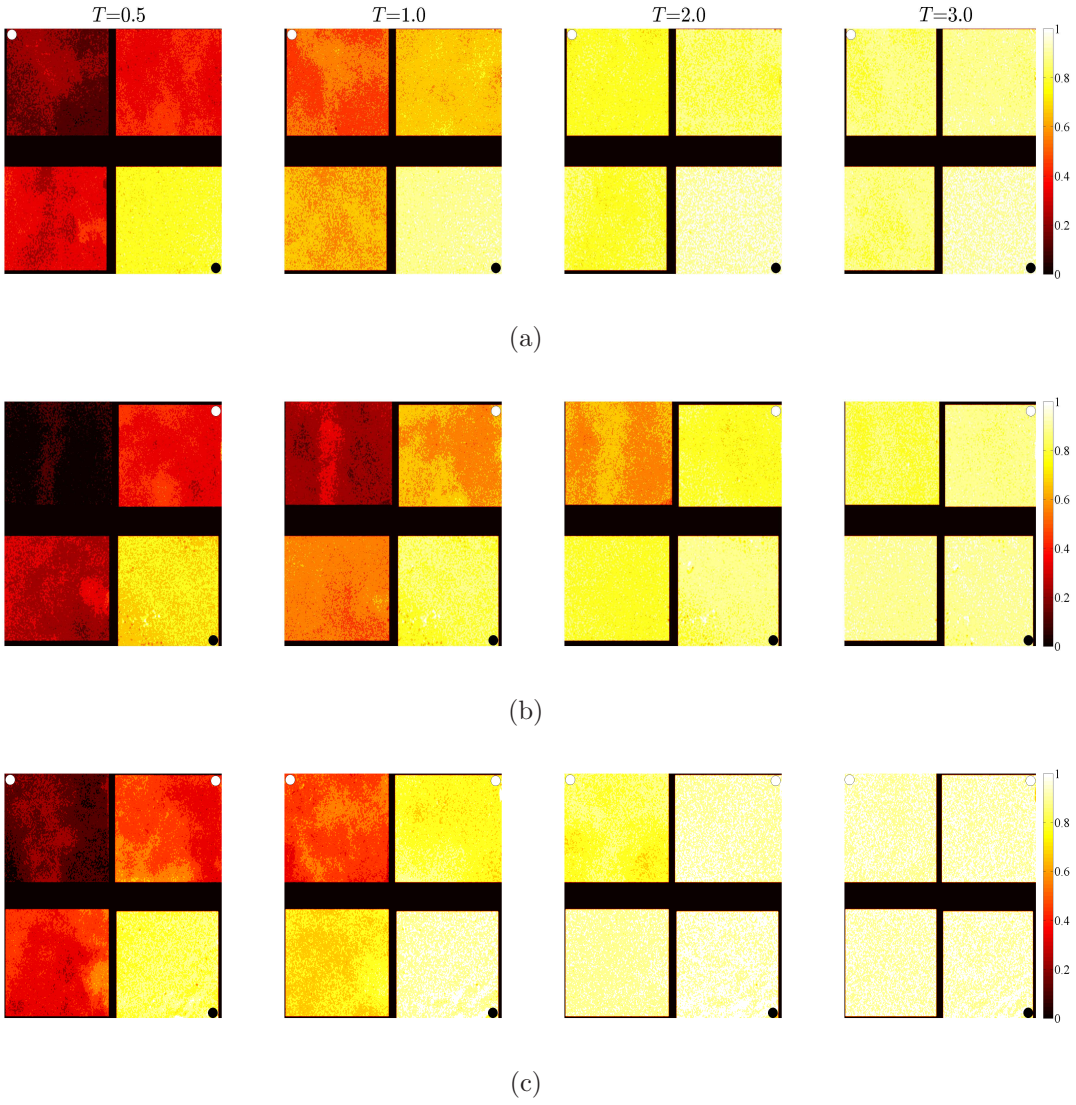

Figure 5.2: The vertically integrated flushed fraction field from the plan view of the 2×2 tank at T =0.5, 1.0, 2.0, and 3.0 in the flushing experiment. The inlet on the right bottom, and the two outlets on both sides of the top are indicated by a closed circle and two open circles, respectively. The figures correspond to (a) 'far open', (b) 'near open', and (c) 'both open' cases.

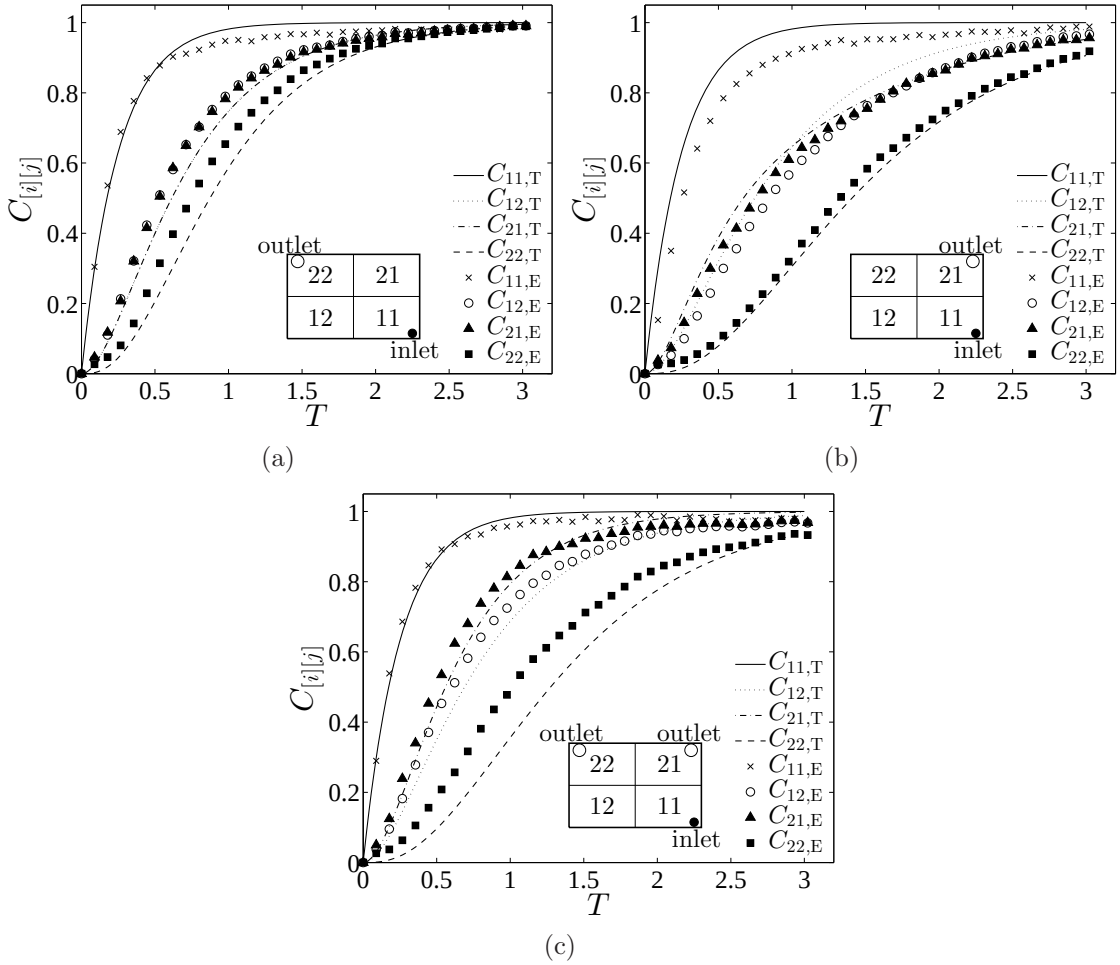

Figure 5.3: The theoretical predictions of the variation in time of the flushed fraction in each compartment are shown on the left hand side, with the corresponding experimental results on the right hand side for the 2×2 tank. '$C_{[i][j],\mathrm{T}}$' represents theoretical prediction, while '$C_{[i][j],\mathrm{E}}$' represents experimental measurement. The figures correspond to (a) 'far open', (b) 'near open', and (c) 'both open' cases.

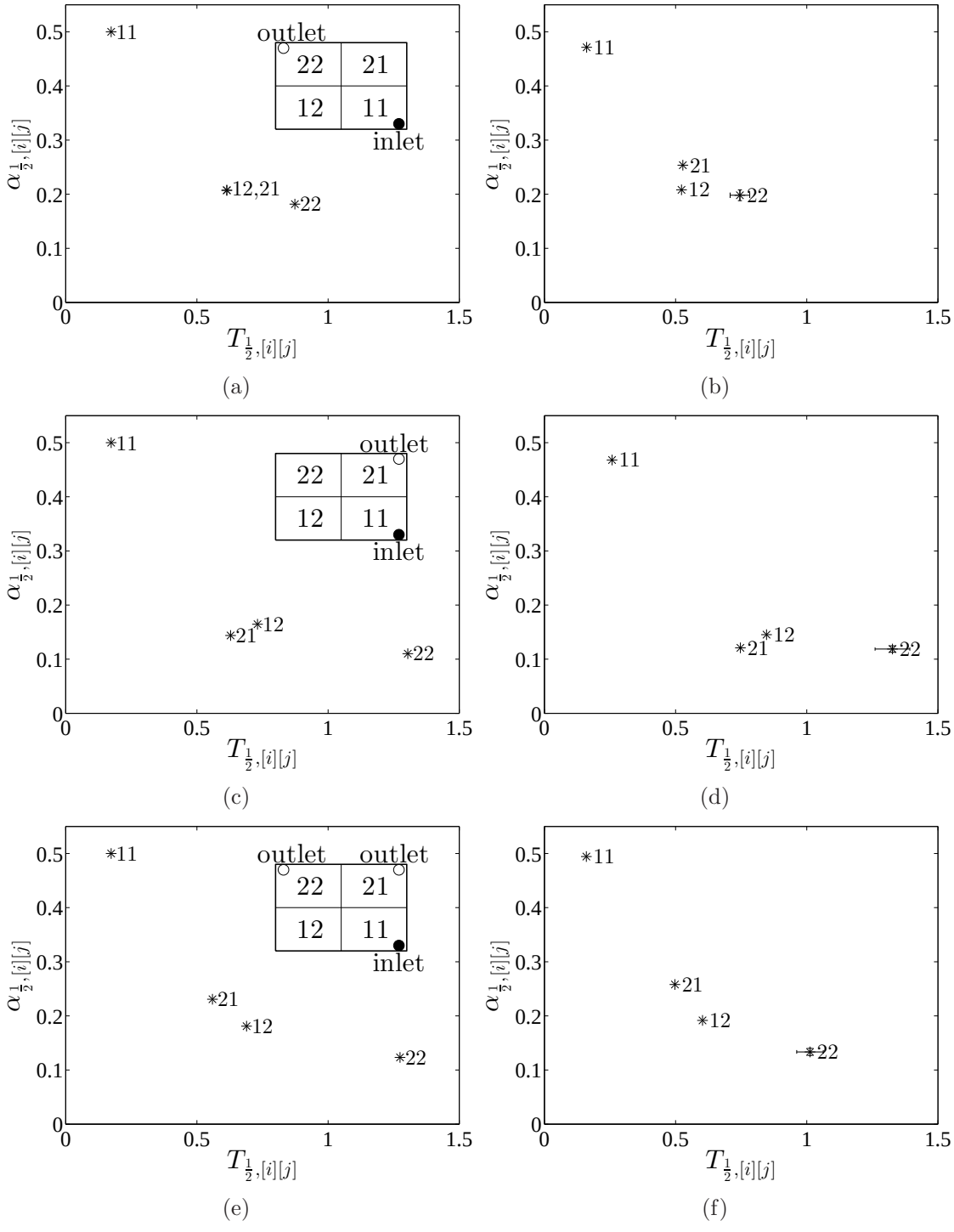

Figure 5.4: The theoretical predictions of the scatter plot $\alpha_{\frac{1}{2},[i][j]}$ versus $T_{\frac{1}{2},[i][j]}$ are shown on the left hand side, with the corresponding experimental results on the right hand side for the 2×2 tank. The figures correspond to (a, b) 'far open', (c, d) 'near open', and (e, f) 'both open' cases.

Figure 5.3 shows the variation in time of the flushed fraction in each compartment of the 2×2 tank for all the three cases considered. The curves represent theoretical predictions ($C_{[i][j],\mathrm{T}}$), while the scatter points represent experimental measurements ($C_{[i][j],\mathrm{E}}$). In all cases, C_{11} increases at the highest rate because the inlet is to compartment 11, which is not influenced by the outlet arrangement; C_{22} is the slowest to be flushed as a consequence of being the farthest from the inlet; Both C_{12} and C_{21} rise between C_{11} and C_{22}. For the 'far open' case, the symmetry in the flow pathways means that $C_{12} = C_{21}$. For the 'near open' case, there is a cross over between C_{12} and C_{21}. This is because while $f_{11,21} > f_{11,12}$ leads to an initially faster increase in C_{21}, at a later time, the fluid with a lower flushed fraction is being transported from compartment 22 to 21 leading to $C_{12} > C_{21}$. For the 'both open' case, the flow largely passes through compartment 21 as $C_{21} > C_{12}$. The experimental measurements compare quite well with the model predictions. For the 'far open' case, C_{12} and C_{21} behaved nearly the same, which is expected due to the inherent symmetry of the flow; for 'near open', C_{21} grew faster from the beginning, until $T \approx 1.5$ when it was exceeded by C_{12}; for 'both open', C_{22} was a little underestimated because the theoretical model simply assumes that $p_{12} = p_{21}$. In fact, compartment 22 was flushed by not only the flow from compartment 12 but also that from compartment 21.

Figure 5.4(a, c, e) summarises the characteristic flushing rate versus the half flushed time in each of the compartments. In all cases, $\alpha_{\frac{1}{2},11} = 1/2$, $T_{\frac{1}{2},11} = \ln 2/4$ since the compartments are all the same size. The increase for compartments 12 and 21 are quite similar in all cases. While Figure 5.4(c) shows that compartment 12 is ultimately flushed slightly faster than 21, the values of $\alpha_{\frac{1}{2}}$ and $T_{\frac{1}{2}}$ do not capture this because they describe the initial characteristics of flushing. Compartment 22 is flushed at similar rates in both the 'near open' and 'both open' cases. Experimentally from figures 5.4(b, d, f), the corresponding $\alpha_{\frac{1}{2},[i][j]}$ versus $T_{\frac{1}{2},[i][j]}$ matched the model predictions. Overall, the experimental results were in close agreement with the model predictions for the 2×2 tank.

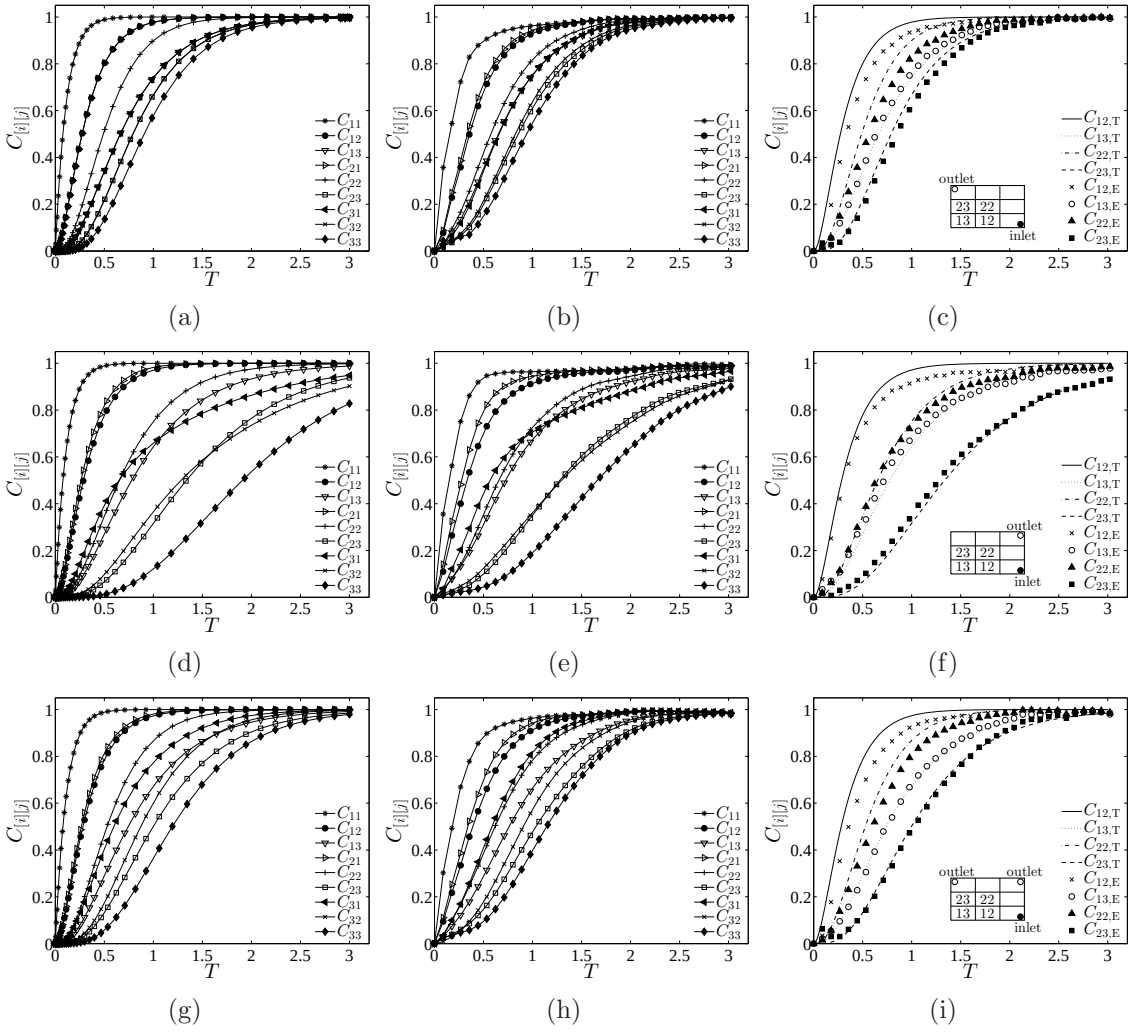

Figure 5.5: The (a, d, g) theoretical predictions and (b, e, h) experimental measurements of the variation in time of the flushed fraction in each compartment of the 3×3 tank. (c, f, i) show the comparison for four selected compartments, where '$C_{[i][j],\mathrm{T}}$' represents theoretical prediction and '$C_{[i][j],\mathrm{E}}$' represents experimental measurement. The figures correspond to (a, b, c) 'far open', (d, e, f) 'near open', and (g, h, i) 'both open' cases.

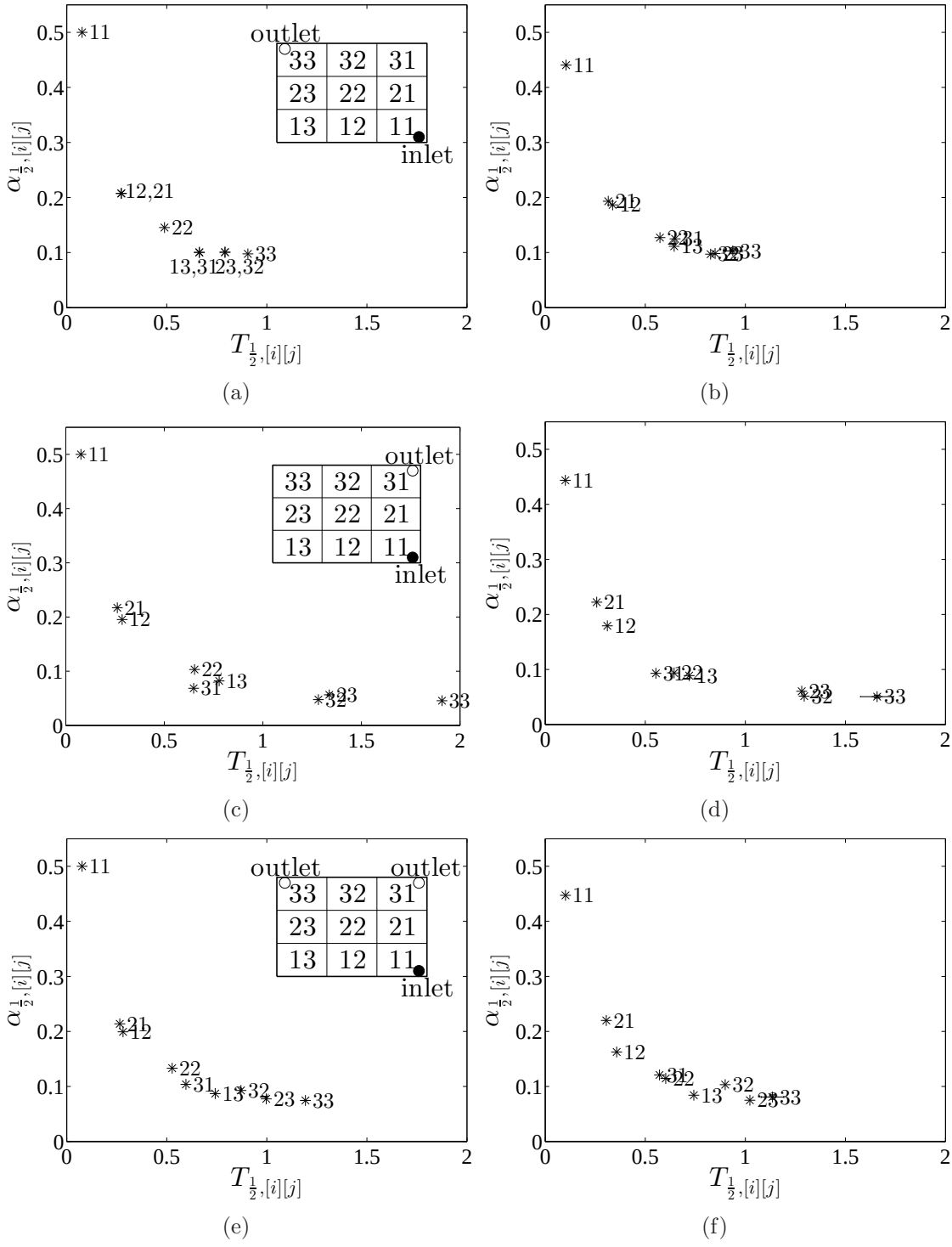

Figure 5.6: The theoretical predictions of the scatter plot $\alpha_{\frac{1}{2},[i][j]}$ versus $T_{\frac{1}{2},[i][j]}$ are shown on the left hand side, with the corresponding experimental results on the right hand side for the 3×3 tank. The figures correspond to (a, b) 'far open', (c, d) 'near open', and (e, f) 'both open' cases.

5.2.2 Flushing the 3×3 square tank

As the number of compartments increases, the complexity of the dynamics increases. The predictions of the variation in time of the flushed fraction and the characteristic flushing rate versus the half flushed time in each compartment of the 3×3 tank are shown in the left column of Figure 5.5 and 5.6, respectively. In all cases, compartment 11 is characterized by $\alpha_{\frac{1}{2},11} = 1/2$ and $T_{\frac{1}{2},11} = \ln 2/9$. Compartments 12 and 21 are flushed in a similar manner for the three cases because the flux through these compartments is weakly dependent by the global influence of the boundary condition. Compartment 33 is always flushed at a slower rate than all the other compartments due to its position. For the 'far open' case, due to the symmetry of the flow, $C_{12} = C_{21}$, $C_{13} = C_{31}$, and $C_{23} = C_{32}$ (see Figures 5.5(a) and 5.6(a)). The farther a compartment is from the inlet, the more slowly it is flushed. Compared with the 'far open' case, most compartments for the 'near open' case are flushed more slowly (see Figure 5.5(d)). From Figure 5.6(c), it can be seen that there are three groups of accumulated points: compartments 21 and 12, compartments 31, 22 and 13, and compartments 32 and 23. For the 'both open' case, most compartments are flushed more slowly than those for the 'far open' case, but faster than those for the 'near open' case (see Figure 5.5(g)). In general, compartments are half flushed at a later time in the 'both open' case than in the 'far open' case, but earlier than those in the 'near open' case (see Figure 5.6(a, c, e)).

The middle column of Figure 5.5 shows the experimental measurements of the flushed fraction in each compartment of the 3×3 tank as a function of time. For all cases, compartment 11 was flushed a little more slowly than expected. The probable reason is that the incoming fluid had not completely mixed with the original fluid in the compartment when it left, that is, the existence of holes between neighbouring compartments challenged the perfect mixing assumption within each compartment; compartment 11 was the first and fastest flushed compartment, so its flushing rate was influenced most severely by the non-perfect mixing condition. For the 'far open' case in Figure 5.5(b), $C_{12} \approx C_{21}$, $C_{13} \approx C_{31}$, and $C_{32} \approx C_{23}$; for the 'near open' case in Figure 5.5(d, e), C_{33} increased a little faster than predicted; for the 'both open' case in Figure 5.5(g, h), compartment 31 was flushed faster than predicted. To further

compare the experimental results with the theoretical results, the model predictions and experimental measurements of the variation in time of the flushed fraction in compartments 12, 13, 22 and 23 are plotted by the curves and scatter points, respectively in the right column of Figure 5.5. For all the three outlet arrangements, $C_{12} > C_{22} > C_{13} > C_{23}$, and C_{12} and C_{22} are a little overestimated. The agreement of the values of $\alpha_{\frac{1}{2},[i][j]}$ versus $T_{\frac{1}{2},[i][j]}$ between the theory and the experiments is quite good (see Figure 5.6); especially for the 'near open' case, the model successfully predicted the three grouped points: 12 and 21; 22, 13 and 31; and 23 and 32 (see Figure 5.6(c, d)). Overall, the theoretical model is able to capture the main character of the flushing in the experiments.

5.2.3 Flushing the 5×4 'J'-type tank

Figure 5.1(c) shows a schematic of a 5×4 tank which consists of compartments which have a rectangular footprint, and holes between neighbouring compartments are not the same in size and number (see Table 4.2). The resistance coefficients used to close the system of equations were estimated using (3.13). The theoretical predictions of the variation in time of the flushed fraction field are shown in Figure 5.7(a, c, e). For all the three outlet arrangements, the tank is flushed from the right bottom to the left top. At $T = 0.25$, the difference of the fraction field among these three cases is not significant. But at a later time, the tank is the most efficiently flushed for the 'far open' case, and more original fluid remains on the left corner compartments for the 'near open' case. The theoretical predictions of the flushed fraction as a function of time in each compartment are shown in Figure 5.8(a, c, e). The difficulty in interpreting Figure 5.8 means that a simpler set of metrics has to be considered. Figure 5.9 shows that the points donating $\alpha_{\frac{1}{2}}$ versus $T_{\frac{1}{2}}$ are grouped into two parts associated with the equal-sized horizontal compartments (the first to the fourth rows of the tank) and the larger vertical compartments (the fifth row). It can be seen that the horizontal compartments behave similarly for each case: in general, the nearer a compartment is located to the inlet, the faster and earlier it is flushed, leading to a bow-shaped decrease of the scatter plot of $\alpha_{\frac{1}{2},[i][j]}$ versus $T_{\frac{1}{2},[i][j]}$ (see Figure

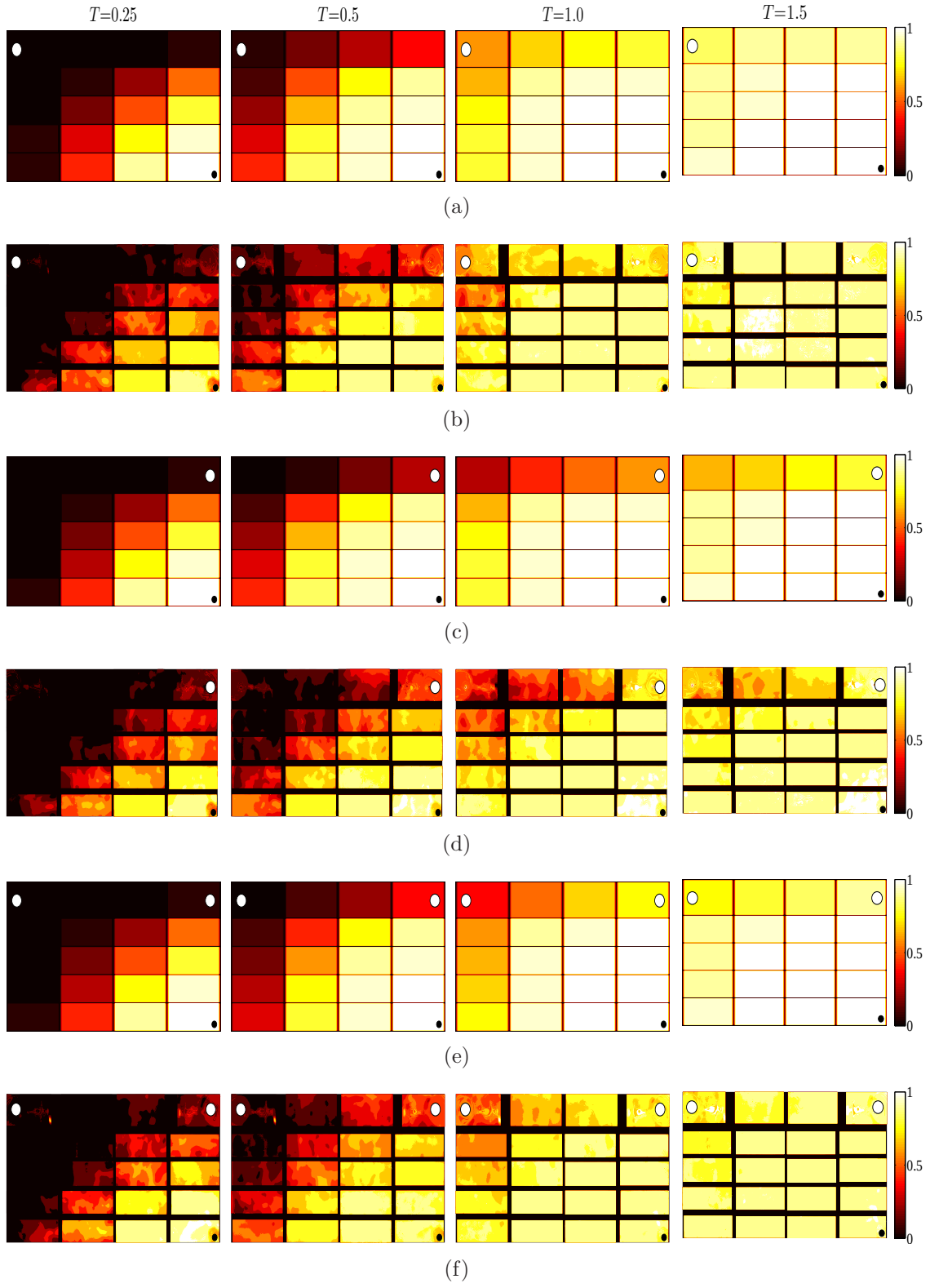

Figure 5.7: The theoretical predictions of the flushed fraction field in each compartment of the 5×4 tank at T =0.25, 0.5, 1 and 1.5 are shown in (a, c, e), with the corresponding experimental measurements in (b, d, f). The figures correspond to (a, b) 'far open', (c, d) 'near open', and (e, f) 'both open' cases. A black circle represents an inlet, and a white circle represents an outlet.

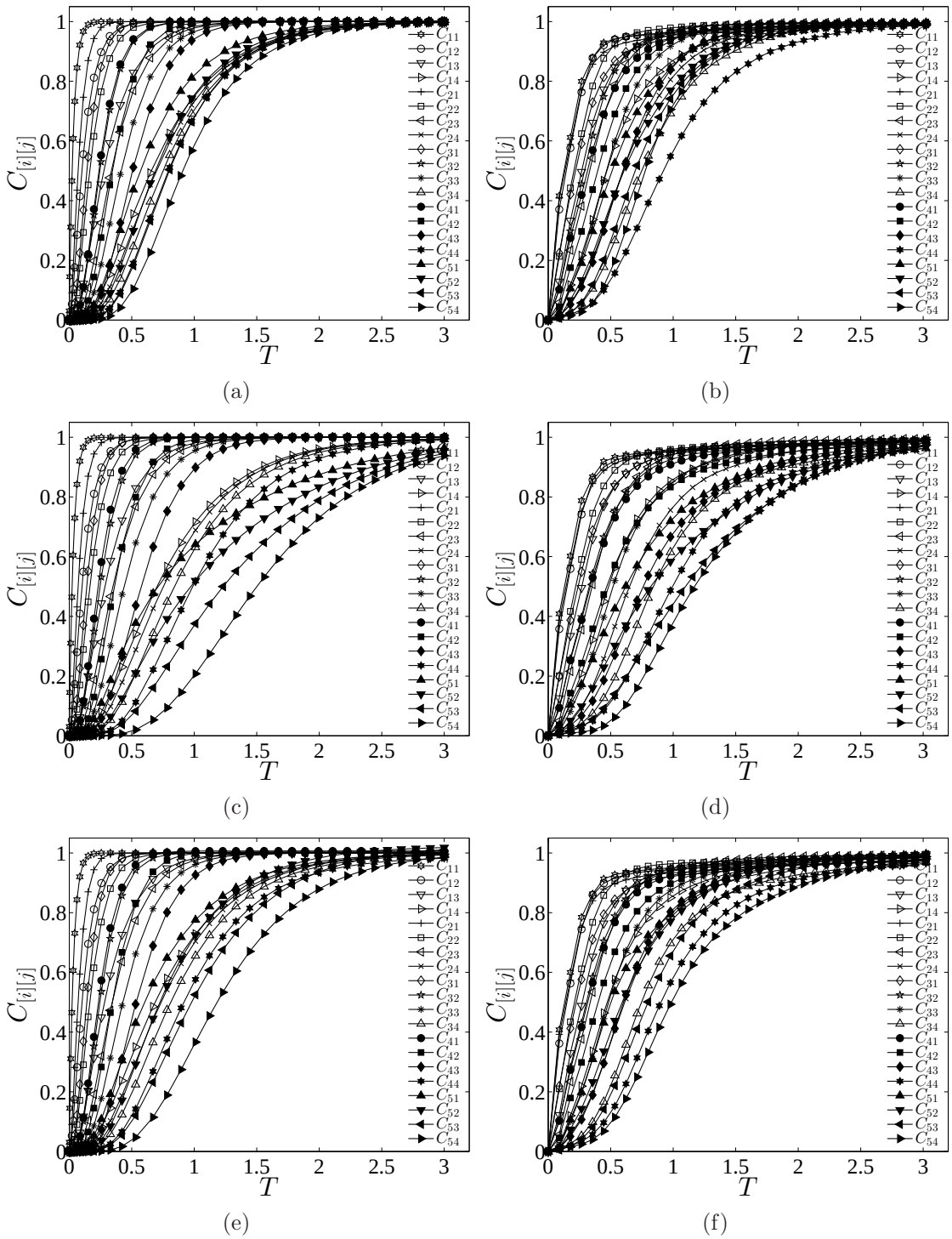

Figure 5.8: The theoretical predictions of the variation in time of the flushed fraction in each compartment are shown on the left hand side, with the corresponding experimental results on the right hand side for the 5×4 tank. The figures correspond to (a, b) 'far open', (c, d) 'near open', and (e, f) 'both open' cases.

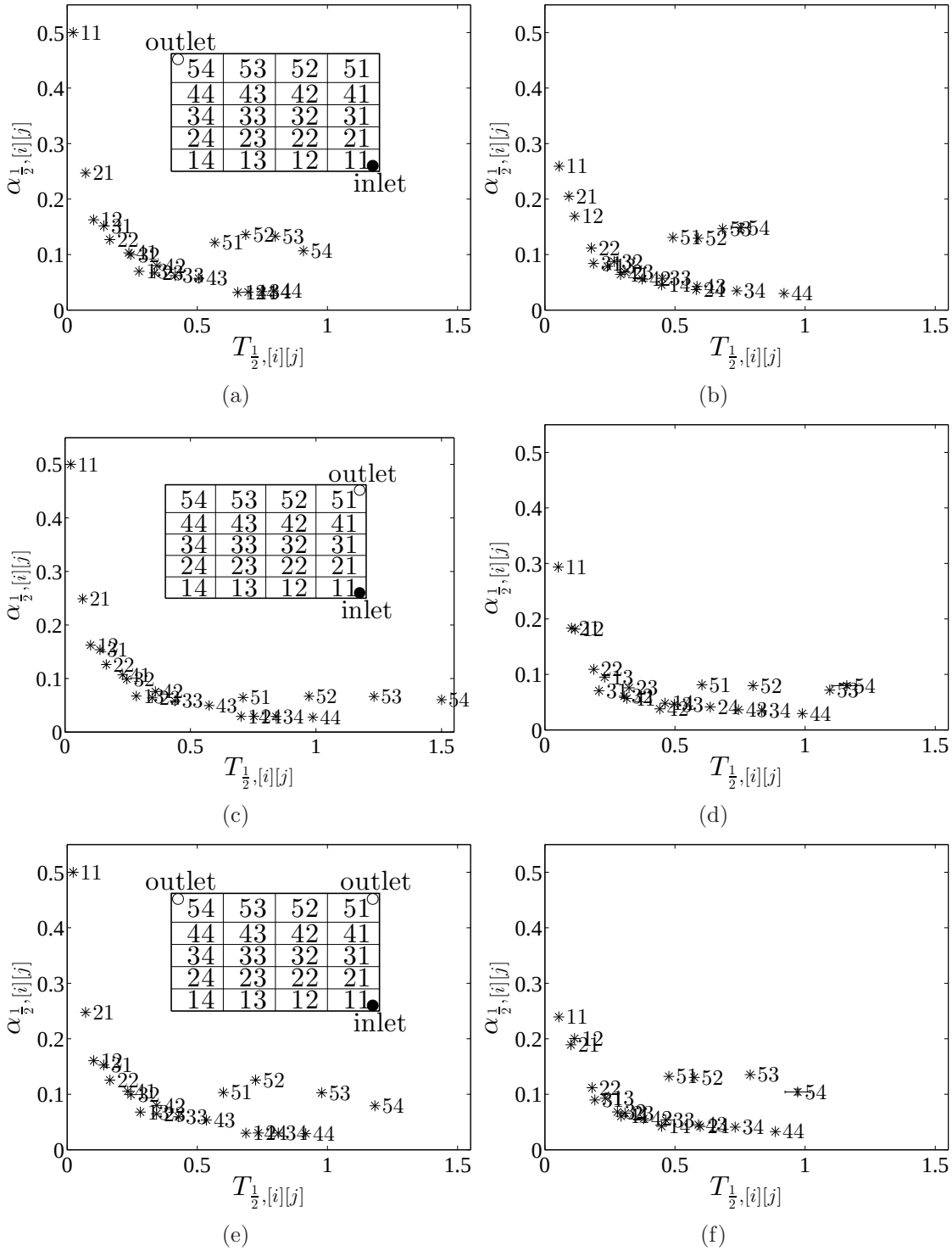

Figure 5.9: The theoretical predictions of the scatter plot $\alpha_{\frac{1}{2},[i][j]}$ versus $T_{\frac{1}{2},[i][j]}$ are shown on the left hand side, with the corresponding experimental results on the right hand side for the 5×4 tank. The figures correspond to (a) 'far open', (b) 'near open', and (c) 'both open' cases.

5.9(a, c, e)). For all cases, $T_{\frac{1}{2},11} = \ln 2V_{11}/V$, $\alpha_{\frac{1}{2},11} = 1/2$. For a large number of compartments, it would tend to be expected that the flow is 'radial' for short time where $u_r \sim 2Q/\pi r H_h$, where r is the distance from the inlet. This gives an approximate relation $\alpha_{\frac{1}{2}} \sim T_{\frac{1}{2}}^{-1}$, which is confirmed by plotting Figure 5.9 on a log-log scale. The relative positions of the points denoting the vertical compartments to those for the horizontal compartments are different for different outlet arrangements. The vertical compartments are flushed more slowly and later in the 'both open' case than in the 'far open' case, but faster and earlier than in the 'near open' case.

The experimental measurements of the variation in time of the flushed fraction field are shown in Figure 5.7(b, d, f). The experimental results agreed well with the model predictions. At an early time, the performance of each compartment was not significantly different among different outlet arrangements; at a later time, the residual fluid was the least for the 'far open' case, but the most for the 'near open' case. The model is able to capture the variation in time of the flushed fraction of each compartment and discern the performance difference of each compartment among the three outlet arrangements. Figure 5.8(b, d, f) shows the variation in time of the flushed fraction in each compartment of the 5×4 tank in the experiment. Generally for each case, the compartments nearer to the inlet began to be flushed earlier than those farther from it. When $T \leq 1.5$, the fraction curves of all the compartments were distributed more sparsely in the 'both open' case than those in the 'far open' case, but denser than those in the 'near open' case. Most flushed fractions of 'both open' got to equilibrium earlier than those of 'near open', but later than those of 'far open'. For all cases, C_{11} increased at the fastest rate, while C_{33} increased most slowly. C_{11} was more underestimated than that in the 3×3 tank. The probable reason is that the perfect mixing assumption of the model was challenged when the ratio of the hole area to the partition wall area between compartments (β) was too large. When the area of the hole of a compartment to its neighbouring compartment was too large, the incoming water could not mix sufficiently with the original water when it left the compartment. In our tests, β=19.6-38.6% for the 5×4 tank, which was much larger than that of the 2×2 tank (β=13.1%) and the 3×3 tank (β=4.91%). In real ballast tanks, the ratio is normally less than 15%. A possible reason for the longer residence

Table 5.1: The theoretical and experimental flushing efficiency at $T = 3$ of the three tanks considered with different outlet arrangements.

Compartment configuration	Theoretical/experimental flushing efficiency (%)		
	Far open	Near open	Both open
2×2	99.5/99.0	96.0/95.7	98.1/97.2
3×3	99.8/99.6	95.6/96.4	99.4/98.4
5×4	99.9/99.3	99.0/97.9	99.7/98.5

of the original water in some compartments (e.g. compartment 44) for the 'near open' and 'both open' cases is that the flux in the peripheral compartments decreased to $\sim 0.2Q$, giving a characteristic Reynolds number of $Re \simeq 600$, so that the turbulent diffusion was weak, leading to insufficient mixing and high residence time for fluid parcels in the recirculating region attached to the outlet holes. The bow-shaped decrease of $\alpha_{\frac{1}{2},[i][j]}$ in Figure 5.9(b, d, f) indicated that the farther a compartment was from the inlet, the more slowly and later it was half flushed. Compartments 12 and 21 were half flushed at relatively high rates, their neighbouring compartments 13, 22 and 31 were flushed at lower rates, and other horizontal compartments were then half flushed at even lower rates. It can be seen that the relative position of the points denoting the vertical compartments to those denoting the horizontal compartments agreed with the predictions.

5.2.4 The average flushing efficiency of the whole tank

The predicted average flushing efficiency of the whole tank (defined by equation (3.5)) is shown in the left of Figure 5.10 for the three tanks, and compared against the pure displacement and perfect mixing. For each case, the flushing efficiency is intermediated between the pure displacement and perfect mixing. Table 5.1 summarises the flushing efficiency at $T = 3$. For all the three tanks, the flushing efficiency is the highest in the 'far open' case, and the lowest in the 'near open' case. This is because when the outlet is placed far from the inlet, the incoming fluid has more chance to

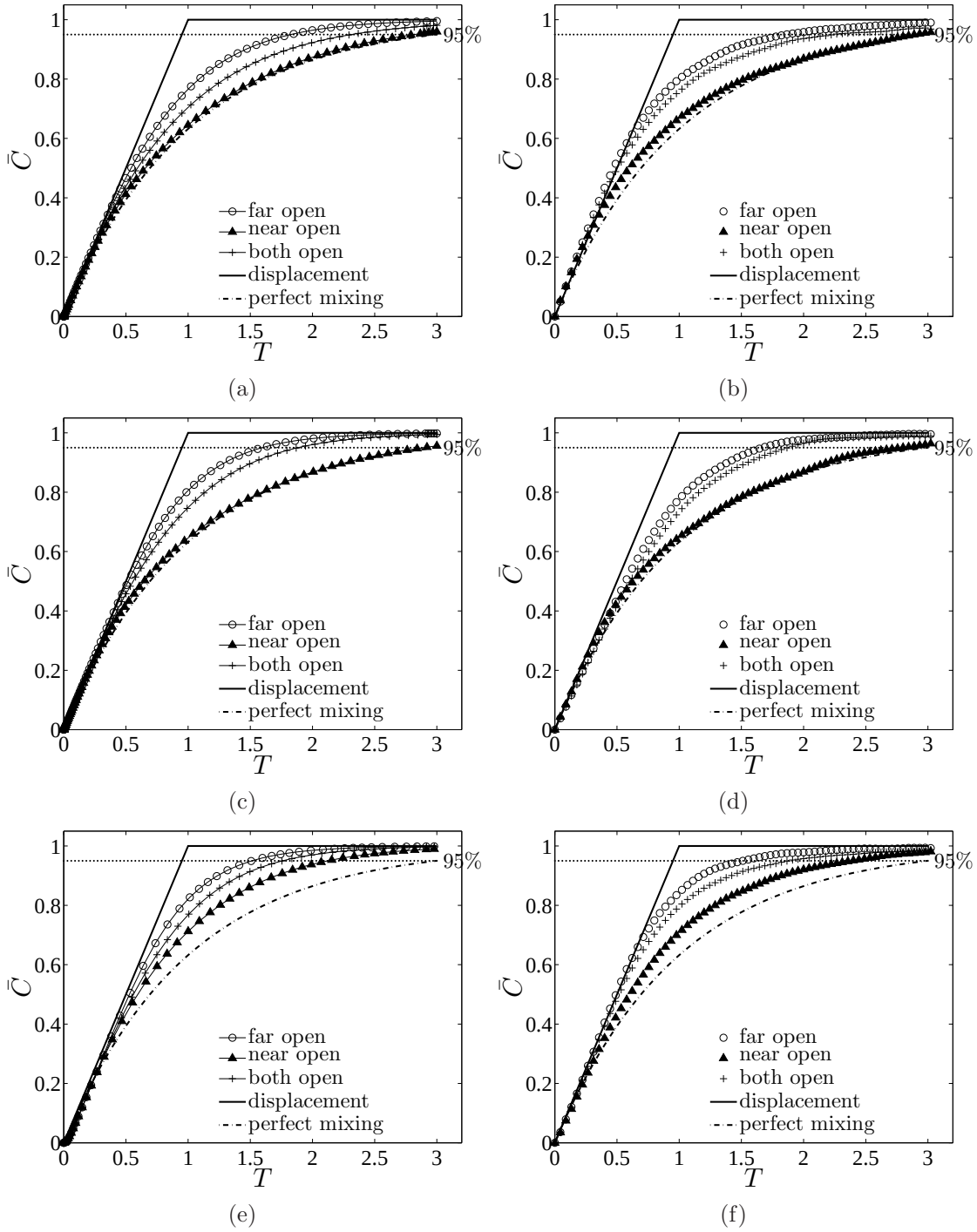

Figure 5.10: The theoretical predictions of the average flushing efficiency of the whole tanks with three outlet arrangements are shown on the left hand side, with the corresponding experimental results on the right hand side. The figures correspond to (a, b) 'far open', (c, d) 'near open', and (e, f) 'both open' cases.

mix with the initial fluid and thus the latter can be replaced more efficiently. Also, it can be seen that when a tank is divided into many compartments, the flow behaves like the displacement mode, as the incoming fluid will leave the tank when it has mixed more sufficiently with the initial fluid (except for some 'near open' cases).

The variation in time of the average flushing efficiency is shown in the right of Figure 5.10. Table 5.1 summarises the flushing efficiency at $T = 3$ for each case. It can be found that for short time, the original fluid was removed by displacement and the increase in $\bar{C}$ was roughly linear; for long time, mixing was important and then $\bar{C}$ followed more closely the perfect mixing rule. For all tank configurations, the flushing efficiency of 'far open' and 'both open' were similar and higher than that of the 'near open' case. For the 'far open' and 'both open' cases, the flushing efficiency increased linearly with time up until $T \simeq 0.6$, because the water exiting consists entirely of water that was initially in the tank. When $T \gtrsim 0.6$, the water exiting the tank consists of an increasing fraction of the water that is being used for flushing the tank. In total, the flushing efficiency at $T = 3$ of these two cases was lower than the pure displacement, but higher than estimates based on perfect mixing in the whole tank. For the 'near open' case, the transition from displacement flushing to mixing occurs earlier at $T \simeq 0.5$, because the incoming water bypassed a large part of the tank and was not able to exchange the initial water efficiently. Generally, the flushing efficiency at $T = 3$ obtained from the experiment was slightly lower than predicted, except for the 'near open' case in the 3×3 tank. In the experiments, the effective Re decreases in the peripheral compartments leading to lower increase rates of flushed fraction and higher residence time. Since the total flushing efficiency is an integrated measure over the whole tank, the impact of the peripheral compartments is not significant and this is why the agreement between the theory and the experiments is generally good (see Figure 5.10 and Table 5.1). The critical point is that for all the tanks considered, the flushing efficiency is greater than 95% at three exchange volumes ($T = 3$), which is required by the IMO protocols.

5.3 Implications to unstratified flushing through homogeneous tanks

In 5.2.4, the flushing efficiency of the three tank configurations was tested among different outlet arrangements. In this section, the predicted flushing efficiency will be compared among different tank configurations with identical compartments, connecting holes and outlet arrangement.

5.3.1 Implications to $m \times 2$ homogeneous tanks

The theoretical predictions of the average flushing efficiency of the 2×2, 3×2 and 4×2 homogeneous tanks with identical compartments and connecting holes is shown in Figure 5.11. It can be seen that for each outlet arrangement, the flushing efficiency increases with m, varying between the displacement mode and the perfect mixing mode. For the 'far open' case shown in Figure 5.11(a), the flushing efficiency of the three tanks performs very similarly to each other, much better than the perfect mixing mode. At $T = 3$, all the three tank are nearly 100% flushed. This is because subdividing a tank provides more time for the incoming fluid to mix with the initial fluid, and thus improves the flushing efficiency. For the 'near open' case shown in Figure 5.11(b), the flushing of 4×2 and 3×2 tanks is much more efficient than that of the 2×2 tank. This is because dividing a tank to more compartments decreases the difference of the flow resistance between pathways $11 \rightarrow 12$ and $11 \rightarrow 21$, and therefore provides more chance to improve mixing and reduce bypassing. For the 'both open' case shown in Figure 5.11(c), the improvement range of the flushing efficiency by the increment of compartments is between the 'far open' case and the 'near open' case.

5.3.2 Implications to $2 \times n$ homogeneous tanks

The theoretical predictions of the average flushing efficiency of 2×2, 2×3 and 2×4 homogeneous tanks with identical compartments and connecting holes is shown in Figure 5.12. For the 'far open' case shown in Figure 5.12(a), the performance of the

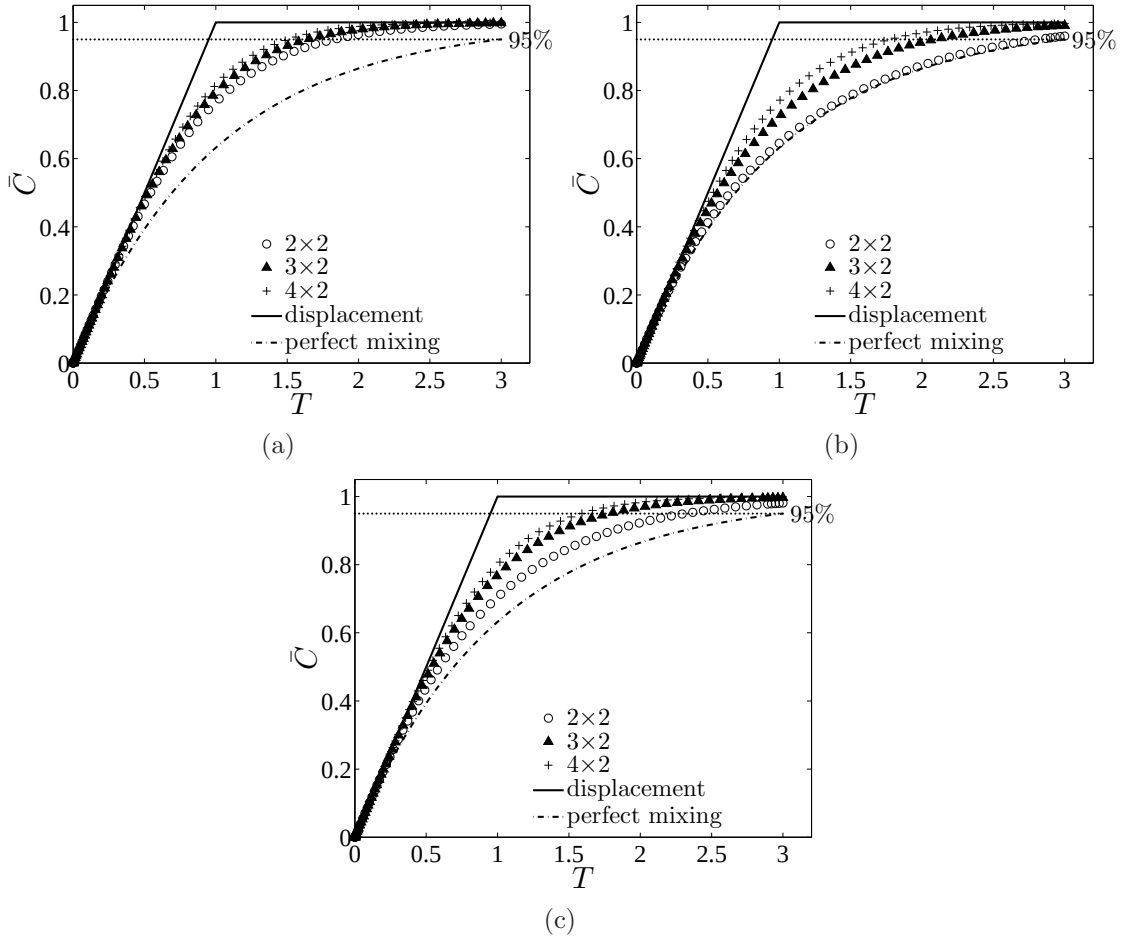

Figure 5.11: Theoretical flushing efficiency of $m \times 2$ identical tanks. The figures correspond to (a) 'far open', (b) 'near open', and (c) 'both open' cases.

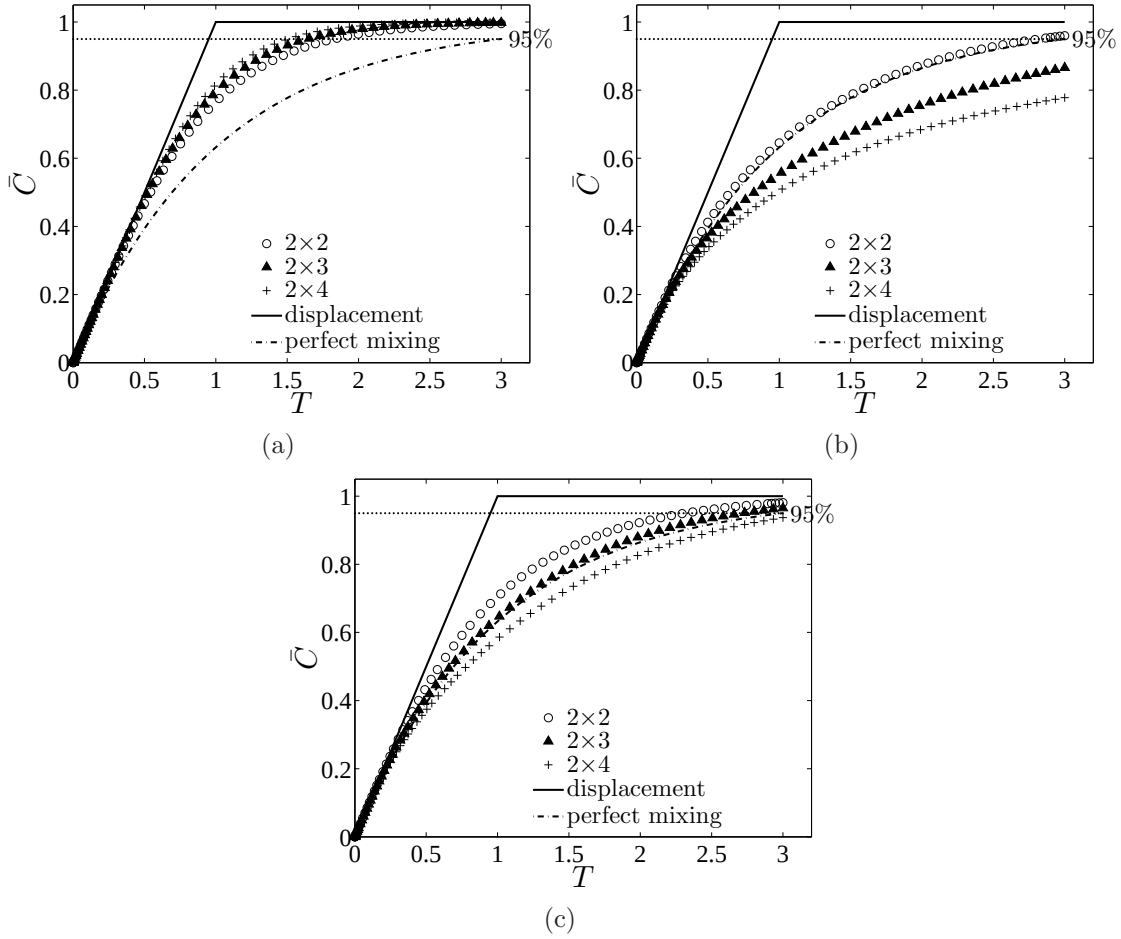

Figure 5.12: Theoretical predictions of the average flushing efficiency of $2 \times n$ homogeneous tanks. The figures correspond to (a) 'far open', (b) 'near open', and (c) 'both open' cases.

flushing efficiency of the $2 \times n$ tanks is the same as that of the $m \times 2$ tanks. This is because when only the far outlet is open, the structure of an $m \times n$ tank and that of an $n \times m$ tank are symmetrical. For the 'near open' and 'both open' cases in Figure 5.12(b, c), the flushing efficiency decreases with n. This is because when compartments are increased, the flow resistance on pathway $11 \rightarrow 12$ is enlarged, so that more incoming fluid will travel through pathway $11 \rightarrow 21$, and then leave the tank without flushing other compartments.

5.3.3 Implications to $m \times m$ homogeneous tanks

The theoretical predictions of the average flushing efficiency of 2×2, 3×3, 4×4 and 5×5 homogeneous tanks with identical compartments and connecting holes are shown in Figure 5.13. For the 'far open' and 'both open' cases shown in Figure 5.13(a, c), all the multi-compartmental flushing cases are more efficient than the perfect mixing in a single tank, but the improvement of flushing efficiency is not remarkable after $m = 3$. For the 'near open' case shown in Figure 5.13(b), the flushing efficiency for each tank configuration is close to the perfect mixing mode in a single tank. The flushing efficiency is not significantly improved by subdividing the tank. The reason is although subdivision provides more chance for mixing, it cannot effectively allocate more fluids to the pathway $11 \rightarrow 12$.

5.4 Summary

In this chapter, the flushing of water from a homogeneous multi-compartment rectangular tank has been examined theoretically and experimentally. A series of detailed experiments on tanks with 2×2 and 3×3 compartment configurations (typical of double bottom ballast tanks) were undertaken to validate the multizone flushing model developed in Chapter 3. When the lightening holes between compartments are identical, the model has no adjustable free parameters. The flushing from a 5×4 tank with more complex geometry, typical of a double hull ballast tank, was also analysed. When the holes between compartments of a tank are different in size, an empirical

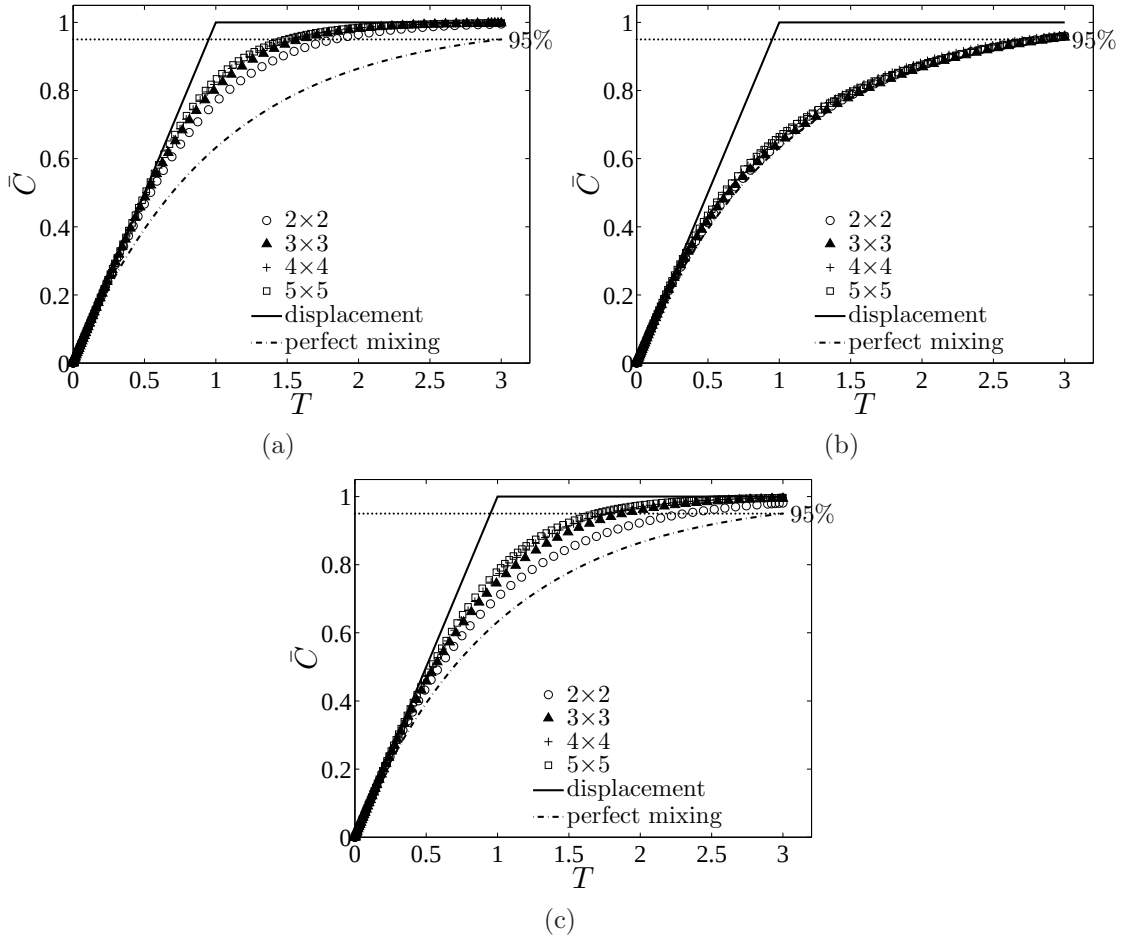

Figure 5.13: Theoretical flushing efficiency of $m \times m$ homogeneous tanks. The figures correspond to (a) 'far open', (b) 'near open', and (c) 'both open' cases.

Table 5.2: The exchange volumes required to achieve $\bar{C} = 95\%$ for different tank configurations.

Tank configuration	Required exchange volumes		
	Far open	Near open	Both open
2×2	1.83	2.82	2.31
2×3	1.64	>3	2.72
2×4	1.51	>3	>3
3×2	1.64	2.08	1.78
3×3	1.60	2.89	1.88
4×2	1.51	1.78	1.59
4×4	1.52	2.73	1.76
5×4	1.51	2.12	1.76
5×5	1.49	2.83	1.69

closure model is required to estimate pressure loss coefficients. The experimental results agree with the model predictions to within 1.2%.

The flushing efficiency of a ballast tank is dependent on the outlet arrangement and compartment configuration. Table 5.2 summarises the exchange volumes required to achieve the 95% average flushing efficiency for the tested tank configurations in this chapter. It can be seen that for each tank configuration, setting a single outlet far from the inlet may achieve an efficient water exchange and thus the exchange volumes required to achieve $\bar{C} = 95\%$ can be significantly reduced. When only the far outlet is open, subdividing a tank may improve the flushing efficiency. When the outlet is close to the inlet, part of the incoming flow may bypass much region of the tank, as the flow through the edge compartments is reduced. Insufficient mixing, caused by weak turbulent diffusion in some compartments where flow rate was low, led to a long residence time of the original fluid and thus a slow exchange, and this is why the American Bureau of Shipping (2010) requires aft and fore peak tanks are to be provided with additional pipe work to improve the mixing conditions.

The IMO requires that the average flushing efficiency of the whole tank should be greater than 95% and these estimates were based on a perfect mixing model for

the whole tank. The theoretical model and experiments show that for unstratified fluids within multi-compartment homogeneous tanks, in most cases, flushing is more efficient than estimated by the IMO, see Table 5.2. The results show to enhance flushing the outlet should be placed far from the inlet to reduce bypassing, which is consistent with the requirement by the American Bureau of Shipping.

This chapter focuses on the homogeneous tanks. The influence of the inhomogeneity of a multi-compartment tank will be further tested in next chapter.

Chapter 6

Flushing Inhomogeneous Tanks

6.1 Introduction

The geometry of a ballast tank is rather complicated, even in most cases, the latitudinal and longitudinal section of a ballast tank do not have the same size, which further increases the structural complexity (Eames et al., 2008). It is necessary to understand how the flushing efficiency depends on the hole resistance and compartment capacitance. In this chapter, the 2×2 tank at a fixed flow rate with different outlet arrangements is further tested to study the influence of the structural inhomogeneity on the flushing efficiency. As described at the end of Section 3.5, this study will further examine the influence of (3) hole resistance and (4) compartment capacitance on the flushing. These are achieved by setting the following parameters:

(3) fixed capacitance, $k_1 = k_2 = 1/2$, and varying the flow allocation ϕ, where $k_1(= L_1/L)$, $k_2(= W_1/W)$ are the ratio of compartment length to tank length (see Figure 3.4) and $\phi(= f_{11,12}/Q)$ is the flow allocation.

(4) fixed resistance, $\zeta_{11,12} = \zeta_{12,22} = \zeta_{11,21} = \zeta_{21,22}$, and varying k_1, k_2, where ζ is the pressure drop coefficient.

The experimental measurements will be compared with the theoretical predictions on the flushed fraction of each compartment. The single outlet cases are flux constrained,

and the double outlets case is pressure constrained. The two following sections show the influence of varying resistance and capacitance, respectively.

6.2 Effect of hole resistance on flushing

In this section, the effect of hole resistance on flushing is tested (corresponding to test (3)). The capacitance of the compartments was kept constant by fixing $k_1 = k_2 = 1/2$ (k_1 and k_2 are illustrated in Figure 3.4(a)). For the case of varying resistance, the inhomogeneity is characterized by ϕ (see Table 3.1), which differs depending on whether the flow is flux or pressure constrained. The diameters of the connecting holes are explicitly shown in Figures 6.1, 6.2 and 6.3. At $k_1 = k_2 = 1/2$, C_{11} increases fastest, as compartment 11 is the inlet compartment, which is not influenced by the sizes of the connecting holes in the tank.

6.2.1 Flushing in the 'far open' case

Figure 6.1 shows the variation in time of $C_{[i][j]}$ with time for the 'far open' case in the 2×2 tank. The theoretical ϕ is (a) 0.65, (b) 0.74 and (c) 0.84, respectively. There are two flow pathways in the tank: $11 \rightarrow 12 \rightarrow 22$ and $11 \rightarrow 21 \rightarrow 22$. When the diameter of the holes on $11 \rightarrow 12 \rightarrow 22$ is larger than that on $11 \rightarrow 21 \rightarrow 22$, $f_{11,12} = f_{12,22} > f_{11,21} = f_{21,22}$, thus $\phi > 0.5$. When the diameter ratio $D_{11,12}/D_{11,21}$ is increased, the flow allocation ϕ becomes larger. It can be seen that when ϕ increases from 0.65 to 0.84, compartment 12 is flushed faster, while compartments 21 and 22 are flushed more slowly, because of the increment of the ratio $f_{11,12}/f_{11,21}$. For each case, C_{21} and C_{22} intersect. The larger the value of ϕ is, the earlier C_{21} is exceeded by C_{22}. This is because C_{12} is relatively low initially, but at a later time, a large amount of original fluid in compartment 12 has been flushed out due to $f_{11,12} > f_{11,21}$, the flow from compartment 12 can flush more original fluid out of compartment 22 than that from compartment 11 can flush out of compartment 21, leading to $C_{22} > C_{21}$.

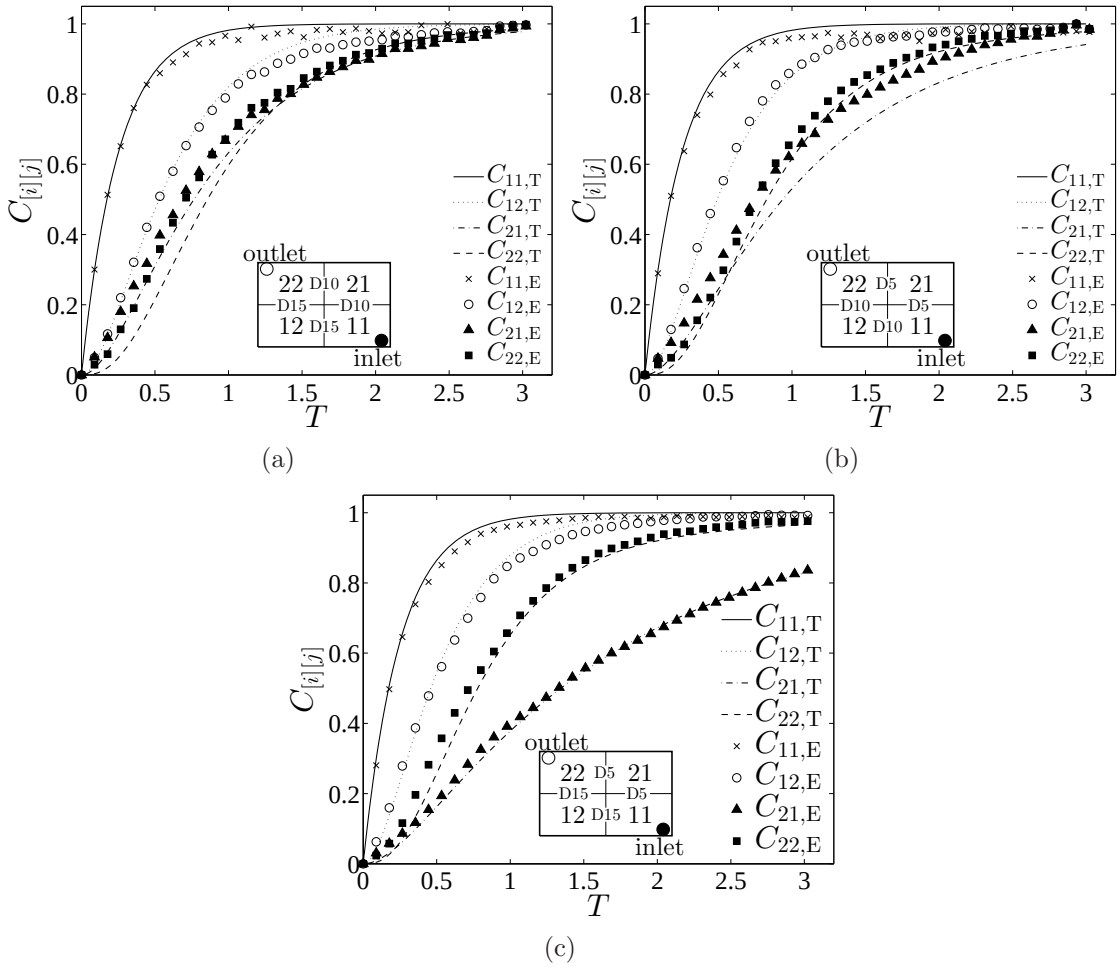

Figure 6.1: The variation in time of the flushed fraction in each compartment of the 2×2 tank for the 'far open' case. '$C_{[i][j],\mathrm{T}}$' represents theoretical predictions, while '$C_{[i][j],\mathrm{E}}$' represents experimental measurements. The figures correspond to $\phi =$ (a) 0.65, (b) 0.74 and (c) 0.84.

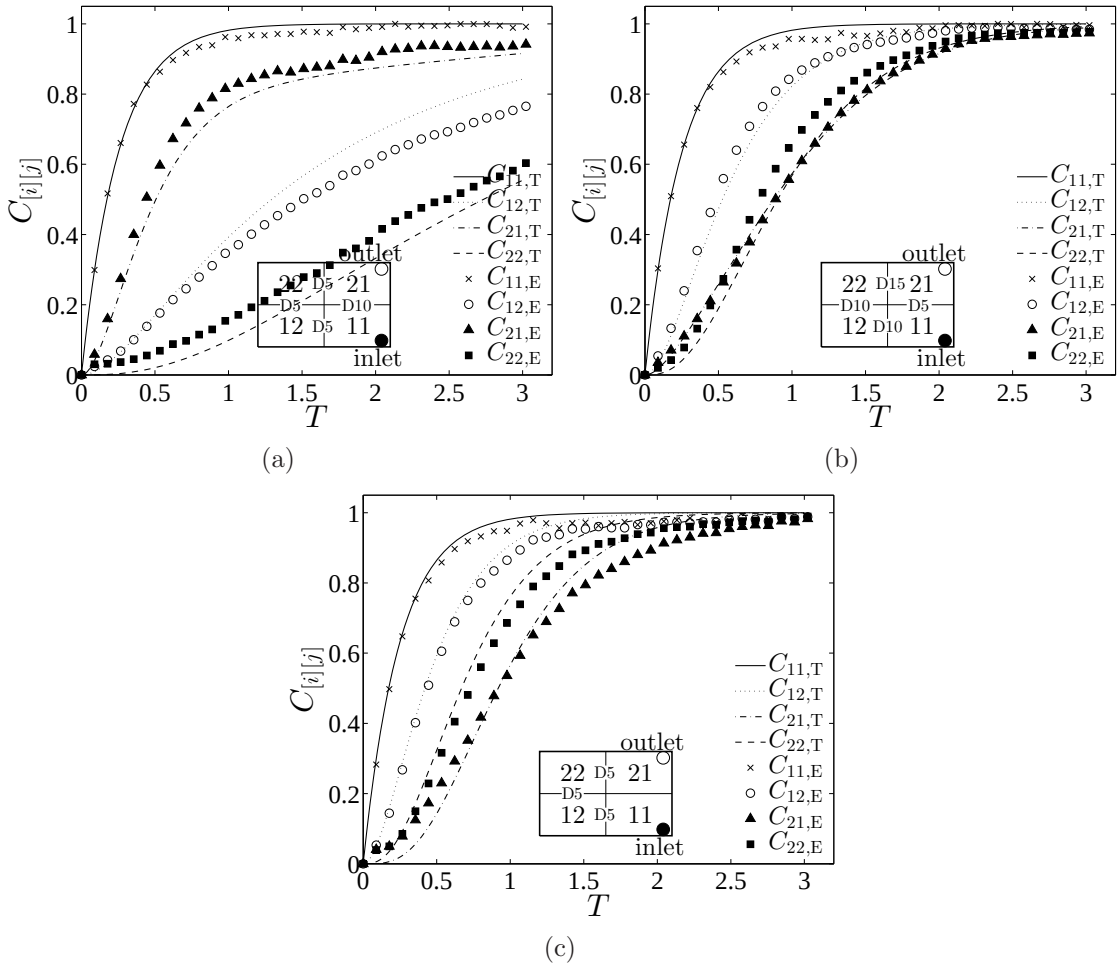

Figure 6.2: The variation in time of the flushed fraction in each compartment of the 2×2 tank for the 'near open' case. '$C_{[i][j],\mathrm{T}}$' represents theoretical predictions, while '$C_{[i][j],\mathrm{E}}$' represents experimental measurements. The figures correspond to $\phi =$ (a) 0.17, (b) 0.65 and (c) 1.

6.2.2 Flushing in the 'near open' case

Figure 6.2 shows the variation in time of $C_{[i][j]}$ with time for the 'near open' case in the tank. The theoretical ϕ is (a) 0.17, (b) 0.65 and (c) 1. There are two flow pathways: $11 \rightarrow 12 \rightarrow 22 \rightarrow 21$ and $11 \rightarrow 21$. When $\phi = 0.17$, $C_{21} > C_{12} > C_{22}$, because $f_{11,21} > f_{11,12} = f_{12,22}$ (see Figure 6.2(a)). When ϕ increases, compartments 12 and 22 are flushed faster, but compartment 21 is flushed more slowly, because of the increment of the ratio $f_{11,12}/f_{11,21}$. When $\phi = 0.65$, C_{21} and C_{22} intersects (see Figure 6.2(b)). Initially, the flow from compartment 11 can flush compartment 11 more efficiently than that from compartment 12 can flush compartment 22, thus $C_{21} > C_{22}$; but at a later time, as C_{12} becomes higher, compartment 22 is flushed more efficiently. As a result of being flushed by a large amount of original fluid from compartment 22, $C_{21} < C_{22}$. When $\phi = 1$, there is no hole between compartment 11 and 21, so $f_{11,21} = 0$. The 2×2 system evolves to a 1×4 linear network. The four compartments are flushed through $11 \rightarrow 12 \rightarrow 22 \rightarrow 21$, so $C_{11} > C_{12} > C_{22} > C_{21}$ (see Figure 6.2(c)). The experimental results matched the theoretical predictions.

6.2.3 Flushing in the 'both open' case

Figure 6.3 shows the variation in time of $C_{[i][j]}$ for the 'both open' case. The theoretical ϕ is (a) 0.2, (b) 0.67 and (c) 0.79. As it is assumed that $f_{21,22} = 0$, there are two flow pathways: $11 \rightarrow 12 \rightarrow 22$ and $11 \rightarrow 21$. When $\phi = 0.2$, $C_{21} > C_{12} > C_{22}$, as $f_{11,21} > f_{11,12}$; experimentally, C_{22} increases faster than expected (see Figure 6.3(a,ii)). This is because $f_{21,22} > 0$ due to $p_{21} > p_{22}$ in fact, compartment 22 was flushed by the flow from both compartments 12 and 21. When ϕ increases, C_{12} and C_{22} increase faster, but C_{21} increases more slowly; C_{21} is exceeded by C_{22} earlier. The discrepancy between the theoretical predictions and the experimental results is caused by the assumption that $f_{21,22} = 0$ while the pressure difference between compartments 21 and 22 cannot be ignored in reality.

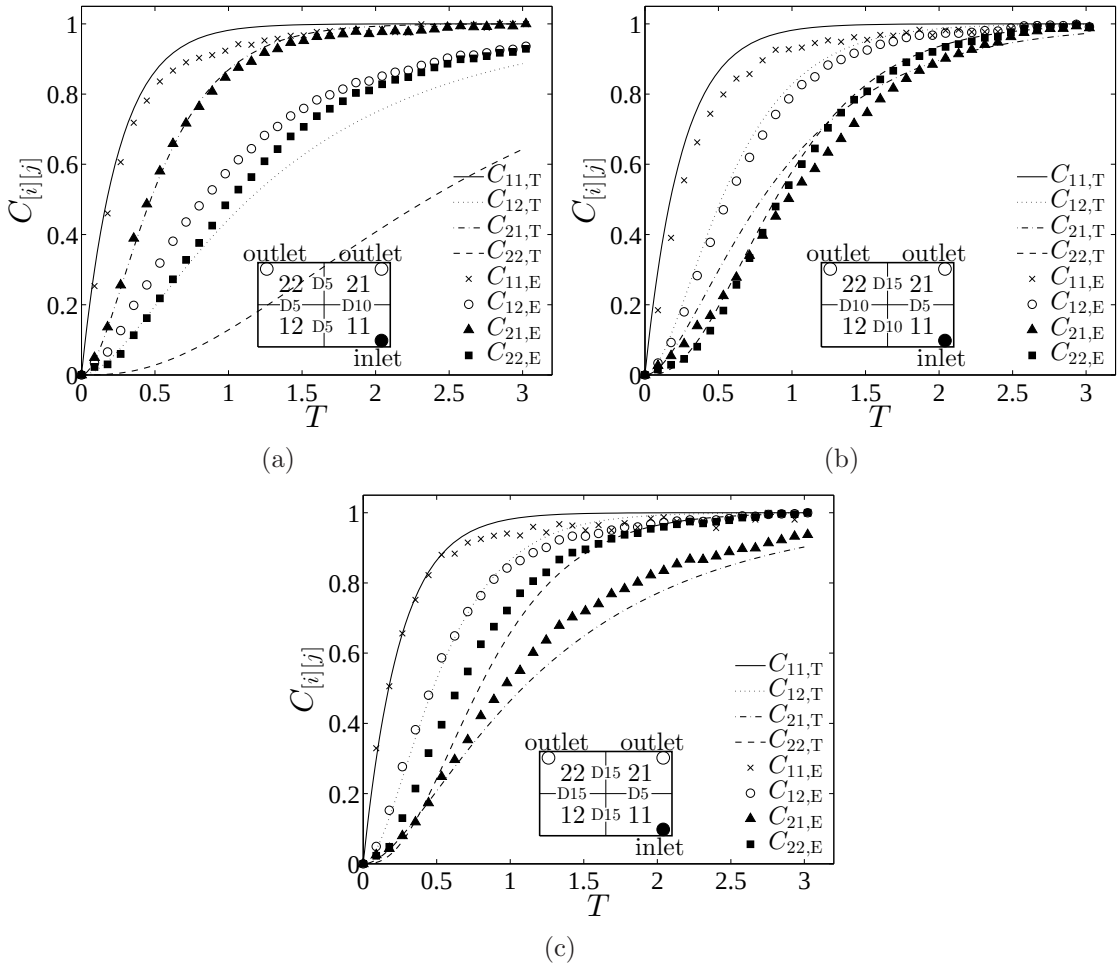

Figure 6.3: The variation in time of the flushed fraction in each compartment of the 2×2 tank for the 'both open' case. '$C_{[i][j],\mathrm{T}}$' represents theoretical predictions, while '$C_{[i][j],\mathrm{E}}$' represents experimental measurements. The figures correspond to $\phi =$ (a) 0.2, (b) 0.67 and (c) 0.79.

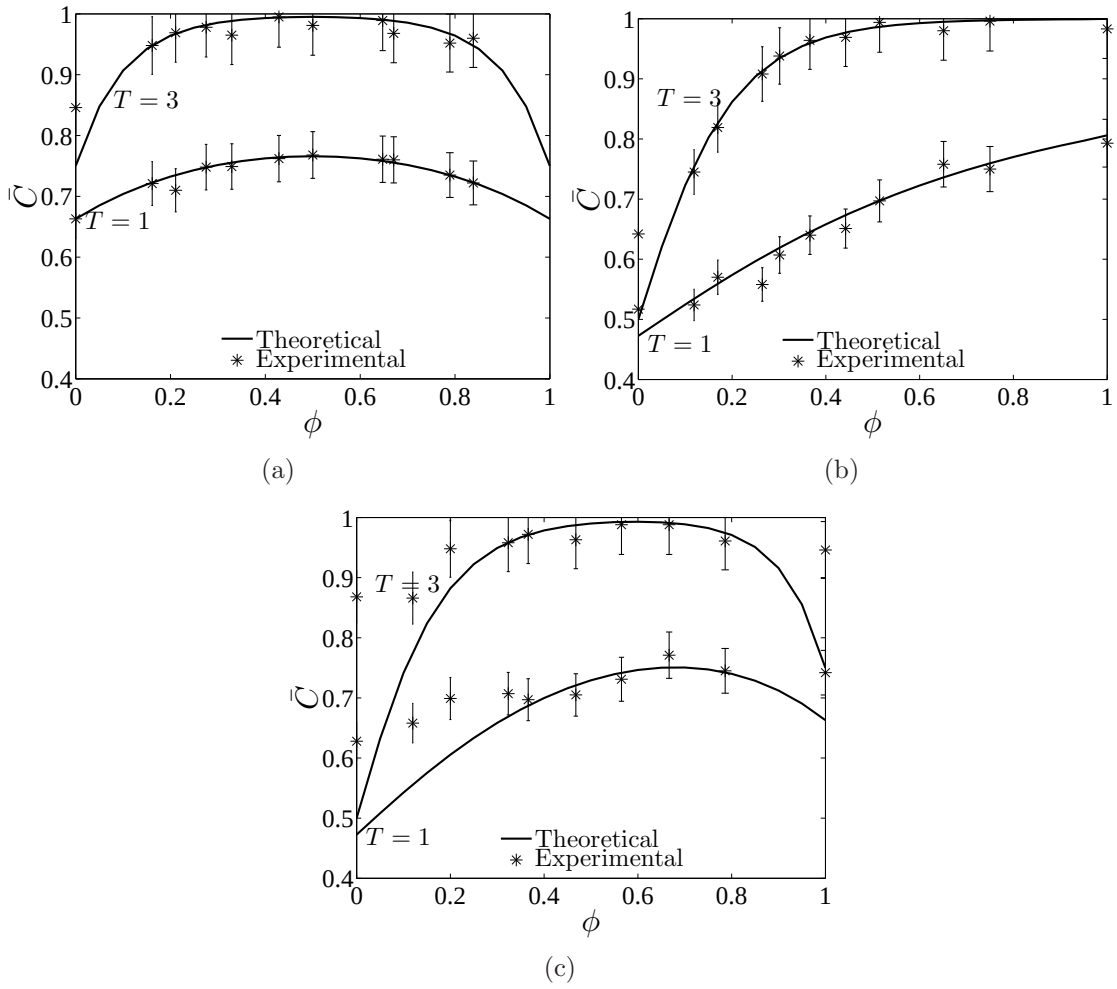

Figure 6.4: The theoretical predictions and experimental results of $\bar{C}$ at $T = 1$ and $T = 3$ versus ϕ in the 2×2 tank. The figures correspond to (a) 'far open', (b) 'near open', and (c) 'both open' cases.

6.2.4 The average flushing efficiency of the whole tank

Figure 6.4 summarises the influence of the flow allocation on the flushing efficiency at $T = 1$ and $T = 3$ of the 2×2 tank for the three cases considered. $\bar{C}$ at $T = 1$ and $T = 3$ is plotted against ϕ for the 'far open' case in Figure 6.4(a). It can be seen that $\bar{C}$ is symmetrical about $\phi = 0.5$. $\bar{C}$ reaches the maximum value at $\phi = 0.5$, $\bar{C}|_{T=3} > 0.95$ when $0.2 \lessapprox \phi \lessapprox 0.8$, and the further from 0.5 ϕ is, the lower the corresponding $\bar{C}$ will be. When $\phi = 0$ or 1, $\bar{C}|_{T=3} \approx 0.75$ because only three of the four compartments are flushed. At $\phi = 0$, $\bar{C}|_{T=3}$ was underestimated in practice because of the existence of fluid exchange between compartment 22 and 12 as $C_{22} \gg C_{12}$ after the tank had been flushed for some time. Figure 6.4(b) shows $\bar{C}$ versus ϕ for the 'near open' case. When ϕ increases, $\bar{C}$ increases. At $\phi = 0$, $\bar{C}|_{T=3} \approx 0.5$, as only compartments 11 and 21 are flushed; $\bar{C}|_{T=3} > 0.95$ when $\phi \gtrapprox 0.3$; at $\phi = 1$, the four compartments are flushed through $11 \to 12 \to 22 \to 21$ and $\bar{C}|_{T=3} \approx 1$. This means that the linear network is the best flushing strategy. At $\phi = 0$, $\bar{C}$ was underestimated by the model due to the fluid exchange between compartment 21 and 22. Figure 6.4(c) shows $\bar{C}$ versus ϕ for the 'both open' case. At $\phi = 0$, $\bar{C}|_{T=3} \approx 0.5$, as only compartments 11 and 21 are flushed; $\bar{C}$ increases with $\phi \lessapprox 2/3$, but decreases with $\phi \gtrapprox 2/3$; at $\phi = 1$, $\bar{C}|_{T=3} \approx 0.75$, as only compartments 11, 12 and 22 are flushed. The further from 2/3 ϕ was, the higher than estimated $\bar{C}$ was. This inconsistency has been analysed above: when ϕ was far from 2/3, the pressure difference between compartment 21 and 22 was high, which contradicted the model assumption that $f_{21,22} = 0$. From Figure 6.4(a,c), it can be inferred that if the network cannot be made linear, the best strategy for flushing is to keep the flow allocation to one pathway equal to the ratio of the volume that is to be flushed on this way. For instance, for the 'both open' case, the flow from compartment 11 is to flush compartments 12 and 22 on one pathway, and to flush compartment 21 on the other way. $\phi = 2/3$ is the best strategy because two out of three volumes is to be flushed on this way. There are significant challenges to keep $\Delta p = 0$.

The agreement between experiments and the theory is good except for the pressure constrained case and large differences in resistance (i.e. when $\phi < 0.2$ or > 0.9), because the fluid exchange between compartments 21 and 22 cannot be completely

ignored in these cases. This difference is largely attributed to the difficulty of maintaining the same pressure in compartments 21 and 22.

6.3 Effect of compartment capacity on flushing

In this section, the effect of compartment capacity on flushing is tested (corresponding to test (4)). The resistance between neighbouring compartments is fixed to be the same. For the case of varying capacitance in the 2×2 tank, the inhomogeneity is characterized by k_1 and k_2. Because of the way the resistance measure is defined, ϕ is different for each outlet arrangement, see Table 3.1. The ratios of the length and width of each compartment are shown in Figures 6.5, 6.6 and 6.7. For each case, C_{11} increases fastest as compartment 11 is the first flushed with the incoming fluid. But different to the previous section, C_{11} behaves differently when the capacitance of compartment 11 is different.

6.3.1 Flushing in the 'far open' case

Figure 6.5 shows the variation in time of $C_{[i][j]}$ with time for the 'far open' case when the holes between neighbouring compartments of the 2×2 tank are the same in size and height. Theoretically, $\phi = 1/(1+((k_2^{-1/2}+(1-k_1)^{-1/2})/(k_1^{-1/2}+(1-k_2)^{-1/2}))^{1/2})$ (see Table 3.1). When $k_1 = k_2 = 1/3$, $C_{12} = C_{21} > C_{22}$ (see Figure 6.5(a)). $C_{12} = C_{21}$ is caused by the equal flow rates $f_{11,12} = f_{11,21}$ due to the equal resistances on the two flow pathways $11 \rightarrow 12 \rightarrow 22$ and $11 \rightarrow 21 \rightarrow 22$, and the equal volumes $V_{12} = V_{21}$. C_{22} increases the most slowly because compartment 22 is latest flushed in the network. When $k_1 = 2/3$, k_2 =1/3 or 1/2, $C_{12} > C_{21}$ because although compartments 12 and 22 are flushed by compartment 11 at the same rate ($f_{11,12}$=$f_{11,21}$), as a result of the compartment capacity difference $V_{12} < V_{21}$, C_{12} increases faster than C_{21} does. Originally, $C_{21} > C_{22}$ as compartment 21 is directly flushed by compartment 11; at a later stage, compartment 12 has been sufficiently flushed so that C_{12} is high and contributes a lot to the increment of C_{22} (see Figure 6.5(b,c)). The experimental results supported the theoretical predictions, although the theory does not consider

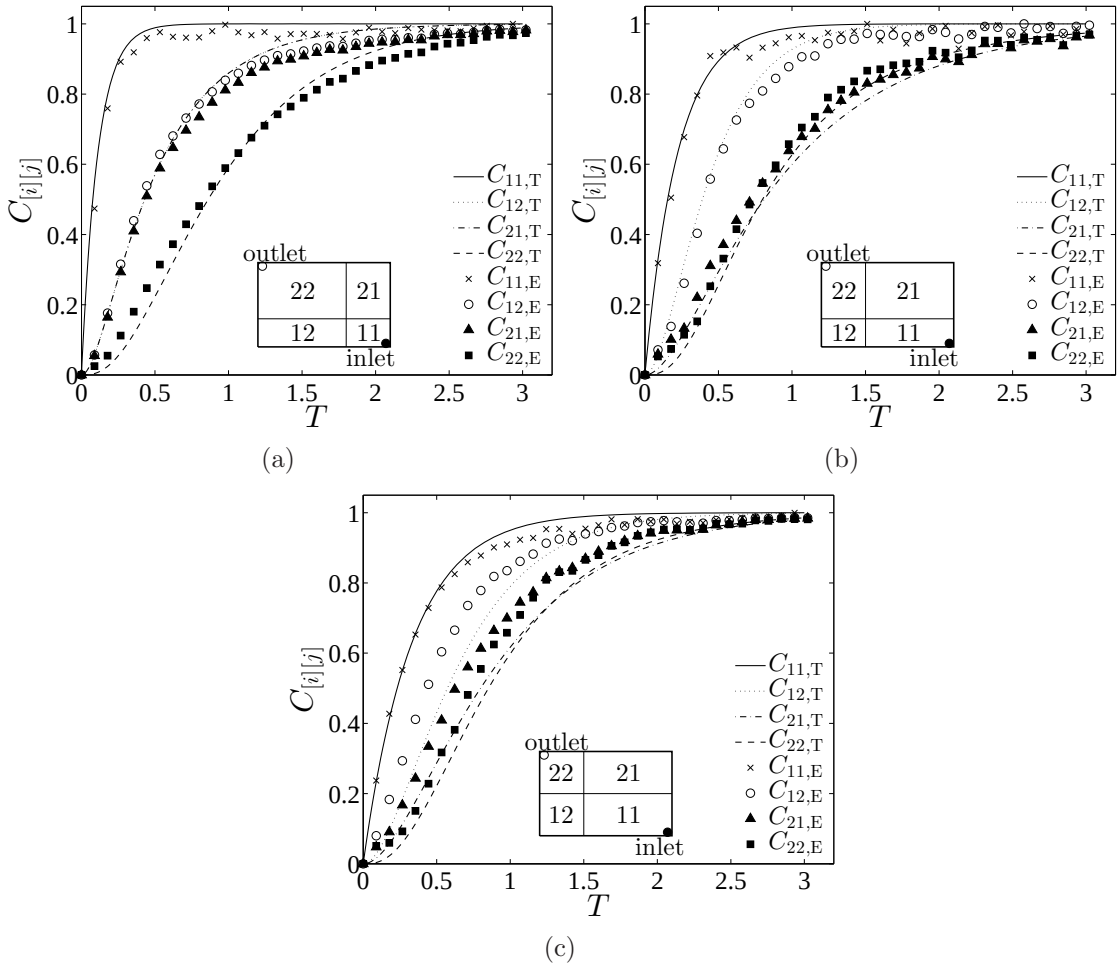

Figure 6.5: The variation in time of $C_{[i][j]}$ in the 2×2 tank for the 'far open' case. '$C_{[i][j],\mathrm{T}}$' represents theoretical predictions, while '$C_{[i][j],\mathrm{E}}$' represents experimental measurements. The figures correspond to (a) $k_1 = k_2 = 1/3$, (b) $k_1 = 2/3$, $k_2 = 1/3$, and (c) $k_1 = 2/3$, $k_2 = 1/2$.

the impact of the compartment size on the flow resistance. This means that the pressure drop of the fluid flow in the tank was mainly caused by contraction of the flow area due to existence of the holes between compartments, rather than the flow friction within compartments.

6.3.2 Flushing in the 'near open' case

Figure 6.6 shows the variation in time of $C_{[i][j]}$ for the 'near open' case with identical connecting holes in the 2×2 tank. Theoretically, $\phi = 1/(1 + ((k_2^{-1/2} + (1 - k_1)^{-1/2} + (1 - k_2)^{-1/2})/k_1^{-1/2})^{1/2})$. For each case, C_{22} is the lowest because compartment 22 locates the furthest from the inlet. When $k_1 = 1/3$, $k_2 = 1/2$, initially $C_{21} > C_{12}$, because $f_{11,21} > f_{11,12}$ and $V_{21} > V_{12}$ (see Figure 6.6(a)); but later $C_{21} < C_{12}$, because compartment 21 is flushed by a large amount of unexchanged fluid from compartment 22. When k_1 =1/2 or 2/3, $k_2 = 2/3$, $C_{21} > C_{12}$ (see Figure 6.6(b,c)). The agreement between the model predictions and the experimental results was quite good.

6.3.3 Flushing in the 'both open' case

Figure 6.7 shows the variation in time of $C_{[i][j]}$ for the 'both open' case with identical connecting holes in the tank. In this case, $\phi = 1/(1+((k_2^{-1/2}+(1-k_1)^{-1/2})/k_1^{-1/2})^{1/2})$. Theoretically for each case, $C_{11} > C_{21} > C_{12} > C_{22}$. When $k_1 = k_2 = 1/3$, C_{21} was overestimated and C_{22} was underestimated, because in reality there was fluid exchange between compartment 21 and 22, as a result, C_{21} increased more slowly, but C_{22} increased faster than expected. When $k_1 = 1/2$, $k_2 = 2/3$, the underestimation of C_{22} was caused by the assumption that $f_{21,22} = 0$. In fact, $p_{21} > p_{22}$, so C_{22} increased faster than expected because of the flow from compartment 21 to 22 ($f_{21,22} > 0$). There are significant challenges to keep $\Delta p = 0$. The experimental result was consistent with the model prediction when $k_1 = k_2 = 2/3$ (see Figure 6.7(c)).

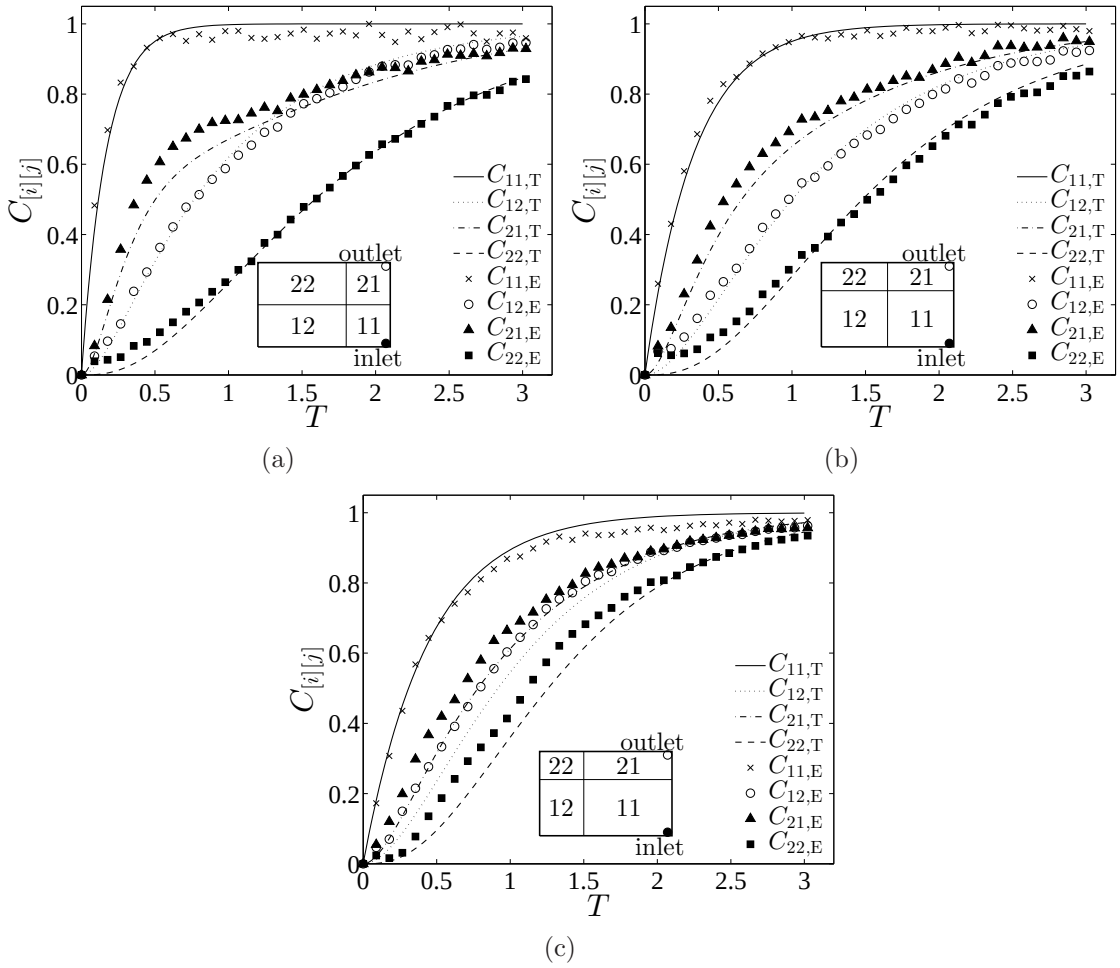

Figure 6.6: The variation in time of $C_{[i][j]}$ in the 2×2 tank for the 'near open' case. '$C_{[i][j],\mathrm{T}}$' represents theoretical predictions, while '$C_{[i][j],\mathrm{E}}$' represents experimental measurements. The figures correspond to (a) $k_1 = 1/3$, $k_2 = 1/2$, (b) $k_1 = 1/2$, $k_2 = 2/3$, and (c) $k_1 = k_2 = 2/3$.

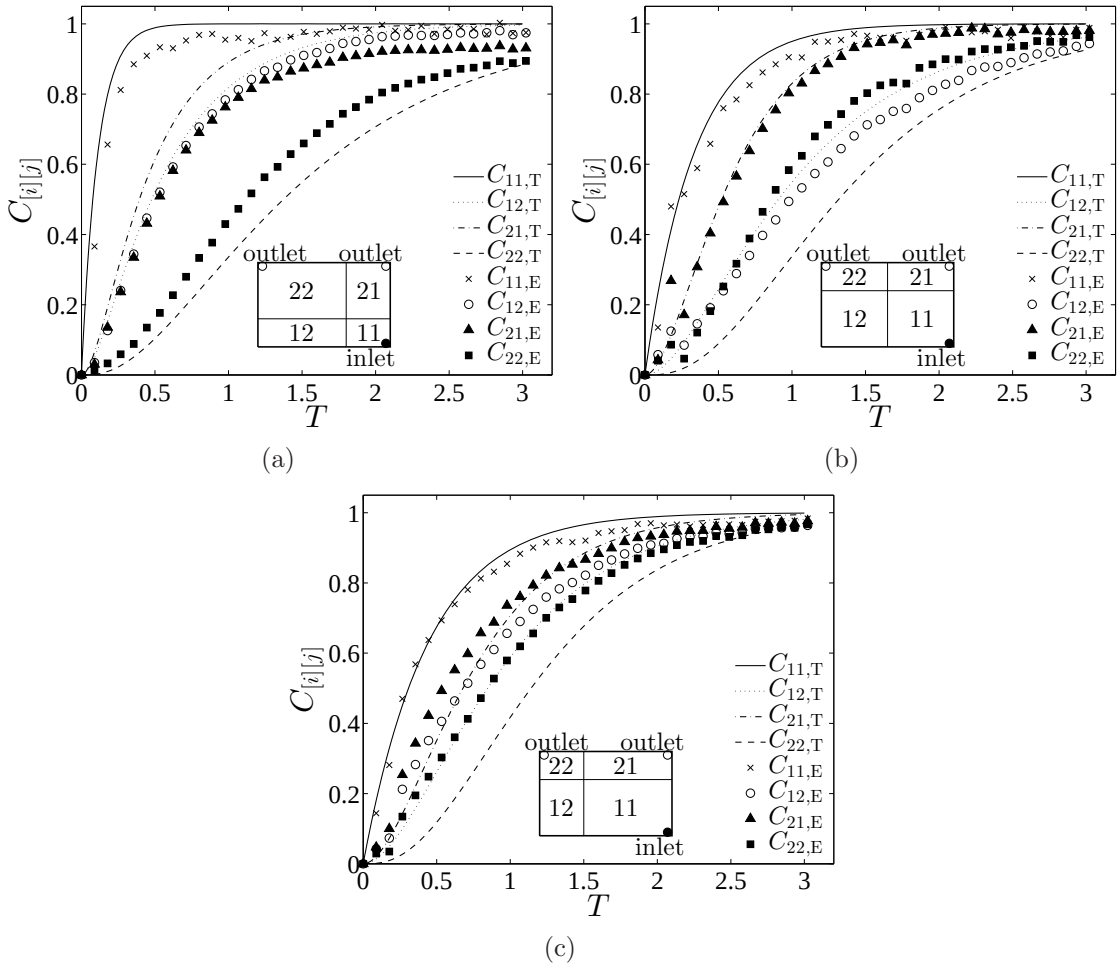

Figure 6.7: The variation in time of $C_{[i][j]}$ in the 2×2 tank for the 'both open' case. '$C_{[i][j],\mathrm{T}}$' represents theoretical predictions, while '$C_{[i][j],\mathrm{E}}$' represents experimental measurements. The figures correspond to (a) $k_1 = k_2 = 1/3$, (b) $k_1 = 1/2$, $k_2 = 2/3$, and (c) $k_1 = k_2 = 2/3$.

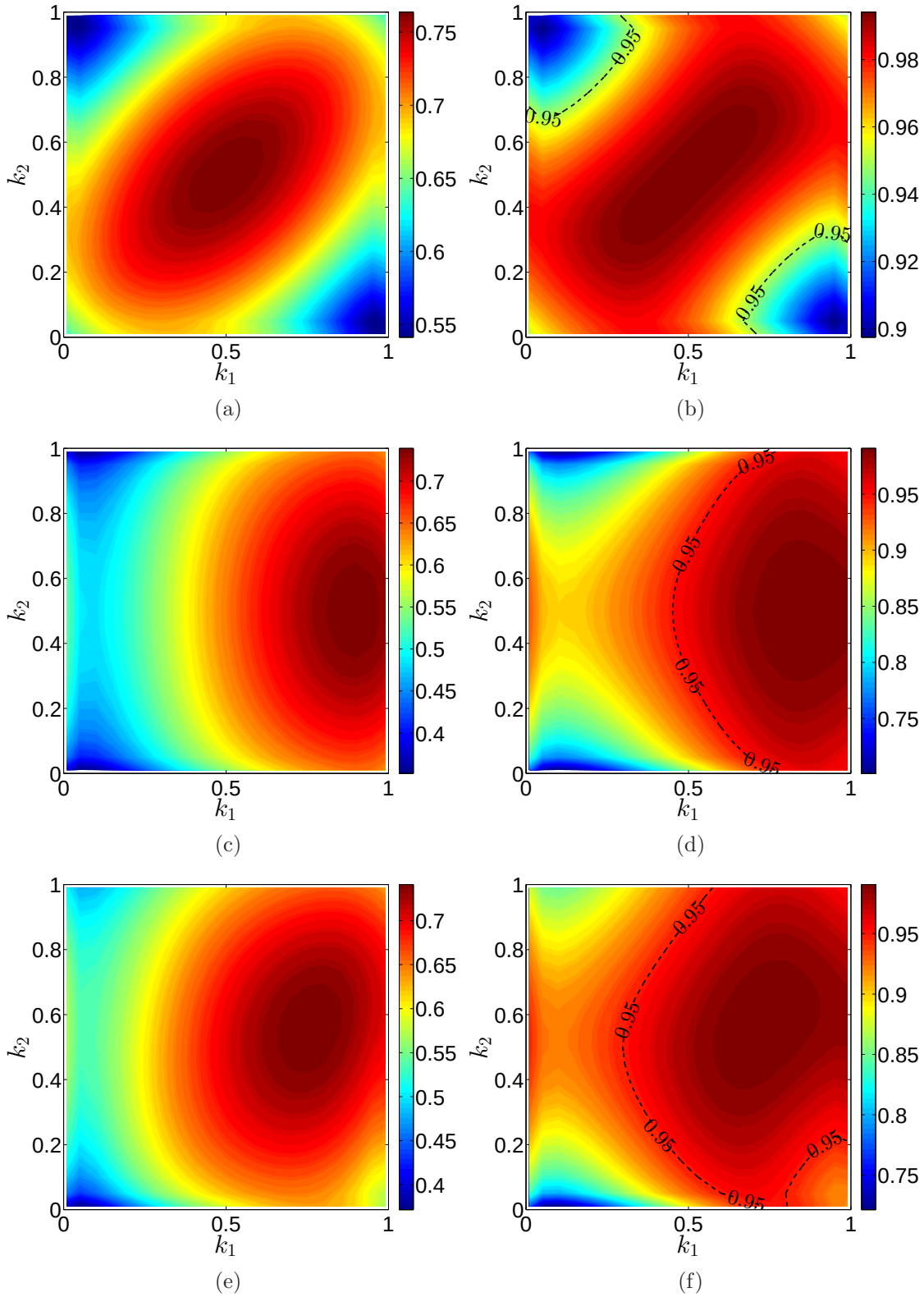

Figure 6.8: The theoretical predictions of $\bar{C}$ considered with different combinations of k_1 and k_2 in the 2×2 tank. The figures correspond to (a) 'far open', $T = 1$; (b) 'far open', $T = 3$; (c) 'near open', $T = 1$; (d) 'near open', $T = 3$; (e) 'both open', $T = 1$; (f) 'both open', $T = 3$.

Table 6.1: The theoretical and experimental flushing efficiency at $T = 1$ and $T = 3$ considered with k_1 and k_2 in the 2×2 tank.

k_1	k_2	Theoretical/experimental flushing efficiency (%)					
		Far open		Near open		Both open	
		$T = 1$	$T = 3$	$T = 1$	$T = 3$	$T = 1$	$T = 3$
1/3	1/3	75.5/74.1	99.4/97.5	56.7/53.4	91.5/89.5	64.0/64.7	94.7/92.7
1/3	1/2	75.4/72.7	99.1/98.3	57.2/57.4	92.5/91.2	64.4/64.1	95.6/94.2
1/3	2/3	72.9/71.1	97.9/95.5	56.7/55.2	91.5/89.0	63.3/60.0	94.8/93.7
1/2	1/3	75.4/75.0	99.1/98.4	63.9/63.7	95.2/94.1	69.6/67.5	97.6/97.3
1/2	2/3	75.4/75.6	99.1/97.3	64.5/65.1	95.2/93.5	69.5/69.9	97.5/96.3
2/3	1/3	72.9/73.5	97.9/97.5	69.5/72.6	98.0/97.7	72.4/70.4	98.6/98.4
2/3	1/2	75.4/74.4	99.1/97.8	70.3/69.1	98.5/98.5	73.9/76.6	99.2/98.4
2/3	2/3	75.5/75.1	99.4/99.2	69.5/72.1	98.0/96.6	73.2/76.0	99.0/97.6

6.3.4 The average flushing efficiency of the whole tank

Figure 6.8 shows the influence of compartment division on the flushing efficiency at $T = 1$ and $T = 3$ in the 2×2 tank. It can be seen that for the 'far open' case in the 2×2 tank, the flushing efficiency $\bar{C}$ is symmetrical according to the line $k_1 = k_2$ and $k_1 + k_2 = 1$, respectively (see Figure 6.8(a,b)). When the sum of k_1 and k_2 is fixed, the smaller the difference between k_1 and k_2 is, the higher the flushing efficiency will be achieved. The maximum $\bar{C}$ is achieved at $k_1 = k_2 = 1/2$. That is, geometrical symmetry improves flushing. For the 'near open' case in the 2×2 tank, $\bar{C}$ is symmetrical according to $k_2 = 0.5$ (see Figure 6.8(c,d)). When k_2 is fixed, the highest $\bar{C}$ will be achieved at $k_1 \simeq 0.8 - 0.9$. The reason why k_1 should be kept larger than 0.5 is that $f_{11,21} > 0.5Q$. For the 'both open' case, the optimal flushing can be achieved at $k_1 \simeq 0.7$ and $k_2 \simeq 0.6$ (see Figure 6.8(e,f)). Table 6.1 summarises the theoretical and experimental flushing efficiency for different divisions of compartment volume. The discrepancy between the experiment and the theory is within ±3.3% for $\bar{C}|_{T=1}$, and within ±2.5% for $\bar{C}|_{T=3}$, which proves the accuracy of the theory in assessing the flushed efficiency in the tank.

The model predictions agree with measurements for the flux constrained cases. For

the pressure constrained cases, the flow is sensitive to bypassing (due to the difficulty of maintaining the same pressure of the two exits). However, the discrepancy for the average flushing efficiency of the tank is small at three exchange volumes because the compartments which are not accurately predicted are always small in volume and do not contribute a lot to the average flushing efficiency of the whole tank.

6.4 Implications to unstratified flushing through inhomogeneous tanks

In this section, the mathematical model is extended to analyse the flushing through an inhomogeneous 2×2 and 3×2 tank.

6.4.1 Implications to a 2×2 inhomogeneous tank

Figure 6.9 shows the influence of flow allocation and compartment capacity on the flushing efficiency at $T = 3$ when $k_1 = k_2 = k$. For the 'far open' case, $\bar{C}$ is symmetrical according to the line $\phi = 0.5$ and $k = 0.5$, respectively (see Figure 6.9(a)). When k is fixed, $\bar{C}$ reaches the highest at $\phi = 0.5$. This is because when $k_1 = k_2$, the tank is geometrically symmetrical according to the diagonal line across compartments 11 and 22, so that the best flushing strategy is to allocate the incoming fluid equally to the two flow pathways. When ϕ is fixed around 0.5, the most efficient strategy for the system configuration is to keep $k = 0.5$; but when ϕ is close to 0 or 1, k needs to be calculated. For the 'near open' case, no matter how k varies, $\bar{C}$ is always the highest at $\phi = 1$, that is, the flow network becomes a linear system (see Figure 6.9(b)). When ϕ is close to 0, the optimal flushing is achieved at $k = 1$, that is, the network regresses to a single-compartment system; when ϕ is larger, k needs to be calculated. For the 'both open' case, $\bar{C}$ reaches the highest at $\phi \simeq 0.5 - 0.7$ and $k \simeq 0.5 - 0.7$ (see Figure 6.9(c)).

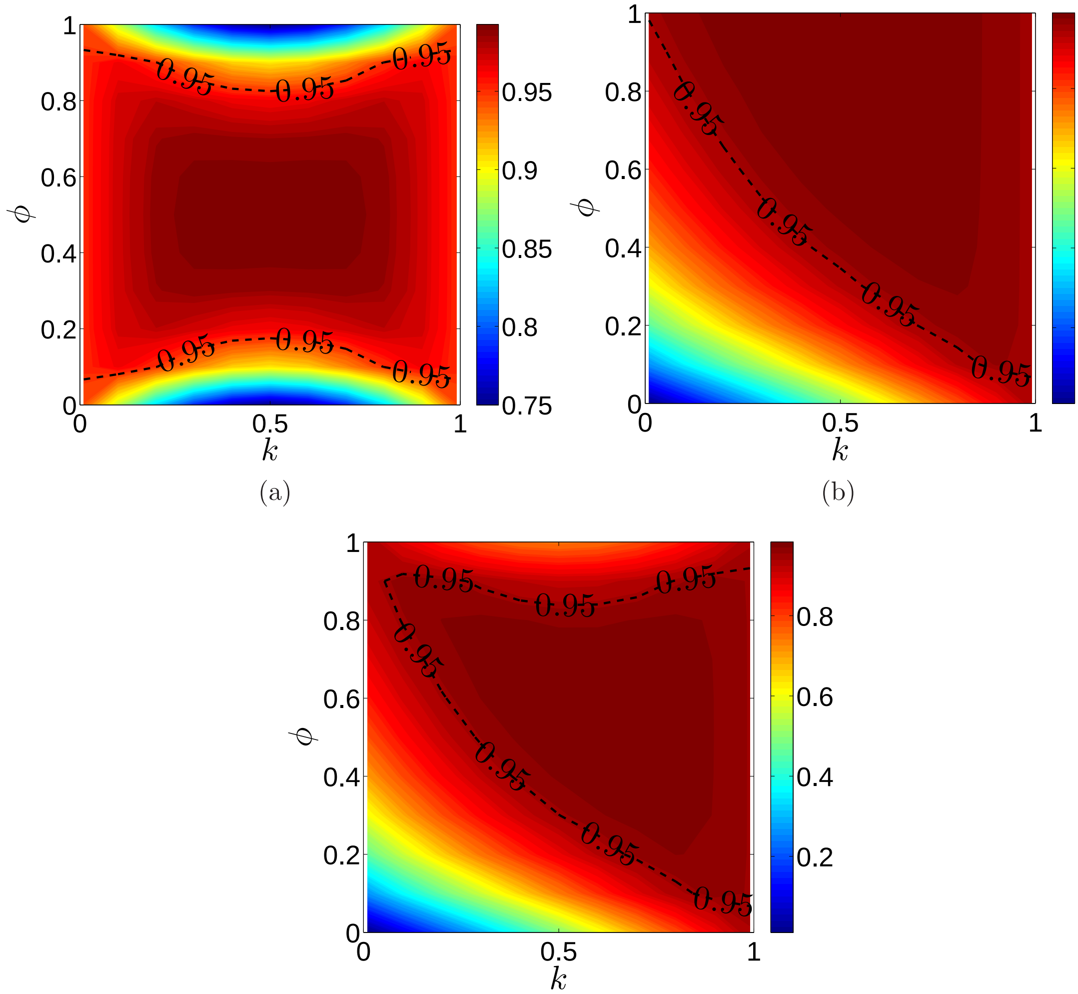

Figure 6.9: The theoretical predictions of $\bar{C}$ at $T = 3$ considered with ϕ and k in the 2×2 inhomogeneous tank. The figures correspond to (a) 'far open', (b) 'near open', and (c) 'both open'.

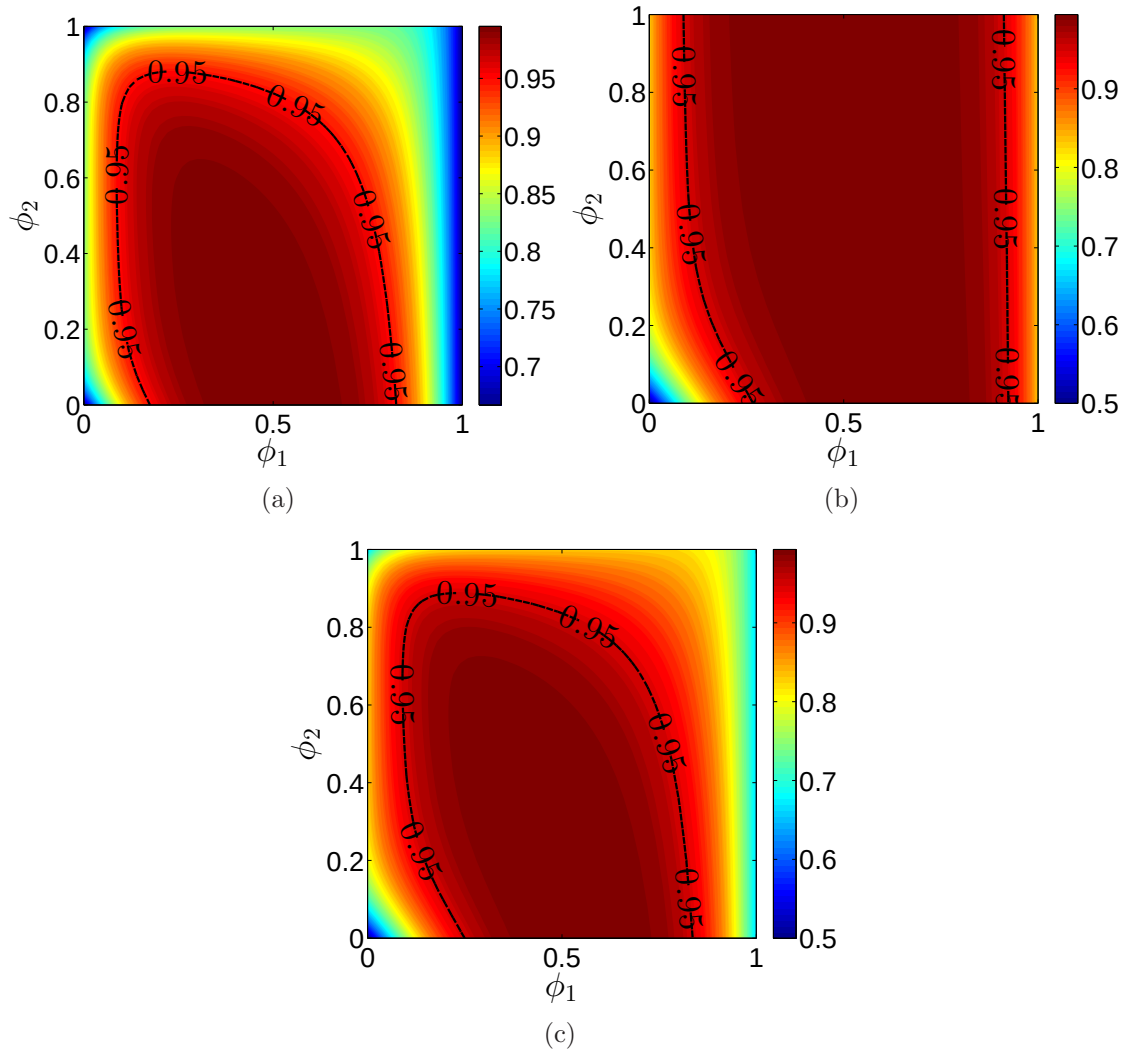

Figure 6.10: The theoretical predictions of $\bar{C}$ at $T = 3$ considered with ϕ_1 and ϕ_2 in a 3×2 inhomogeneous tank. The figures correspond to (a) 'far open', (b) 'near open' and (c) 'both open'.

Table 6.2: The existence of Hamiltonian path from the inlet to the outlet in an $m \times n$ tank.

	Far open		Near open	
	n is odd.	n is even.	n is odd.	n is even.
m is odd.	Yes	Yes	Yes	No
m is even.	Yes	No	Yes	Yes

6.4.2 Implications to a 3×2 inhomogeneous tank

A 3×2 tank is shown in Figure 3.4(b). $L_1 = L_2$ and $W_1 = W_2 = W_3$. Let $\phi_1 = f_{11,12}/Q$, $\phi_2 = f_{21,22}/f_{11,21}$. Figure 6.10 shows the influence of ϕ_1 and ϕ_2 on the flushing efficiency at $T = 3$ of the 3×2 tank under the condition that all compartments are identical. For the 'far open' and 'both open' cases, the optimal flushing may be achieved at $\phi_1 \simeq 0.3-0.8$ and $\phi_2 \simeq 0-0.8$ (see Figure 6.10(a,c)). When $\phi_1 < 0.2$ or $>$ 0.8, compartment 12 or 21 cannot be effectively flushed, respectively; when $\phi_2 > 0.9$, compartment 31 cannot be flushed very well. But when ϕ_2 is large, compartment 22 can be flushed by compartment 12, so a high flushing efficiency can still be achieved in this case. For the 'near open' case, the flushing efficiency is mainly dependent on ϕ_1 (see Figure 6.10(b)). When ϕ_1 is neither too high (>0.9) nor too low (<0.2), all the six compartments can be effectively flushed in theory. The most efficient flushing may be achieved at $\phi_1 = 0.25 - 0.9$.

6.5 Topological analysis

For an $m \times n$ tank with a single inlet and a single outlet, whether it can be made linear depends on whether there exists a Hamiltonian path (Montalbano, 1962), which starts from the inlet compartment, visits each compartment once and only once, and ends at the outlet compartment. Table 6.2 lists the rule to determine the existence of Hamiltonian path from the inlet to the outlet in an $m \times n$ tank, which depends on the parity of m and n. For the 'far open' case, there is no Hamiltonian path from

the inlet to the outlet when both m and n are even; for the 'near open' case, there is no Hamiltonian path when m is odd and n is even. In these cases, the tank cannot be made linear, and thus the optimal flushing strategy needs to be calculated.

6.6 Summary

The multizone network model is further validated against a series of detailed experimental tests in a 2×2 tank for the inhomogeneous case. The influence of the hole resistance on the flushing through a 2×2 tank with equal-sized compartments, as well as the influence of the compartment capacitance on the flushing through the tank with equal-sized connecting holes have been studied. The model predictions agree extremely well with the measurements when the flow is constrained by volume flux. When there are two outlets and the flow is pressure controlled, the difference between the experimental and theoretical results is about 10%. This difference is likely due to the difficulty of realising this situation in the laboratory, rather than a model failure.

The flushing efficiency of a multi-compartment tank depends on hole resistance, compartment capacitance and the boundary conditions applied to the problem. The mixing within each compartment is perfect. The small lightening holes with sharp edge in ballast tanks generate a turbulent flow where the RMS velocity is comparable to the mean. For a tank with a single outlet, the optimal flushing strategy is to form a linear network by blocking some flow pathways (e.g. the 'near open' case of the 2×2 tank). However, although connecting all the ballast tanks in series is more effective for flushing, the added complexity of retrofitting the additional pipework makes it less practical. Generally, fluid of a compartment needs to be allocated more to the pathway that has a larger capacity by reducing the resistance on the way. Especially for the symmetrical tank, the flow needs to be allocated equally (e.g. $k = 0.5$ for the 'far open' case of the 2×2 tank). If the hole resistance is fixed, the best configuration needs to be calculated.

The current analysis is applicable to cases when the initial ballast water and the water used for flushing have the same density. There are a number of scenarios where the density contrast may be important. The next chapter will extend the analysis to

stratified flushing.

Chapter 7

Stratified Flushing from In-line Tanks

Here 'an in-line tank' is defined as a tank composed of a series of compartments that are connected in line. Each compartment have only one inlet and only one outlet.

7.1 Introduction

When ballast water is taken at ports in warm shallow seas or near fresh water sources, density difference between the flushing water and the initial ballast water is important. In this chapter, the discussion in Chapters 5 and 6 is extended to include the case when there is density difference between the incoming fluid and the original fluid. This involves flushing a tank with water that is denser or lighter than the existing water in the tank. The influence of stratification means that there is a vertical distribution of NIS in each compartment. In contrast to the $Ri = 0$ case, the compartments from the side, rather than from the plan view, needs to be accurately followed to identify the vertical stratification. The physics in a tank composed of identical compartments connected in line are described. Three models that account for stratification and mixing are developed, and their predictions are tested against a specific set of experiments with a 1×7 network. A detailed critical analysis of the three modelling approaches is described in §7.7.

7.2 Description of physical processes

To provide a starting point for developing a model that captures the physics of stratified flushing, a brief overview of the observed physics is presented. The observations are limited to in-line exchange, where the stratification can be assessed. As summarised in Chapter 3, the key variables are the Richardson number Ri and the Reynolds number Re, defined as

$$Ri = \frac{\Delta\rho g L}{\rho U^2}, \qquad Re = \frac{UL}{\nu}, \tag{7.1}$$

where ρ is the density of the denser fluid, $\Delta\rho$ the density difference between the incoming fluid and the existing fluid, g the gravitational acceleration, ν the kinematic viscosity, U and L the characteristic velocity and length. In an in-line tank composed of identical compartments, characterised by a hole diameter D, Re and Ri are the same in each compartment.

A general categorisation of the physical processes that occur in a stratified exchange in a ballast tank is presented. For immiscible fluids at high Ri, e.g. water is injected to fill an empty tank, shown in Figure 7.1(a, b), stratification is very significant. The exchange process is limited by the loss of momentum at the connecting holes, which can lead to a hydraulically controlled horizontal exchange. The tank is separated to two regions - the lower region with dye water and the upper region with air. At the first stage, water descends into the adjacent compartment through the lightening holes to fill the lower region of the tank, and the stable height of the water is the same among the previous compartments that have been flushed, which is higher than the lower edge of the connecting holes. During the next stage, after all compartments have been filled to the same stable height, the water height in all compartments rises at the same rate to the upper edge of the connecting holes. At the final stage, water fills up the whole region of the last compartment, but in other compartments, air remains in the trapped region above the upper edge of the connecting holes.

For miscible fluids, the physical processes change as Ri decreases. At high Ri, e.g. a tank full of fresh water is flushed with salt water at a low flow rate, shown

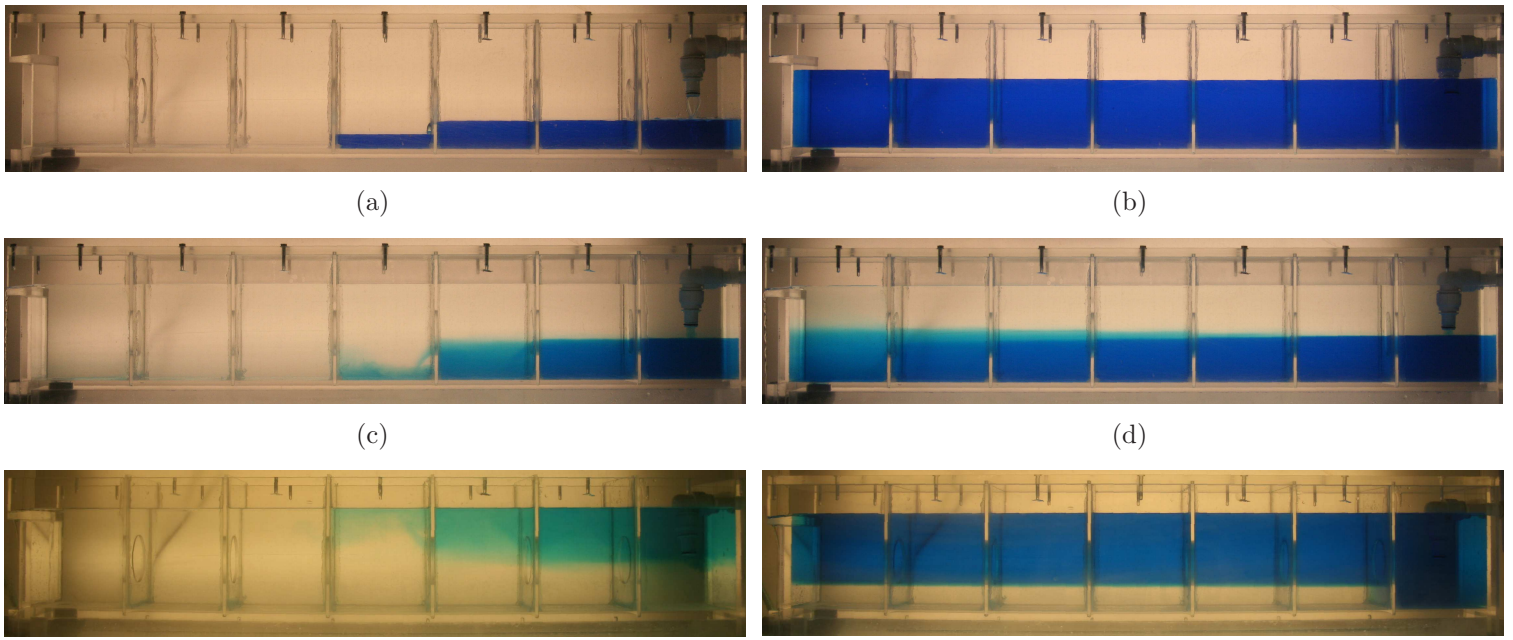

Figure 7.1: Images of stratified flushing from a 1×7 tank at high Ri. The tank is filled or flushed at a fixed rate with dye water. The figures correspond to (a, b) water to air ($Ri = 22953$), (c, d) salt water to fresh water ($Ri = 450$) and (e, f) fresh water to salt water ($Ri = -450$); (a, c, e) short time and (b, d, f) long time.

in Figure 7.1(c, d), the incoming water will first exchange the existing water in the lower region. Mixing occurs at the same time, due to an overspilling flow, that appears to form a plume, which descends to the bottom of the neighbouring compartment. Entrainment causes dilution and the volume flux of the dyed fluid to increase. When the lower region of the tank has been displaced with the incoming water, the interface of the last compartment rises first and flows back to the middle region of the previous compartments. At the final stage, only the last compartment is fully flushed; in other compartments, the water in the region above the upper edge of the holes is not exchanged. When the salt water tank is slowly flushed with fresh water ($Ri < 0$), the incoming light water will mix with and displace the dense water from the upper region of the tank (see Figure 7.1(e)). The upper region of the tank is flushed from the inlet compartment to the outlet compartment. When the flow bypasses the upper region, shear mixing occurs in the middle region so that the interface decreases. Finally, the tank is stably separated to two regions. The top region is occupied with the incoming light water, and the original dense water remains on the bottom (see Figure 7.1(f)).

Lower Ri increases turbulence at the sharp edge of the connecting holes. Figure 7.2 shows the perfect mixing ($Ri = 0$) and weakly stratified flushing ($Ri = \pm 4.5$) from a 1×7 tank. When the water tank is flushed with water at a high Re, due to turbulent diffusion, the exchange process almost follows the perfect mixing mode in each compartment. Water in the tank is mixed evenly from the inlet compartment to the outlet compartment when there is no density difference between the existing water and the external water (see Figure 7.2(a, b)). There is no trapped region in each compartment of the tank after a sufficiently long time flushing. When salt water enters a tank to flush fresh water at a high Re (see Figure 7.2(c, d)), the compartments that are close to the inlet are strongly mixed and can be fully displaced after a long time flushing; a portion of the original fresh water will remain in the top region of the compartments far from the inlet. When the salt water tank is flushed with fresh water at a high Re, (see Figure 7.2(e, f)), the compartments near the inlet are well mixed and then fully displaced by the incoming water; a small amount of the original salt water will be trapped in the bottom of the compartments far from the inlet.

For immiscible fluids, a displacement model is developed to describe the movement

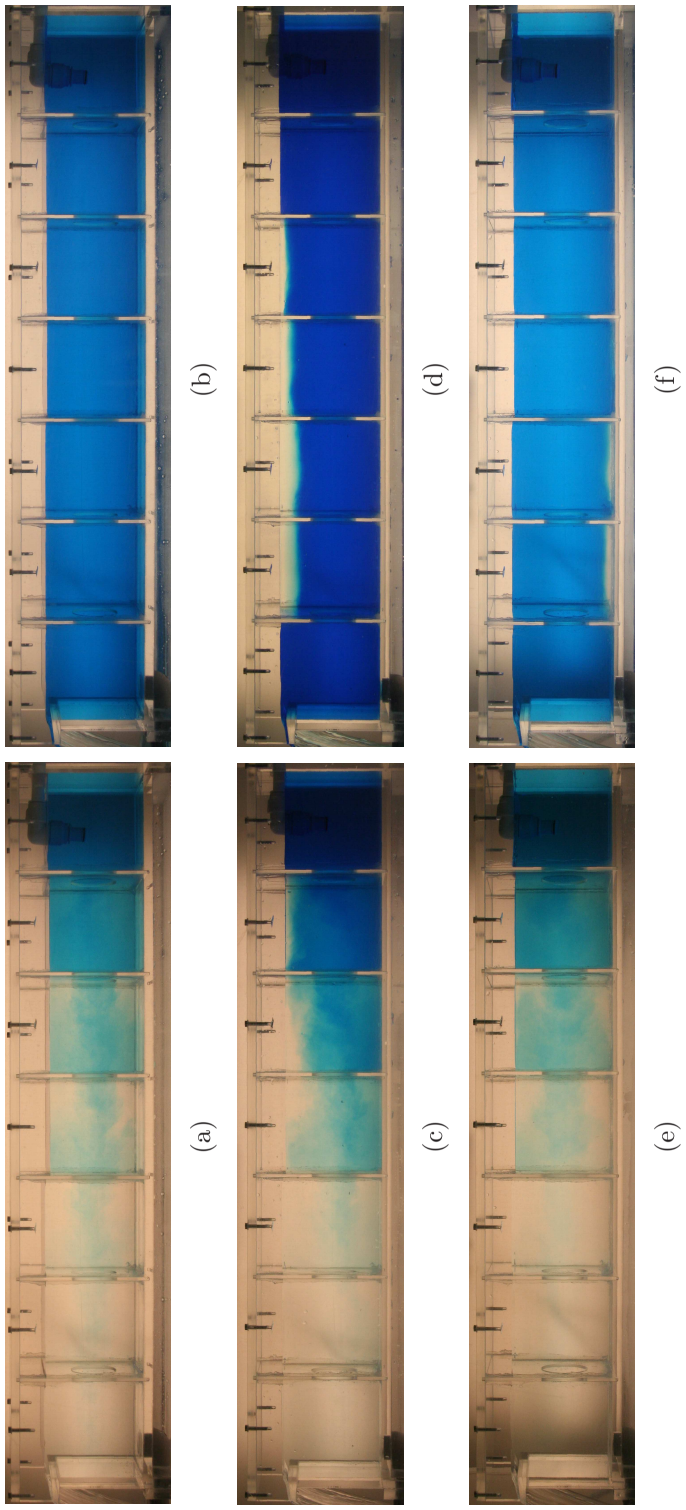

Figure 7.2: Images of flushing from a 1×7 tank at low Ri. The figures correspond to Ri = (a, b) 0, (c, d) 4.5 and (e, f) -4.5; (a, c, e) short time and (b, d, f) long time.

of the incoming fluid. For miscible fluids, a stratified mixing model and a plume model are developed to describe the fluid exchange; the plume model is more theoretically strict but the stratified mixing model is more applicable to real ballast tanks.

7.3 Displacement model

When $Ri \to \pm\infty$, the flow is so slow that it can be considered stagnant. For miscible fluids, diffusion still operates, but since it operates over a time scale of $H^2/\mathcal{D} \sim 10^6$s (in real ballast tanks), it can be ignored over the typical time scale of flushing. In the limit of $Ri \to \pm\infty$, the momentum equation and the convection equation reduce to

$$0 = -\boldsymbol{\nabla} p + \Delta\rho g \hat{\boldsymbol{z}} \quad \text{and} \quad \frac{\mathrm{D}C}{\mathrm{D}t} = 0. \tag{7.2}$$

These equations essentially describe a geometric process of filling where the interface in interconnected spaces rises at the same rate.

There are two separate cases to consider: denser fluid injected into lighter fluid ($Ri > 0$) and lighter fluid injected into denser fluid ($Ri < 0$). In order to simplify the discussion, all compartments of the tank are assumed to be identical with height H, and the upper and lower edges of holes between each two neighbouring compartments are at the same height, H_u and H_l, respectively.

7.3.1 Denser fluid to lighter fluid ($Ri \gg 1$)

When $Ri \gg 1$, the incoming denser fluid essentially fills up the tank from the bottom, pushing out the lighter fluid. The pressure and the flushed fraction of a point at height z (a distance from the tank bottom) in compartment i are

$$p(z) = \Delta\rho g(h_i - z)\mathcal{H}(h_i - z) + \rho g(H - z) \quad \text{and} \quad C(z) = \mathcal{H}(h_i - z), \tag{7.3}$$

where h_i is the height of the interface between the denser fluid and the lighter fluid in compartment i, H the height of the tank, and $\mathcal{H}(X)$ the Heaviside-step function with the properties $\mathcal{H}(X) = 0$ for $X < 0$ and 1 for $X \geq 0$. From (7.3), the flushed

fraction in compartment i is

$$C_i = \frac{h_i}{H}. \tag{7.4}$$

The lower region of each compartment is flushed one by one through the lightening holes from the inlet compartment to the outlet. This stage is hydraulically controlled by the processes of the lightening holes. The side view and front view of compartment i that is being flushed are shown in Figure 7.3(a, b), respectively. When lighter fluid in compartment i is flushed with denser fluid from compartment $i-1$, there are two layers in both compartments. In compartment $i-1$, the interface between the upper lighter fluid and the lower denser fluid is stable. The lower region of compartment i is flushed with the dense fluid from the lower region of compartment $i-1$. The interface in compartment i rises from the bottom to the height of the lower edge of the hole.

When denser fluid from compartment i passes over a circular sharp-crested weir to compartment $i+1$, energy conservation requires

$$p + \Delta\rho g z + \frac{\rho u^2}{2} = \text{const}, \tag{7.5}$$

where p is pressure and u flow velocity. Ignoring the approach velocity and the change of pressure,

$$u_{i,i+1}(z) = \sqrt{2\frac{\Delta\rho}{\rho} g(h_i - z)}, \tag{7.6}$$

where $u_{i,i+1}(z)$ is the velocity of a point over the weir from compartment i to $i+1$ at height z.

The theoretical volume flow rate of the denser fluid over the weir of compartment i to $i+1$, $f^*_{i,i+1}$, can be written as

$$f^*_{i,i+1} = \int_{H_l}^{h_i} u_{i,i+1} w \mathrm{d}z, \tag{7.7}$$

where $w = 2\sqrt{(z - H_l)(H_l + D - z)}$ is the width of the weir cross section at height

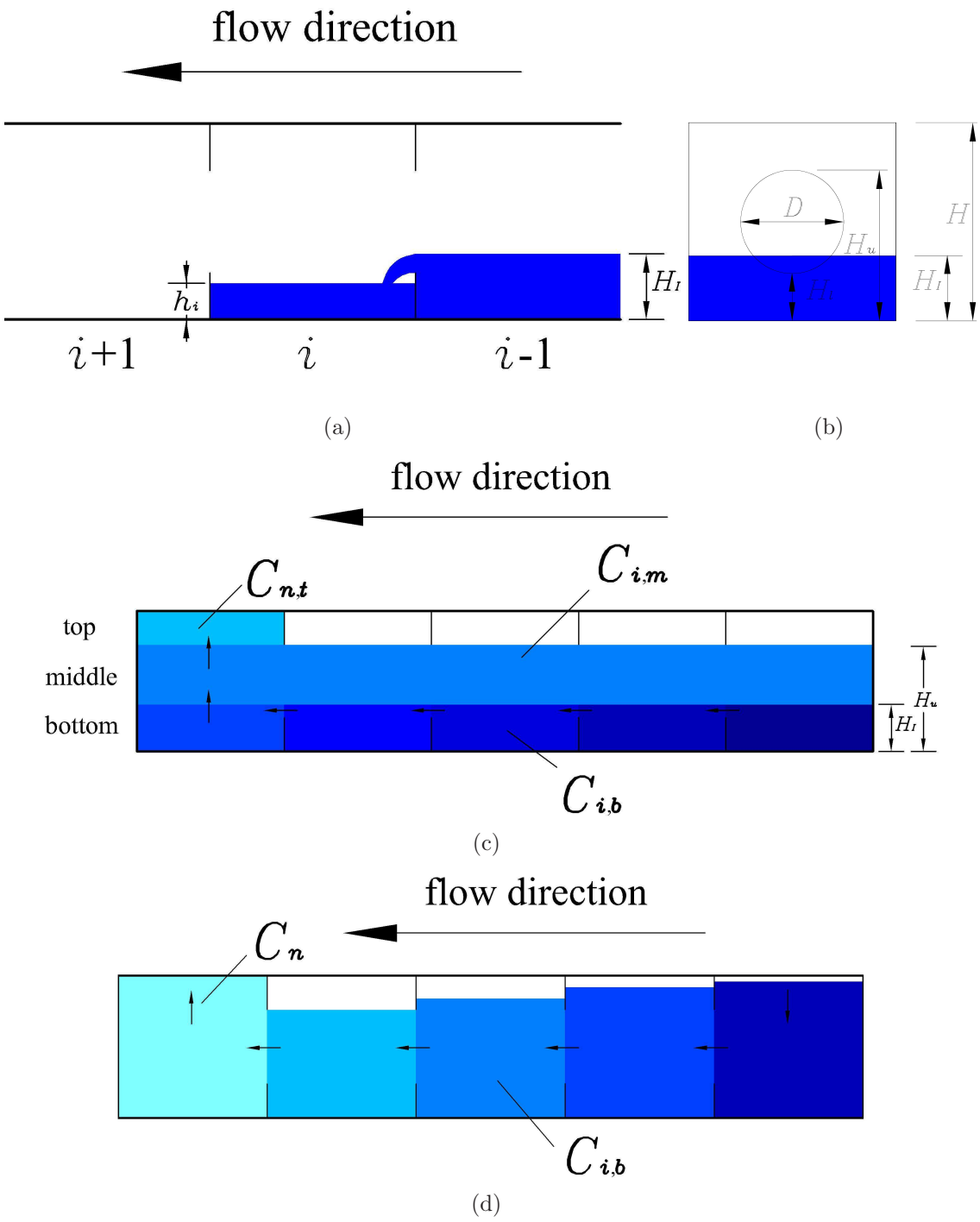

Figure 7.3: Schematics of a tank that is flushed with denser fluid. H, H_l and H_u are the height of the compartment, the lower edge and the upper edge of the hole, respectively. The figures correspond to the (a) side view and (b) front view of immiscible fluids, and the side view of miscible fluids at (c) high Ri and (d) low Ri.

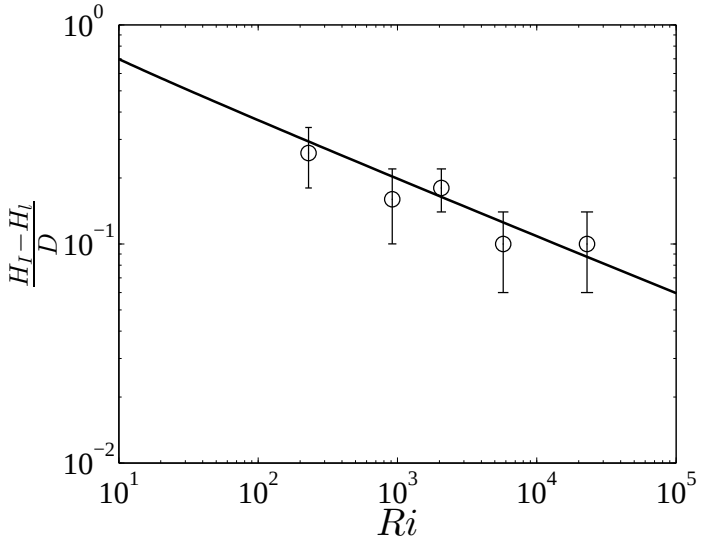

Figure 7.4: $(H_I - H_l)/D$ is plotted against Ri in a log-log scale. The points with errorbars are experimental measurements (described in 7.6.1).

z, and D the diameter of the circular hole in the wall between neighbouring compartments. Vatankhah (2010) used the numerical integration and curve cutting method, and by introducing the discharge coefficient (C_d) to (7.7) to take into account the effect of approach velocity head and correct other non-realistic assumptions, obtained

$$f_{i,i+1} = 0.3926 C_d \sqrt{2\frac{\Delta\rho}{\rho} g D} (h_i - H_l)^2 \left(\sqrt{1 - 0.22\frac{h_i - H_l}{D}} + \sqrt{1 - 0.773\frac{h_i - H_l}{D}} \right). \tag{7.8}$$

C_d is determined using curve fitting method based on Greve's data (Greve, 1932) as

$$C_d = \frac{0.728 + 0.24(h_i - H_l)/D}{1 + 0.668\sqrt{(h_i - H_l)/D}}. \tag{7.9}$$

The relative density contrast, $\Delta\rho/\rho$, is assumed to be the same for each compartment, so in the hydraulically controlled stage, the height of the stable interface of all compartments, H_I, corresponds to h_i at $f_{i,i+1} = Q$ in (7.8). When $h_i = H_I$ at

$f_{i,i+1} = Q$, by using $Q = \pi u D^2/4$ and $Ri = \Delta\rho g D/\rho u^2$,

$$Ri = \frac{2.001}{\left(\frac{0.728+0.24(H_I-H_l)/D}{1+0.668\sqrt{(H_I-H_l)/D}}\right)^2 \left(\frac{H_I-H_l}{D}\right)^4 \left(\sqrt{1-0.22\frac{H_I-H_l}{D}}+\sqrt{1-0.773\frac{H_I-H_l}{D}}\right)^2}. \tag{7.10}$$

Figure 7.4 shows the influence of Ri on $(H_I - H_l)/D$ in a log-log scale. $(H_I - H_l)/D$ decreases with Ri. This means that the stable height of the interface increases with the flow rate, but decreases with the density contrast or hole diameter. The relationship between the stable interface height and Ri was confirmed by the experimental observations (see the scatter points in Figure 7.4).

The flushing of the tank can be expressed into how the interface between denser and lighter fluid in each compartment changes in time. The height of the interface in compartment i is normalised as

$$\hat{h}_i = \frac{h_i}{H}, \tag{7.11}$$

so $\hat{h}_i = C_i$.

When denser fluid is injected, it will first displace the fluid below H_l in compartment 1. When $\hat{h}_1 = 0 \to H_l/H$, $\hat{h}_1$ increases linearly as

$$\frac{\mathrm{d}\hat{h}_1}{\mathrm{d}T} = n; \tag{7.12}$$

when the interface between the lower denser fluid and the upper lighter fluid rises to the lower edge of the connecting hole, compartment 1 starts to flush compartment 2; when $\hat{h}_1 = H_l/H \to H_I/H$, $\hat{h}_1$ increases more and more slowly as

$$\frac{\mathrm{d}\hat{h}_1}{\mathrm{d}T} = n\left(1 - \frac{f_{1,2}}{Q}\right), \tag{7.13}$$

where $f_{1,2}$ can be expressed by replacing h_i with h_1 on the right side of (7.8); since compartment i starts to be flushed until compartment i starts to flush compartment

$i+1$, that is, when $\hat{h}_{i-1} = H_l/H \rightarrow \hat{h}_i = H_l/H$, $i = 2, 3, \cdots, n-1$, $\hat{h}_i$ increases as

$$\frac{\mathrm{d}\hat{h}_i}{\mathrm{d}T} = n\frac{f_{i-1,i}}{Q}; \tag{7.14}$$

since compartment i starts to flush compartment $i+1$ until h_i rises to H_I, that is, when $\hat{h}_i = H_l/H \rightarrow H_I/H$, $i = 2, 3, \cdots, n-1$, $\hat{h}_i$ increases as

$$\frac{\mathrm{d}\hat{h}_i}{\mathrm{d}T} = n\frac{f_{i-1,i} - f_{i,i+1}}{Q}; \tag{7.15}$$

since compartment n starts to be flushed until h_n rises to H_I, that is, when $\hat{h}_{n-1} = H_l/H \rightarrow \hat{h}_n = H_I/H$, $\hat{h}_n$ increases as

$$\frac{\mathrm{d}\hat{h}_n}{\mathrm{d}T} = n\frac{f_{n-1,n}}{Q}; \tag{7.16}$$

then the incoming denser fluid flushes all the compartments at the same rate, and the height of the interface rises at a constant rate until $\hat{h}_i = H_u/H$, that is, $\hat{h}_i$ increases as

$$\frac{\mathrm{d}\hat{h}_i}{\mathrm{d}T} = 1 \tag{7.17}$$

for $T = H_I/H \rightarrow H_u/H$; after that, only the last compartment is flushed until all the original fluid in it is replaced, that is, $\hat{h}_n$ increases as

$$\frac{\mathrm{d}\hat{h}_n}{\mathrm{d}T} = n \tag{7.18}$$

for $T = H_u/H \rightarrow H_u/H + (H - H_u)/nH$. The initial condition is $\hat{h}_i|_{T=0} = 0$.

7.3.2 Lighter fluid into denser fluid ($Ri \ll -1$)

Nowthe case when the fluid is highly vertically stratified ($Ri \ll -1$) is considered, which occurs when lighter fluid is introduced slowly into the tank. The pressure and

the flushed fraction of a point at height z in compartment i are

$$p(z) = -\Delta\rho g(h_i - z)\mathcal{H}(h_i - z) + (\rho + \Delta\rho)g(H - z), \qquad C(z) = 1 - \mathcal{H}(h_i - z), \tag{7.19}$$

and the flushed fraction in each compartment is

$$C_i = 1 - \hat{h}_i = 1 - \frac{h_i}{H}. \tag{7.20}$$

In this case, the flow rate from compartment i to $i+1$ can be expressed as

$$f_{i,i+1} = 0.3926 C_d \sqrt{2\frac{\Delta\rho}{\rho} g D (H_u - h_i)^2} \left(\sqrt{1 - 0.22\frac{H_u - h_i}{D}} + \sqrt{1 - 0.773\frac{H_u - h_i}{D}} \right) \tag{7.21}$$

(Vatankhah, 2010), where

$$C_d = \frac{0.728 + 0.24(H_u - h_i)/D}{1 + 0.668\sqrt{(H_u - h_i)/D}}. \tag{7.22}$$

The stable height of the interface, H_I, corresponds to h_i at $f_{i,i+1} = Q$ in (7.21).

When lighter fluid is injected to denser fluid, the incoming fluid will first displace the original fluid above the upper edge of the hole in compartment 1, that is, when $\hat{h}_1 = 1 \to H_u/H$, $\hat{h}_1$ decreases linearly as

$$\frac{\mathrm{d}\hat{h}_1}{\mathrm{d}T} = -n; \tag{7.23}$$

when the interface between the lower denser fluid and the upper lighter fluid declines to the upper edge of the holes, the lighter fluid starts to flush compartment 2; when $\hat{h}_1 = H_u/H \to H_I/H$, $\hat{h}_1$ decreases more and more slowly as

$$\frac{\mathrm{d}\hat{h}_1}{\mathrm{d}T} = -n\left(1 - \frac{f_{1,2}}{Q}\right); \tag{7.24}$$

since compartment i starts to be flushed until h_i declines to the upper edge of the connecting hole, that is, when $\hat{h}_{i-1} = H_u/H \to \hat{h}_i = H_u/H$, $i = 2, 3, \cdots, n-1$, $\hat{h}_i$

decreases as

$$\frac{\mathrm{d}\hat{h}_i}{\mathrm{d}T} = -n\frac{f_{i-1,i}}{Q}; \tag{7.25}$$

when h_i decreases to H_u, compartment i starts to flush compartment $i+1$; since compartment i starts to flush compartment $i+1$ until h_i declines to H_I, that is, when $\hat{h}_i = H_u/H \to H_I/H$, $i = 2, 3, \cdots, n-1$, $\hat{h}_i$ decreases as

$$\frac{\mathrm{d}\hat{h}_i}{\mathrm{d}T} = -n\frac{f_{i-1,i} - f_{i,i+1}}{Q}. \tag{7.26}$$

Then the lighter fluid bypasses the tank, while the fluid of compartment n is not exchanged. There forms two layers in the whole tank: the incoming lighter fluid is in the upper region, while the original denser fluid in the lower region.

7.4 Stratified mixing model

The disadvantage of the displacement model is that it is only valid for immiscible fluids because it does not describe the mixing processes shown in §7.2. For miscible fluids, the model is extended to incorporate the stratified mixing with weir effect. The basis of the model is that each compartment is separated into three or two layers and perfect mixing occurs in the layers that are not entrained in the tank.

7.4.1 Denser fluid into lighter fluid

When denser fluid is injected into the lighter fluid in a $1\times n$ tank, the fluid is separated into three layers (bottom, middle and top region) in each compartment, and the top region of compartments 1, 2, $\cdots$, $n-1$ is entrained. The height of the interface between the bottom and the middle region is H_I (determined by (7.10)), and that between the middle and the top region is H_u (the top height of the connecting holes). In compartment i, the flushed fraction in the lower, middle and upper region is $C_{i,l}$, $C_{i,m}$ and $C_{i,u}$, respectively. The flushed fraction of compartment i, can be expressed

as a combination of the flushed fraction in each layer, i.e.

$$C_i = \frac{H_I}{H} C_{i,b} + \frac{H_u - H_I}{H} C_{i,m} + \left(1 - \frac{H_u}{H}\right) C_{i,t}. \tag{7.27}$$

Figure 7.3(c) illustrates the stratified mixing model in a $1 \times n$ tank that is flushed with denser fluid. When a tank with fluid is flushed with denser fluid, the external fluid enters the inlet compartment and mixes with the fluid in the bottom region of the compartment (below H_I). The mixed fluid in the bottom region of compartment 1 flushes the bottom region of compartment 2, and the mixed fluid in the bottom region of compartment $i-1$ flushes the bottom region of compartment i, until the mixed fluid in the bottom region of compartment $n-1$ flushes the bottom region of compartment n. The mixed fluid in the bottom region of compartment n flushes the middle region (between H_I and H_u) of the whole tank, and the mixed fluid in the middle region of the tank flushes the top region of compartment n. Some original fluid remains in the top region of compartments 1, 2, $\cdots$, $n-1$. The flushed fraction in compartment i is described by

$$\frac{\mathrm{d}C_{1,l}}{\mathrm{d}T} = \frac{nH}{H_I}(1 - C_{1,l}), \tag{7.28}$$

$$\frac{\mathrm{d}C_{i,l}}{\mathrm{d}T} = \frac{nH}{H_I}(C_{i-1,l} - C_{i,l}), \quad i = 2, 3, \cdots, n, \tag{7.29}$$

$$\frac{\mathrm{d}C_{i,m}}{\mathrm{d}T} = \frac{H}{H_u - H_I}(C_{n,l} - C_{i,m}), \quad i = 1, 2, \cdots, n, \tag{7.30}$$

$$\frac{\mathrm{d}C_{n,u}}{\mathrm{d}T} = \frac{nH}{H - H_u}(C_{n,m} - C_{n,u}). \tag{7.31}$$

The variation of the flushed fraction in a mixed region is a result of the combination of being flushed by the upstream neighbouring section and flushing its downstream neighbouring section. For each section, the sum of the inflow rate is equal to the sum of the outflow rate.

At a low Ri and high Re, the flow is strongly turbulent. From the observation shown in Figure 7.2(d), the further a compartment lies from the inlet, the thicker the entrained region exists on the top of the compartment. The stable interface in some compartments can be higher than H_u because the region above the lower

edge of these compartments is partly perturbed, illustrated in Figure 7.3(d). The height of the stable interface is different among compartments because the extent of turbulence in each compartment is different, although the Ri and Re are the same among compartments. The stratified flushing from a $1\times n$ tank can be described by perfect mixing in the whole or part of each compartment. In this case, each compartment is assumed to be divided to two regions - the upper region and the lower region. For compartment i, the flushed fraction in the upper region and lower region are $C_{i,u}$ and $C_{i,l}$, respectively. $C_{i,u} = 0$. $C_i = C_{i,l}H_{i,I}/H$. The flushed fraction varies as

$$\frac{\mathrm{d}C_{1,l}}{\mathrm{d}T} = \frac{nH}{H_{1,I}}(1 - C_{1,l}), \tag{7.32}$$

$$\frac{\mathrm{d}C_{i,l}}{\mathrm{d}T} = \frac{nH}{H_{i,I}}(C_{i-1,l} - C_{i,l}), \quad i = 2, 3, \cdots, n-1, \tag{7.33}$$

$$\frac{\mathrm{d}C_n}{\mathrm{d}T} = n(C_{n-1,l} - C_n), \tag{7.34}$$

where $H_{i,I}$ is the interface height of compartment i.

7.4.2 Lighter fluid into denser fluid

When lighter fluid is injected to flush the denser fluid in a $1\times n$ tank, the fluid is separated into three layers (top, middle and bottom region) in each compartment, and the lower region of the tank is entrained. The height of the interface between the upper and the lower region, H_I, is determined by (7.21) at $f_{i,i+1} = Q$. In compartment i, the flushed fraction in the upper, middle and lower region is $C_{i,u}$, $C_{i,m}$ and $C_{i,l}$, respectively. $C_{i,b} = 0$. The flushed fraction of compartment i, can be expressed as

$$C_i = \left(1 - \frac{H_I}{H}\right) C_{i,u} + \frac{H_I - H_l}{H} C_{i,m}. \tag{7.35}$$

From the experimental observation shown in Figure 7.1(e, f), it can be seen that when the incoming lighter fluid bypasses the tank, shear mixing occurs in the middle region. A portion of the flow from the inlet compartment mixes with the fluid in the

middle region of the tank. When $Ri \to 0$, there is not much density gradient and the fluid flow nearly follows the perfect mixing rule; when $Ri \to \infty$, the stratification is so strong that the vertical velocity is inhibited (Park et al., 1994). It is widely accepted that at a certain range of local Ri, the vertical flow speed, v, can be expressed as

$$\frac{v}{u} \propto |Ri|^{-n}, \tag{7.36}$$

where u is the horizontal flow speed and n is a positive constant. Many theoretical and experimental studies have focused on determining the value of n and the proportional coefficient. Here a form which has been verified by the experiments to estimate the vertical flow speed is adopted, that is,

$$\frac{v}{u} = 0.6|Ri|^{-\frac{1}{2}} \tag{7.37}$$

for $30 < |Ri| < 1000$ (Kranenburg, 1984). When density difference increases or flow speed decreases, the entrainment rate (v/u) decreases with $|Ri|^{-1/2}$. The region between H_I and H_l of the tank is assumed to be diffused by the flow from the upper region of compartment 1 at a rate of Q_v, where $Q_v = vL_1W_1$, L_1 and W_1 are the length and width of compartment 1. This region is assumed to be mixed very well across all compartments. The flushed fraction in compartment i is described by

$$\frac{\mathrm{d}C_{1,u}}{\mathrm{d}T} = \frac{nH}{H - H_I}(1 - C_{1,u}), \tag{7.38}$$

$$\frac{\mathrm{d}C_{i,u}}{\mathrm{d}T} = \frac{nH}{H - H_I}\left(1 - \frac{Q_v}{Q}\right)(C_{i-1,u} - C_{i,u}), \quad i = 2, 3, \cdots, n, \tag{7.39}$$

$$\frac{\mathrm{d}C_{i,m}}{\mathrm{d}T} = \frac{H}{H_I - H_l}\frac{Q_v}{Q}(C_{1,u} - C_{i,m}), \quad i = 1, 2, \cdots, n. \tag{7.40}$$

The top region of the tank is flushed at a rate of $Q - Q_v$.

For the strongly turbulent case at $Ri \ll -1$, shown in Figure 7.2(e, f), each compartment is divided to two regions, with flushed fraction $C_{i,u}$ in the upper region and $C_{i,l}$ in the bottom region. $C_{i,l} = 0$. $C_i = C_{i,u}(1 - H_{i,I}/H)$. The flushed fraction

in compartment i varies as

$$\frac{\mathrm{d}C_{1,u}}{\mathrm{d}T} = \frac{nH}{H - H_{1,I}}(1 - C_{1,u}), \tag{7.41}$$

$$\frac{\mathrm{d}C_{i,u}}{\mathrm{d}T} = \frac{nH}{H - H_{i,I}}(C_{i-1,u} - C_{i,u}), \quad i = 2, 3, \cdots, n. \tag{7.42}$$

7.5 Plume model

The disadvantage of the stratified mixing model is that it simply assumes that fluid is perfectly mixed in a region but in fact the fluid exchange is vertically different. From Figure 7.1(c, e), it can be seen that there forms a plume from the edge of the connecting hole from one compartment to another. Therefore, a plume model is developed to consider the vertical distribution of the flushed fraction.

7.5.1 Denser fluid into lighter fluid

The vertical dynamics of a plume are characterized by a volume flux Q_p, a specific momentum flux M_p and a mass flux F_p, defined as

$$Q_p = \pi b^2 w, \tag{7.43}$$

$$M_p = \pi b^2 w^2, \tag{7.44}$$

$$F_p = Q_p C_p, \tag{7.45}$$

where b is the radius of the cross-section of the plume, w the vertical flow velocity, C_p the flushed fraction of the plume which is a function of height and time and serves as proxy to salinity. A top hat model is used where the volume flux in the plume

increases due to entrainment, i.e.

$$\frac{\mathrm{d}Q_p}{\mathrm{d}z} = -2\pi bw\kappa = -2\pi^{\frac{1}{2}} M_p^{\frac{1}{2}} \kappa, \tag{7.46}$$

$$\frac{\mathrm{d}M_p}{\mathrm{d}z} = -\pi b^2 g \frac{\Delta\rho}{\rho}(C_p(z) - C_t(z)) = -\frac{Q_p^2}{M_p} g \frac{\Delta\rho}{\rho}(C_p(z) - C_t(z)), \tag{7.47}$$

$$\frac{\mathrm{d}F_p}{\mathrm{d}z} = -2\pi bwC_t(z)\kappa, \tag{7.48}$$

where $\kappa = 0.1$ is the empirically determined entrainment coefficient (Ülpre et al., 2013), and $C_t(z,t)$ the flushed fraction of the tank at height z and time t, respectively. The negative sign is used because the plume is going down.

Figure 7.5 shows the physics of the plume model in a compartment for dense fluid into light fluid. Near one side of a compartment, a downward plume takes place at height H_I, and the surrounding fluid in the compartment rises and exits at height H_I to the next compartment. Entrainment occurs on the surface of the plume. In a compartment, the horizontally integrated flushed fraction of the plume increases from the bottom to H_I, while that of the tank decreases from the bottom to H_u. The compartment can be vertically divided to N layers. The region below H_I in each compartment is vertically divided to NH_I/H layers. At layer j below H_I,

$$Q_{t,j} = Q_{p,j}, \tag{7.49}$$

where Q_t and Q_p are volume flux of the tank compartment and the plume, respectively; the original fluid in the region below H_I is advected by the vertical flow and removed by an entrainment into the plume,

$$A\frac{\partial C_t}{\partial t} + \frac{\partial (Q_t C_t)}{\partial z} = -2\pi bwC_t\kappa, \tag{7.50}$$

that is,

$$A_j(C_{t,j}^t - C_{t,j}^{t-1})\delta z + (Q_{t,j}C_{t,j}^{t-1} - Q_{t,j-1}C_{t,j-1}^{t-1})\delta t = -2\pi^{\frac{1}{2}} M_{p,j-1}^{\frac{1}{2}} C_{t,j-1}^{t-1}\kappa\delta t\delta z, \tag{7.51}$$

where $A_j = A - \pi b_j^2$ is cross-sectional area surrounding the plume cross-section, δz

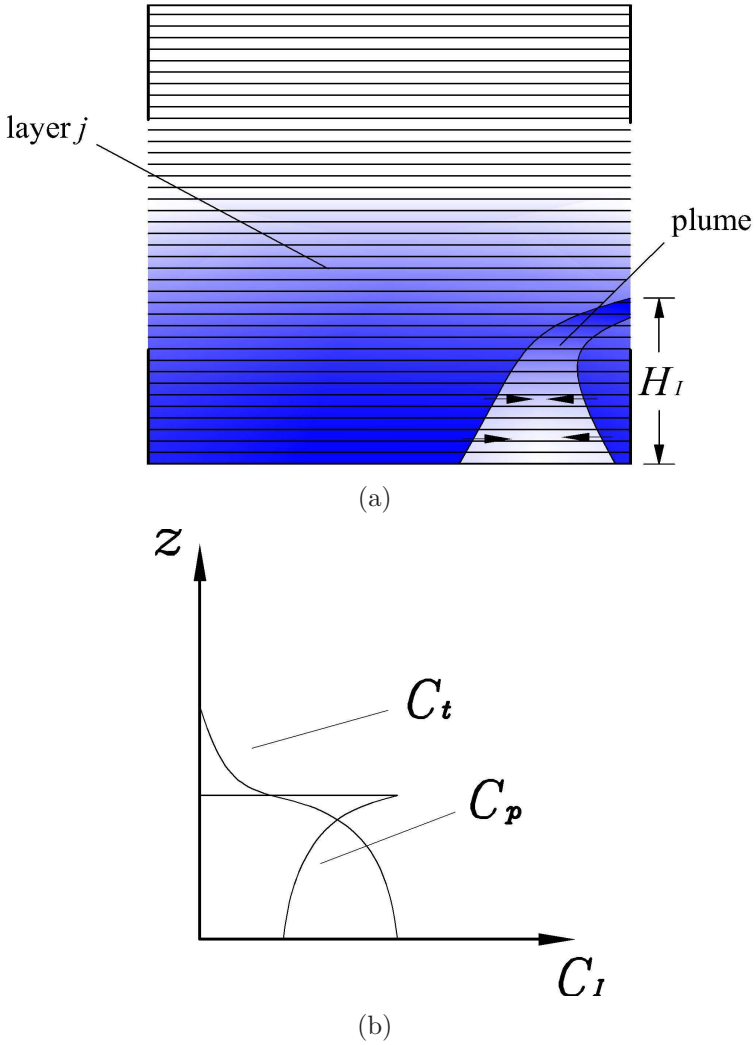

Figure 7.5: The plume model for the case of denser fluid into lighter fluid. (a) shows the schematic of the model in a compartment, and (b) shows the vertical distribution of the horizontal integrated flushed fraction of the plume and the tank.

vertical distance interval and δt time interval. The layer at height H_I in compartment $i-1$ is the source of the plume in compartment i, i.e.

$$Q_{p,i} = Q_{t,i-1}, \tag{7.52}$$

$$M_{p,i} = M_{p,i-1}, \tag{7.53}$$

$$F_{p,i} = F_{t,i-1} = Q_{t,i-1}C_{t,i-1}. \tag{7.54}$$

The whole region between H_I and H_u in the tank is vertically divided to $N(H_u - H_I)/H$ layers. The fluid from the lower layer is assumed to displace the fluid in the upper layer, so the flushed fraction at a layer between H_I and H_u is the same among all compartments. The layer at height H_I in compartment n is the source of the layer just above H_I in all compartments. The fluid at layer j between H_I and H_u is advected as

$$nA\frac{\partial C}{\partial t} + Q\frac{\partial C}{\partial z} = 0, \tag{7.55}$$

that is, at layer j between H_I and H_u in compartment i,

$$nA(C_{t,j}^{t} - C_{t,j}^{t-1})\delta z + Q(C_{t,j}^{t-1} - C_{t,j-1}^{t-1})\delta t = 0. \tag{7.56}$$

The region above H_u in compartment n which is flushed by the lower region from all compartments is divided to $N(1 - H_u/H)$ layers, and the source is the layer at height H_u. The fluid at layer j between H_u and H in compartment n is advected as

$$A\frac{\partial C}{\partial t} + Q\frac{\partial C}{\partial z} = 0, \tag{7.57}$$

that is,

$$A(C_{t,j}^{t} - C_{t,j}^{t-1})\delta z + Q(C_{t,j}^{t-1} - C_{t,j-1}^{t-1})\delta t = 0. \tag{7.58}$$

Compartment n can be completely flushed at the end, but the region above H_u in other compartments is trapped. The flushed fraction of the tank at layer j can be estimated by

$$C_j = A_j C_{t,j} + (A - A_j)C_{p,j}. \tag{7.59}$$

For compartment i, the flushed fraction C_i is calculated by

$$C_i = \frac{\sum_{j=1}^{N} C_{i,j}}{N}, \tag{7.60}$$

where $C_{i,j}$ is the flushed fraction at layer j in compartment i.

7.5.2 Lighter fluid into denser fluid

For lighter fluid into denser fluid, the governing equations become

$$\frac{\mathrm{d}Q_p}{\mathrm{d}z} = 2\pi^{\frac{1}{2}} M_p^{\frac{1}{2}} \kappa, \tag{7.61}$$

$$\frac{\mathrm{d}M_p}{\mathrm{d}z} = \frac{Q_p^2}{M_p} g \frac{\Delta\rho}{\rho} (C_p(z) - C_t(z)), \tag{7.62}$$

$$\frac{\mathrm{d}F_p}{\mathrm{d}z} = 2\pi b w C_t(z) \kappa. \tag{7.63}$$

Each compartment is vertically divided to N layers, and the interface layer is determined by using (7.21) to estimate H_I. The region above H_I in each compartment is vertically divided to $N(1 - H_I/H)$ layers. The original fluid in the region above H_I is removed by an entrainment into the plume,

$$A_j(C_{t,j}^t - C_{t,j}^{t-1})\delta z + (Q_{t,j} C_{t,j}^{t-1} - Q_{t,j+1} C_{t,j+1}^{t-1})\delta t = -2\pi^{\frac{1}{2}} M_{p,j+1}^{\frac{1}{2}} C_{t,j+1}^{t-1} \kappa \delta t \delta z. \tag{7.64}$$

The whole region between H_I and H_l in the tank is vertically divided to $N(H_I - H_l)/H$ layers. The fluid from the inlet compartment at H_I is assumed to displace the original fluid between H_I and H_l in the whole tank,

$$A(C_{t,j}^t - C_{t,j}^{t-1})\delta z + Q(C_{t,j}^{t-1} - C_{t,j+1}^{t-1})\delta t = 0. \tag{7.65}$$

The original fluid in the region below H_l in each compartment of the tank is assumed not to be exchanged by the incoming fluid.

7.6 Experimental study

In this section, the experimental results will be compared with the model predictions at different Ri. For the immiscible fluids, the displacement model will be tested; for the miscible fluids, both the stratified mixing model and the plume model will be tested. The Ri was varied by changing the flow rate or the density contrast.

7.6.1 Immiscible fluids

Figure 7.6 shows the weir effect when an empty 1×7 tank is filled with water at different flow rates. H_l/H=0.25, H_u/H=0.75. $\hat{h}_1$ is removed from Figure 7.6(a, b) because during the experiment at high Re, a large number of bubbles were generated in the highly turbulent flow falling down to compartment 1, leading to the failure of image processing. For all cases, the incoming water occupies the bottom of the empty tank compartment by compartment, so the normalised height of each compartment increases one by one. When a compartment starts to be filled, the height of water in it increases linearly; when the water height reaches the lower edge of the connecting hole (H_l), the increase rate of the water height starts to decrease, because it starts to fill the neighbouring compartment; the water height becomes stable when it reaches H_I, due to weir effect. When the water height of the last compartment reaches H_I, the water height of all compartments increases at the same rate. The stable height H_I depends on the Ri. When the Ri increases from 230 to 22953, H_I decreases from $0.40H$ to $0.29H$. Therefore, the water height of all compartments reaches H_I at 0.4 and 0.29 exchange volumes, respectively. In the experiments, the water height in a compartment was not as stable as predicted when the following compartments were filled, especially when the flow rate was high. The probable reason was that the flow friction increased when the downstream water height increased, resulting in the rise of upstream water height.

The horizontally integrated flushed fractions in compartment 4 are plotted against the normalised height at a certain time interval ($\Delta T = 0.02$) in Figure 7.7. The horizontal lines in Figure 7.7(a) represent the interface heights. Theoretically for immiscible fluids, the horizontally integrated flushed fraction should be either 1 or 0

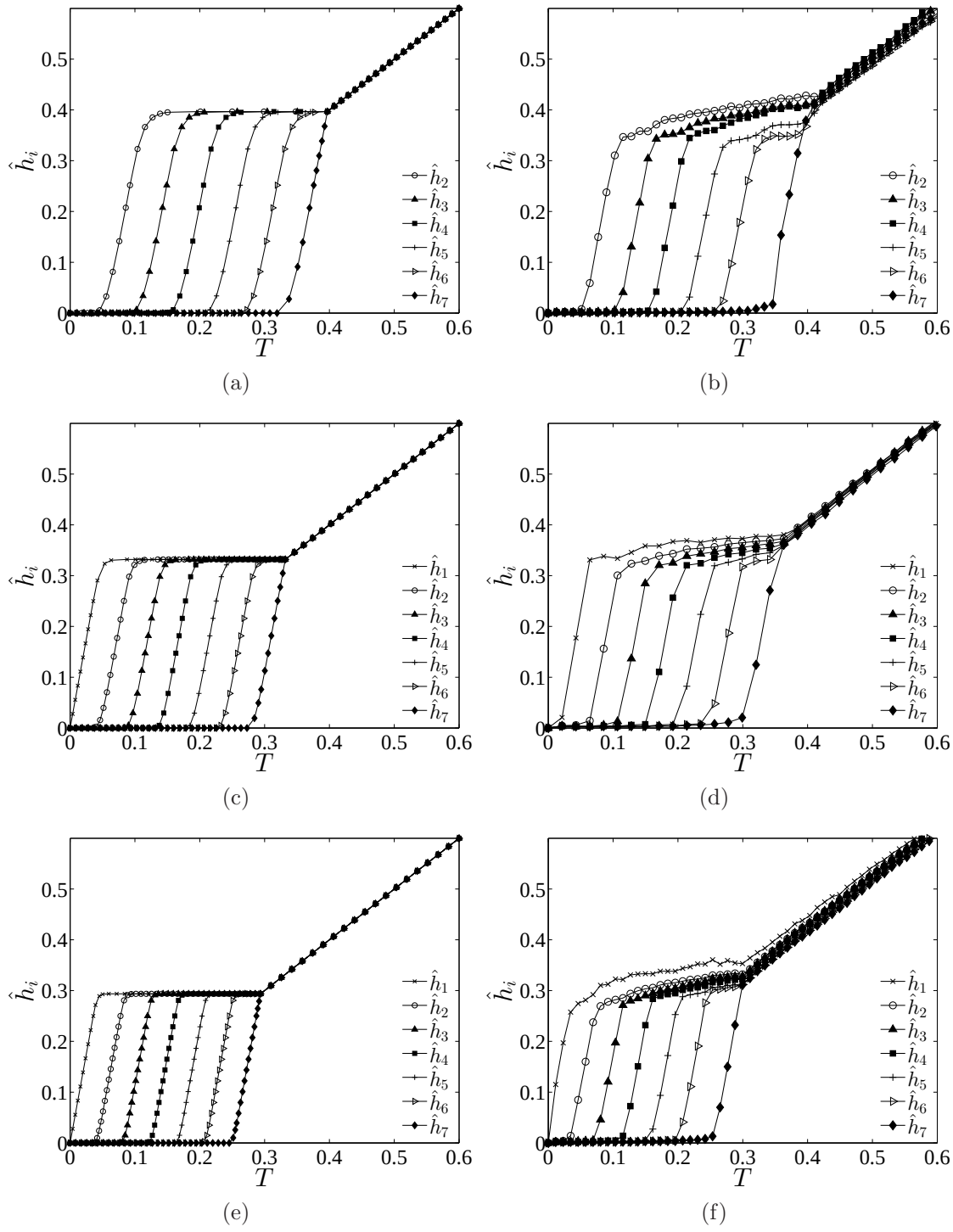

Figure 7.6: The (a, c, e) theoretical predictions and (b, d, f) experimental measurements of the variation in time of the normalised water height in each compartment of the 1×7 tank when it is filled with water at different flow rates. H_l/H=0.25, H_u/H=0.75. The figures correspond to (a, b) Ri =230, Re =6366, (c, d) Ri =2066, Re =3183 and (e, f) Ri =22953, Re =1273.

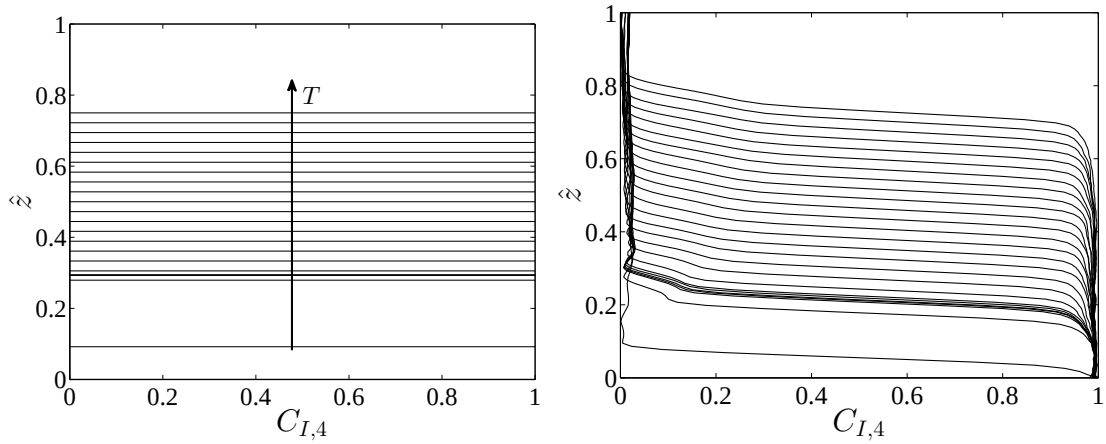

Figure 7.7: The (a) theoretical prediction and (b) experimental measurement of the vertical distribution of the normalised interface height of compartment 4 in the 1×7 tank at $Ri = 22953$. The time interval between two neighbouring curves is $\Delta T = 0.02$.

at a certain height. Initially, the integrated flushed fraction does not increase at a constant rate. When the previous compartments were flushed, the flushed fraction in compartment 4 is 0. When compartment 4 starts to be flushed, the interface increases fast. When the interface rises over the lower edge of the hole, compartment 4 starts to flush compartment 5. When the last compartments are flushed, the interface in compartment 4 rises slowly. When the lower region of the whole tank has been flushed, all compartments are flushed at the same rate. That is why the interface rises at an even rate at this stage. The experimental observation of the variation in time of the interface height is plotted in Figure 7.7(b). During the flushing experiment, the camera was fixed in front of the tank, so when the interface increased, the camera captured the inclined top view of the interface. That is why the interface curves obtained from the image processing are parallel but not horizontal. It can be seen that the displacement model has successfully captured the character of the rise of the interface.

The good agreement between the displacement model predictions and the experimental measurements validates the weir effect.

7.6.2 Miscible fluids

High positive Ri

The contour of the front view of the 1×7 tank with fresh clear water when it was flushed with dyed salt water at $Ri = 450$ is plotted in Figure 7.8. At the initial stage, the bottom region of the tank was flushed from the inlet compartment to the outlet compartment, and there existed a stable interface between the lower salt water and the upper fresh water. In each compartment, the flushed fraction increased with the depth of the fluid. A plume was observed over the lower edge of the connecting hole. These observations supported the assumption of the plume model. When the bottom region of the tank was exchanged, the interface in each compartment rose together, but in the outlet compartment, the interface rose faster because of the stronger vertical flow in it. At the final stage, only the last compartment was fully flushed; a portion of the original fluid in the top region was exchanged due to diffusion, especially in those compartments close to the outlet.

Figure 7.9(a, b) shows the experimental measurements of the variation in time of the flushed fraction in each compartment of the 1×7 tank when it was flushed with denser water at $Ri = 900$ and 450, respectively. At high Ri, the performance of the flushed fractions for these two Ri was nearly the same, where density effect was very important. Initially, the lower region of the tank was flushed one by one. When a compartment (except compartment 1) started to be flushed, the increase rate of the flushed fraction was relatively low, because the interface in the previous compartment had not yet become stable; the flushing rate increased with the interface height in the previous compartment. After the height of the incoming denser water of a compartment rose over the lower edge of the connecting hole, the increase rate of C_i became lower and lower because the denser fluid in it flushed the neighbouring compartment. When the height of the interface in the last compartment reached H_I, the increase rate of the flushed fraction in the compartments close to the inlet became higher. All C_i except C_7 increased together, because the interface in these compartments rose at the same time. Finally, only the last compartment was fully flushed; the flushed fraction of other compartments was a little higher than 75%,

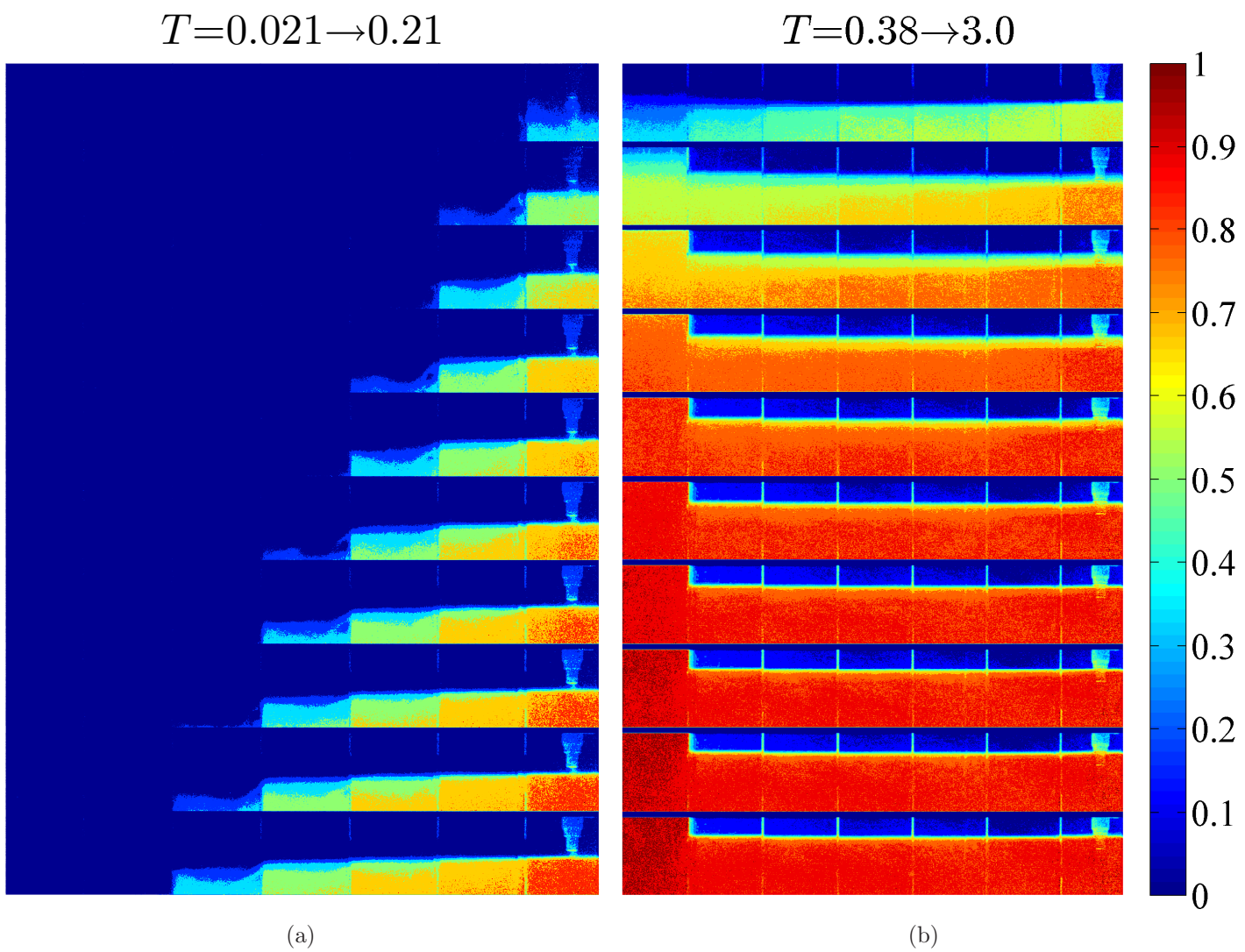

Figure 7.8: The experimental measurements of the variation in time of the flushed fraction field in a 1×7 tank when the tank with fresh water was flushed with salt water at $Ri = 450$. $H_l/H = 0.25$, $H_u/H = 0.75$. The ten contours from top to bottom are plotted at a time interval of $\Delta T =$ (a) 0.021 and (b) 0.29, respectively.

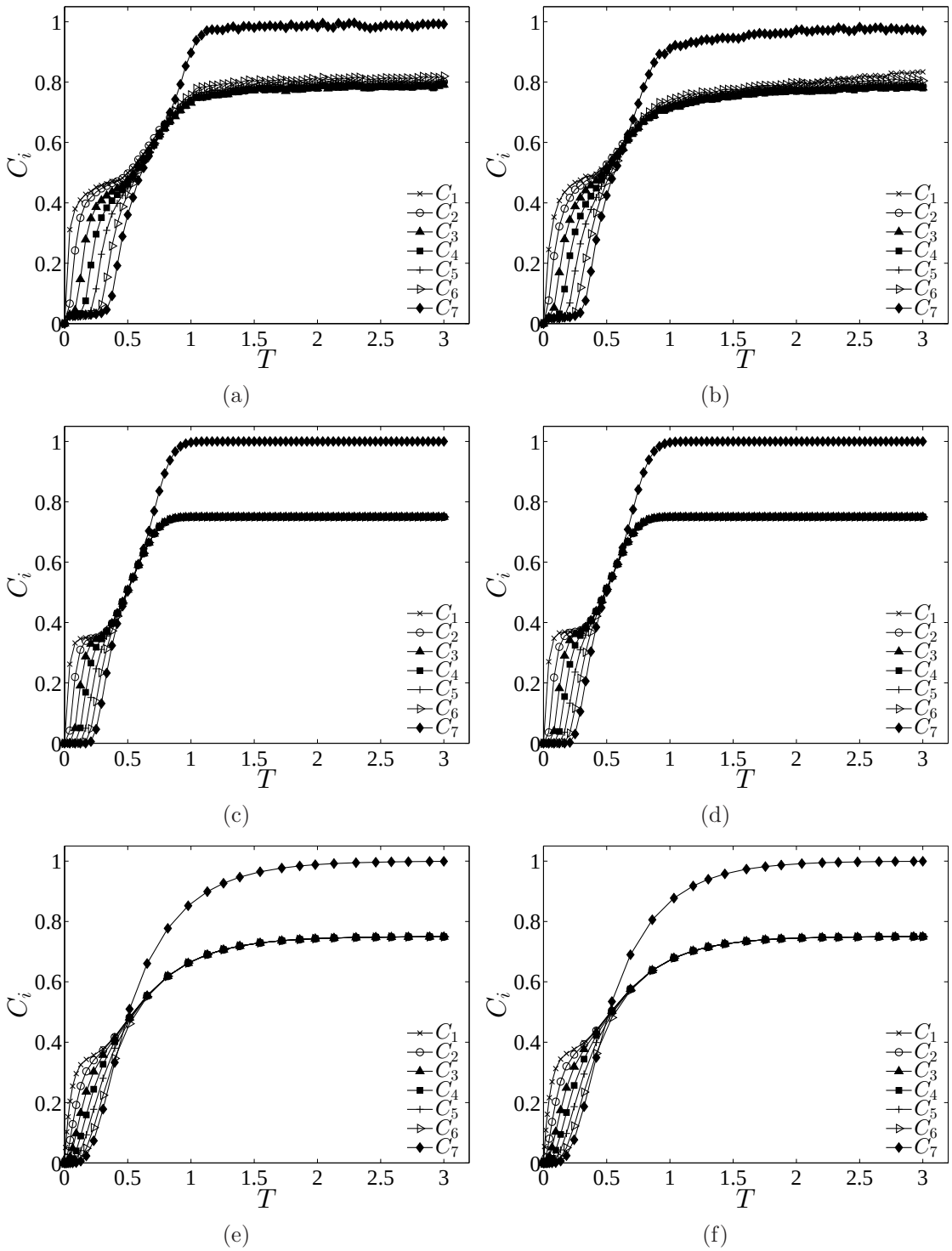

Figure 7.9: The (a, b) experimental measurements, (c, d) plume model predictions and (e, f) stratified mixing model predictions of the variation in time of C_i in a 1×7 tank when the tank with fresh water was flushed with salt water at $Ri =$ (a, c, e) 900 and (b, d, f) 450. $H_l/H = 0.25$, $H_u/H = 0.75$.

because the interface height of these compartments stayed at about $H_u = 0.75H$ and mixing existed between the trapped top region and the exchanged lower region.

The predictions on the flushed fractions by the plume model are shown in Figure 7.9(c, d). The agreement between the model and the measurements is quite good, although the theory underestimated a little the flushed fraction of the previous six compartments at the two stable stages. The probable reason is that the mixing in reality was stronger than expected. The predictions by the stratified mixing model are shown in Figure 7.9(e, f). It can be seen that these predictions can capture the character of the variation in time of the flushed fraction in each compartment, but the agreement is not as good as that between the experiments and the plume model. The stratified mixing model is not able to estimate the linear rise of the flushed fraction when all compartments are flushed at the same time. The reason is that when the fluid flow is highly stratified, displacement dominates mixing. However, the flushed fractions at three volumes exchange are nearly the same between the stratified mixing model and the plume model.

The time series of the vertical distribution of the horizontally integrated flushed fraction in compartment 4 predicted by the plume model is compared with the experimental measurement in Figure 7.10. It was confirmed by the observation that there were three layers in the compartment, although the interface in reality was not so obvious as predicted by the model. At the initial stage, the lower region of the compartment was exchanged, and the top region was trapped. At a later stage, the interface became obvious; the vertical difference of the flushed fraction in the lower region became smaller; the middle region was vertically advected by the flow from the lower region; the top region was slightly exchanged with the incoming fluid due to diffusion. At the final stage, the flushed fraction in the lower region of the compartment was a little less than 1, probably because a small portion of the original fluid remained due to mixing. From comparison, although the plume model does not contain the slight mixing in the top region, it is able to capture the main character of the fluid exchange in different layers.

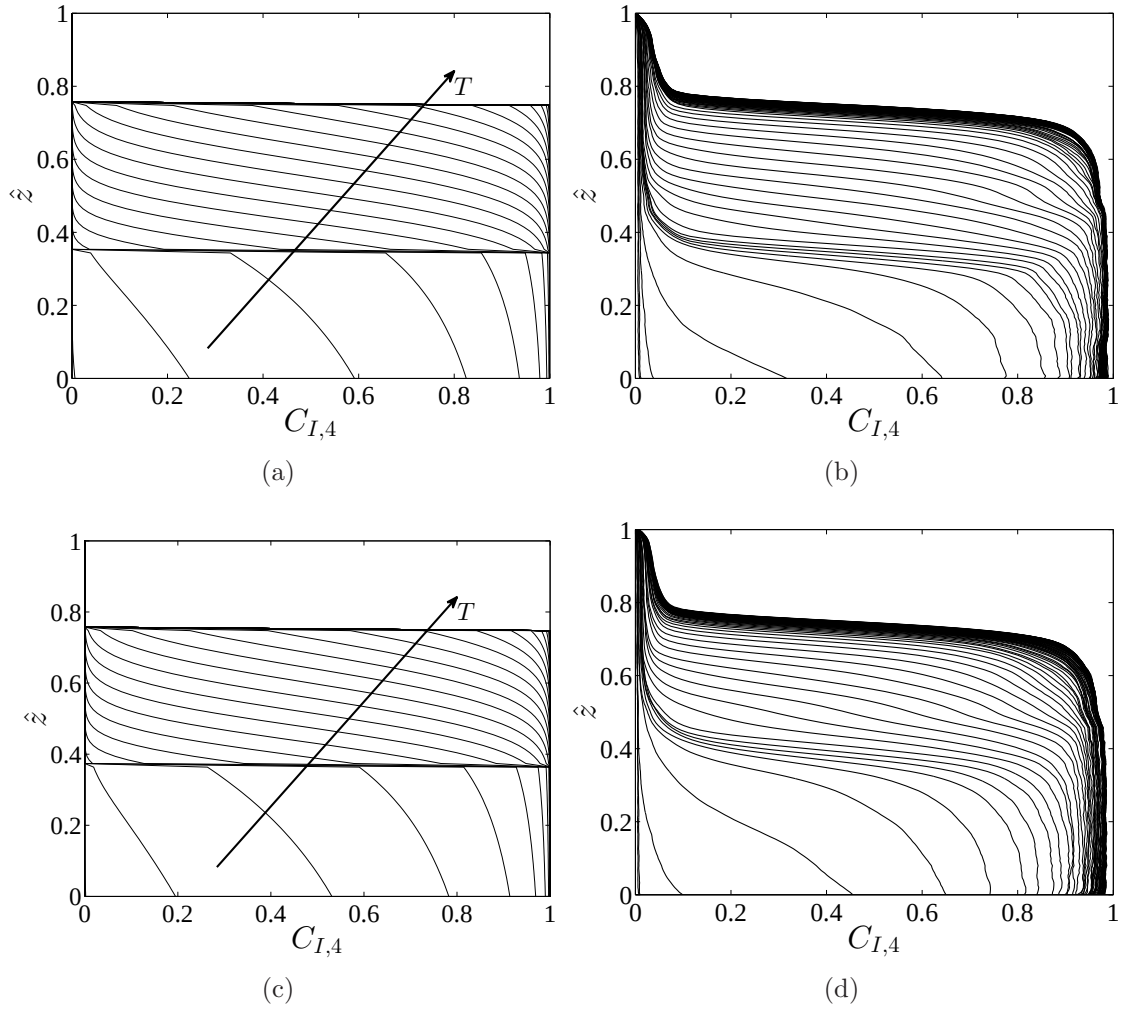

Figure 7.10: The (a, c) plume model predictions and (b, d) experimental measurements of the vertical distribution of the horizontally integrated flushed fraction of compartment 4 in the 1×7 tank at $Ri =$ (a, b) 900 and (c, d) 450. The time interval between two neighbouring curves is $\Delta T = 0.04$.

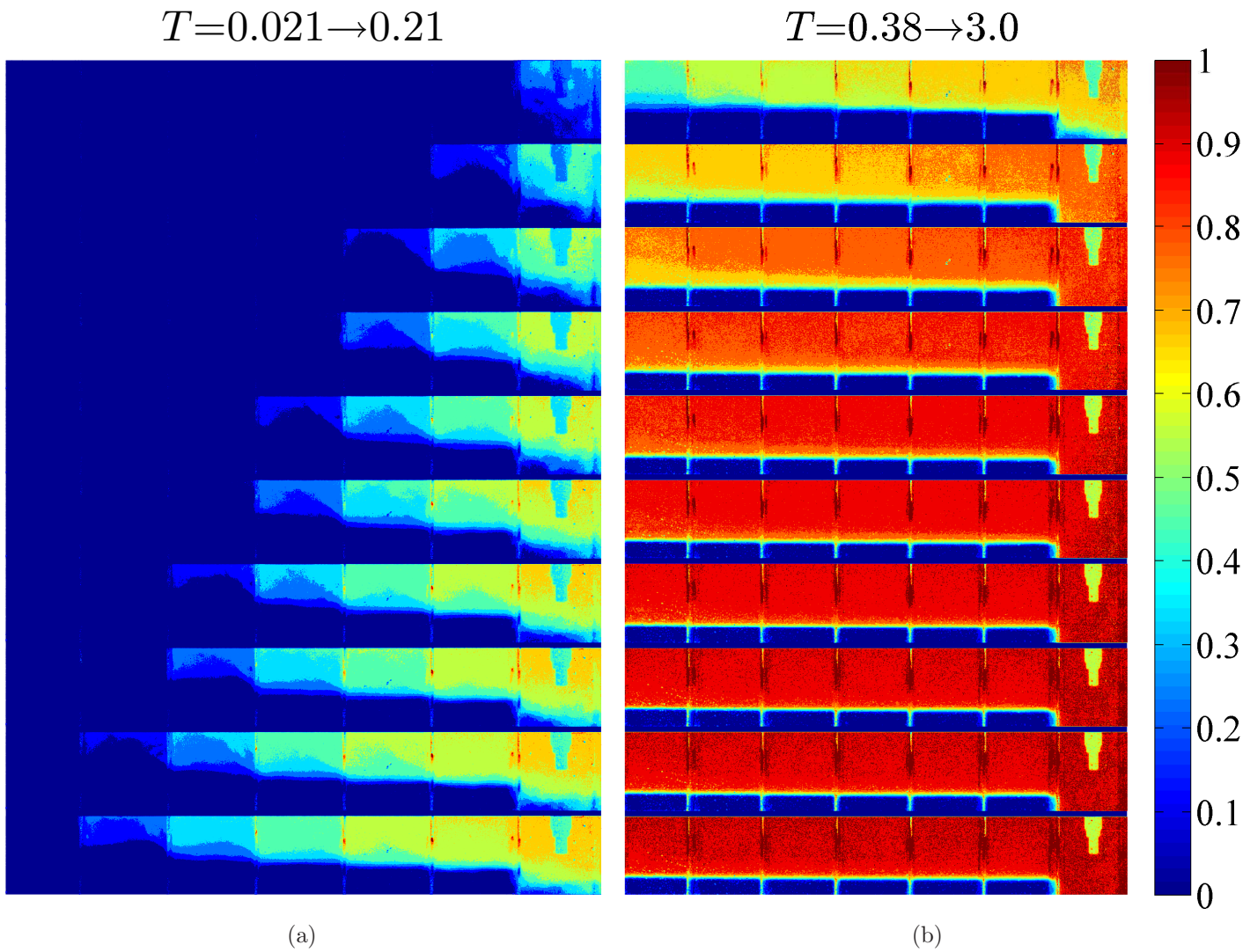

Figure 7.11: The experimental measurements of the variation in time of the flushed fraction field in a 1×7 tank when the tank with fresh water was flushed with salt water at $Ri = -450$. $H_l/H = 0.25$, $H_u/H = 0.75$. The ten contours from top to bottom are plotted at a time interval of $\Delta T =$ (a) 0.021 and (b) 0.29, respectively.

High negative Ri

Figure 7.11 shows the contour of the front view of the 1×7 tank with clear salt water when it was flushed with dyed fresh water at $Ri = -450$. Initially, the top region of the tank was exchanged. Between neighbouring compartments, the plume was not obvious, but the vertical difference of the fluid exchange could be observed. In the inlet compartment, the mixing was intense to a lower distance because of the inflow direction was opposite to the buoyancy. The original fluid in the middle region of the tank was exchanged by shear mixing. Finally, the inlet compartment was completely flushed. The bottom region of other compartments was slightly mixed.

Figure 7.12(a, b) shows the variation in time of the flushed fraction in each compartment when the 1×7 tank with fresh water was flushed with salt water at $Ri = -900$ and -450, respectively. At $Ri = -900$, the tank was slowly flushed and the original fluid was weakly exchanged due to density effect. The top region of the tank was first flushed by the incoming lighter fluid compartment by compartment. When the top region was occupied by the incoming fluid, on one side, the incoming fluid bypassed the tank; on the other side, the middle region of the tank was exchanged due to shear mixing. Therefore, each flushed fraction curve increased approximately linearly at this stage. At the final stage, C_1 increased faster than other flushed fractions because the mixing in compartment 1 was more intense so that the lower region in it was exchanged at the end. At three exchange volumes, the flushed fraction was over 80% in compartment 1, but under 80% in other compartments. Due to the existence of the density difference between the incoming fresh water and the original salt water, the bottom region of these compartments could hardly be exchanged. At $Ri = -450$, the tank was flushed a little more effective. The flushed fraction in compartment 1 was higher than that in other compartments because when the lighter fluid was injected through the inlet pipe from above to below, mixing in compartment 1 was enhanced. The flushed fraction in each compartment increased faster than that at $Ri = -900$, because the density contrast was lower so that the exchange was more efficient. At three exchange volumes, the flushed fraction was achieved at over 90% in compartment 1, but around 80% in other compartments.

Figure 7.12(c, d) shows the flushed fractions predicted by the stratified mixing

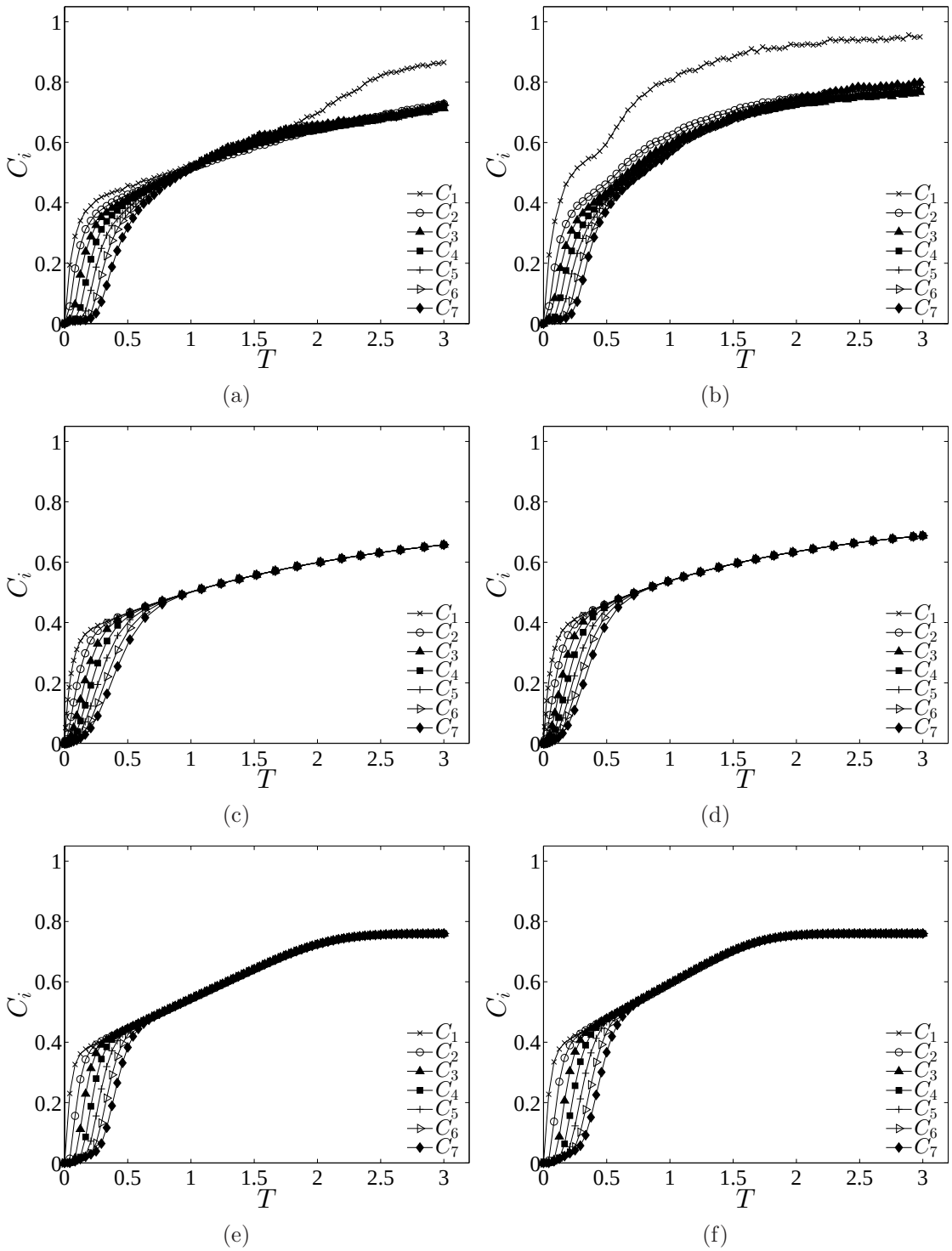

Figure 7.12: The (a, b) experimental measurements, (c, d) stratified mixing model predictions and (e, f) plume model predictions of the variation in time of the flushed fraction in each compartment of a 1×7 tank when the tank with salt water was flushed with fresh water at Ri = (a, c, e) -900 and (b, d, f) -450. H_l/H=0.25, $H_u/H = 0.75$.

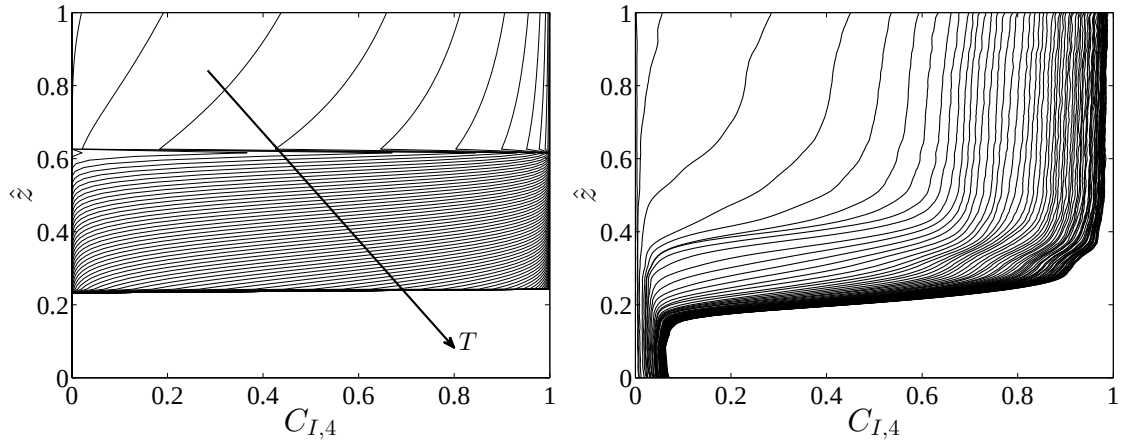

Figure 7.13: The (a) theoretical prediction and (b) experimental measurement of the vertical distribution of the horizontally integrated flushed fraction of compartment 4 in a 1×7 tank when the tank with salt water was flushed with fresh water at $Ri = -450$. The time interval between two neighbouring curves is $\Delta T = 0.04$.

model. C_i is underestimated especially for compartment 1 because the model does not consider the fluid exchange in the bottom region of the compartments. Figure 7.12(e, f) shows the flushed fractions predicted by the plume model. It can be seen that at $Ri = -900$, the predicted flushed fraction is lower than reality at $T = 2.5 \rightarrow 3$ because it does not account for the shear mixing in the lower region. Similarly at $Ri = -450$, the increase rate is overestimated at $T = 0.5 \rightarrow 1.5$, and underestimated at $T = 2 \rightarrow 3$. However, both the stratified mixing model and the plume model are able to describe the main physics for the case of lighter fluid injected into denser fluid.

The theoretical and experimental vertical distribution of the fluid exchange is shown in Figure 7.13(a, b), respectively. From the observation in the experiment, the compartment was flushed from top to bottom at the initial period. At a later period, the integrated flushed fraction in the upper region became nearly the same vertically; the fluid in the middle region was vertically advected by the fluid flow from the upper region so that the interface descended horizontally at this period; a portion of the fluid in the bottom region of the compartment was mixed by the incoming fluid on the upper side. The plume model succeeds to describe the character of the fluid

exchange in each of the three layers, but fails to accurately estimate the height of the interface. This is possibly because the bottom source of the plume was lower in reality when lighter fluid was injected into denser fluid.

Low positive Ri

At $Ri = 113$ and 18, the experimental flushed fractions are plotted in Figure 7.14(a, b), respectively. At a relatively low positive Ri, weir effect was not obvious. At $Ri = 113$, when the interface height of the middle compartments (2-6) reached H_u, the flushed fractions did not rise any more because the top region of these compartments was entrained. C_1 increased continuously because the original fluid in the top region of compartment 1 was exchanged by shear mixing. At $T = 3$, $C_1 \approx 1$ because almost the whole compartment was exchanged. At $Ri = 18$, the flushing was more effective to exchange the original fluid. The performance of C_1 almost followed the perfect mixing mode because of the high turbulence in it. C_2 was higher than C_i $(i = 3 - 6)$ because compartment 2 was closer to the inlet so that the turbulence in it was stronger. Compartment 7 was completely flushed because the outlet was on the top of it so that the fluid flow passed the whole compartment. The other four compartments (3-6) could not be completely flushed due to the existence of the entrainment on the top region of these compartments. The turbulence in these compartments was not strong enough to exchange the trapped original fluid on the top.

The predicted flushed fractions were plotted in Figure 7.14(c-f). The discrepancy between the theory and the experiment mainly appeared in the initial stage of the flushing. Both the plume model (shown in Figure 7.14(c, d)) and the stratified mixing model (shown in Figure 7.14(e, f)) underestimated the increase of the flushed fractions especially in the compartments close to the inlet. This is because the models do not consider the high turbulence caused by the small inlet nozzle. However, at the later stable stage, the discrepancy for estimating the performance of the compartments farther from the inlet is not large, although the models do not describe the shear mixing existing in the top region of these compartments.

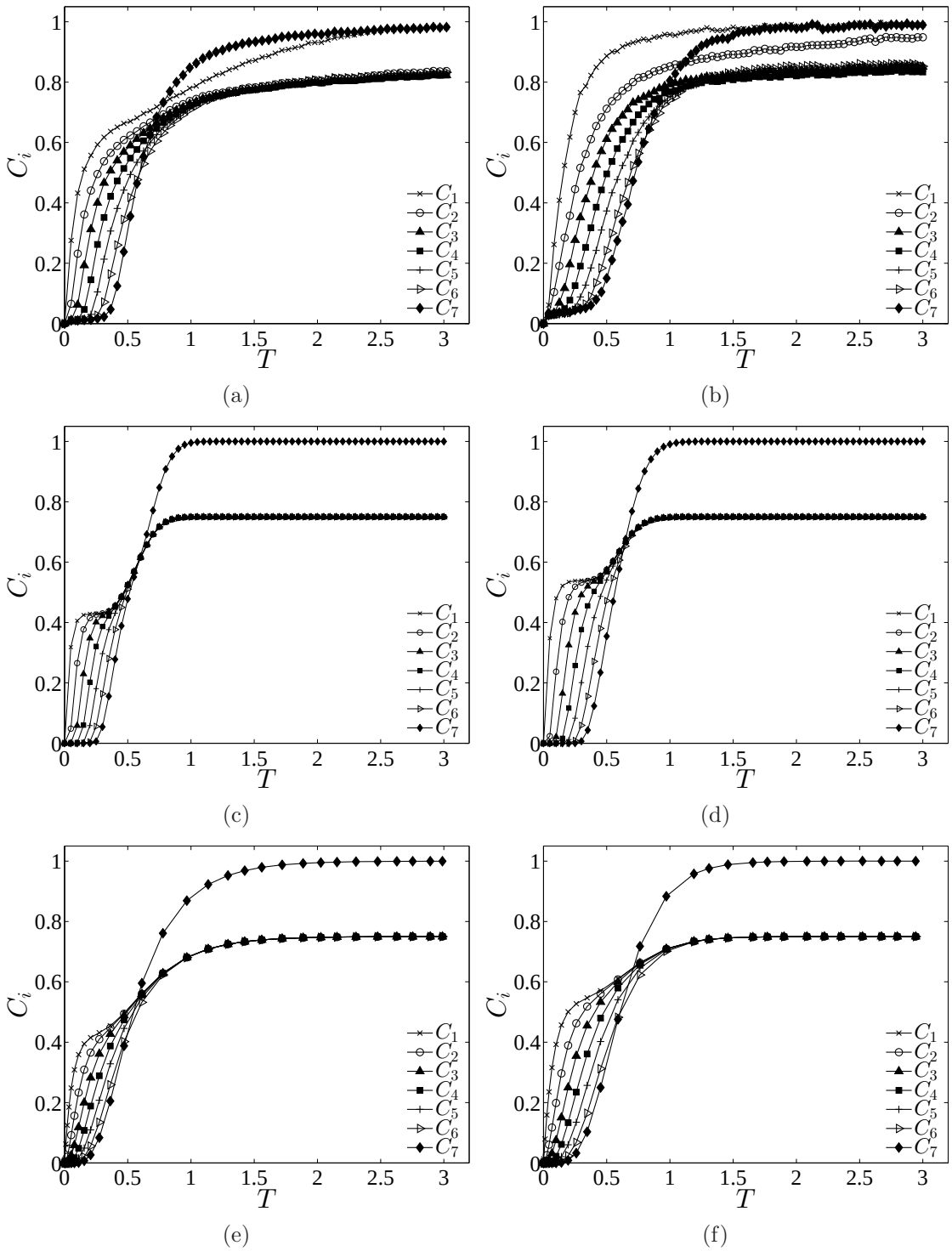

Figure 7.14: The (a, b) experimental measurements, (c, d) plume model predictions and (e, f) stratified mixing model predictions of the variation in time of C_i in a 1×7 tank when the tank with fresh water was flushed with salt water at $Ri =$ (a, c, e) 113 and (b, d, f) 18. $H_l/H = 0.25$, $H_u/H = 0.75$.

Low negative Ri

Figure 7.15(a, b) shows the experimental variation in time of the flushed fractions at low negative Ri. At $Ri = -113$, the top region of all the compartments was exchanged with the incoming light fluid at the initial stage. At the time when the incoming fluid bypassed the top region of the whole tank, the bottom region of the tank was exchanged by shear mixing. Compartment 1 was almost fully exchanged at $T = 3$ because the mixing was more intense in it. For other compartments, the flushed fractions were close to 80% at $T = 3$, a little higher than the fraction of the top and middle region, which is $1 - H_l/H = 0.75$. At $Ri = -18$, compartments 1 and 2 almost followed the perfect mixing mode, because the flow in it was highly turbulent. In other compartments, density effect was obvious so that the flushed fraction could not reach 100% after three exchange volumes. The further a compartment located from the inlet, the more the original water remained in its bottom region. In compartment 7, about 80% of the original water was flushed out at three exchange volumes. The predictions of the flushed fractions by the stratified mixing model are shown in Figure 7.15(c, d). It can be seen that the model underestimates the flushed fraction especially for the compartments close to the inlet when density effect is not significant, as the model does not consider the high turbulence in these compartments.

$Ri = 0$ **(No density contrast)**

Figure 7.16 shows the variation in time of the flushed fraction in each compartment of the 1×7 tank when there is no density contrast between the existing water and the external water. For compartment i, the flushed fraction C_i evolves as

$$C_i = 1 - \sum_{j=1}^{i} \frac{T^{i-j}}{(i-j)!} e^{-T}, \tag{7.66}$$

shown in Figure 7.16(a). The water tank is flushed from the inlet compartment to the outlet compartment. The exchange follows the unstratified mixing mode. A group of laboratory experiments were conducted at different Re. The model predictions agreed very well with the experimental measurements at Re =1273, 3183 and 6366, shown in

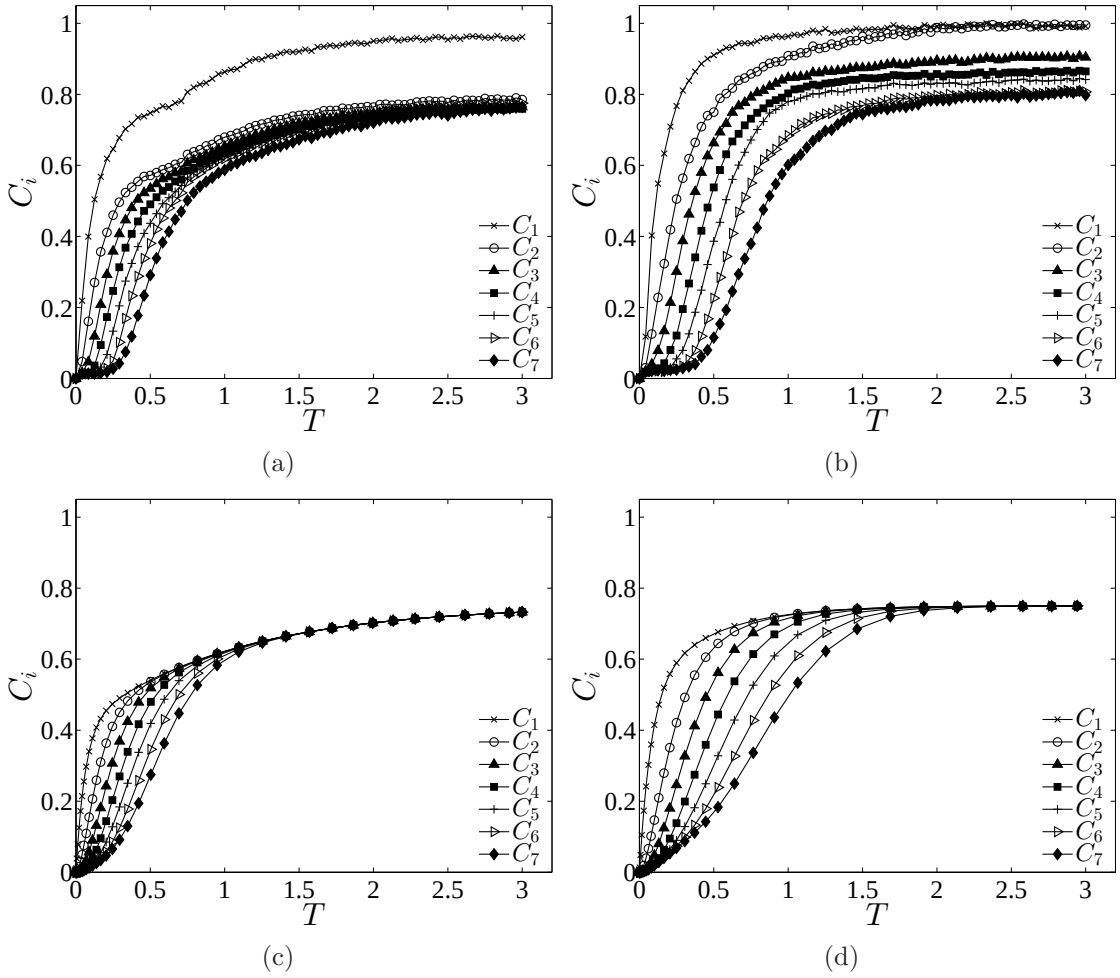

Figure 7.15: The (a, b) experimental measurements and (c, d) stratified mixing model predictions of the variation in time of C_i in a 1×7 tank when the tank with salt water was flushed with fresh water at Ri = (a, c) -113 and (b, d) -18. $H_l/H = 0.25$, $H_u/H = 0.75$.

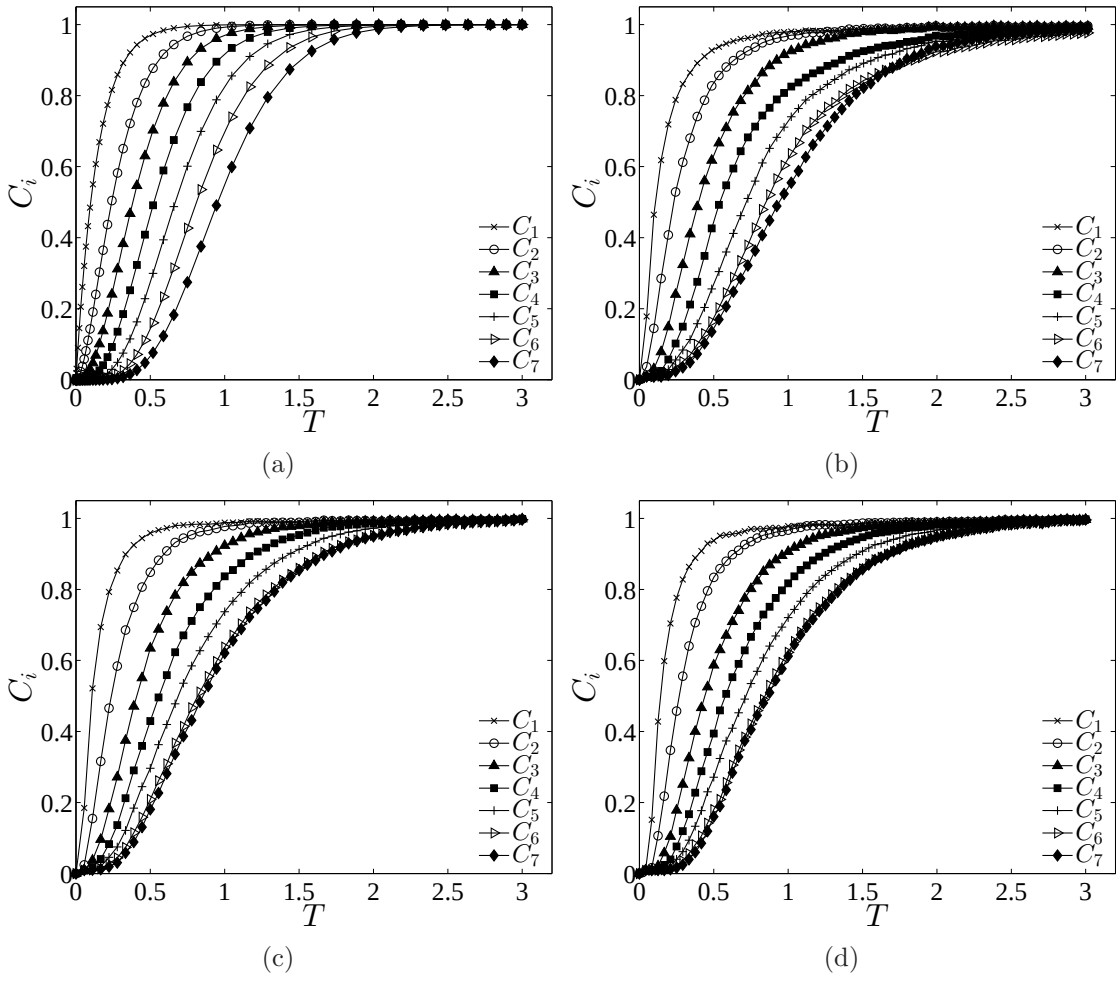

Figure 7.16: The (a) theoretical prediction and (b, c, d) experimental measurements of the variation in time of the flushed fraction in each compartment of the 1×7 tank at $Ri = 0$. The figures correspond to $Re =$ (b) 1273, (c) 3183 and (d) 6366.

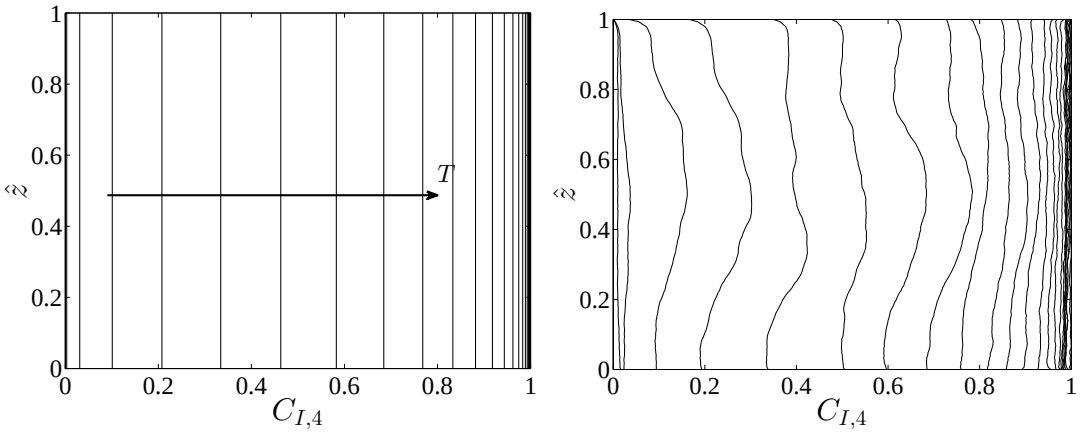

Figure 7.17: The (a) theoretical prediction and (b) experimental measurement of the vertical distribution of the horizontally integrated flushed fraction of compartment 4 in the 1×7 tank at $Ri = 0$ and $Re = 6366$. The time interval between two neighbouring curves is $\Delta T = 0.08$.

Figure 7.16(b), (c) and (d), respectively. It can be seen that at $Re = 1273$, the fluid flow in some compartments was not highly turbulent to mix sufficiently. As a result, the retention time of these compartments was a little longer than expected; at three exchange volumes, the flushed fraction in these compartments did not achieve 1. But at higher Re, mixing was more sufficient so that all compartments could be exchanged completely after a long time flushing. It can be seen that C_7 increased faster than expected, because the flow state in compartment 7 was different from the previous compartments. The fluid was pumped out of the tank from the top of compartment 7, so the flow in this compartment had a 90 degree rotation, which improved mixing and thus increased the flushing efficiency in it.

For $Ri = 0$ and $Re = 6366$, the theoretical and experimental time series of the vertical distribution of the horizontally integrated flushed fraction in compartment 4 is plotted in Figure 7.17(a) and (b), respectively. Theoretically, the whole compartment was evenly mixed so the predicted flushed fraction is assumed to be vertically identical. At a certain time interval ($\Delta T = 0.08$), the increase rate of the flushed fraction

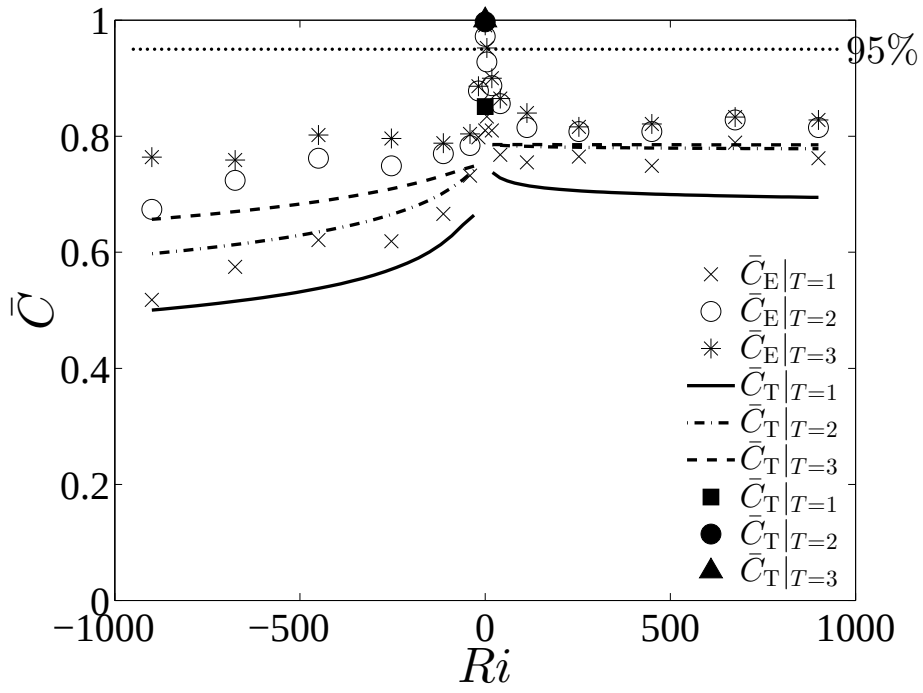

Figure 7.18: The average flushing efficiency of the whole tank at $T = 1$, 2 and 3 versus Ri. $\bar{C}_{\mathrm{T}}$ represents the theoretical prediction, and $\bar{C}_{\mathrm{T}}$ represents the experimental measurement.

increases at the initial period, but decreases at the later period. This is because when compartment i starts to be flushed, the difference between C_{i-1} and C_i is high; but after it has been flushed for some time, the difference becomes lower. From the flushing experiment, the flushed fraction in the middle region of compartment 4 was relatively higher than that in the top and bottom region, because the middle region was first flushed by the flow from the previous compartment. At the final stage, the vertical difference is not obvious because the whole compartment has been completely mixed and efficiently exchanged. The model is successful to reflect the increase rate of the integrated flushed fraction in the compartment.

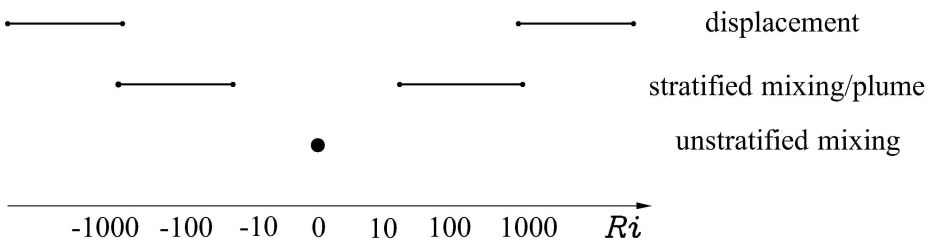

Figure 7.19: The applicable range of the models according to Ri.

7.6.3 Influence of Ri on the average flushing efficiency

From the above discussion in this section, the performance of the flushing in the tank depends on Ri. The average flushing efficiency at $T = 1$, 2 and 3 of the whole tank is plotted as a function of Ri in Figure 7.18. The curves are estimated by the stratified mixing model. The average flushing efficiency is the highest at $Ri = 0$. When density effect does not exist, there is no trapped region in the top or bottom and the whole tank can be efficiently flushed. When Ri increases from 0 to $+\infty$, the average flushing efficiency decreases, because when density effect becomes more significant, more of the original light fluid will be trapped in the region above H_u. When Ri decreases from 0 to $-\infty$, the average flushing efficiency decreases, as the incoming lighter fluid has less energy to disturb the original denser fluid in the region below H_l in the tank so that less original fluid can be exchanged. At $T = 1$, the flushing efficiency is underestimated by the stratified mixing model because the model does not describe displacement; at the later stage, the underestimation is caused by ignition of the shear mixing in the top region (at $Ri > 0$) or the bottom region (at $Ri < 0$). The flushing efficiency at $T = 3$ is underestimated by about 5% for $30 < Ri < 1000$, and about 10% for $-1000 < Ri < -30$.

Table 7.1: Summarisation of the stratification models.

Models	Advantages	Disadvantages	Applicable range
Displacement model	Technically simple	Mixing is not considered.	Immiscible fluids, $\|Ri\| > 100$
Stratified mixing model	Technically simple	Vertical distribution is not considered.	Miscible fluids in multi-compartment tanks, $30 < \|Ri\| < 1000$
Plume model	Vertical distribution is described.	Technically complex	Miscible fluids in in-line tanks, $30 < \|Ri\| < 1000$
Unstratified mixing model	Technically simple	Density effect is not considered.	Miscible fluids in multi-compartment tanks, $Ri \to 0$

7.7 Critical analysis of the models

The displacement model, stratified mixing model and plume model have been developed for stratified flushing in an in-line tank. These models as well as the unstratified mixing model are summarised in Table 7.1, in terms of advantages, disadvantages and applicable range. Meanwhile, their applicable range is drawn in Figure 7.19 according to Ri. The assumption of the displacement model is that the two fluids are immiscible so that there exists strict stratification in each compartment when one fluid is injected to another. The flushing is rigorously controlled by the hydraulics. Since the displacement model does not describe mixing, it is applicable to immiscible stratified fluids or extremely stratified fluids ($Ri > 1000$). The displacement model proves the weir effect, which will be considered by the stratified mixing model and the plume model. The stratified mixing model divides each compartment of a tank to a few layers, and the incoming fluid is assumed to mix perfectly with the original fluid in each layer. This modelling technique is simple, which has been validated by the laboratory experiments at $30 < |Ri| < 1000$. The disadvantage of the stratified mixing model is the ignorance of the vertical difference of the fluid exchange. The plume model provides physical information on the vertical distribution of the horizontally integrated flushed fraction, but this technique is too complex to apply to complex tank structure. The stratified mixing model is more applicable for complex multi-compartment tanks. The unstratified mixing model can be widely used when density effect is not important ($Ri \to 0$), as discussed in Chapters 5 and 6.

7.8 Summary

The stratified flushing in an in-line tank has been tested from both the theoretical and experimental aspects. Three types of mathematical models have been developed to interpret the physical processes. The displacement model is suitable to the case when the incoming fluid and the original fluid are immiscible, which is validated by the experiments of filling an empty tank. For miscible fluids, a stratified mixing model is used to quantify the fluid exchange in the tank during flushing; a more

theoretically strict model - the plume model is employed to describe the physics when the tank is flushed. The plume model works well for high positive Ri, and the stratified mixing model works well for high negative Ri. The flushing efficiency at $T = 3$ is underestimated by about 5% for $30 < Ri < 1000$, and about 10% for $-1000 < Ri < -30$. For low Ri, mixing due to turbulence in reality is stronger than expected. In practice, when the density of the incoming water is largely different from that of the existing ballast water, increasing the flow rate may improve mixing and thus the flushing efficiency.

Chapter 8

Stratified Flushing from Rectangular Tanks

8.1 Introduction

In Chapter 7, the stratified flushing was tested in an in-line tank. It can be seen that there exists a gap between the theory and the experiment at low Ri, especially for $|Ri| < 30$. The experimental observations showed that when the trapped region where the original fluid was not exchanged was large in the inlet compartment, the compartments farther from the inlet were largely trapped as well; when the inlet compartment was highly turbulent at low Ri, the height of the trapped region in a compartment depended on the location of the compartment. The closer a compartment located to the inlet, the stronger the turbulence and thus the smaller the trapped region were in it. The assumption of the stratified mixing model was based on a local Ri. The difficulty of incorporating the density effect on the trapped height into the model is that the local Ri in all of these compartments was the same but the turbulence intensity in each was different.

In order to understand more about the density effect on the fluid exchange in multi-compartment tanks at low Ri, the analysis is extended to the situation where the local Ri is the same between compartments. This is achieved by considering the stratified flushing in a 2×2 square tank. To reduce the complexity, the geometrical configuration

was fixed but the stratification was varied. The four square compartments and the four circular connecting holes are identical in size and height, respectively. This tank structure is tested because on one aspect, it is the simplest multi-compartment square tank to analyse; on the other aspect, the flow network in it is symmetrical so that the density effect on flushing the two corner compartments (12 and 21) are the same. It will be seen how to modify the mathematical model to close the experimental results.

The main aim of this chapter is to extend the analysis of stratified flushing from an in-line tank to more complex structure in practice so that the physics can be interpreted in the context of the practical situation. As many real ballast tanks have limber holes on the top and bottom of the connecting walls, which may influence the fluid exchange when density difference exists between the incoming water and the original water, the flushing through a more complex configuration - a 5×4 'J'-type tank with limber holes will be further tested experimentally.

8.2 Flushing a 2×2 square tank

In this section, the influence of Ri on the flushing of the 2×2 square tank is investigated.

8.3 Experimental results

To reduce the complexity, a 2×2 tank (of volume $V = 0.075$ m^3) with identical compartments (of width 0.3 m and height 0.2 m each) and lightening holes (of diameter $D = 0.05$ m each) was employed, shown in Figure 5.1(a). During the flushing, only the far outlet was kept open so that the tank is geometrically symmetrical. The tank was flushed at a steady rate Q. The height of each compartment, the lower and upper edge of the connecting holes are $H = 0.2$ m, $H_l = 0.075$ m and $H_u = 0.125$ m, respectively.

Table 8.1: Ri and Re in the 2×2 tank when it was flushed at different inflow rates.

Q (m^3/s)	Re		Ri			
	Inlet	Holes	Inlet	Holes	Inlet	Holes
5×10^{-5}	3185	637	1.6	59	-0.8	-30
1.25×10^{-4}	7960	1593	0.26	9	-0.26	-9
2.5×10^{-4}	15920	3185	0.06	2	-0.06	-2

Dense water into light water

The influence of the inflow rate on the flushing efficiency was tested at $Ri > 0$. The water originally existing inside the tank was fresh water, and the salinity of the water that was used to flush the tank was 20‰. Thus the ratio of density contrast is $\Delta\rho/\rho = 0.02$. Three Ri were tested: 59, 9 and 2 at the connecting holes.

For the three tested inflow rates, the variation in time of $C_{[i][j]}$ and $\bar{C}$ was shown on the left side of Figure 8.1 and 8.2, respectively. The Ri and Re at the inlet and the connecting holes of the tank were listed in Table 8.1. The water exchange of the tank was driven by both displacement and mixing. For all the three cases, after three volumes exchange, C_{11} and C_{22} were close to 1; but C_{12} and C_{21} were less than 1. This is because in compartments 12 and 21, the original water was trapped on the top region due to the stratification caused by the larger density of the incoming water. When $Ri = 59$ (see Figure 8.1(a)), C_{11} increased more slowly than that when $Ri = 9$ or 2 (see Figure 8.1(c, e)), because at a relatively low flow rate, after the region lower than the hole in the tank was occupied by the denser water, the incoming water in compartment 11 would flush compartments 12 and 21 faster than the perfect mixing condition. Also, when $Ri = 9$ or 59, C_{12} and C_{21} were lower than those were when $Ri = 2$ at $T = 3$. The reason was that the higher flow rate in the last case led to a stronger turbulence in compartments 12 and 21, where Ri was relatively lower and Re was relatively higher, which increased the mixing and thus reduced the trapped region in these compartments. It can be seen from Figure 8.2(a) that at $T = 3$, the higher the inflow rate was, the higher the flushing efficiency was achieved. This

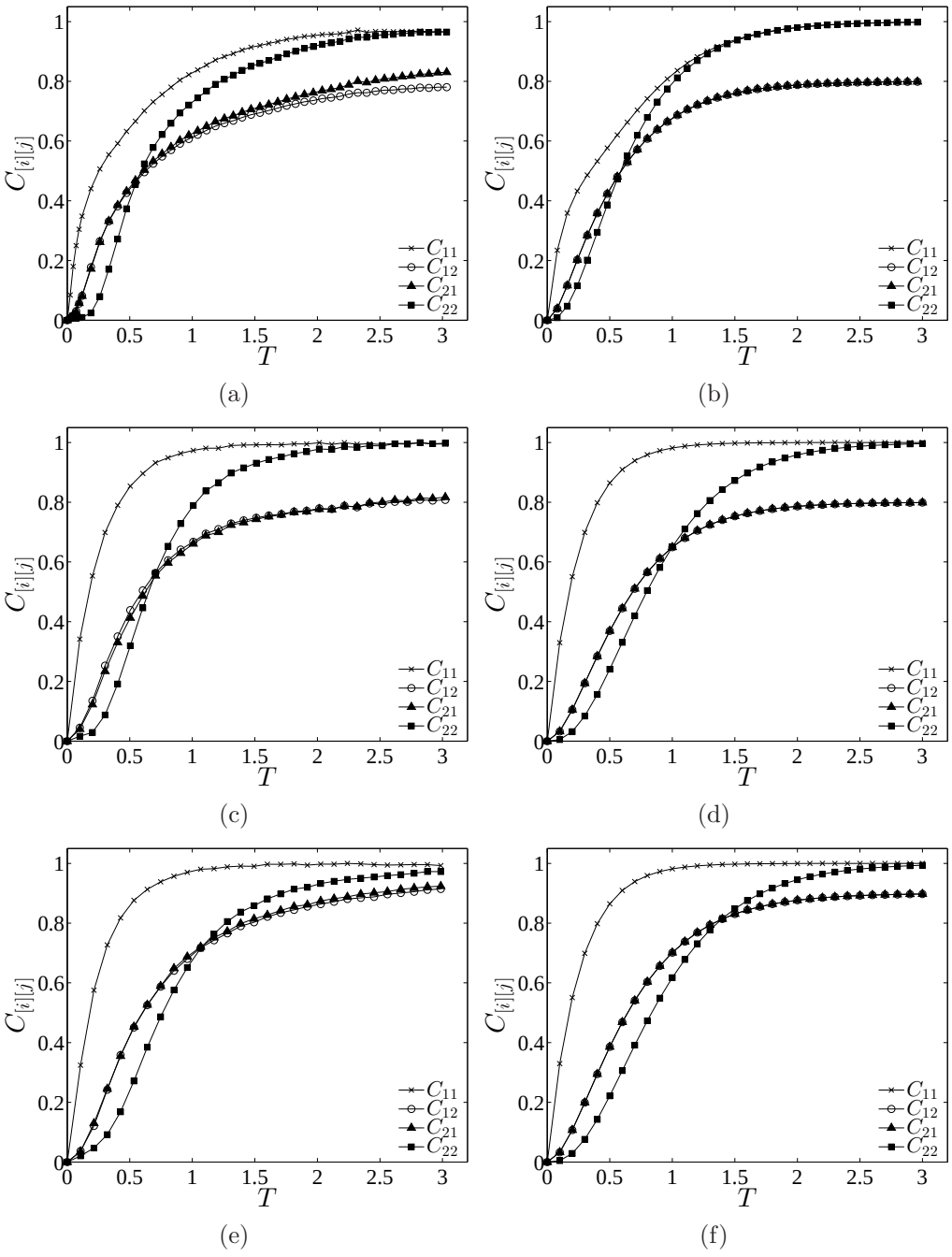

Figure 8.1: The (a, c, e) experimental measurements and (b, d, f) model predictions of the variation in time of the flushed fractions in the 2×2 tank when the tank with fresh water was flushed with salt water at different flow rates. The figures correspond to $Ri =$ (a, b) 59, (c, d) 9 and (e, f) 2.

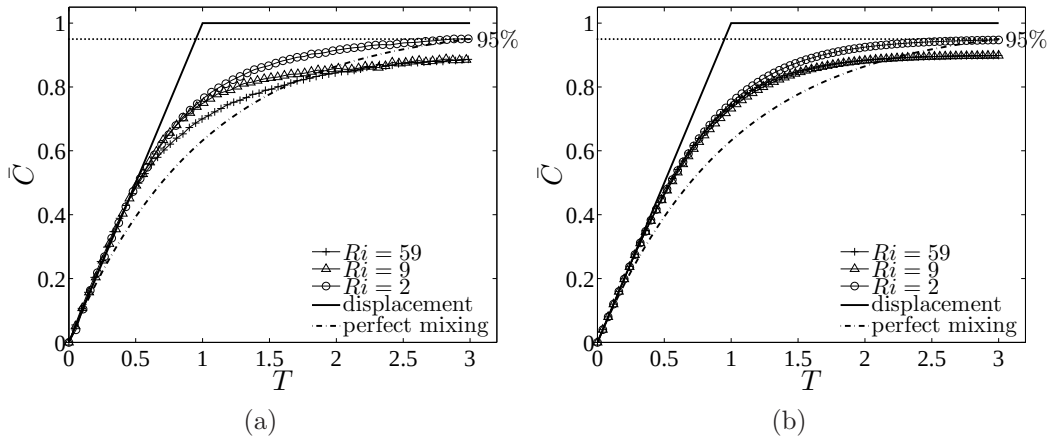

Figure 8.2: The (a) experimental measurements and (b) model predictions of the average flushing efficiency in the 2×2 tank when the tank with fresh water was flushed with salt water at different flow rates.

means that when water in a multi-compartment tank with no limber holes on the walls is flushed with water of higher density, increasing the inflow rate can enhance mixing and reduce the trapped region within compartments, and thus improve the water exchange rate in the whole tank, although some original water may remain on the top of those compartments where there is not sufficient vertical water exchange.

Fresh water into salt water

The influence of inflow rate and density contrast on the flushing efficiency was tested at $Ri < 0$. The water originally existing inside the tank was salt water, with salinity about 20‰and the water used to flush the tank was fresh water. Three Ri were tested: -30, -9 and -2. The variation in time of $C_{[i][j]}$ and $\bar{C}$ was shown on the left side of Figure 8.3 and 8.4, respectively. The Ri and Re at the inlet and the holes of the tank were listed in Table 8.1. It can be seen that for all cases, at $T = 3$, C_{11} reached close to 1, but the other three compartments were about half flushed. This is because due to the existence of the vertical flow from the inlet, the mixing in compartment 11 was stronger so that the incoming water might flush most of the original water out of it; but in other compartments the lighter water was not able to

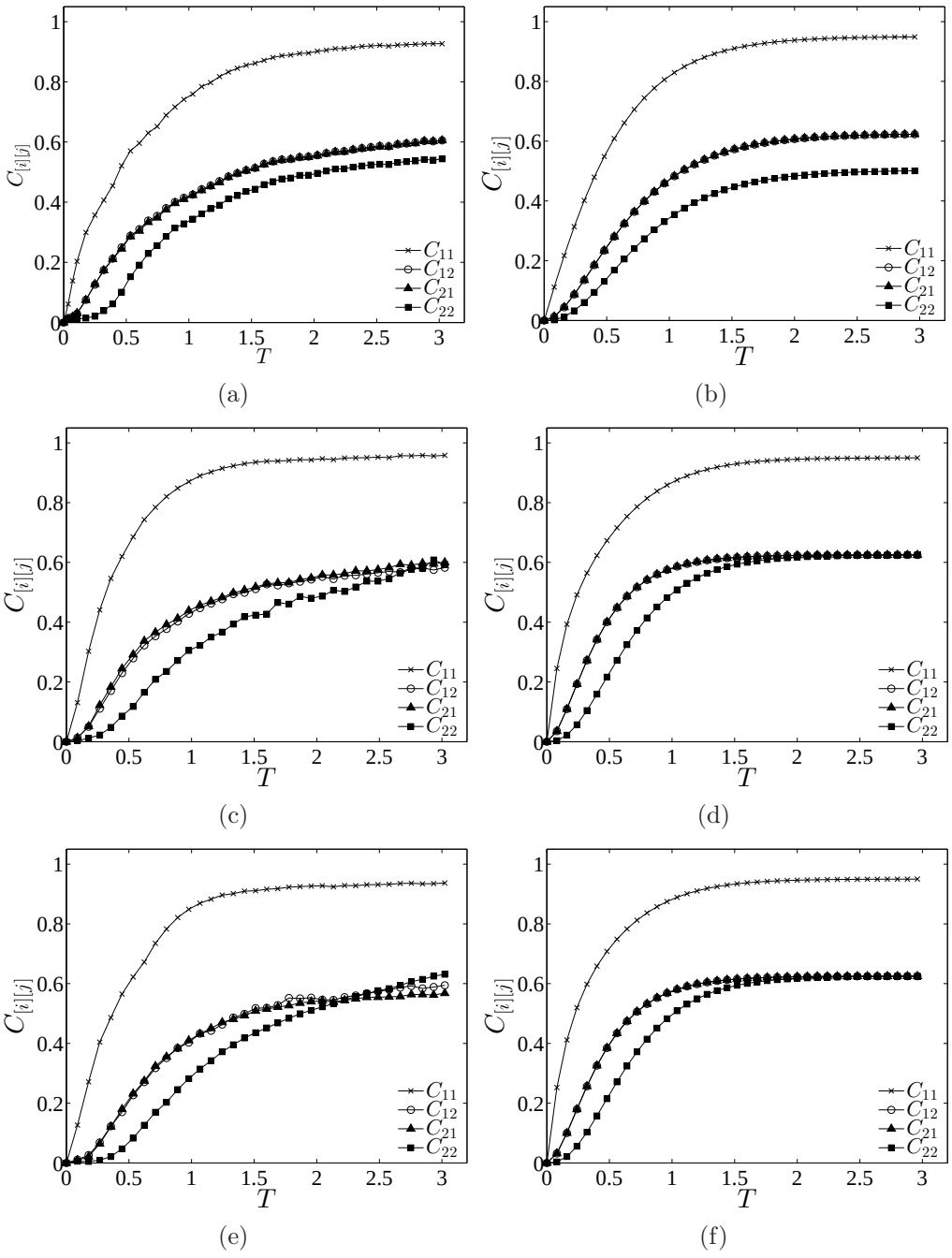

Figure 8.3: The (a, c, e) experimental measurements and (b, d, f) model predictions of the variation in time of the flushed fractions in the 2×2 tank when the tank with salt water was flushed with fresh water at different flow rates. The figures correspond to $Ri =$ (a, b) -30, (c, d) -9 and (e, f) -2.

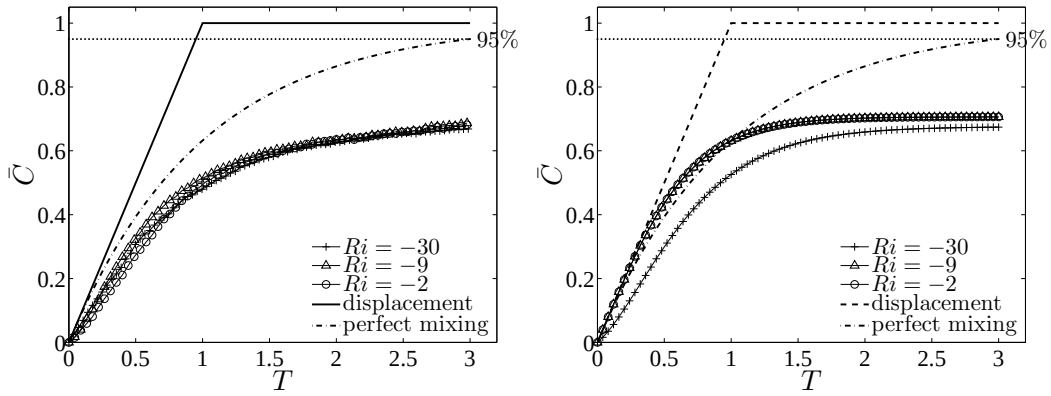

Figure 8.4: The (a) experimental measurements and (b) model predictions of the variation in time of the average flushing efficiency in the 2×2 tank when the tank with salt water was flushed with fresh water at different flow rates.

mix with the original denser water in the lower region. At $Ri = -30$, C_{11} increased more slowly than that at the other two higher flow rates (see Figure 8.3(a, c, e)), because the relatively lower Ri and Re led to insufficient mixing in compartment 11. At $Ri = -2$, C_{22} at $T = 3$ was a little higher than that at the other two lower inflow rates, because the relatively higher Ri and Re resulted in a faster water exchange in compartment 22. From Figure 8.4(a), $\bar{C}$ at $T = 3$ was around 65-70%. Even though the inflow rate was increased 4 times higher, there was no significant improvement of the flushing efficiency.

It is indicated that when lighter water is used to flush denser water, a significant amount of the original water cannot be exchanged and will remain in the lower region. Therefore, water of higher density in a multi-compartment tank cannot be efficiently removed by being flushed with water of lower density.

8.3.1 Modification of the stratified mixing model at low Ri

In order to interpret the experimental results, the stratified mixing model is modified to describe the flushing processes in the 2×2 tank. Since the Ri is relatively low, turbulence is intense. The model is modified as a transition from the stratified mixing

to unstratified mixing case. $H_l/H = 0.375$ and $H_u/H = 0.625$.

Denser fluid into lighter fluid

From the experimental measurements shown on the left side of Figure 8.1, it can be seen that the flushed fractions at $T = 3$ were higher than H_u/H, which means that the top region of the compartments were not trapped. For $Ri = 59$ at $T = 3$, C_{11}, C_{12}, C_{21} and C_{22} were close to 1, 0.8, 0.8 and 1, respectively. As described in Chapter 7, at $Ri > 0$, the bottom of each compartment of the tank is first exchanged. There forms a fluid interface, and the height H_I is assumed to be determined by (7.10). As the tank is structurally simple, the region between H_I and H in compartments 11 and 22, as well as the region between H_I and $0.8H$ in compartments 12 and 21, can be simply assumed as an integral region. Therefore, the model becomes two-layer; the flushed fraction in a compartment is assumed to be composed of the flushed fractions in the lower and upper sections, that is,

$$C_{11} = \frac{H_I}{H} C_{11,l} + \left(1 - \frac{H_I}{H}\right) C_{11,u}, \tag{8.1}$$

$$C_{12} = \frac{H_I}{H} C_{12,l} + \left(0.8 - \frac{H_I}{H}\right) C_{12,u}, \tag{8.2}$$

$$C_{21} = \frac{H_I}{H} C_{21,l} + \left(0.8 - \frac{H_I}{H}\right) C_{21,u}, \tag{8.3}$$

$$C_{22} = \frac{H_I}{H} C_{22,l} + \left(1 - \frac{H_I}{H}\right) C_{22,u}, \tag{8.4}$$

where $C_{[i][j],l}$ and $C_{[i][j],u}$ are the flushed fraction in the lower region and upper region of compartment $[i][j]$, respectively. The upper region of the tank is flushed by the mixed fluids from the lower region of compartment 22. The variation in time of the flushed fraction in each section of each compartment follows the rule of mass

conservation, evolving as

$$\frac{\mathrm{d}C_{11,l}}{\mathrm{d}T} = \frac{4H}{H_I}(1 - C_{11,l}), \tag{8.5}$$

$$\frac{\mathrm{d}C_{12,l}}{\mathrm{d}T} = \frac{2H}{H_I}(C_{11,l} - C_{12,l}), \tag{8.6}$$

$$\frac{\mathrm{d}C_{21,l}}{\mathrm{d}T} = \frac{2H}{H_I}(C_{11,l} - C_{21,l}), \tag{8.7}$$

$$\frac{\mathrm{d}C_{22,l}}{\mathrm{d}T} = \frac{2H}{H_I}(C_{12,l} + C_{21,l} - 2C_{22,l}), \tag{8.8}$$

$$\frac{\mathrm{d}C_{[i][j],u}}{\mathrm{d}T} = \frac{2H}{(H - H_I) + (H_S - H_I)}(C_{22,l} - C_{[i][j],u}), \tag{8.9}$$

where H_S is trapped height. Here H_S is empirically assumed to be $0.8H$ at $Ri = 59$.

For $Ri = 9$ or 2, the turbulence in each compartment was even stronger. From the observations, it can be inferred that compartment 11 followed the unstratified mixing rule. Perfect mixing occurred in compartment 22 as well, where the stratification effect was not significant. At $T = 3$, compartments 11 and 22 were almost 100% flushed, but about 80% or 90% of the lower region in compartments 12 and 21 were flushed. For compartments 12 and 21, since the increase of the flushed fractions after $T = 2$ was not so obvious, perfect mixing could be assumed to take place in the lower region in each of the two compartments that was not trapped. Based on the rule of mass conservation, the flushed fraction in each region is assumed to vary as

$$\frac{\mathrm{d}C_{11}}{\mathrm{d}T} = 4(1 - C_{11}), \tag{8.10}$$

$$\frac{\mathrm{d}C_{12,l}}{\mathrm{d}T} = \frac{2H}{H_S}(C_{11} - C_{12,l}), \tag{8.11}$$

$$\frac{\mathrm{d}C_{21,l}}{\mathrm{d}T} = \frac{2H}{H_S}(C_{11} - C_{21,l}), \tag{8.12}$$

$$\frac{\mathrm{d}C_{22}}{\mathrm{d}T} = 2(C_{12,l} + C_{21,l} - 2C_{22}), \tag{8.13}$$

where H_S is assumed to be $0.8H$ and $0.9H$ at $Ri = 9$ and 2, respectively. $C_{12} = C_{12,l}H_S/H$ and $C_{21} = C_{21,l}H_S/H$.

Figure 8.1(b, d, f) shows the variation in time of $C_{[i][j]}$ in the 2×2 tank closed by

the stratified model at $Ri = 59$, 9 and 2, respectively. The main character of the flushing can be captured by modifying the stratified mixing model. At $Ri = 59$, C_{11} does not behave like the perfect mixing rule. However, the whole of the top region in the inlet compartment, and part of the top region in compartments 12 and 21 are flushed due to turbulent mixing. At $Ri = 9$ or 2, the region that is not trapped in the tank follows the unstratified mixing mode. The incoming fluid is transported from one compartment to its downstream compartment(s) and mixes perfectly with the original fluid in the untrapped section it enters. Figure 8.2(b) shows the model predicted variation in time of $\bar{C}$ in the 2×2 tank for three tested Ri. The predictions reflect the main character of the experimental measurements. The flushing efficiency at $T = 3$ depends on the model assumption on the height of the trapped region in the corner compartments.

Lighter fluid into denser fluid

At $Ri < 0$, the flushing in compartment 11 was not perfect mixing, see Figure 8.3. The two-layer assumption is adopted here. The height of the interface, H_I, is determined by equation (7.21). From the experimental measurements, C_{11} became almost steady at about 0.95 after $T = 1.5$ or 2. So the bottom trapped height H_S is assumed to be $0.05H$. At $Ri = -30$, the upper region of compartments 11, 12 and 21 is first exchanged, and the region between H_S and H_I in compartment 11, the region between H_l and H_I in compartment 12 and 21, as well as the region above H_I in compartment 22, are assumed as an integral region to be flushed. The flushed fractions in the four compartments can be expressed as

$$C_{11} = \frac{H_I - H_S}{H} C_{11,l} + \left(1 - \frac{H_I}{H}\right) C_{11,u}, \tag{8.14}$$

$$C_{12} = \frac{H_I - H_l}{H} C_{12,l} + \left(1 - \frac{H_I}{H}\right) C_{12,u}, \tag{8.15}$$

$$C_{21} = \frac{H_I - H_l}{H} C_{21,l} + \left(1 - \frac{H_I}{H}\right) C_{21,u}, \tag{8.16}$$

$$C_{22} = \left(1 - \frac{H_I}{H}\right) C_{22,u}. \tag{8.17}$$

The region above H_I in compartments 12 and 21 are assumed to be flushed by the region above H_I in compartment 11 at a rate of $Q - Q_v$, where $Q_v = vL_1W_1$ and v is determined by (7.36). The region between H_S and H_I in compartment 11, as well as the region between H_l and H_I in compartments 12 and 21, are assumed as an integral region, which is flushed by the flow from the upper region in compartment 11 at a rate of Q_v. The region above H_I in compartment 22 is assumed to be flushed by the flow from both the upper and lower region of compartments 12 and 21. Based on mass conservation, the flushed fraction in each section is assumed to vary as

$$\frac{\mathrm{d}C_{11,u}}{\mathrm{d}T} = \frac{4H}{H - H_I}\left(1 - \frac{Q_v}{Q}\right)(1 - C_{11,u}), \tag{8.18}$$

$$\frac{\mathrm{d}C_{12,u}}{\mathrm{d}T} = \frac{2H}{H - H_I}\frac{Q_v}{Q}(C_{11,u} - C_{12,u}), \tag{8.19}$$

$$\frac{\mathrm{d}C_{21,u}}{\mathrm{d}T} = \frac{2H}{H - H_I}\frac{Q_v}{Q}(C_{11,u} - C_{21,u}), \tag{8.20}$$

$$\frac{\mathrm{d}C_{[i][j],l}}{\mathrm{d}T} = \frac{3H}{(H_I - H_S) + 2(H_I - H_l)}\frac{Q_v}{Q}(C_{11,u} - C_{[i][j],l}), \tag{8.21}$$

$$\frac{\mathrm{d}C_{22,u}}{\mathrm{d}T} = \frac{2H}{H - H_I}\left(\frac{Q_v}{Q}C_{12,u} + \frac{Q_v}{Q}C_{21,u} + 2\left(1 - \frac{Q_v}{Q}\right)C_{[i][j],l} - 2C_{22,u}\right). \tag{8.22}$$

At $Ri = -9$ and -2, the flow in the tank is more turbulent. The region above H_I in compartments 12 and 21 are assumed to be flushed by the region above H_I compartment 11. For simplicity, the region between H_S and H_I in compartment 11, the region between H_l and H_I in compartments 12 and 21, as well as the region above H_l in compartment 22 are assumed to be integral, which is flushed by the flow from the upper region of compartments 12 and 21. Based on mass conservation, the flushed

fractions are assumed to evolve as

$$\frac{\mathrm{d}C_{11,u}}{\mathrm{d}T} = \frac{4H}{H-H_I}(1-C_{11,u}), \tag{8.23}$$

$$\frac{\mathrm{d}C_{12,u}}{\mathrm{d}T} = \frac{2H}{H-H_I}(C_{11,u}-C_{12,u}), \tag{8.24}$$

$$\frac{\mathrm{d}C_{21,u}}{\mathrm{d}T} = \frac{2H}{H-H_I}(C_{11,u}-C_{21,u}), \tag{8.25}$$

$$\frac{\mathrm{d}C_{[i][j],l}}{\mathrm{d}T} = \frac{2H}{(H_I-H_S)+2(H_I-H_l)+(H-H_l)}(C_{12,u}+C_{21,u}-2C_{[i][j],l}). \tag{8.26}$$

In this case,

$$C_{22} = \left(1-\frac{H_l}{H}\right)C_{[i][j],l}.$$

Figure 8.3(b, d, f) shows the variation in time of $C_{[i][j]}$ in the 2×2 tank estimated by modifying the stratified mixing model at $Ri = -30$, -9 and -2, respectively. At different Ri, the difference between the performance of C_{11} and C_{22} is reflected by the model. When Ri increases from -30 to -2, the increase of the turbulence intensity improves the flushing. Figure 8.4(b) shows the model predicted average flushing efficiency for the three tested Ri. At $Ri = -30$, $\bar{C}$ increases lower than the displacement mode due to bypassing of the incoming fluid from the top region. The model predicted flushing efficiency is higher than the experimental measurements, because the amount of bypassing fluids is underestimated.

8.4 Flushing a 5×4 'J'-type tank

In this section, the influence of Ri on the stratified flushing is further tested in a more complex structure - a 5×4 'J'-type tank with limber holes, shown in Figures 4.1(d) and 5.1(c). The bottom section of the tank can be considered as an extension from the 2×2 square configuration to 5×4 rectangular configuration, but the compartments of the last row stand higher than those of the other four rows, which has the geometrical character of a real ballast tank. The number of the connecting holes on the longitudinal walls is different from that on the transverse walls. During the flushing experiments, only the far outlet was kept open.

8.4.1 Salt water into fresh water

Figure 8.5(a, d, g) shows the variation in time of $C_{[i][j]}$ in the 5×4 tank with fresh water when it was flushed with salt water. At the first stage, the lower region of the compartments that are closer to the inlet was earlier flushed. After the lower region of the tank was flushed, all the flushed fractions increased. In this stage, all the horizontal compartments except compartment 11 behaved similarly, and the four vertical compartments performed the same. C_{11} increased higher than other flushed fractions, which was largely influenced by Ri as the inlet nozzle located in compartment 11. At $Ri = 94$, the increase rate of $C_{[5][j]}$ was lower than that of the horizontal compartments (on rows 1, 2, 3 and 4) because the vertical compartments (on the 5th row) were larger in size. Although the height of the vertical compartments is three times that of the horizontal compartments, the increase rate of $C_{[5][j]}$ was larger than a third of that of the horizontal compartments. This was because the mixed fluids above the displaced fluids were transported to the vertical compartments through the lightening holes and the turning section. At $T = 3$, almost all compartments were completely flushed, due to the existence of the limber holes on the top of the connecting walls between neighbouring compartments.

The main differences among the three tested cases occurred at the initial stage. The variation in time of $C_{[i][j]}$ at $T = 0 \rightarrow 0.38$ was shown in Figure 8.5(b, e, h). For $Ri = 94$ at $T = 0.1$, C_{11} increased to about 0.35 and became stable, higher than $H_l/H = 0.25$ because of the weir effect. At this period, the flushed fractions of the horizontal compartments close to the inlet reached a stable state to 'wait' for the lower region of the downstream compartments to be flushed. The closer a compartment located to the inlet, the higher the stable flushed fraction was. The stable flushed fractions at $Ri = 94$ were lower than that at $Ri = 7.8$ and 5.5, because when the incoming flow was not sufficiently turbulent, density effect was significant.

The variation in time of the average flushed fraction of each case is shown in Figure 8.5(c, f, i). At the first stage, $\bar{C}$ increased linearly, following the displacement mode, because mixing in the upper region of the tank was not significant. At a later stage, the increase rate of the flushing efficiency decreased because the mixed fluids left the tank from the top outlet. At three exchange volumes, the flushing efficiency

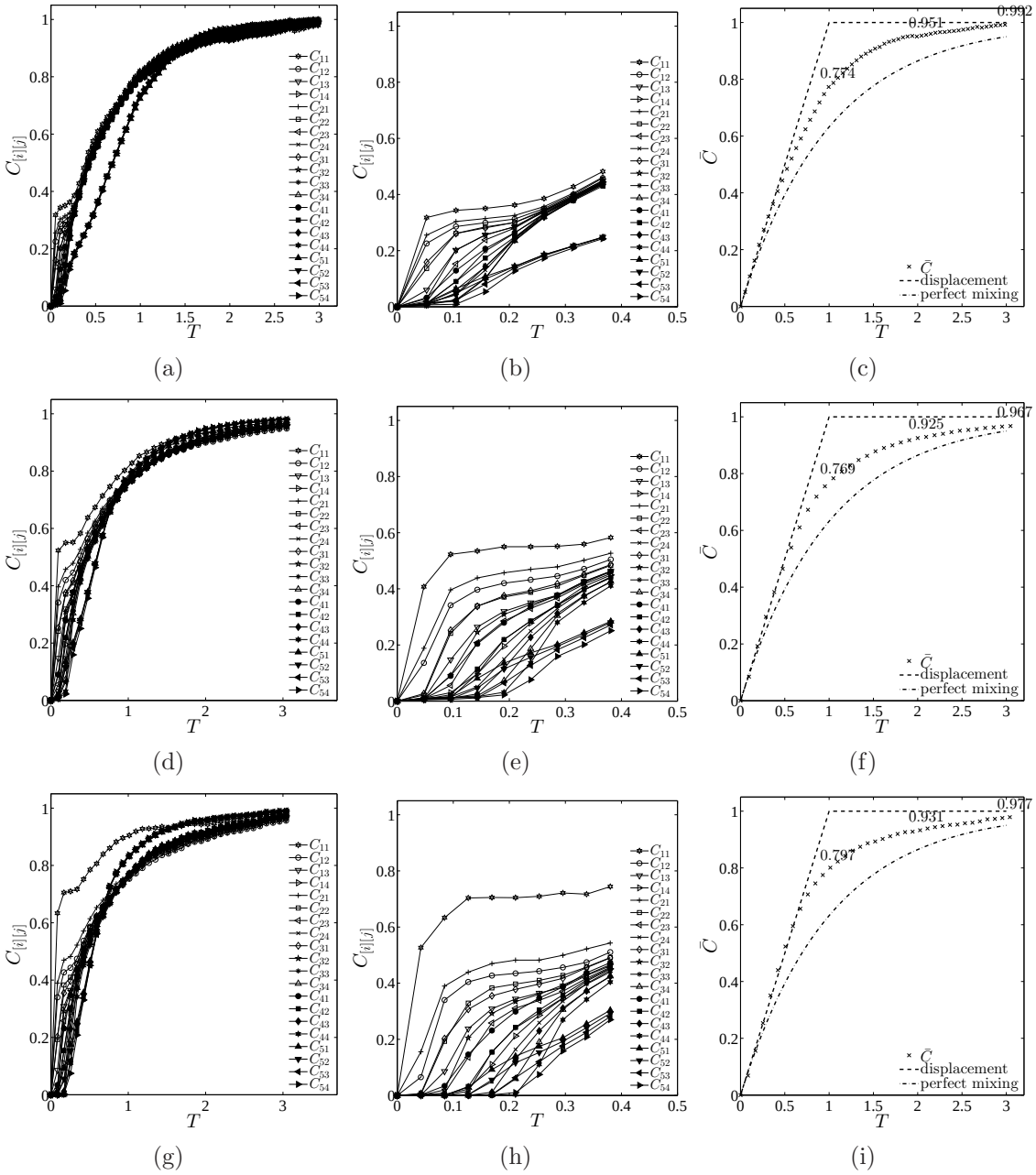

Figure 8.5: The variation in time of (a, b, d, e, g, h) $C_{[i][j]}$ and (c, f, i) $\bar{C}$ in the 5×4 tank with only the far outlet open for the salt water into fresh water case. The figures correspond to Ri = (a, b, c) 94, (d, e, f) 7.8 and (g, h, i) 5.5. The three numbers in (c, f, i) correspond to $\bar{C}$ at T =1, 2 and 3, respectively.

in each case was over 95%. This indicates that adding limber holes onto the top of the connecting walls in ballast tanks may help remove the original fluid in the top region for the case of injecting dense water into light water.

8.4.2 Fresh water into salt water

The case of injecting fresh water into salt water was tested, and the variation in time of $C_{[i][j]}$ at $T = 0 \rightarrow 3$ for different Ri was shown in Figure 8.6(a, d, g). For all cases, C_{11} rose highest, as the turbulence in compartment 11 was the most intense. The flushing was composed of two main processes. The first stage was dominated by displacement in the upper region of each compartment, which was followed by a shear mixing stage. After the upper region of the tank was displaced with the incoming lighter fluid, the original fluid in the lower region was exchanged by the shear mixing between the two fluids. The flushed fractions of the horizontal compartments were exceeded by those of the vertical compartments at a certain time, because the ratio of the region which could be mixed in the horizontal compartments was smaller than that in the vertical compartments. At a later period, the increase of the flushed fractions seemed approximately linear due to shear mixing.

The variation in time of $C_{[i][j]}$ at $T = 0 \rightarrow 0.8$ was shown in Figure 8.6(b, e, h) for the three tested Ri. Similarly to the dense water into fresh water case, there existed quasi-stable stage for each compartment after the upper region was flushed at the initial stage. At $Ri = -105$, the stable flushed fractions were quite low, because the density effect was important. When Ri increased to -10.5 and -3.9, the influence of the turbulence caused by the inlet nozzle on mixing became stronger. The closer a compartment located to the inlet, the more intensely the mixing occurred in it. As a result, the stable flushed fractions became higher and the difference between neighbouring flushed fractions became remarkably larger.

The average flushing efficiency of the tank is shown in Figure 8.6(c, f, i). Unlike the dense water into fresh water case, the increase of the flushing efficiency did not follow the displacement rule at the initial stage of the flushing. The reason was that due to the existence of the limber holes on the top of the connecting walls, the incoming light

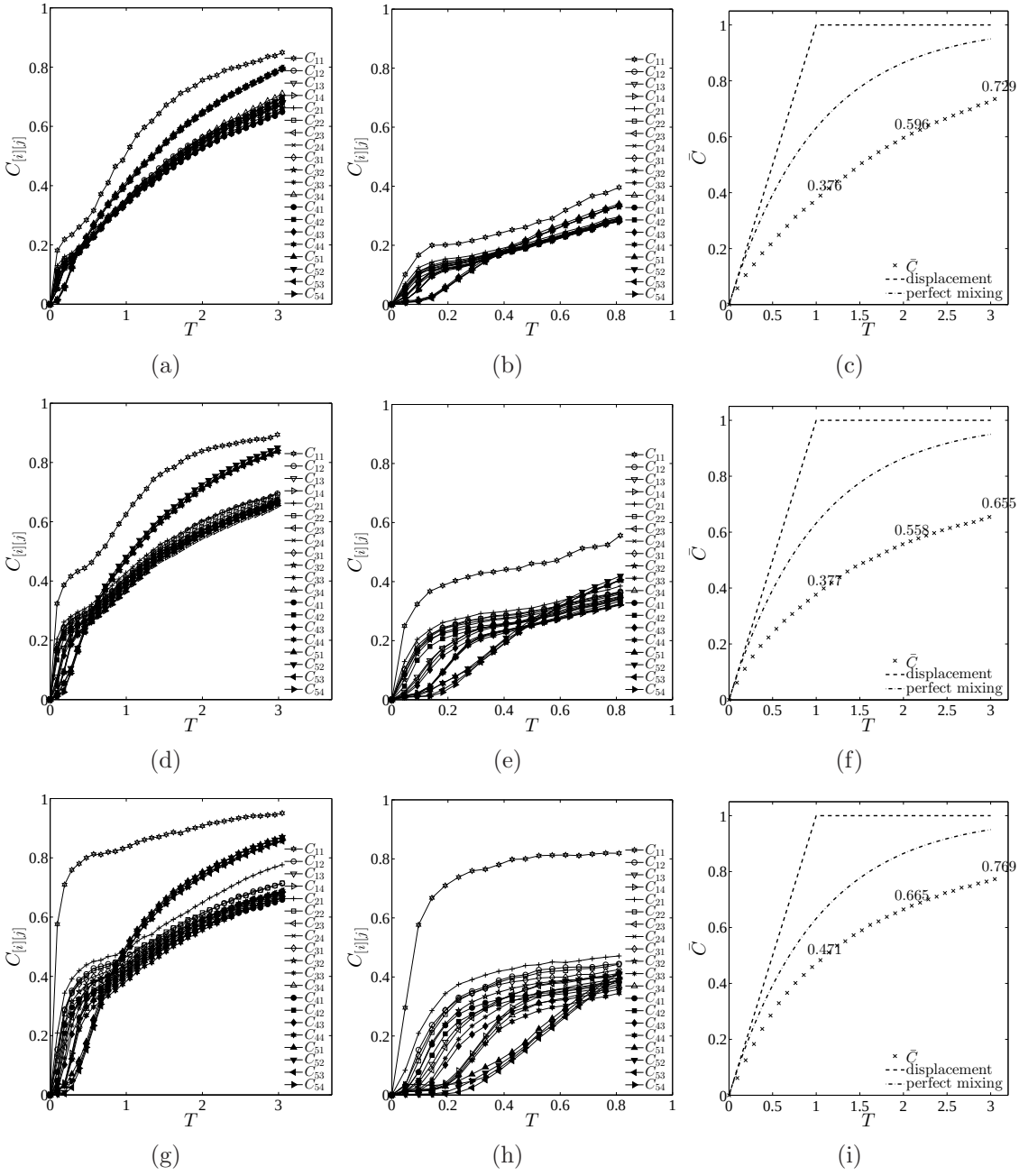

Figure 8.6: The variation in time of (a, b, d, e, g, h) $C_{[i][j]}$ and (c, f, i) $\bar{C}$ in the 5×4 tank with only the far outlet open for the fresh water into salt water case. The figures correspond to $Ri =$ (a, b, c) -105, (d, e, f) -10.5 and (g, h, i) -3.9. The three numbers in (c, f, i) correspond to $\bar{C}$ at T =1, 2 and 3, respectively.

fluid bypassed the uppermost region of the tank. The flushing efficiency increased when Ri increased from -105 to -3.9, because when density effect became weaker, the incoming fluid had more energy to mix with and exchange the original fluid.

8.5 Summary

The stratified flushing from multi-compartment tanks has been tested. The flushing efficiency depends on density effect in terms of Ri. At high Ri, the weir effect is significant, and the original fluid may be trapped in the top or bottom region of the tank; when the Ri is low, the turbulence is intense, and the incoming fluid has more energy to displace and mix with the original fluid. The stratified mixing model can be modified to reflect the character of the stratified flushing in multi-compartment tanks. Meanwhile, adding limber holes to the connecting walls may allow the incoming fluid to exchange the original fluid in the trapped region and thus improve the flushing efficiency, especially for the case of injecting denser fluid into lighter fluid.

Chapter 9

Model Application to Ballast Water Flushing Systems

9.1 Introduction

When the structure of a ballast tank is known, it is necessary to understand how the flushing efficiency can be estimated. To put the theoretical work into context, the new modelling methodology is applied to the flushing from two typical ballast tanks in this chapter. The influence of tank structure on the flushing efficiency will be analysed in open-looped systems under both unstratified and stratified cases. The results have implications on saving costs of running ballast pumps as well as collecting ballast water samples.

In this chapter, the validated models will be applied to analyse the flushing in typical ballast tanks. The unstratified flushing in the typical hopper side and upper wing tank is first analysed to see how the flushing efficiency depends on the setting of the outlet and the position of the connecting pipes. Then both the unstratified and stratified flushing in the typical 'J'-type bottom and side tank are considered to investigate the possibility of relaxing the exchange volumes and the influence of the geometry on the flushing.

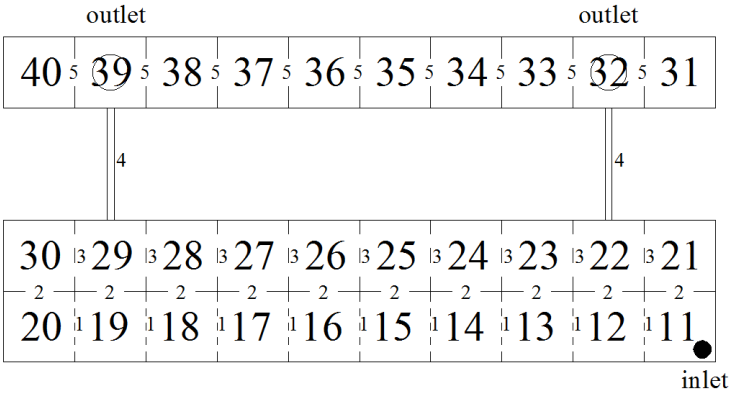

Figure 9.1: Model of the hopper side and upper wing tank in Figure 2.2(c) from the plan view, including double bottom compartments (row 1), hopper side compartments (row 2), and upper wing compartments (row 3).

9.2 Application to the hopper side and upper wing tank

The hopper side and upper wing tank typical of a bulk carrier which has been drawn in Figure 2.2(c) is modelled as a network in Figure 9.1. The network has in total 3 rows by 10 columns of nodes, including 10 double bottom compartments in row 1, 10 hopper side compartments in row 2, and 10 upper wing compartments in row 3. The external water is pumped into compartment 11 and exits from compartments 32 and 39. All these 30 compartments are assumed to have the same volume. There are 4, 2 and 1 hole between compartments within the double bottom compartments, hopper side compartments, and upper wing compartments, respectively (numbered as 1, 3 and 5 in Figure 9.1); and 1 hole connects a double bottom compartment to a hopper side compartment (numbered as 2). One pipe connects the hopper side compartment 22 to the upper wing compartment 32, and another pipe connects compartment 29 to 39 (numbered as 4). The inflow rate is normalised as 1. Usually both outlets are kept open during the flushing, and the internal flow rates estimated by the unstratified flushing model developed in Chapter 3 are listed in the column under 'Case 1' in Table 9.1. Usually both outlets are kept open during the flushing, but there is little flow

between the upper wing compartments of the tank. Figure 9.2 and 9.4(a) show the variation of the concentration field and $\bar{C}$ with time, respectively. It can be seen that for the 'both open' case, the upper wing compartments except 32 and 39 are hardly flushed, leading to a flushing efficiency of 73.3% at $T = 3$. For other compartments, $C_{[i][j]}$ reaches close to 1 at $T = 3$. Initially, $\bar{C}$ increases between the displacement and the perfect mixing mode; at $T = 0.5 - 2.0$, $\bar{C}$ increases more slowly, below the perfect mixing mode; after $T = 2$, $\bar{C}$ is almost steady. Therefore, the outlet setting needs to be changed for a more effective flushing.

In an earlier work, Kent and Parsons (2004) suggested that care is needed in detailed tank design to ensure complete exchange by the flow-through method. The setting of the outlet and the position of the connecting pipes can be altered to improve the flushing efficiency. Firstly the outlet in compartment 32 is closed and only the outlet in compartment 39 is kept open. The internal flow rates among some compartments for the 'far open' case are shown under 'Case 2' in Table 9.1, where the inflow rate is normalised as 1. In this case, there exists fluid flow from compartment 32 to compartment 39. From Figure 9.3, it can be seen that except compartments 31 and 40, all compartments are flushed effectively, with $C_{[i][j]}$ close to 1 at $T = 3$. The performance of $\bar{C}$ is much better than that of the 'both open' case, which rises between the displacement and the perfect mixing mode from initially to $T = 2.7$ (see Figure 9.4(b)). It does not achieve 0.95 because the two corner compartments 31 and 40 are not flushed. Secondly, if the far outlet is further moved from compartment 39 to 40, compartment 40 can be flushed (see 'Case 3' in Table 9.1). In this case, $\bar{C}$ is over 95% after around $T = 1.9$ (see Figure 9.4(c)). Thirdly, the position of the two connection pipes can be further changed to improve the flushing. When compartment 22 is connected to 32, compartment 31 cannot be effectively flushed. So the pipe is moved from between compartments 22 and 32 to between 21 and 31. To form a symmetrical structure, the pipe is also moved from between compartments 29 and 39 to between 30 and 40. In this case, all compartments are flushed efficiently (see 'Case 4' in Table 9.1). From Figure 9.4(d), $\bar{C}$ is over 95% at $T = 1.8$, and 99.8% at $T = 3$. This finding is consistent with the CFD result of Kent and Parsons (2004) that the dual-trunk, single-port design gives the best flushing performance for the

Table 9.1: The predicted internal normalised flow rates in the hopper side and upper wing tank for the four cases considered. 'Case 1', 'Case 2', 'Case 3' and 'Case 4' correspond to the 'both open' case, the 'far open' case, the 'far open' case with revised outlet position and the 'far open' case with revised outlet position and connecting pipes, respectively.

	Case 1	Case 2	Case 3	Case 4
$f_{21,22}$	0.242	0.240	0.240	0.055
$f_{22,23}$	-0.066	-0.071	-0.071	0.193
$f_{23,24}$	0.061	0.058	0.058	0.256
$f_{24,25}$	0.132	0.130	0.130	0.272
$f_{25,26}$	0.161	0.160	0.160	0.274
$f_{26,27}$	0.170	0.170	0.170	0.275
$f_{27,28}$	0.193	0.194	0.194	0.295
$f_{28,29}$	0.257	0.257	0.257	0.365
$f_{29,30}$	-0.113	-0.113	-0.113	0.524
$f_{21,31}$	0	0	0	0.179
$f_{22,32}$	0.500	0.499	0.499	0
$f_{29,39}$	0.500	0.501	0.501	0
$f_{30,40}$	0	0	0	0.821
$f_{31,32}$	0	0	0	0.179
$f_{32,33}$	0	0.499	0.499	0.179
$f_{33,34}$	0	0.499	0.499	0.179
$f_{34,35}$	0	0.499	0.499	0.179
$f_{35,36}$	0	0.499	0.499	0.179
$f_{36,37}$	0	0.499	0.499	0.179
$f_{37,38}$	0	0.499	0.499	0.179
$f_{38,39}$	0	0.499	0.499	0.179
$f_{39,40}$	0	0	1	0.179

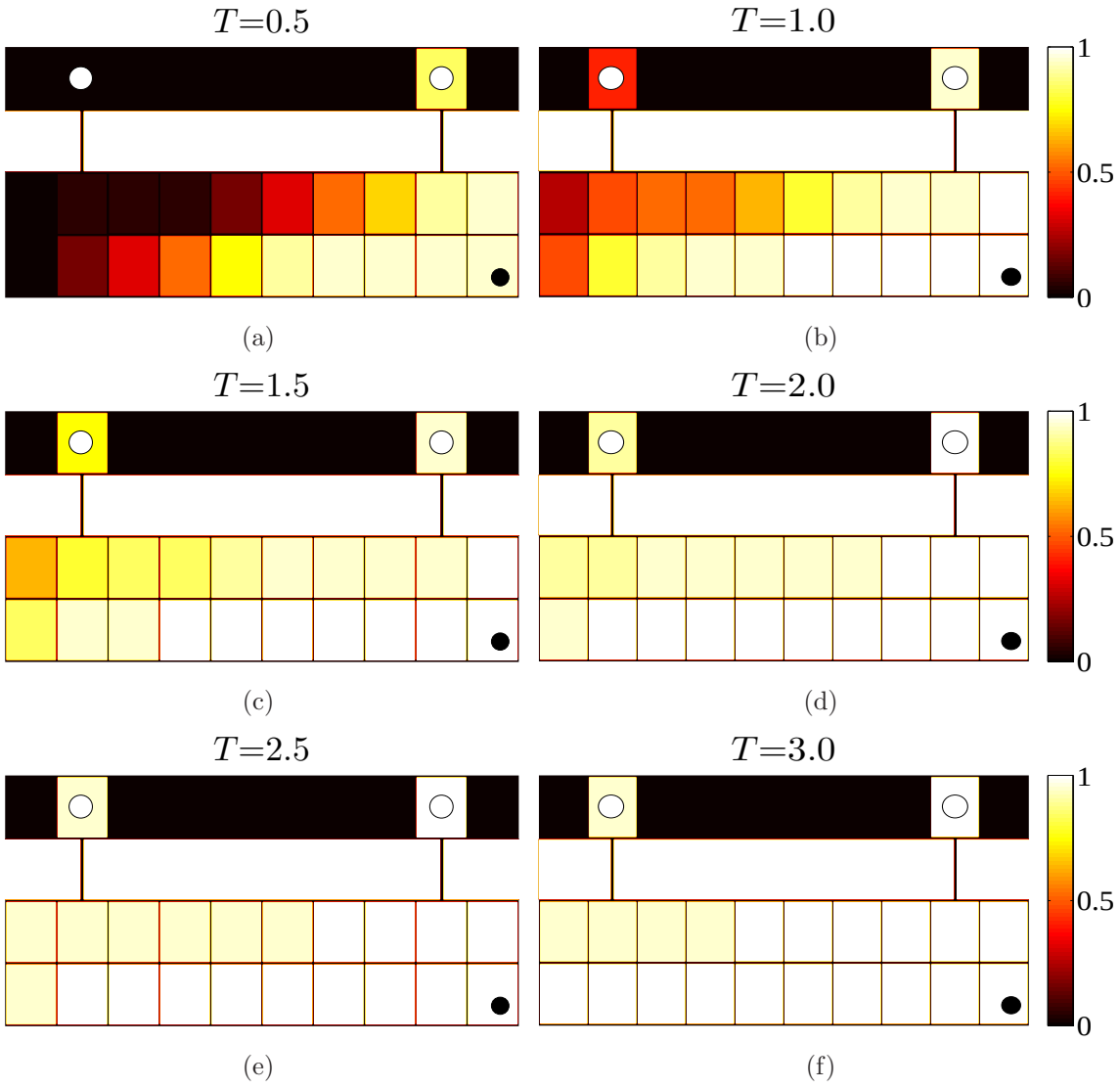

Figure 9.2: The variation of the concentration field in the hopper side and upper wing tank under the unstratified mixing condition for the 'both open' case ('Case 1').

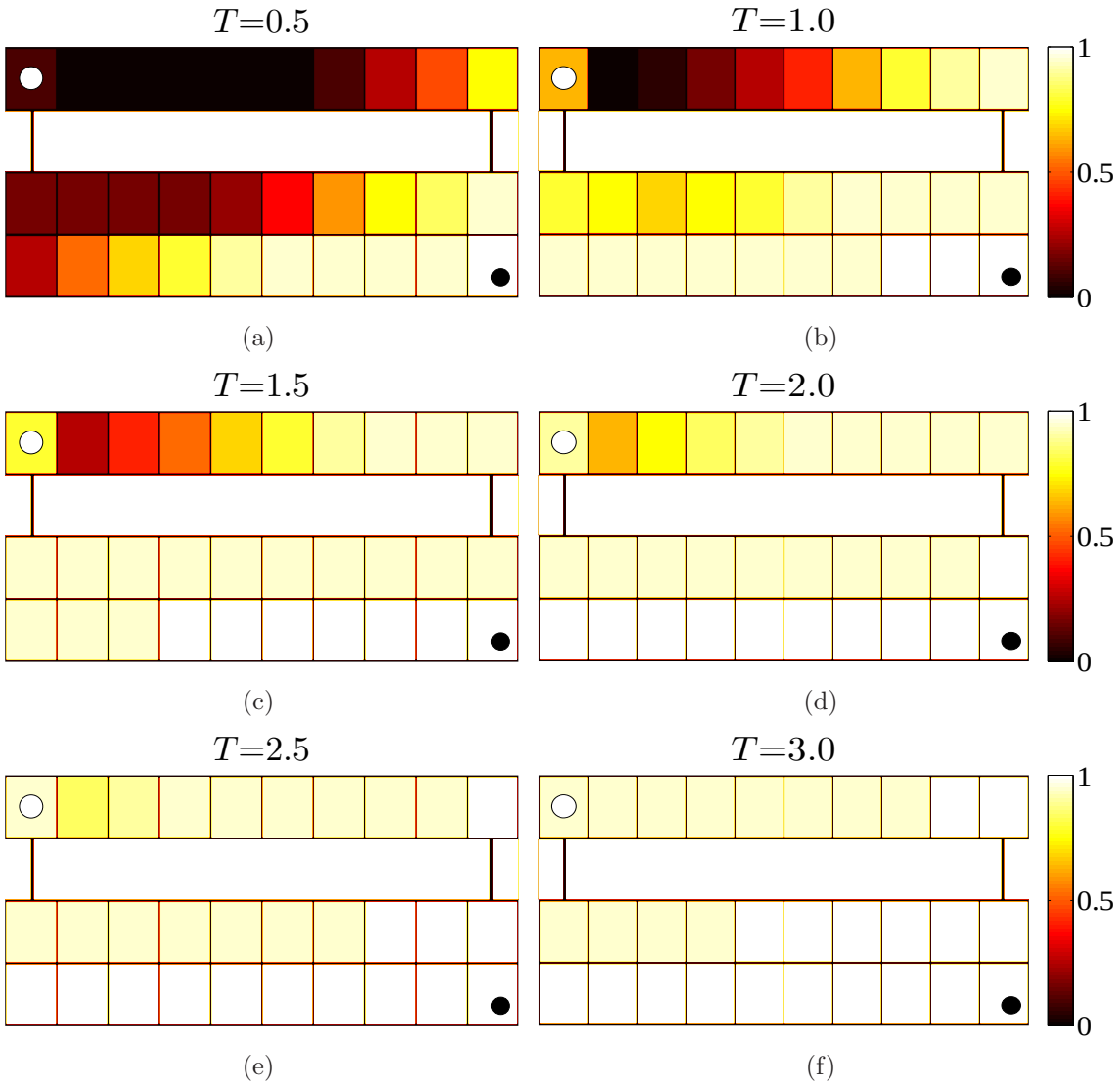

Figure 9.3: The variation of the flushed fraction field in the hopper side and upper wing tank under the unstratified mixing condition for the 'far open' case ('Case 2').

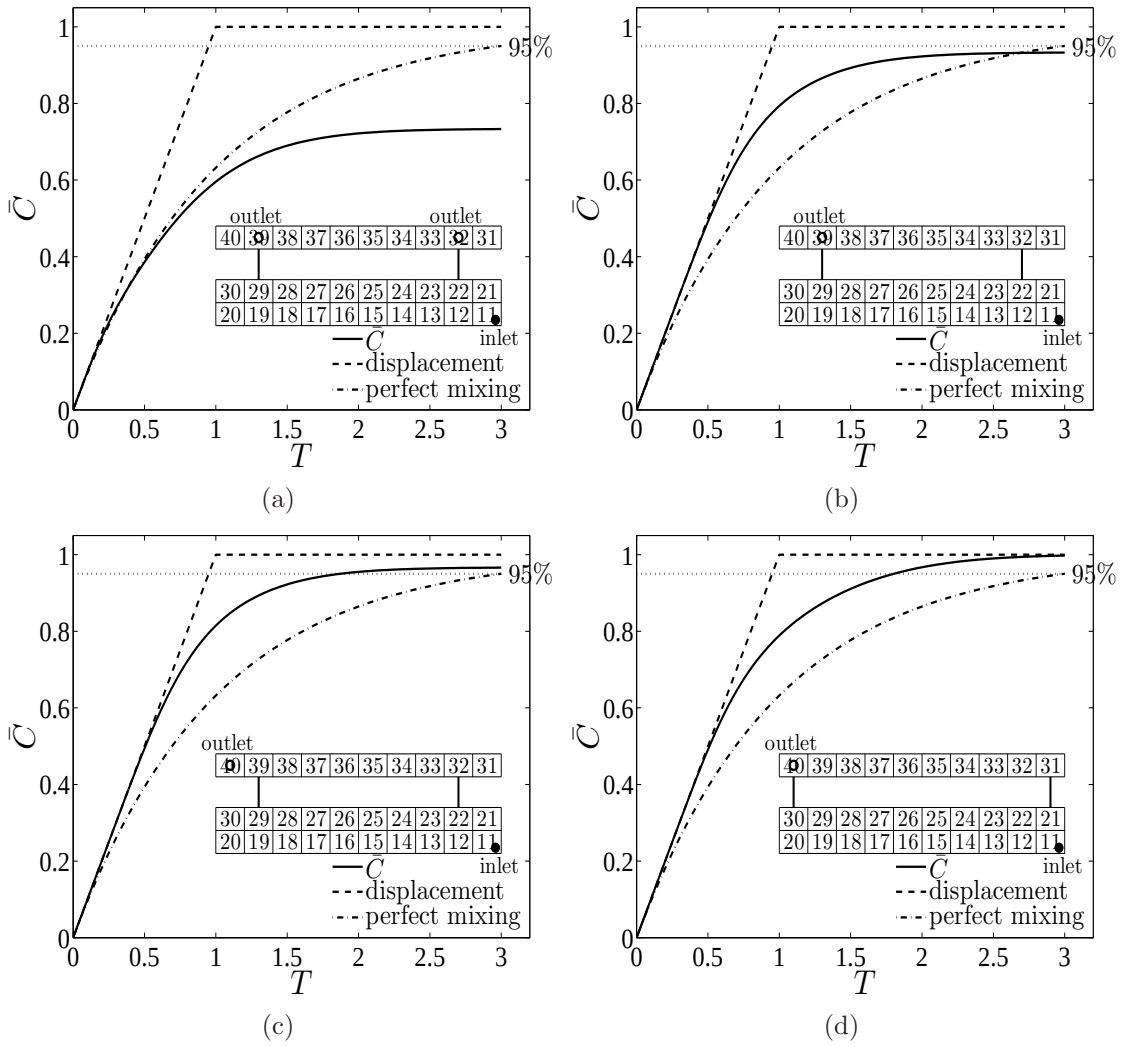

Figure 9.4: The variation of $\bar{C}$ in the hopper side and upper wing tank under the unstratified mixing condition. The figures correspond to (a) the 'both open' case ('Case 1'), (b) the 'far open' case ('Case 2'), (c) the 'far open' case with revised outlet position ('Case 3') and (d) the 'far open' case with revised outlet position and connecting pipes ('Case 4').

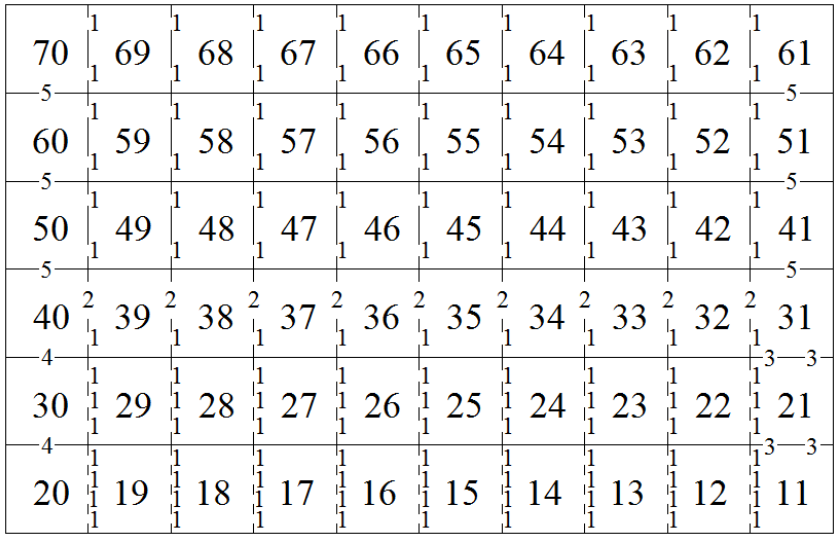

Figure 9.5: Model of the 'J'-type bottom and side tank in Figure 2.2(d) from the plan view, including double bottom tanks (rows 1 and 2), hopper tanks (row 3) and side tanks (rows 4, 5 and 6). Numbers in the figure represent holes of different sizes.

hopper side/upper wing tank, where $\bar{C}$ =99.9% at $T = 3$. Generally, to achieve an effective flushing, the setting of the outlets and the position of the connecting pipes should be adjusted to generate a flow system that can connect all compartments in the tank.

9.3 Application to the 'J'-type bottom and side tank

The geometry of a 'J'-type bottom and side tank (typical of container vessels) which has been drawn in Figure 2.2(d) is modelled in Figure 9.5. There are in total 6 rows by 10 columns of compartments, including 20 double bottom compartments in rows 1 and 2, 10 hopper compartments in row 3, and 30 side compartments in rows 4, 5 and 6. The external water is pumped into compartment 11 and exits from compartment 70. All compartments of a row are connected longitudinally. On the transverse direction, the compartments of the 1st and 10th columns, which are on

Table 9.2: The predicted internal normalised flow rates in the 'J'-type tank.

$f_{11,12}$	0.272	$f_{12,13}$	0.272	$f_{13,14}$	0.272	$f_{14,15}$	0.272
$f_{15,16}$	0.272	$f_{16,17}$	0.272	$f_{17,18}$	0.272	$f_{18,19}$	0.272
$f_{19,20}$	0.272	$f_{11,21}$	0.728	$f_{20,30}$	0.272	$f_{21,22}$	0.080
$f_{22,23}$	0.080	$f_{23,24}$	0.080	$f_{24,25}$	0.080	$f_{25,26}$	0.080
$f_{26,27}$	0.080	$f_{27,28}$	0.080	$f_{28,29}$	0.080	$f_{29,30}$	0.080
$f_{21,31}$	0.648	$f_{30,40}$	0.352	$f_{31,32}$	0.166	$f_{32,33}$	0.166
$f_{33,34}$	0.166	$f_{34,35}$	0.166	$f_{35,36}$	0.166	$f_{36,37}$	0.166
$f_{37,38}$	0.166	$f_{38,39}$	0.166	$f_{39,40}$	0.166	$f_{31,41}$	0.482
$f_{40,50}$	0.518	$f_{41,42}$	0.068	$f_{42,43}$	0.068	$f_{43,44}$	0.068
$f_{44,45}$	0.068	$f_{45,46}$	0.068	$f_{46,47}$	0.068	$f_{47,48}$	0.068
$f_{48,49}$	0.068	$f_{49,50}$	0.068	$f_{41,51}$	0.414	$f_{50,60}$	0.586
$f_{51,52}$	0.149	$f_{52,53}$	0.149	$f_{53,54}$	0.149	$f_{54,55}$	0.149
$f_{55,56}$	0.149	$f_{56,57}$	0.149	$f_{57,58}$	0.149	$f_{58,59}$	0.149
$f_{59,60}$	0.149	$f_{51,61}$	0.265	$f_{60,70}$	0.735	$f_{61,62}$	0.265
$f_{62,63}$	0.265	$f_{63,64}$	0.265	$f_{64,65}$	0.265	$f_{65,66}$	0.265
$f_{66,67}$	0.265	$f_{67,68}$	0.265	$f_{68,69}$	0.265	$f_{69,70}$	0.265

the side of the tank, are connected, respectively. There are different numbers and sizes of holes between two connected compartments. On the longitudinal direction, two neighbouring compartments on row 1 and row 2 are connected by 4 and 3 holes, respectively; and those on all the other 4 rows by 2 holes. The sizes of the holes along row 3 are different, noted as 1 and 2, respectively, and those along the other 5 rows are the same, noted as 1. On the 1st column, there are 2 holes between two neighbouring compartments of rows 1, 2 and 3, noted as 3; 1 hole between those of rows 3, 4, 5 and 6, noted as 5. On the 10th column, there is 1 hole between two neighbouring compartments of rows 1, 2 and 3, noted as 4; 1 hole between those of rows 3, 4, 5 and 6, noted as 5. The volumes of the compartments are the same in each row, but different among different rows.

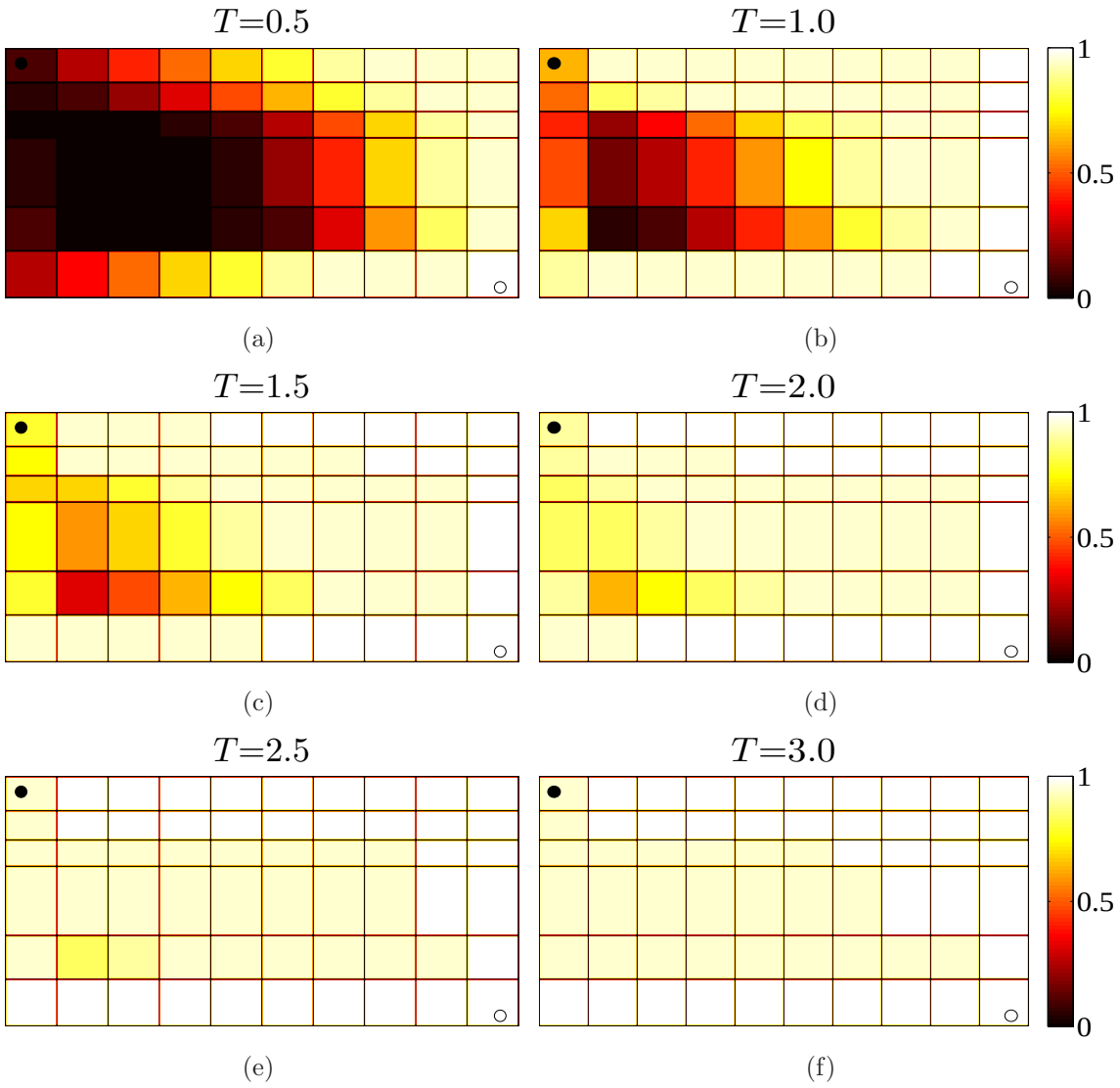

Figure 9.6: The variation of the flushed fraction field at $T = 0.5 - 3.0$ in the 'J'-type bottom and side tank under the unstratified mixing condition.

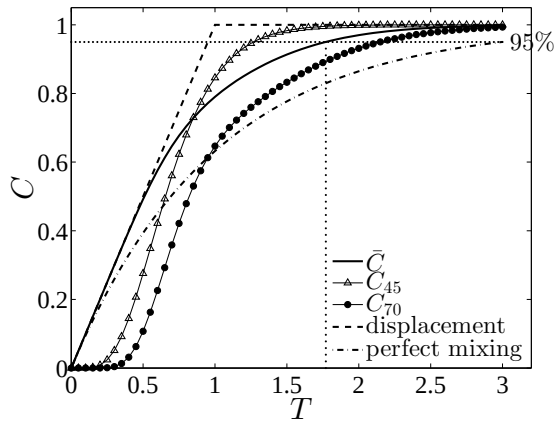

Figure 9.7: The variation of $\bar{C}$, C_{45} and C_{70} is plotted against exchange volumes, compared with the displacement and perfect mixing mode, in the 'J'-type bottom and side tank. The dotted line showing $\bar{C} = 90\%$ is the IMO exchange requirement.

9.3.1 Unstratified case

External water is pumped into the right bottom compartment of the tank and exits from the left top. When density effect is negligible, the unstratified model can be employed to analyse the flushing in the tank. The internal flow rates are calculated and listed in Table 9.1, where the inflow rate is normalised as 1. Figure 9.6 shows the time evolution of the flushed fraction field in the tank. The compartments of the 1st row and those of the right top are flushed relatively faster. After one exchange volume, most of the initial fluid remains in the compartments on the left middle of the tank. At $T = 2$, almost all compartments have been flushed. Figure 9.7 shows the variation of the tank flushing efficiency $\bar{C}$, C_{45} and C_{70} in time. Compartment 45 is a middle side compartment and compartment 70 is the outlet compartment (see Figure 2.2(d)). The performance of $\bar{C}$ is much better than the perfect mixing mode. Initially, $\bar{C}$ follows the displacement rule until $T \simeq 0.5$, because the incoming fluid mixes sufficiently with the original fluid in the compartments close to the inlet, leading to little incoming fluid bypassing the tank. The flushing efficiency is 99.9% at three exchange volumes, which agrees with the CFD result of Kent and Parsons (2004) that the three volumes pumping-through method for the 'J'-type tank can

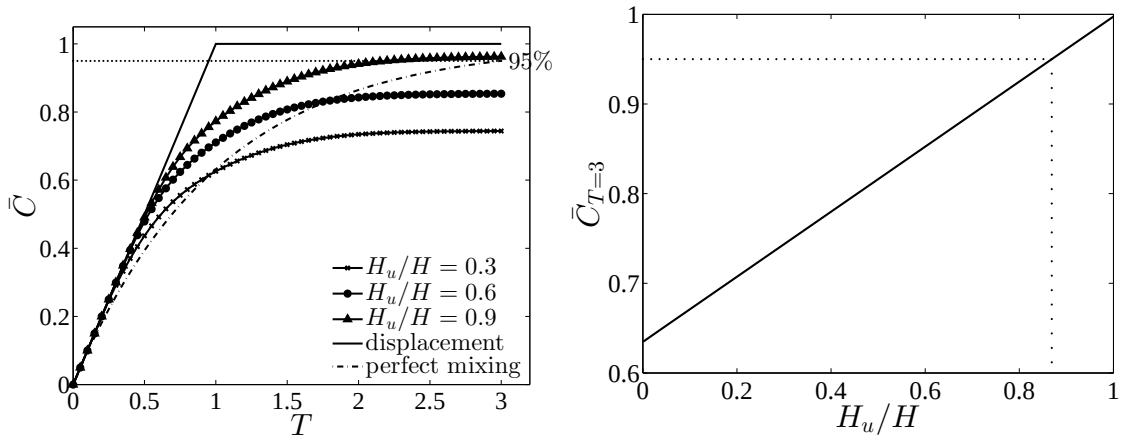

(a) (b)

Figure 9.8: Analysis of the stratified flushing from the double hull tank. (a) shows the variation of $\bar{C}$ against T at $H_u/H = 0.3$, 0.6 and 0.9, respectively, compared with the displacement and perfect mixing mode; (b) shows the flushing efficiency at three exchange volumes against H_u/H. The dotted line in (b) shows the corresponding H_u/H for $\bar{C}|_{T=3} = 95\%$.

achieve a flushing efficiency of 99.7% when a single outlet is open. For $T \geq 1.8$, the flushing efficiency of the whole tank is over 95%. This means that when this ballast tank has been flushed with 1.8 volumes of clean water, the flushing efficiency can meet the IMO exchange standard. The cost of ballast exchange is estimated at about \$0.23-0.32 per m^3 ballast water (adjusted for oil price increase from 2000 to 2014, see Gramling, 2000), so the cost saving of running the ballast pumps for a ship containing 4 considered 'J'-type tanks is about \$22,314-31,045 per stop when the flushing is reduced from 3 to 1.8 exchange volumes. The reductions of NIS concentration are different among compartments. At $T \geq 1.8$, the flushing efficiency in compartment 45 and 70 is 87% and 99%, respectively. This means that at three exchange volumes, the NIS concentration in the water collected from the discharge port has not been reduced by 95% compared to the initial water.

9.3.2 Stratified case

When density effect is important during the flushing, the stratified mixing model can be employed. Here the case when salt water is injected to flush the fresh water in the tank is considered. The region above the upper edge of the connecting holes (of height H_u) in the double bottom tanks (of height H) is assumed to be trapped, and perfect mixing is assumed to occur in the region below H_u of each bottom tank and the whole of each hopper and side tank. The variation of the average flushing efficiency of the entire tank is plotted against exchange volumes at different ratios of H_u/H in Figure 9.8(a). The flushing efficiency increases with the ratio of H_u/H, because the higher the upper edge of the connecting holes is, the smaller the trapped region exists in the tank. At three exchange volumes, the flushing efficiency is over 95% at $H_u/H = 0.9$, but lower than 95% at $H_u/H = 0.6$ and 0.3. The flushing efficiency at three exchange volumes is plotted against H_u/H is Figure 9.8(b). $\bar{C}|_{T=3}$ increases almost linearly with the height of the upper edge of the connecting holes in the bottom tanks. To achieve a flushing efficiency of 95% at three exchange volumes, the upper edge of the connecting holes needs to be at least 87% the height of the connecting walls.

9.4 Summary

In many cases, change of the outlet setting and position of connecting pipes can improve the flushing efficiency in a ballast tank. Generally, it is useful to improve the flushing efficiency by setting a single outlet far from the inlet. To achieve an effective flushing, there needs to form a flow system that can connect all compartments in the tank. In some cases, it is not necessary to flush three tank volumes of water to meet the 95% standard, and thus the running time of the ballast pumps can be reduced to save costs. For the 'J'-type bottom and side tank considered, the requirement for exchange volumes can be relaxed. The cost saving of running the ballast pumps for a ship containing 4 considered 'J'-type tanks is about $22,314-31,045 per stop when the flushing is reduced from 3 to 1.8 exchange volumes. In the case of stratified flushing, to achieve a flushing efficiency of 95% at three exchange volumes, the upper edge of

the connecting holes in the double bottom compartments needs to be at least 87% the height of the connecting walls. There is currently no guidance about where the water in the ballast tanks should be sampled. This is not trivial because there are usually multiple sampling ports on a ship (David, 2013). And as seen from the flushed fraction curves there is a significant variability between compartments, which means that the NIS reduction of the samples may be different when the flushing efficiency of the whole tank is 95%. When ballast water sampling is undertaken from the discharge port, the NIS reduction of the sample is not necessary to be 95% at three exchange volumes.

Chapter 10

Conclusions and future work

10.1 Summary

Currently, ballast tank flushing is in widespread use and will continue to be so for quite some time. In the future, a number of onboard cleaning technologies adopted by ships will recycle treated ballast water to flush ballast tanks. The NIS removal rate depends on both the flushing and cleaning efficiency. Numerous studies have been attempted in the aspect of treatment technologies, but there is limited research on ballast tank flushing from the viewpoint of fluid mechanics. In this thesis, a detailed experimental and modelling study on how ballast water is exchanged in a multi-compartment ballast tank has been undertaken and a robust methodology has been developed to study the influencing factors on ballast water exchange.

The thesis starts off with a detailed literature review that summarises the key environmental issues related to ballast tanks. The key features of fluid flow and NIS spreading in a ballast tank are identified, particularly the role of turbulence and stratification. The link between reported methods for treating ballast water and how these methods change the properties of ballast water is made. The methodologies adopted in this thesis (laboratory scale experiments and modelling) for studying ballast tank flushing are justified. The flushing efficiency of a multi-compartment tank depends on the tank geometry (in terms of compartment division, outlet setting, hole resistance

and compartment capacitance), inflow rate and density contrast between the incoming fluid and the initial fluid. The lightening holes with sharp edge between ballast tank compartments generate a turbulent flow where the RMS velocity is comparable to the mean.

The unstratified flushing from multi-compartment ballast tanks is theoretically analysed. A multizone model is developed based on perfect mixing within compartments and advection between compartments. The model is characterised in terms of pressure differences between compartments and is driven by a volumetric flow rate, and an empirical closure is required to estimate the pressure drop coefficients. Three clear model tanks are required to be constructed to test various aspects of the exchange process. An optical method is used to analyse the variation of dye concentration in each compartment of the tank; this technique provides a means of testing the model predictions within an error of 3%. A cascade of experiments, with increasing complexity, have been designed and undertaken to understand the influence of buoyancy in geometrically complex ballast tanks. This series of tests start with unstratified fluid with geometrically simple tanks, before increasing the complexity of structure and before introducing stratification.

The flushing from 2×2, 3×3 to 5×4 internal tank configurations are undertaken. For all cases, the agreement between the predictions and measurements for the flushing efficiency is good. Insufficient mixing, caused by weak turbulent diffusion in some compartments where flow rate is low, leads to a long residence time of the original fluid, that is why the aft and fore peak tanks are required to be provided with additional pipework to improve the mixing conditions. The results show that the flushing efficiency of a multi-compartment tank may be improved by subdividing the tank or setting a single outlet far from the inlet. For a tank with a single outlet, the optimal flushing strategy is to form a linear network by blocking some flow pathways. If the hole resistance is fixed, the best configuration needs to be calculated.

When ballast water is taken at ports in warm shallow seas or near fresh water sources, density effect is important. The stratified flushing in an in-line tank has been tested from both the theoretical and experimental aspects. Three types of mathematical models have been developed to interpret the physical processes. The

displacement model is suitable to the case when the incoming fluid and the original fluid are immiscible, which is validated by the experiments of filling an empty tank at $230 < Ri < 23000$. For miscible fluids, a stratified mixing model is used to quantify the fluid exchange in the tank during flushing; a more theoretically strict model - the plume model is employed to describe the physics when the tank is flushed. The plume model works well at high positive Ri, and the stratified mixing model works well for high negative Ri. The flushing efficiency at three exchange volumes is underestimated by about 5% for $30 < Ri < 1000$, and about 10% for $-1000 < Ri < -30$. For low Ri, mixing due to turbulence in reality is stronger than expected. In practice, when the density difference is large, increasing the flow rate may enhance mixing. The final test comes from studying the flushing from a tank which is geometrically complex and where stratification is important. The flushing efficiency depends on density effect in terms of typical Ri. At high Ri, the weir effect is significant, and the original fluid may be trapped in the top or bottom region of the tank; when the Ri is low, the turbulence is intense, and the incoming fluid has more energy to displace and mix with the original fluid. Meanwhile, adding limber holes to the connecting walls may allow the incoming fluid to exchange the original fluid in the trapped region and thus improve the flushing efficiency, especially for the case of injecting denser fluid into lighter fluid. The stratified mixing model can be modified to reflect the main character of the stratified flushing in multi-compartment tanks.

To put the results from the theoretical study into context, the new modelling methodology is applied to the flushing from two typical ballast tanks. The flushing efficiency is significantly influenced by the setting of outlet and the position of connecting pipes. For unstratified flow within the 'J'-type bottom and side tank considered, the flushing is more efficient than estimated by the IMO. In this case, the requirement for exchange volumes can be relaxed so that the running time of the ballast pumps can be reduced to save costs. The cost saving of running the ballast pumps for a ship containing 4 considered 'J'-type tanks is about $22,314-31,045 per stop when the flushing is reduced from 3 to 1.8 exchange volumes. When ballast water sampling is undertaken from the discharge port, the NIS reduction of the sample is not necessary to be 95% at three exchange volumes. For the case of stratified

flushing, to achieve a flushing efficiency of 95% at three exchange volumes, the upper edge of the connecting holes in the 'J'-type tank needs to be at least 87% the height of the connecting walls.

10.2 Recommendation for ship ballast system design

(1) To enhance flushing, a single outlet should be placed far from the inlet of a ballast tank to reduce bypassing.

(2) If possible, a ballast tank should be designed so that an in-line flow network can be formed.

(3) A single compartment ballast tank should be subdivided to form a multi-compartment tank.

(4) To achieve an effective flushing, the position of the connecting pipes should be adjusted to generate a flow system that can connect all compartments in the tank.

(5) To avoid fluid trappage, limber holes need to be dug on the connecting walls between neighbouring compartments; when there is no limber hole, the upper edge of the lightening holes needs to be as high as possible.

10.3 Future work

10.3.1 Closed-loop ballast water treatment system

As pointed out in Chapter 2, flushing ballast tanks and treating ballast water itself are two major cleaning methods. There is a need to study how the NIS removal can be enhanced by the potential circulated flushing system (see Figure 2.5(b)). The section shows a method of assessing the combined effect of using both flushing and treatment technology. The NIS removal rate (R) is defined as $R = (C_0 - C(t))/C_0 \times 100\%$, where

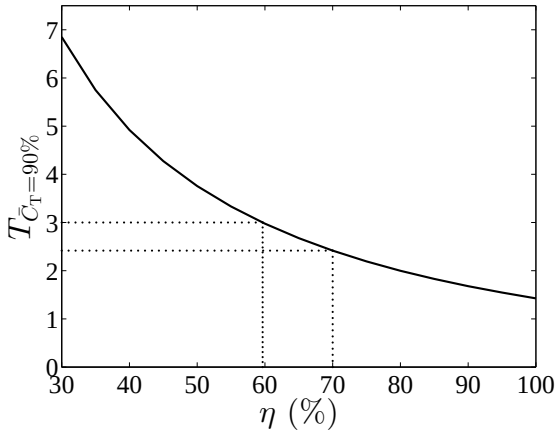

(a)

Figure 10.1: The exchange volumes required to achieve the 90% NIS removal rate against treatment efficiency (η) in the 'J'-type tank.

C_0 is the original NIS average concentration of the ballast system and $C(t)$ is the NIS average concentration of the system varying with time. R measures the total removal of NIS from the whole system. If the ballast water treatment technology is employed, there may form a closed-loop system. The treatment efficiency η is defined as $\eta = (C_0 - C)/C_0 \times 100\%$, where C_0 is the original NIS concentration in the water before entering the treatment unit and C is the NIS concentration after treatment. In this system, ballast water is taken and kept in ballast tank before treatment. During the voyage, the tank water is continuously pumped through the treatment unit. During the circulation, the NIS are killed or deactivated by the adopted treatment technology. The treated water is continuously pumped back to flush the ballast tank. If the water exchange in a single compartment tank follows the perfect mixing rule, the NIS concentration decrease can be expressed as $C/C_0 = \exp(-\eta T)$. This means that the lower the treatment efficiency is, more than three times flushing is needed to achieve the 90% reduction. The unstratified multizone model is applied to analyse the total NIS removal rate when the 'J'-type tank employs this kind of cleaning system, and the effect of the treatment efficiency and exchange volumes on the NIS removal.

If the model is applied to the closed-loop system, the flow out of the outlet (compartment 70) which is then treated by the treatment unit is set as the source flow of the inlet (compartment 11). For example, for the 'J'-type tank with a treatment unit, C_{11} varies as

$$\frac{\mathrm{d}C_{11}}{\mathrm{d}T} = \frac{V}{V_{11}}(QC_{70} + Q\eta(1 - C_{70}) - f_{11,12}C_{11} - f_{11,21}C_{11}), \tag{10.1}$$

where C_{70} is the flushed fraction of the outlet compartment, 2 and 11 are compartments connected to compartment 1. The mass flux of the backflow to compartment 1 is $Q(C_{70} + \eta(1 - C_{70}))$. Figure 10.1 shows the exchange volumes required to achieve the 90% NIS removal rate against the treatment efficiency (η). It can be seen that the lower the treatment efficiency is, the longer flushing time is needed to achieve the required NIS removal rate. The treatment efficiency needs to be at least 59% to achieve the 90% NIS removal rate at three exchange volumes. When the treatment efficiency is greater than 59%, the flushing required for the tank treated to 90% of the initial concentration is less than three exchange volumes. At a treatment efficiency of $\eta = 70\%$, 2.4 exchange volumes is required to achieve the 90% NIS removal rate. Future work is required to prove the effectiveness of treating NIS by this system.

10.3.2 Density effect in complex ballast tanks

From the tests of the stratified flushing in a linearly connected tank at relatively low Ri, the portion of the original water trapped in the top of each compartment varies, as the intensity of turbulence in a compartment depends on its distance from the inlet of the tank. The discrepancy between the experimental measurements and the theoretical predictions has indicated the necessity of requesting aid from CFD. CFD is a common engineering tool and it would be useful, in the future, to examine its potential for being applied to examine flushing from ballast tanks. However, there are two important points that need to considered. First, the structure of a ballast tank is extremely complex so that the creation of the geometry (within CAD) and the mesh represents a challenge. The tank structure in the published work is poorly resolved. Since there are various lengthscales (limber holes to compartments up to

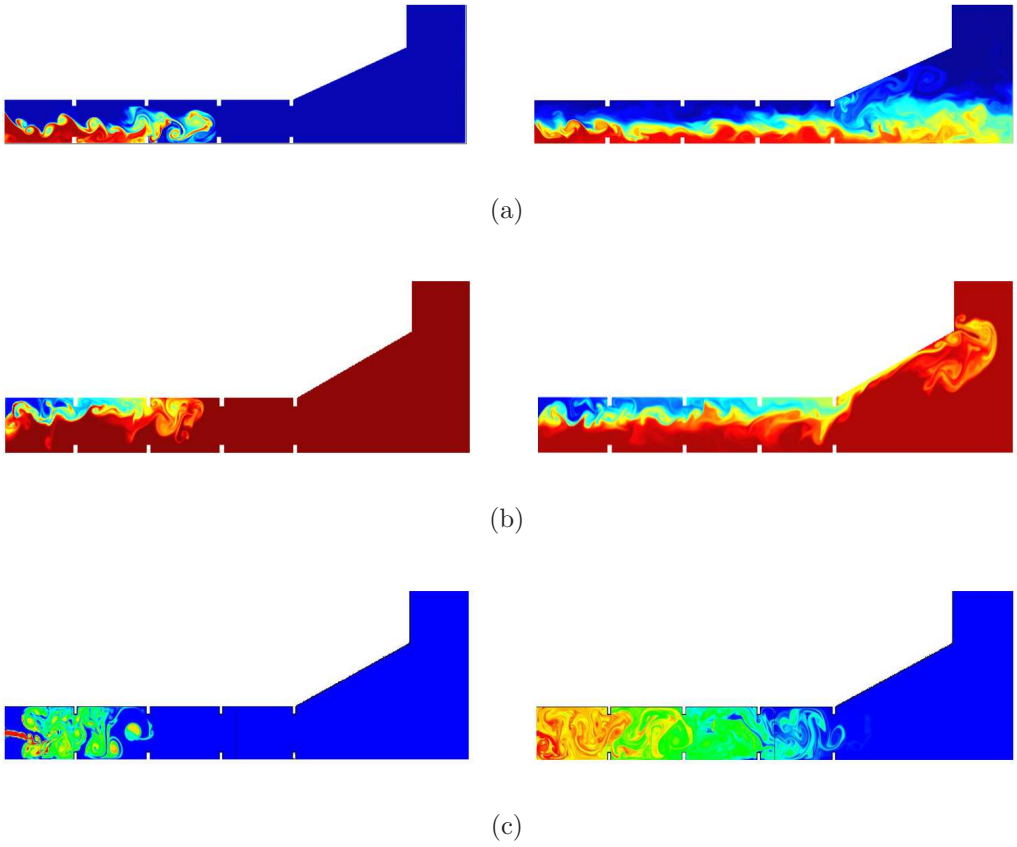

Figure 10.2: CFD simulation (DNS) of the flushing from the front view of a 2D tank. The figures correspond to Ri = (a) 400, (b) -400 and (c) 0.

tank), the mesh will be very large. Typically, after about meshes greater than 2M nodes, a small computational cluster is required whose size grows as the meshes size grows. Second, the critical physics are turbulence generation at sharp edges and the influence of stratification. Stratification tends to mean that there are large gradients of fluid property (such as density) in the vertical direction requiring anisotropic meshes; turbulence near the sharp edges requires finer meshes. Combined together, while the application of CFD should be considered, there are certainly a number of challenges that need to be overcome.

An initial understanding of the processes could be undertaken by studying simpler 2D confined flushing problems. Figure 10.2 shows some initial tests using ACEsim to examine the flushing of a 2D tank from the front view. At different Ri, the vertical difference of the fluid exchange is indicated by the output graphics. Displacement dominates mixing at $Ri = \pm 400$, when stratification takes place; vertically even mixing mode occurs at $Ri = 0$. The computational tools have the potential to reveal how the geometrical and dynamical conditions in a ballast tank influence the turbulent mixing and provide detailed information on the fluid exchange.

Finally, CFD calculations must be tested against available experimental work to have faith that they are accurate. One of the strengths of the Chapters 5 and 7 is that geometry and boundary conditions are well-defined, so that the reported experimental observations can form the basis of future validation test case.

10.3.3 Sediment transport

The NIS can not only float with ballast water, but also settle out of ballast water within a ship. According to the 2004 BWM Convention, all ships should remove and dispose of sediments from spaces designated to carry ballast water. A way of removing sediments is to mix the residual ballast water with the sea water through the motion of a vessel or injecting the water against the bottom of tanks so that the sediments become resuspended and then discharge the mixed water (Prange and Pereira, 2013). On one side, due to the existence of non-passive substances in the water that is used to fill the tank, further work is required to extend the analysis

to account for the settling dynamics, which involves the study of the main physics of sediment transport in multi-compartment tanks. A potential method to include the settling effect is to add a sink term -$v_T A_{[i][j]} C_{[i][j]}$ (where v_T is the terminal fall velocity) to the right side of (3.14). On the other side, a deep understanding of how the sediment suspension/sticking depends on the geometrical and dynamical conditions in ballast tanks is required.

Studying experimentally will represent a challenge because of the difficulty in collecting the sediments from the bottom of each compartment of the model tanks and accurately measuring the weight. To understand the influencing factors of the settling physics, it is necessary to measure the time series of the sediment distribution in the tank, which is even more difficult.

Appendix A

Matrix form of the mass equation array for flushing an $m \times n$ tank

The equation array (3.14) can be expressed in a matrix form as

$$\frac{\mathrm{d}\boldsymbol{C}}{\mathrm{d}\tau} = \boldsymbol{F}\boldsymbol{C} + \boldsymbol{f}, \tag{A.1}$$

where $\boldsymbol{F}$ is an $mn \times mn$ matrix, $\boldsymbol{F}_{11} = -1$, $\boldsymbol{F}_{ij} = 0$ for $1 \leq i < j \leq mn$. $\boldsymbol{C}$ and $\boldsymbol{f}$ are both $mn \times 1$ vectors.

$$\boldsymbol{C} = [C_{11} \quad C_{12} \quad \cdots \quad C_{1n} \quad C_{21} \quad C_{22} \quad \cdots \quad C_{2n} \quad \cdots \quad \cdots \quad C_{m1} \quad C_{m2} \quad \cdots \quad C_{mn}]^T.$$

The forcing for the system is

$$\boldsymbol{f} = [1 \quad 0 \quad 0 \quad \cdots \quad 0]^T.$$

The solution is

$$\boldsymbol{C}(\tau) = \boldsymbol{\Phi}(\tau) \int_0^\tau \boldsymbol{\Phi}^{-1}(t)\boldsymbol{f}\mathrm{d}t, \tag{A.2}$$

where $\boldsymbol{\Phi}$ is the fundamental matrix that is a square matrix whose columns are linearly independent solutions of

$$\frac{\mathrm{d}\boldsymbol{C}}{\mathrm{d}\tau} = \boldsymbol{F}\boldsymbol{C}. \tag{A.3}$$

The form of $\boldsymbol{\Phi}$ depends on the number of linearly independent eigenvectors of $\boldsymbol{F}$. If $\boldsymbol{F}$ has mn linearly independent eigenvectors $\boldsymbol{v}_1, \boldsymbol{v}_2, \cdots, \boldsymbol{v}_{mn}$, and their corresponding eigenvalues are $\lambda_1, \lambda_2, \cdots, \lambda_{mn}$, then

$$\boldsymbol{\Phi} = [e^{\lambda_1 \tau}\boldsymbol{v}_1 \quad e^{\lambda_2 \tau}\boldsymbol{v}_2 \quad \cdots \quad e^{\lambda_{mn} \tau}\boldsymbol{v}_{mn}];$$

if the multiplicity of eigenvalue λ_i is r $(1 < r \leq mn)$, and the number of the linearly independent eigenvectors associated with λ_i is p, $p < r$, then the deficient $r-p$ column vector(s) associated with λ_i in Φ are

$$e^{\lambda_i \tau}\sum_{k=0}^{1}\frac{\tau^k}{k!}\boldsymbol{v}_{1-k} \quad e^{\lambda_i \tau}\sum_{k=0}^{2}\frac{\tau^k}{k!}\boldsymbol{v}_{2-k} \quad \cdots \quad e^{\lambda_i \tau}\sum_{k=0}^{r-p}\frac{\tau^k}{k!}\boldsymbol{v}_{r-p-k},$$

satisfying $(\boldsymbol{F} - \lambda_i \boldsymbol{I})\boldsymbol{v}_j = \boldsymbol{v}_{j-1}$, j =1, 2, $\cdots$, $r-p$, where $\boldsymbol{v}_0$ is any of the known eigenvectors associated with λ_i.

Appendix B

Analytical solution to $C_{[i][j]}$ for unstratified flushing in a 2×2 tank

Under the condition of unstratified mixing in a 2×2 tank, where the flux between each compartment is known, the flushed fraction can be explicitly determined from (3.23) in the case of $k_1 = k_2 = 1/2$.

$$\boldsymbol{C} = \begin{bmatrix} C_{11} \\ C_{12} \\ C_{21} \\ C_{22} \end{bmatrix}, \boldsymbol{f} = \begin{bmatrix} 1 \\ 0 \\ 0 \\ 0 \end{bmatrix}. \tag{B.1}$$

For the 'far open' case,

$$\boldsymbol{F} = \begin{bmatrix} -1 & 0 & 0 & 0 \\ \phi & -\phi & 0 & 0 \\ 1-\phi & 0 & -(1-\phi) & 0 \\ 0 & \phi & 1-\phi & -1 \end{bmatrix}, \tag{B.2}$$

which has 4 eigenvalues: $\lambda_1 = -1$, $\lambda_2 = -1$, $\lambda_3 = -\phi$, and $\lambda_4 = -(1-\phi)$ and 4

corresponding eigenvectors:

$$\boldsymbol{v_1} = \begin{bmatrix} 0 \\ 0 \\ 0 \\ 1 \end{bmatrix}, \boldsymbol{v_2} = \begin{bmatrix} 0 \\ 0 \\ 0 \\ 1 \end{bmatrix}, \boldsymbol{v_3} = \begin{bmatrix} 0 \\ \frac{1-\phi}{\phi} \\ 0 \\ 1 \end{bmatrix}, \boldsymbol{v_4} = \begin{bmatrix} 0 \\ 0 \\ \frac{\phi}{1-\phi} \\ 1 \end{bmatrix}. \tag{B.3}$$

The solution is

$$\begin{aligned} C_{11} =& 1 - \exp(-\tau), \\ C_{12} =& 1 - \frac{1}{1-\phi}\exp(-\phi\tau) + \frac{\phi}{1-\phi}\exp(-\tau), \\ C_{21} =& 1 - \frac{1}{\phi}\exp(-(1-\phi)\tau) + \frac{1-\phi}{\phi}\exp(-\tau), \\ C_{22} =& 1 - \frac{\phi}{(1-\phi)^2}\exp(-\phi\tau) - \frac{1-\phi}{\phi^2}\exp(-(1-\phi)\tau) \\ &+ \left(\left(\frac{1}{\phi(1-\phi)} - 3\right)\tau + \frac{1}{\phi^2(1-\phi)^2} - \frac{3}{\phi(1-\phi)} - 1\right)\exp(-\tau). \end{aligned} \tag{B.4}$$

For the 'near open' case,

$$\boldsymbol{F} = \begin{bmatrix} -1 & 0 & 0 & 0 \\ \phi & -\phi & 0 & 0 \\ 1-\phi & 0 & -1 & \phi \\ 0 & \phi & 0 & -\phi \end{bmatrix}, \tag{B.5}$$

which has 4 eigenvalues: $\lambda_1 = -1$, $\lambda_2 = -1$, $\lambda_3 = -\phi$, and $\lambda_4 = -\phi$ and 4 corresponding eigenvectors:

$$\boldsymbol{v_1} = \begin{bmatrix} 0 \\ 0 \\ 1 \\ 0 \end{bmatrix}, \boldsymbol{v_2} = \begin{bmatrix} 0 \\ 0 \\ 1 \\ 0 \end{bmatrix}, \boldsymbol{v_3} = \begin{bmatrix} 0 \\ 0 \\ \frac{\phi}{1-\phi} \\ 1 \end{bmatrix}, \boldsymbol{v_4} = \begin{bmatrix} 0 \\ 0 \\ \frac{\phi}{1-\phi} \\ 1 \end{bmatrix}. \tag{B.6}$$

The solution is

$$\begin{aligned}
C_{11} =& 1 - \exp(-\tau), \\
C_{12} =& 1 - \frac{1}{1-\phi}\exp(-\phi\tau) + \frac{\phi}{1-\phi}\exp(-\tau), \\
C_{21} =& 1 - \left(\frac{\phi^2}{(1-\phi)^2}\tau - \frac{3\phi^2-\phi}{(1-\phi)^3}\right)\exp(-\phi\tau) \\
& - \left(\frac{3\phi^2-3\phi+1}{(1-\phi)^2}\tau - \frac{\phi^3-6\phi^2+4\phi-1}{(1-\phi)^3}\right)\exp(-\tau), \\
C_{22} =& 1 - \left(\frac{\phi}{1-\phi}\tau - \frac{2\phi-1}{(1-\phi)^2}\right)\exp(-\phi\tau) - \frac{\phi^2}{(1-\phi)^2}\exp(-\tau).
\end{aligned} \tag{B.7}$$

For the 'both open' case,

$$\boldsymbol{F} = \begin{bmatrix} -1 & 0 & 0 & 0 \\ \phi & -\phi & 0 & 0 \\ 1-\phi & 0 & -(1-\phi) & 0 \\ 0 & \phi & 0 & -\phi \end{bmatrix}, \tag{B.8}$$

which has 4 eigenvalues: $\lambda_1 = -1$, $\lambda_2 = -(1-\phi)$, $\lambda_3 = -\phi$, and $\lambda_4 = -\phi$ and 4

corresponding eigenvectors:

$$\boldsymbol{v_1} = \begin{bmatrix} \frac{(1-\phi)^2}{\phi^2} \\ -\frac{1-\phi}{\phi} \\ -\frac{(1-\phi)^3}{\phi^3} \\ 1 \end{bmatrix}, \boldsymbol{v_2} = \begin{bmatrix} 0 \\ 0 \\ 1 \\ 0 \end{bmatrix}, \boldsymbol{v_3} = \begin{bmatrix} 0 \\ 0 \\ 0 \\ 1 \end{bmatrix}, \boldsymbol{v_4} = \begin{bmatrix} 0 \\ 0 \\ 0 \\ 1 \end{bmatrix}. \tag{B.9}$$

The solution is

$$\begin{aligned} C_{11} =& 1 - \exp(-\tau), \\ C_{12} =& 1 - \frac{1}{1-\phi}\exp(-\phi\tau) + \frac{\phi}{1-\phi}\exp(-\tau), \\ C_{21} =& 1 - \frac{1}{\phi}\exp(-(1-\phi)\tau) + \frac{1-\phi}{\phi}\exp(-\tau), \\ C_{22} =& 1 - \left(\frac{\phi}{1-\phi}\tau - \frac{2\phi-1}{(1-\phi)^2}\right)\exp(-\phi\tau) - \frac{\phi^2}{(1-\phi)^2}\exp(-\tau). \end{aligned} \tag{B.10}$$

Bibliography

N. C. Añasco, J. Koyama, S. Imai, and K. Nakamura. Toxicity of Residual Chlorines from Hypochlorite-treated Seawater to Marine Amphipod *Hyale barbicornis* and Estuarine Fish *Oryzias javanicus*. *Water Air. Soil Pollut.*, 195:129–136, 2008.

V. Alekseev, A. Makrushin, and J.-S. Hwang. Does the survivorship of activated resting stages in toxic environments provide cues for ballast water treatment? *Mar. Pollut. Bull.*, 61:254–258, 2010.

G. Altug, S. Gurun, M. Cardak, P. S. Ciftci, and S. Kalkan. The occurrence of pathogenic bacteria in some ships' ballast water incoming from various marine regions to the Sea of Marmara, Turkey. *Mar. Environ. Res.*, 81:35–42, 2012.

American Bureau of Shipping. *Inert gas system for ballast tanks*, 2004.

American Bureau of Shipping. *Guide for ballast water exchange*, 2010.

G. Armstrong. Ballast system design for flow-through exchange of ballast water. *Trans. IMarE.*, 109:257–269, 1997.

O. O. Badran and M. M. Abu-Khader. Ballast water separator performance for solid particulate removal. In *Proceedings of the World Engineers' Convention 2004, Vol F-A, Resources and Energy*, pages 515–518, 2004.

S. H. Baek, S. W. Jung, M. C. Jang, B. Hyun, and K. Shin. Survival potential of autotrophic phytoplankton species collected from ballast water in international commercial ships. *N. Z. J. Mar. Freshwater Res.*, 46:125–136, 2012.

M. Bai, Z. Zhang, M. Bai, B. Yang, and X. Bai. Effects of Hydroxyl Radicals on Introduced Organisms of Ships Ballast Water Based Micro-Gap Discharge. *Plasma Sci. Technol.*, 9:206–210, 2007.

O. C. Basurko and E. Mesbahi. Statistical representativeness of ballast water sampling. *P. I. Mech. Eng. M: J. Eng.*, 225:183–190, 2011.

P. Brodie, C. Blatchley, M. Balcer, Y. Sasson, I. Kreisel, Y. Kolodni, D. Sorek, N. Shimron, W. Cairns, and R. Braun. Ship ballast water treatment: the closed-loop option. In *2nd International Ballast Water Treatment R&D Symposium*, 2003.

J. Burkholder, G. Hallegraeff, G. Melia, A. Cohen, H. Bowers, D. Oldach, M. Parrow, M. Sullivan, P. Zimba, and E. Allen. Phytoplankton and bacterial assemblages in ballast water of U.S. military ships as a function of port of origin, voyage time, and ocean exchange practices. *Harmful Algae*, 6:486–518, 2007.

R. Cao, Y. S. Liu, and C. Yan. A criterion for flow mechanisms through vertical sharp-edged orifice and model for the orifice discharge coefficient. *Pet. Sci.*, 8: 108–113, 2011.

K. J. Carney, O. C. Basurko, K. Pazouki, S. Marsham, J. E. Delany, D. V. Desai, A. C. Anil, and E. Mesbahi. Difficulties in obtaining representative samples for compliance with the Ballast Water Management Convention. *Mar. Pollut. Bull.*, 68:99–105, 2013.

CATDS Ocean Salinity Expert Center. Salinity distribution at the ocean surface. http://www.salinityremotesensing.ifremer.fr, 2013.

T. J. Chang, M. Y. Huang, Y. T. Wu, and C. M. Liao. Quantitative prediction of traffic pollutant transmission into buildings. *J. Environ. Sci. Heal. A*, 38:1025–1040, 2003.

P. Chang III, W. Wilson, J. Carneal, P. Atsavapranee, S. Verosto, D. Reid, and P. Jenkins. Final Report: Computational modeling of ballast water tanks to improve understanding and maximize effectiveness of management practices and

treatment mechanisms. phase ii – extension of laboratory study. Technical report, NOAA Technical Memorandum GLERL-148., NOAA Great Lakes Environmental Research Laboratory, Ann Arbor, MI and NSWCCD-50-TR-2009/028, Naval Surface Warfare Center Carderock Division, West Bethesda, MD, 78 pp., 2009.

J. Chen, Y. Lin, J. Huo, M. Zhang, and Z. Ji. Optimization of Ships' Diagonal Ballast Water Exchange Sequence Using a Multiobjective Genetic Algorithm. *J. Ship Res.*, 54:257–267, 2010a.

J. Chen, Y. Lin, J. Z. Huo, M. X. Zhang, and Z. S. Ji. Optimization of ships subdivision arrangement for offshore sequential ballast water exchange using a non-dominated sorting genetic algorithm. *Ocean Eng.*, 37:978–988, 2010b.

J. Chen, Y. Lin, J. Z. Huo, M. X. Zhang, and Z. S. Ji. Optimal ballast water exchange sequence design using symmetrical multitank strategy. *J. Mar. Sci. Technol.*, 15: 280–293, 2010c.

J. Chen, J. Z. Huo, Y. Zhang, D. Y. Zhang, W. Y. Zhang, and Y. Lin. Heuristic Solution Strategy for the Sequential Ballast Water Exchange Problem. *J. Waterw. Port C.-ASCE*, 139:72–80, 2013.

Q. Y. Chen. Ventilation performance prediction for buildings: A method overview and recent applications. *Build. Environ.*, 44:848–858, 2009.

Q. Y. Chen, K. Lee, S. Mazumdar, S. Poussou, L. Z. Wang, M. Wang, and Z. Zhang. Ventilation performance prediction for buildings: Model assessment. *Build. Environ.*, 45:295–303, 2010d.

C. R. Chu and Y.-w. Wang. Experimental Study of the Discharge Coefficient of Internal Openings in Partitioned Buildings. In *The Seventh Asia-Pacific Conference on Wind Engineering*, 2009.

C. R. Chu and Y. W. Wang. The loss factors of building openings for wind-driven ventilation. *Build. Environ.*, 45:2273–2279, 2010.

C. R. Chu, Y. H. Chiu, Y. J. Chen, Y. W. Wang, and C. P. Chou. Turbulence effects on the discharge coefficient and mean flow rate of wind-driven cross-ventilation. *Build. Environ.*, 44:2064–2072, 2009.

C. R. Chu, Y. H. Chiu, and Y. W. Wang. An experimental study of wind-driven cross ventilation in partitioned buildings. *Energy Build.*, 42:667–673, 2010.

K. Curran and M. Davies. Spectral intensity mapping and analysis of dyed microflows. *Microfluid. Nanofluid.*, 1:146–154, 2004.

M. David. Ballast water sampling for compliance monitoring - ratification of the ballast water management convention. Technical report, Final report of research study for WWF International. 66 pp., 2013.

M. David and M. Perkovic. Ballast water sampling as a critical component of biological invasions risk management. *Mar. Pollut. Bull.*, 49:313–318, 2004.

M. David, M. Perkovic, V. Suban, and S. Gollasch. A generic ballast water discharge assessment model as a decision supporting tool in ballast water management. *Decis. Support Syst.*, 53:175–185, 2012.

Y. de Lafontaine and S.-P. Despatie. Performance of a biological deoxygenation process for ships' ballast water treatment under very cold water conditions. *Sci. Total Environ.*, 472:1036–1043, 2014.

Y. de Lafontaine, Y. Chambers, S. P. Despatie, C. Gagnon, and C. Blaise. Effectiveness and potential environmental impact of a yeast-based deoxygenation process for treating ship ballast waters. *Water Qual. Res. J. Can.*, 48:55–75, 2013.

M. D. de Oliveira, A. M. Takeda, L. F. de Barros, D. S. Barbosa, and E. K. de Resende. Invasion by *Limnoperna fortunei* (Dunker, 1857) (Bivalvia, Mytilidae) of the Pantanal wetland, Brazil. *Biol. Invasions*, 8:97–104, 2006.

B. E. Deagle, N. Bax, C. L. Hewitt, and J. G. Patil. Development and evaluation of a PCR-based test for detection of Asterias (Echinodermata : Asteroidea) larvae in

Australian plankton samples from ballast water. *Mar. Freshwater Res.*, 54:709–719, 2003.

C. DiBacco, D. B. Humphrey, L. E. Nasmith, and C. D. Levings. Ballast water transport of non-indigenous zooplankton to Canadian ports. *ICES J. Mar. Sci.*, 69:483–491, 2012.

A. I. Dittel and C. E. Epifanio. Invasion biology of the Chinese mitten crab *Eriochier sinensis*: A brief review. *J. Exp. Mar. Biol. Ecol.*, 374:79–92, 2009.

L. A. Drake, G. M. Ruiz, B. S. Galil, T. L. Mullady, D. O. Friedmann, and F. C. Dobbs. Microbial ecology of ballast water during a transoceanic voyage and the effects of open-ocean exchange. *Mar. Ecol. Prog. Ser.*, 233:13–20, 2002.

G. Drillet, C. Schmoker, A. Trottet, M. S. Mahjoub, M. Duchemin, and M. Andersen. Effects of temperature on type approval testing of ballast water treatment systems. *Integr. Environ. Assess. Manag.*, 9:192–195, 2013.

L. Dunsby. The effect of density contrast on the rate of flushing in a model ballast tank. Master's thesis, University College London, 2009.

I. Eames, M. Landeryou, A. Greig, and J. Snellings. Continuous flushing of contaminants from ballast water tanks. *Mar. Pollut. Bull.*, 56:250–260, 2008.

I. Eames, D. Shoaib, C. A. Klettner, and V. Taban. Movement of airborne contaminants in a hospital isolation room. *J. R. Soc. Interface*, 6:757–766, 2009.

K. Emami, V. Askari, M. Ullrich, K. Mohinudeen, A. C. Anil, L. Khandeparker, J. G. Burgess, and E. Mesbahi. Characterization of Bacteria in Ballast Water Using MALDI-TOF Mass Spectrometry. *PLOS One*, 7:e38515, 2012.

O. y. Endresen, H. Lee Behrens, S. Brynestad, A. Bjørn Andersen, and R. Skjong. Challenges in global ballast water management. *Mar. Pollut. Bull.*, 48:615–623, 2004.

F. Engdahl. Stability of mechanical exhaust systems. *Indoor Air*, 9:282–289, 1999.

M. M. Flagella, M. Verlaque, A. Soria, and M. C. Buia. Macroalgal survival in ballast water tanks. *Mar. Pollut. Bull.*, 54:1395–1401, 2007.

S. Flöder and C. Kilroy. *Didymosphenia geminata* (Protista, Bacillariophyceae) invasion, resistance of native periphyton communities, and implications for dispersal and management. *Biodivers. Conserv.*, 18:3809–3824, 2009.

E. M. Fykse, T. Nilsen, A. D. Nielsen, I. Tryland, S. Delacroix, and J. M. Blatny. Real-time PCR and NASBA for rapid and sensitive detection of Vibrio cholerae in ballast water. *Mar. Pollut. Bull.*, 64:200–206, 2012.

C. Gladstone, A. Woods, J. Philips, and C. Caulfield. Experimental study of mixing in a closed room by doorway exchange flow. *Proc. Roomvent*, 2:555–561, 1998.

S. Gollasch, M. David, M. Voigt, E. Dragsund, C. Hewitt, and Y. Fukuyo. Critical review of the IMO international convention on the management of ships ballast water and sediments. *Harmful Algae*, 6:585–600, 2007.

A. A. Goncalves and G. A. Gagnon. Recent Technologies for Ballast Water Treatment. *Ozone: Sci. Eng.*, 34:174–195, 2012.

J. Gramling. Ballast water and shipping patterns in puget sound - considerations for siting of alternative ballast water exchange zones. Technical report, Puget Sound Water Quality Action Team, Olympia, Washington, 2000.

F. W. Greve. *Flow of water through circular, parabolic, and triangular vertical notch weirs.*, volume 16. Engineering Bulletin of Purdue University, 1932.

F. Haghighat. Air infiltration and indoor air quality models - a review. *Int. J. Ambient Energy*, 10(3):115–122, 1989.

G. M. Hallegraeff and C. J. Bolch. Transport of diatom and dinoflagellate resting spores in ships' ballast water: implications for plankton biogeography and aquaculture. *J. Plankton Res.*, 14:1067–1084, 1992.

Hamworthy. http://www.hamworthy.com, 2012.

V. Hanby, M. Cook, D. Infield, Y. Ji, D. Loveday, and L. Mei. Nodal network and cfd simulation of airflow and heat transfer in double skin facades with blinds , in:. In *The 7th International Conference on System Simulation in Buildings, 11-13 December 2006, Liege, Belgium.*, 2006.

J. B. J. Harvey, M. S. Hoy, and R. J. Rodriguez. Molecular detection of native and invasive marine invertebrate larvae present in ballast and open water environmental samples collected in Puget Sound. *J. Exp. Mar. Biol. Ecol.*, 369:93–99, 2009.

P. Heiselberg, K. Svidt, and P. V. Nielsen. Characteristics of airflow from open windows. *Build. Environ.*, 36:859–869, 2001.

S. Helu. Treatment of ballast water using acoustic cavitation techniques coupled with advanced oxidants. *Ethnic. Dis.*, 15:24–25, 2005.

O.-K. Hess-Erga, K. J. Kihle Attramadal, and O. Vadstein. Biotic and abiotic particles protect marine heterotrophic bacteria during UV and ozone disinfection. *Aquat. Biol.*, 4:147–154, 2008.

A. Heyer, F. D'Souza, C. F. L. Morales, G. Ferrari, J. M. C. Mol, and J. H. W. de Wit. Ship ballast tanks a review from microbial corrosion and electrochemical point of view. *Ocean Eng.*, 70:188–200, 2013.

T. Hirano, S. Kato, S. Murakami, T. Ikaga, and Y. Shiraishi. A study on a porous residential building model in hot and humid regions: part 1the natural ventilation performance and the cooling load reduction effect of the building model. *Build. Environ.*, 41:21–32, 2006.

E. R. Holm, D. M. Stamper, R. A. Brizzolara, L. Barnes, N. Deamer, and J. M. Burkholder. Sonication of bacteria, phytoplankton and zooplankton: Application to treatment of ballast water. *Mar. Pollut. Bull.*, 56:1201–1208, 2008.

J. Hua and W. H. Hwang. Effects of voyage routing on the survival of microbes in ballast water. *Ocean Eng.*, 42:165–175, 2012.

International Maritime Organization. *International convention for the control and management of ships ballast water and sediments*. London, 2004.

International Maritime Organization. *Guidelines for approval of ballast water management systems (G8)*. London, 2008.

V. Joekar-Niasar, S. M. Hassanizadeh, and H. K. Dahle. Non-equilibrium effects in capillarity and interfacial area in two-phase flow: dynamic pore-network modelling. *J. Fluid Mech.*, 655:38–71, 2010.

H. Juretić, S. Dobrović, N. Ružinski, J. Lovrić, M. Pećarević, J. Mikuš, M. Crnčević, E.-J. Marčelja, M. M. Rajčić, S. Širac, W. J. Cooper, D. Grewell, and J. H. van Leeuwen. Pilot Studies of Ozonation for Inactivation of Artemia salina Nauplii in Ballast Water. *Ozone: Sci. Eng.*, 33:3–13, 2011.

K. Kamada, K. Minami, K. Shoji, S. Shiotani, and H. Ishida. Study of ballast water exchange by pumping-through method. In *Oceans '04 MTS/IEEE Techno-Ocean '04, Vols 1-2, Conference Proceedings, Vols. 1-4*, pages 707–712, 2004.

C. P. Kent and M. G. Parsons. Computational fluid dynamics study of the effectiveness of flow-through ballast exchange. *Trans. SNAME*, 112:241–270, 2004.

N. Kim, M. C. Murphy, S. A. Soper, and D. E. Nikitopoulos. Liquid-liquid segmented flows in polymer microfluidic channels. In *ASME 2009 7th International Conference on Nanochannels, Microchannels and Minichannels*, pages 1155–1165, 2009.

S.-J. Kim and S.-K. Jang. Corrosion characteristics of steel in seawater containing various chloride concentrations generated by electrochemical method. *Trans. Nonferrous Met. Soc. China*, 19:s50–s55, 2009.

D. M. King, P. T. Hagan, M. Riggio, and D. A. Wright. Preview of global ballast water treatment markets. *J. Mar. Eng. Technol.*, 11:3–16, 2012.

C. Kranenburg. Wind-induced entrainment in a stably stratified fluid. *J. Fluid. Mech.*, 145:253–273, 1984.

S. Krüger and F. Kluwe. Development of threshold values for a minimum stability criterion based on full scale accidents. Technical report, Technischen Universität Hamburg Harburg, 2010.

Z. Kurtela and P. Komadina. Application of Hydrocyclone and UV Radiation as a Ballast Water Treatment Method. *Promet*, 22:183–191, 2010.

J. Leichsenring and J. Lawrence. Effect of mid-oceanic ballast water exchange on virus-like particle abundance during two trans-Pacific voyages. *Mar. Pollut. Bull.*, 62:1103–1108, 2011.

Y. J. P. Lin and P. F. Linden. Buoyancy-driven ventilation between two chambers. *J. Fluid Mech.*, 463:293–312, 2002.

P. F. Linden. The fluid mechanics of natural ventilation. *Annu. Rev. Fluid. Mech.*, 31:201–238, 1999.

B. MacPhee. Alien flotillas: the expansion of invasive species through ship ballast water. In *EarthTrends Environmental Essay Competition Winner*, pages 1–8, 2006.

S. H. Magill, H. Thetmeyer, and C. J. Cromey. Settling velocity of faecal pellets of gilthead sea bream (*sparus aurata* l.) and sea bass (*dicentrarchus labrax* l.) and sensitivity analysis using measured data in a deposition model. *Aquaculture*, 251: 295–305, 2006.

R. Mamlook, O. Badran, M. M. Abu-Khader, A. Holdo, and J. Dales. Fuzzy sets analysis for ballast water treatment systems: best available control technology. *Clean Technol. Environ. Policy*, 10:397–407, 2007.

L. Maranda, A. M. Cox, R. G. Campbell, and D. C. Smith. Chlorine dioxide as a treatment for ballast water to control invasive species: Shipboard testing. *Mar. Pollut. Bull.*, 75:76–89, 2013.

L. F. Martínez, A. G. Lavín, M. M. Mahamud, and J. L. Bueno. Improvements in hydrocyclone design flow lines stabilization. *Powder Technol.*, 176:1–8, 2007.

D. K. McCluskey, A. E. Holdo, and R. K. Calay. An overview of ballast water treatment methods. In *Proceedings of the ASME Pressure Vessels and Piping Conference 2005, Vol 4*, volume 4 of *Pressure Vessel and Piping Division of the American Society of Mechanical Engineers*, pages 317–325, 2005.

T. McCollin, G. Quilez-Badia, K. D. Josefsen, M. E. Gill, E. Mesbahi, and C. L. J. Frid. Ship board testing of a deoxygenation ballast water treatment. *Mar. Pollut. Bull.*, 54:1170–1178, 2007.

H. D. Meizig and P. K. Schmidt. Pressure distribution during parachute opening. Technical report, Deutsche Forschungsanstalt fuer Luft- und Raumfahrt E V Brunswick (West Germany) Institut fuer Flugmechanik, 1965.

F. J. Millero and A. Poissont. International one-atmosphere equation of state of seawater. *Deep-Sea Res.*, 28:625–629, 1981.

E. L. Mills, J. H. Leach, J. T. Carlton, and C. L. Secor. Exotic Species in the Great Lakes: A History of Biotic Crises and Anthropogenic Introductions. *J. Great Lakes Res.*, 19:1–54, 1993.

M. Montalbano. Tables, flow-charts, and program logic. *IBM Syst. J.*, 1:51–63, 1962.

H. Montazeri, F. Montazeri, R. Azizian, and S. Mostafavi. Two-sided wind catcher performance evaluation using experimental, numerical and analytical modeling. *Renew. Energ.*, 35:1424–1435, 2010.

L. Mora, A. J. Gadgil, and E. Wurtz. Comparing zonal and CFD model predictions of isothermal indoor airflows to experimental data. *Indoor Air*, 13:77–85, 2003.

K. Murphy, J. Boehme, P. Coble, J. Cullen, P. Field, W. Moore, E. Perry, R. Sherrell, and G. Ruiz. Verification of mid-ocean ballast water exchange using naturally occurring coastal tracers. *Mar. Pollut. Bull.*, 48:711–730, 2004.

K. R. Murphy, J. R. Boehme, C. Brown, M. Noble, G. Smith, D. Sparks, and G. M. Ruiz. Exploring the limits of dissolved organic matter fluorescence for determining

seawater sources and ballast water exchange on the US Pacific coast. *J. Mar. Syst.*, 111:157–166, 2013.

D. Olorunfemi, E. Duru, and F. Okieimen. Induction of chromosome aberrations in Allium cepa L. root tips on exposure to ballast water. *Caryologia*, 65:147–151, 2012.

M. I. Orlova, T. W. Therriault, P. I. Antonov, and G. K. Shcherbina. Invasion ecology of quagga mussels (*Dreissena rostriformis bugensis*): a review of evolutionary and phylogenetic impacts. *Aquatic Ecology*, 39:401–418, 2005.

Y.-G. Park, J. A. Whitehead, and A. Gnanadeskian. Turbulent mixing in stratified fluids: layer formation and energetics. *J. Fluid Mech.*, 279:279–311, 1994.

M. G. Parsons. Flow-through ballast water exchange. *Trans. SNAME*, 106:485–493, 1998.

M. G. Parsons. Considerations in the Design of the Primary Treatment for Ballast Systems. *Mar. Technol.*, 40:49–60, 2003.

M. G. Parsons and R. W. Harkins. Full-Scale Particle Removal Performance of Three Types of Mechanical Separation Devices for the Primary Treatment of Ballast Water. *Mar. Technol. Sname N.*, 39:211–222, 2002.

G. Partnerships. http://globallast.imo.org, 2012.

J. G. Patil, R. M. Gunasekera, B. E. Deagle, N. J. Bax, and S. I. Blackburn. Development and evaluation of a PCR based assay for detection of the toxic dinoflagellate, Gymnodinium catenatum (Graham) in ballast water and environmental samples. *Biol. Invasions*, 7:983–994, 2005.

A. N. Perakis and Z. Y. Yang. Options for nonindigenous species control and their economic impact on the Great Lakes and St. Lawrence seaway: A survey. *Mar. Technol. Sname N.*, 40:34–41, 2003.

D. Pimentel, L. Lach, R. Zuniga, and D. Morrison. Environmental and economic costs of nonindigenous species in the united states. *Bioscience*, 5:53–65, 2000.

G. J. Prange and N. N. Pereira. Ship ballast tank sediment reduction methods. *Nav. Eng. J.*, 125:127–134, 2013.

R. A. Rahim, M. H. F. Rahiman, C. L. Goh, S. Z. M. Muji, H. A. Rahim, and Y. M. Yunos. Modeling orthogonal and rectilinear mixed-modality projection of optical tomography for solid-particles concentration measurement. *Sensor. Actuat. A: Phys*, 161:53–61, 2010.

G. Rigby and G. Hallegraeff. The transfer and control of harmful marine organisms in shipping ballast water: behaviour of marine plankton and ballast water exchange trials on the mv iron whyalla. *J. Marine Env. Engg.*, 1:91–110, 1994.

I. N. G. Rivera, K. M. C. Souza, C. P. Souza, and R. M. Lopes. Free-living and plankton-associated vibrios: assessment in ballast water, harbor areas, and coastal ecosystems in brazil. *Front. Microbiol.*, 3:443, 2012.

J. D. Rothlisberger and D. M. Lodge. The laurentian great lakes as a beachhead and a gathering place for biological invasions. *Aquatic Invasions*, 8:361–374, 2013.

D. A. Rudnick, K. Hieb, K. F. Grimmer, and V. H. Resh. Patterns and processes of biological invasion: The Chinese mitten crab in San Francisco Bay. *Basic Appl. Ecol.*, 4:249–262, 2003.

G. M. Ruiz and D. F. Reid. Current state of understanding about the effectiveness of ballast water exchange (BWE) in reducing aquatic nonindigenous species (ANS) introductions to the great lakes basin and chesapeake bay, usa: Synthesis and analysis of existing information. Technical report, National Oceanic and Atmospheric Administration, United States Department of Commerce, 2007.

G. M. Ruiz, T. K. Rawlings, F. C. Dobbs, L. A. Drake, T. Mullady, A. Huq, and R. R. Colwell. Global spread of microorganisms by ships - Ballast water discharged from vessels harbours a cocktail of potential pathogens. *Nature*, 408:49–50, 2000.

G. M. Ruiz, K. R. Murphy, E. Verling, G. Smith, S. Chaves, and A. H. Hines. Ballast water exchange: Efficacy of treating ships ballast water to reduce marine species transfers and invasion success? Technical report, Report submitted to Prince William Sound Regional Citizens Advisory Council and the US Fish & Wildlife Service, 14p., 2005.

M. Sandberg. The multi-chamber theory reconsidered from the viewpoint of air quality studies. *Build. Environ.*, 19(4):221–233, 1984.

V. Santosh, S. K. Mitra, M. Vinjamur, and R. Singh. Experimental and Numerical Investigations of Waterflood Profiles with Different Well Configurations. *Energy Fuels*, 21:3353–3359, 2007.

K. E. See and B. E. Feist. Reconstructing the range expansion and subsequent invasion of introduced European green crab along the west coast of the United States. *Biol. Invasions*, 12:1305–1318, 2009.

B. P. Shrestha, B. Gautam, and T. R. Bajracharya. Computational analysis of Pelton bucket tip erosion using digital image processing. In *Electronic Imaging and Multimedia Technology V, Pts 1 and 2*, volume 6833 of *Proceedings of the Society of Photo-optical Instrumentation Engineers (SPIE)*, page C8333, 2008.

N. Simard, S. Plourde, M. Gilbert, and S. Gollasch. Net efficacy of open ocean ballast water exchange on plankton communities. *J. Plankton Res.*, 33:1378–1395, 2011.

F. W. Sinden. Multi-chamber theory of air infiltration. *Build. Environ.*, 13:21–28, 1978.

Y. X. Song, J. Z. Wang, J. D. Yang, Y. B. Wu, N. Li, N. Gong, X. X. Pan, Y. Q. Sun, and D. Q. Li. Algae Detection and Ship's Ballast Water Analysis by a Microfluidic Lab-on-chip Device. *Instrum Sci. Technol.*, 40:305–315, 2012.

F. Steinhauer. Ballast water exchange and the destruction of non-indigeneous species. Master's thesis, University College London, 2007.

K. Suhling, G. Hungerford, R. W. Airey, and B. L. Morgan. A position-sensitive photon event counting detector applied to fluorescence imaging of dyes in sol-gel matrices. *Meas. Sci. Technol.*, 12:131–141, 2001.

B. Sun, N. N. Aye, X. Wang, X. Zhu, and M. Sato. Eradication of Invasive Organisms From Ballast Water With Electrodeless Pulsed-Discharge Hybrid Reactor. *Society*, 47:1079–1085, 2011.

C. A. Sutton, K. Murphy, R. B. Martin, and C. Hewitt. *A review and evaluation of ballast water sampling protocols.*, volume CRIMP at CSIRO. Hobart : CSIRO Division of Marine Research, 1998.

G. Tan and L. Glicksman. Application of integrating multi-zone model with CFD simulation to natural ventilation prediction. *Energy Build.*, 37:1049–1057, 2005.

Z. Tang, M. A. Butkus, and Y. F. Xie. Crumb rubber filtration: a potential technology for ballast water treatment. *Mar. Environ. Res.*, 61:410–423, 2006.

Z. Tang, M. A. Butkus, and Y. F. Xie. Enhanced performance of crumb rubber filtration for ballast water treatment. *Chemosphere*, 74:1396–1399, 2009.

L. B. Tao and K. Thiagarajan. Low kc flow regimes of oscillating sharp edges i. vortex shedding observation. *Appl. Ocean Res.*, 25:21–35, 2003.

T. W. Therriault, M. I. Orlova, M. F. Docker, H. J. Macisaac, and D. D. Heath. Invasion genetics of a freshwater mussel (*Dreissena rostriformis bugensis*) in eastern Europe: high gene flow and multiple introductions. *Heredity*, 95:16–23, 2005.

R. Tovar, P. F. Linden, and L. P. Thomas. Hybrid ventilation in two interconnected rooms with a buoyancy source. *Sol. Energy*, 81:683–691, 2007.

R. Tovar, C. A. C. Garrido, P. F. Linden, and L. P. Thomas. Buoyancy-driven flow in two interconnected rooms: effects of the exterior vent location and size. *J. Sol. Energy Eng.*, 131:021005, 2009.

E. Tsolaki and E. Diamadopoulos. Technologies for ballast water treatment: a review. *J. Chem. Technol. Biotechnol.*, 85:19–32, 2010.

H. Ülpre, I. Eames, and A. Greig. Turbulent acidic jets and plumes injected into an alkaline environment. *J. Fluid Mech.*, 734:253–274, 2013.

UNEP, ITC and ICTSD. *Trade and Environment Briefings: International Transport*. ICTSD Programme on Global Economic Policy and Institutions, International Centre for Trade and Sustainable Development, Geneva, Switzerland, policy brief no. 5 edition, 2012.

A. R. Vatankhah. Flow measurement using circular sharp-crested weirs. *Flow Meas. Instrum.*, 21:118–122, 2010.

D. Violon. Kinetics of intravenous radiographic contrast medium injections as used on ct: simulation with time delay differential equations in a basic human cardiovascular multicompartment model. *Br. J. Radiol.*, 85:e1212–e1218, 2012.

J.-M. Wang and L.-Z. Wang. Experimental Study of a New Hydrocyclone for Multi-Density Particles Separation. *Sep. Sci. Technol.*, 44:2915–2927, 2009.

L. Wang and Q. Chen. Theoretical and numerical studies of coupling multizone and CFD models for building air distribution simulations. *Indoor Air*, 17:348–361, 2007a.

L. Wang and Q. Chen. Validation of a coupled multizone and cfd program for building airflow and contaminant transport simulations. *HVAC&R Res.*, 13(2):267–281, 2007b.

Z.-x. Wang, J.-h. Zhao, X.-h. Jia, J.-g. Fang, B. Zhang, and G.-q. Ding. Influence of inactivation treatment of ships ballast water on corrosion resistance of ship steel plate. *J. Iron. Steel Res. Int.*, 20:85–89, 2013.

J. R. Waters and M. W. Simons. The evaluation of contaminant concentrations and air flows in a model of a building. *Build. Environ.*, 22(4):305–315, 1987.

A. Weinläder, W. Wu, S. Tenbohlen, and Z. Wang. Prediction of the oil flow distribution in oil-immersed transformer windings by network modelling and computational fluid dynamics. *IET Electr. Power Appl.*, 6:82–90, 2012.

B. Werschkun, Y. Sommer, and S. Banerji. Disinfection by-products in ballast water treatment: An evaluation of regulatory data. *Water Res.*, 46:4884–4901, 2012.

W. Wilson, P. Chang, S. Verosto, P. Atsavapranee, D. F. Reid, and P. T. Jenkins. Computational and experimental analysis of ballast water exchange. *Nav. Eng. J.*, 118:25–36, 2006.

K. B. Wong and R. H. Piedrahita. Settling velocity characterization of aquacultural solids. *Aquacult. Eng.*, 21:233–246, 2000.

M. J. Wonham, M. A. Lewis, and H. J. Macisaac. Minimizing Invasion Risk by Reducing Propagule Pressure: A Model for Ballast-Water Exchange. *Front. Ecol. Environ.*, 3:473–478, 2005.

D. A. Wright. Logistics of compliance assessment and enforcement of the 2004 ballast water convention. *J. Mar. Eng. Technol.*, 11:17–24, 2012.

W. Wu, Z. D. Wang, A. Revell, and P. Jarman. Computational fluid dynamics calibration for network modelling of transformer cooling flows part ii: pressure loss at junction nodes. *IET Electr. Power Appl.*, 6:28–34, 2012.

S. B. Yamada and P. M. Kosro. Linking ocean conditions to year class strength of the invasive European green crab, *Carcinus maenas*. *Biol. Invasions*, 12:1791–1804, 2009.

L. Yang, G. Zhang, Y. Li, and Y. Chen. Investigating potential of natural driving forces for ventilation in four major cities in China. *Build. Environ.*, 40:738–746, 2005.

Z. Yang. Multiattribute decision analysis of mandatory ballast water treatment measures in the US Great Lakes. *Transp. Res. D: Transp. Environ.*, 9:81–86, 2004.

Z. Ye, G. Zhang, I. H. Seo, P. Kai, C. K. Saha, C. Wang, and B. Li. Airflow characteristics at the surface of manure in a storage pit affected by ventilation rate, floor slat opening, and headspace height. *Biosyst. Eng.*, 104:97–105, 2009.

N. Y. Zeng, Y. R. Li, and M. Du. Rapid quantitative image analysis of hCG by gold immunochromatographic assay and genetic fast FCM algorithm. In *3rd International Conference on Biomedical Engineering and Informatics*, pages 1560–1564, 2010.

B. Zhao, X. T. Li, and Q. S. Yan. A simplified system for indoor air flow simulation. *Build. Environ.*, 38:543–552, 2003.

Y. Zhao, H. Yoshino, and H. Okuyama. Evaluation of the comis model by comparing simulation and measurement of airflow and pollutant concentration. *Indoor Air*, 8: 123–130, 1998.